

Fluvial organic carbon
losses from tropical
peatland oil palm
plantations in Sarawak,
Malaysia

Sarah Cook

A thesis submitted for the degree of Doctor of
Philosophy at the University of Leicester,
Department of Geography, Geology and the
Environment

Abstract

Currently, there are only very limited estimates of carbon loss from oil palm plantations (OPPs) on tropical peat, with the aquatic fluxes largely unquantified. This thesis presents an annual estimate of exported dissolved (DOC) and particulate (POC) organic carbon from the drainage waters of four OPPs and nearby stands of tropical peat swamp forest (PSF) in Sarawak, Malaysia, subjected to varying degrees of anthropogenic disturbance. Annual total organic carbon (TOC) fluxes ($104 \pm 19.3 \text{ g C m}^{-2} \text{ yr}^{-1}$) from the OPPs explored here are one third larger than those from intact PSFs ($63 \text{ g C m}^{-2} \text{ yr}^{-1}$) and comparable to fluxes from degraded PSFs ($97 \text{ g C m}^{-2} \text{ yr}^{-1}$) as reported in the literature. Forest fluxes measured in this project were of a similar magnitude (71.2 ± 11.0 to $84.5 \pm 13.1 \text{ g C m}^{-2} \text{ yr}^{-1}$), likely as a result of hydrological disturbance from the adjacent plantation drainage system.

Qualitative analysis (^{14}C and spectrophotometric analysis) of DOC derived from the OPP land cover revealed that the majority (> 50 %) originates from aged carbon sources (100 – 499 years, BP) and is both labile and highly oxidised, suggesting loss of carbon from long-term stable storage.

Extrapolation of the plantation sub-catchment fluxes indicates that industrial peatland OPPs across Peninsular Malaysia, Borneo and Sumatra contribute a combined TOC flux of 3.2 Tg C yr^{-1} . This represents one third of the regional TOC flux ($10.4 \text{ Tg C yr}^{-1}$; PSF intact + degraded + industrial OPPs) and suggests a more than two-fold increase in TOC losses since 1990.

Overall, this investigation reinforces the importance of considering alternative fluvial carbon loss pathways when assessing the on-going collapse of tropical peatland carbon stores in response to their continued anthropogenic exploitation.

Acknowledgements

First and foremost, I would like to thank my supervisors, Professor Sue Page and Dr Mick Whelan of the University of Leicester. They offered continuous guidance, support and enthusiasm throughout the past few years and were always on hand whenever I needed their advice. In addition, I am also extremely grateful to my two external supervisors, Professor Vincent Gauci of the Open University and Professor Chris Evans of the Centre for Ecology and Hydrology (CEH) in Bangor who were both eager to support and generous with their time. This research would also not have been possible without the funding provided by the Natural Environment Research Council (NERC), Sarawak Oil Palm Berhad and AXA Research Fund.

I also wish to extend a big thank you to Dr Kho Lip Khoon of the Tropical Peat Research Institute (TROPI) for welcoming me into his research group and supporting me for months at a time in Malaysia during fieldwork. Thank you Lilyen for your tireless fieldwork support and positive attitude every day in the field. An additional thank you to Cecelyea, Elisa, Tus, Steward and Ham who always made me feel welcome on the plantation and for keeping me safe on the plantation roads! Further thanks to Dr Yit Arn Teh of the University of Aberdeen and Dr Tim Hill of the University of Exeter for their useful discussions and continuous project support. Also, a big thank you to Fran Manning, Liyana Zin and Lizzie Telford who offered enormous amounts of emotional support and laughter in the field.

From the Open University I would also like to thank Dr Mike Peacock for his laboratory analysis and assistance, endless peaty advice and for always answering all my questions (no matter how silly they may have been)! I am also grateful to Dr Mark Garnett of the NERC Radiocarbon facility in East Kilbride, Scotland, for putting time aside to show me around the laboratories and analyse my samples.

I would also like to thank many other members of staff and colleagues at the University of Leicester who have made my time here so enjoyable and memorable.

Finally, a huge thank you to my family for which I dedicate this thesis to. Firstly to my parents for their continuous encouragement and support throughout my education, as well as for always believing in me. Particular thanks to my Mum who flew out and spent time on the oil palm plantation and caught dengue fever all to help me! Lastly, but not least, to Logan who went from being my long-term boyfriend, to fiancé to husband throughout the course of this PhD! Not only did you fly out to help set up my field sites, but you also put up with me, and kept me sane, throughout the emotional whirl wind of a ride that is a PhD.

Contents

Abstract.....	i
Acknowledgements	ii
Contents.....	iv
Table of Figures	ix
Tables	xxiii
List of abbreviations and acronyms	xxviii
Chapter One: Introduction	1
1.1 General overview.....	1
1.2 Tropical peatlands	2
1.2.1 <i>The tropical peatlands of Southeast Asia</i>	3
1.3 Tropical peatland characteristics	6
1.3.1 <i>Dome structure</i>	6
1.3.2 <i>Hydrology</i>	9
1.3.3 <i>Vegetation communities</i>	10
1.3.4 <i>Carbon balance on tropical peatlands</i>	11
1.4. Tropical peatland disturbance.....	16
1.4.1 <i>Oil palm plantation expansion</i>	17
1.4.2 <i>Disturbance effects on the carbon balance</i>	19
1.4.3 <i>Summary of emissions factors from drained organic soils under different land-uses</i>	28
1.5 Fluvial carbon overview	31
1.5.1 <i>Peatland fluvial carbon components</i>	32
1.5.2 <i>Peatland fluvial carbon fluxes</i>	33
1.5.3 <i>Peatland fluvial carbon as a source of CO₂</i>	39
1.6 Thesis aims and objectives.....	41
1.7 Thesis outline	42
Chapter Two: Methodology	44
2.1 Introduction	44
2.2 Study sites.....	45
2.2.1 <i>Location</i>	45
2.2.2 <i>Climate</i>	49

2.2.3 <i>Geology and topography</i>	50
2.3 Descriptions of the plantation experimental sites	51
2.3.1 <i>Sebungan Estate</i>	54
2.3.2 <i>Sabaju Estates</i>	58
2.4 Descriptions of the forest experimental sites	66
2.4.1 <i>Peat Swamp Forests</i>	66
2.4.2 <i>Deforested peat swamp forest areas</i>	69
2.5. Sampling methods.....	73
2.5.1 <i>Sample collection</i>	73
2.5.2 <i>Sample filtration</i>	75
2.5.3 <i>Sample preservation</i>	78
2.6 Sample analysis	79
2.6.1 <i>In-situ measurements</i>	79
2.6.2 <i>Dissolved organic carbon</i>	79
2.6.2.1 <i>UV-visible spectrophotometry</i>	81
2.6.2.2 <i>Non-purgeable organic carbon technique</i>	81
2.6.3 <i>Particulate organic carbon</i>	82
2.7 Hydrological measurements	83
2.8 Carbon flux calculations	86
2.8.1 <i>Catchment area</i>	86
2.8.2 <i>Water mass balance approach</i>	87
2.8.2.1 <i>Chloride mass balance</i>	88
2.8.2.2 <i>Soil water balancing model</i>	89
2.8.3 <i>Flow weighted TOC concentrations</i>	91
2.9 Environmental parameters	93
2.9.1 <i>Rainfall</i>	93
2.9.2 <i>Watertable height</i>	93
2.10 Statistical analyses.....	94
Chapter Three: The preservation and quantification of dissolved organic carbon (DOC).....	95
3.1 Introduction.....	95
3.1A Abstract	96
3.2A Introduction.....	97
3.3A Methods	99

3.3.1A Experiment 1. Effect of cold storage on DOC quantity and quality.....	100
3.3.2A Experiment 2. DOC changes during cold storage and the effect of freeze/thaw	101
3.3.3A Statistical analyses.....	102
3.4A Results	102
3.4.1A Experiment 1. Effect of cold storage on DOC quantity and quality.....	102
3.4.2A Experiment 2. DOC changes during cold storage.....	104
3.4.3A Experiment 2. Effect of freezing and thawing on DOC quality	106
3.5A Discussion.....	109
3.1B Abstract	112
3.2B Introduction.....	113
3.3B. Methods	116
3.3.1B <i>Site descriptions and sampling</i>	116
3.3.2B <i>Two-wavelength model description</i>	118
3.3.3B <i>Single-wavelength proxy assessment</i>	119
3.3.4B <i>Two-wavelength proxy assessment</i>	119
3.3.5B <i>Comparisons between approaches</i>	120
3.3.6B <i>Statistical analyses</i>	121
3.4B. Results	122
3.3.1B <i>Single-wavelength approach</i>	122
3.4.2B <i>Two-wavelength approach</i>	124
3.4.3B <i>Overall assessment of models</i>	126
3.5B Discussion.....	129
3.6B Conclusions.....	131
3.7B Data uncertainty	131
3.7.1B <i>Inverse confidence limits</i>	132
Chapter Four: Fluvial organic carbon losses from oil palm plantations on tropical peat.....	135
4.1 Introduction	135
4.2 Methods	135
4.2.1 <i>Hydrological investigations to determine fluvial organic carbon fluxes</i>	136
4.2.1.1 <i>Plantation</i>	138
4.2.1.2 <i>Forest</i>	144
4.3 Results	146
4.3.1 <i>Hydrological investigation results</i>	146

4.3.2	<i>Rainfall and discharge</i>	158
4.3.3	<i>Total organic carbon</i>	161
4.3.3.1	<i>Landcover classes</i>	161
4.3.3.2	<i>TOC seasonality</i>	165
4.3.3.3	<i>Temporal dynamics of TOC</i>	170
4.3.4	<i>Environmental parameters</i>	173
4.3.5	<i>Fluvial carbon fluxes</i>	181
4.5	<i>Discussion</i>	189
4.5.1	<i>TOC concentrations</i>	189
4.5.2	<i>TOC concentration variability</i>	191
4.5.3	<i>Forest hydrology</i>	194
4.5.4	<i>Interaction between watertable and TOC concentrations</i>	195
4.5.6	<i>Water sample properties (pH and EC)</i>	197
4.5.7	<i>Plantation and forest TOC fluxes</i>	198
4.6	<i>Conclusions</i>	200
<i>Chapter Five: Qualitative analysis of tropical dissolved organic carbon</i>		203
5.1	<i>Introduction</i>	203
5.1.1	<i>Spectrophotometric techniques</i>	203
5.1.2	<i>Radiocarbon dating</i>	205
5.2	<i>Methods</i>	209
5.2.1	<i>Sample collection</i>	209
5.2.2	<i>Radiocarbon dating</i>	211
5.3	<i>Results</i>	213
5.3.1	<i>DOC radiocarbon ages</i>	213
5.3.2	<i>Absorptivity and aromaticity</i>	219
5.3.4	<i>Temporal dynamics of SUVA</i>	223
5.3.5	<i>E ratios</i>	228
5.3.6	<i>Intense DOC collection experiment</i>	231
5.4	<i>Discussion</i>	232
5.4.1	<i>DOC radiocarbon ages</i>	232
5.4.2	<i>Bioavailability</i>	233
5.4.3	<i>E ratios</i>	238
5.5	<i>Conclusions</i>	239
<i>Chapter Six: General Discussion</i>		241

6.1 Introduction	241
6.2 Fluvial organic carbon fluxes and carbon quality	241
6.3 The Sebungan and Sabaju estates within a global context	252
6.4 Limitations and future research recommendations	258
6.4.1 TOC fluxes.....	258
6.4.2 TOC upscaling	260
6.4.3 Drivers of TOC variability	260
6.4.4 The fate of DOC.....	262
6.4.5 Forest buffer zones	263
6.4.6 Smallholder oil palm plantations.....	264
6.5 Summary and overall conclusions	265
7. References.....	268
Appendix.....	320
Appendix A: Plantation bulk density estimates.....	321
Appendix B: Flow-weighted TOC concentration fluxes, a worked example	322
Appendix C: Chloride mass balance	324
Appendix D: peat core pH profile	326
Appendix E: Characterisation of the semi-volatile component of Dissolved Organic Matter by Thermal Desorption – Proton Transfer Reaction – Mass Spectrometry (Final submitted manuscript).....	327
Appendix F: Annual TOC flux data calculations for all sites	345
Appendix G: Comparison between dipwell and ditch water.....	359

Table of Figures

	Page
Figure 1.1. Distribution of tropical peatlands found throughout Southeast Asia (Page et al., 2004)	4
Figure 1.2. Distribution of peat soils within Sarawak (Sa'don et al., 2015)	5
Figure 1.3. Representation of a highly developed inland peat dome, with peat swamp forest and freshwater swamp forests at margins (Page et al., 2011a)	7
Figure 1.4. Basic schematic diagram outlining the development of a peat dome (ASEAN, 2011 cited in Crump, 2017)	8
Figure 1.5. Diagram to show the natural drainage system (black arrows) within tropical peatlands, with water retention features i.e. hummocked topography and large buttress rooted trees	9
Figure 1.6. Simplified schematic diagram to highlight the main carbon inputs and output pathways on an intact tropical PSF	10
Figure 1.7 Schematic diagram outlining the basic processes involved in the carbon cycle of an intact peatland, under a low watertable, dry season (a) and high watertable, wet season (b)	14
Figure 1.8. Land cover change on peatland from 2000-2010, figures taken from Miettinen et al., (2011)	16
Figure 1.9 Photos to illustrate the sequence of peatland preparation for oil palm plantation development	25
Figure 1.10 Schematic diagram outlining the effect of drainage on a peat dome (Hooijer et al., 2010; Page et al., 2011a)	27
Figure 1.11. Percentage of the different carbon fractions found in contrasting fluvial systems, along with supporting references. Dashed line indicates division between temperate and tropical peat.	31

	Page
Figure 1.12. Diagram to illustrate the relationship between DOC, POC and TOC	33
Figure 1.13. Feedback mechanisms responsible for accelerating fluvial organic carbon losses, within tropical peatland catchments, as a result of deforestation and drainage (Verwer et al., 2008; Moore et al., 2013). Where: red box= increase; blue box= decrease	38
Figure 1.14 Thesis Chapters and subsections, alongside interlinks between the separate Chapters	43
Figure 2.1. Location of Sarawak State Malaysia.	46
Figure 2.2 Location of the oil palm plantation study sites (Sebungan and Sabaju Estates) in relation to the coastal town of Bintulu.	47
Figure 2.3 Location of the Sebungan and Sabaju oil palm estates in Sebauh Bintulu district Sarawak. The estates are bordered by a network of rivers (left map: grey and white lines; right map: blue lines) namely the Batang Kemena, S. Sebungan, S. Batang and S.Pandan. Arrows indicate direction of water flow.	48
Figure 2.4. Average annual rainfall and evaporation for the Lavang-Sabauh region over a 30-year record (1969-1998) and 35 year record (1964-1998), respectively. Rainfall data was collected from the Sebauh DID rainfall station no. 3132023 and Lavang DID rainfall station no. 3234022, with evapotranspiration data taken from Bintulu Airport Station no. 3130302 (EIA Report, 2006)	49
Figure 2.5 Example of a peatland oil palm plantation (Sebungan estate) layout with the planting blocks, drains and roads highlighted	53
Figure 2.6. Schematic of typical drainage set up on a peat OPP planting block. Where: red box = planting area, black dashed line = field drains, solid black line = collection drain, solid blue line = main drain, blue dashed line = perimeter drain and arrows show the direction of water flow.	54

	Page
Figure 2.7. Photographs to illustrate the height of the oil palm trees and the semi-closed canopy structure in the SE plantation estate.	55
Figure 2.8 Map of the Sebungan estate, including the location of the four point locations and their approximate catchment areas (shaded), arrows indicate the direction of water flow	56
Figure 2.9. Example of wooden weir structures located in the SE main drain, used to artificially modify water channel heights	57
Figure 2.10. Photograph to illustrate the dry collection drains encountered during October 2015	57
Figure 2.11 Photographs to illustrate the exposed peat surface in SA 3 (a) and SA 4 (b) and limited canopy coverage in 6 year old plantation stands	59
Figure 2.12 Large woody PSF debris on the peat surface in SA 4. The debris is stacked into windrows which were observed across the Sabaju plantation estates (photograph taken from SA 4)	60
Figure 2.13 Map of the Sabaju 1 estate, including the location of the four point locations and their approximate catchment areas (shaded), arrows indicate the direction of water flow	61
Figure 2.14 Map of the Sabaju 3 estate, including the location of the five point locations, and their approximate catchment areas (shaded), arrows indicate the direction of water flow. Note there is no SA 3.4 location.	63
Figure 2.15 Example of the flooding experienced in SA 3	64
Figure 2.16 Map of the Sabaju 4 estate, including the location of the four point locations and their approximate catchment areas (shaded), arrows indicate the direction of water flow	65
Figure 2.17. Location of the two PSF study sites in relation to the Sebungan and Sabaju estates	67

	Page
Figure 2.18. Closed canopy and tall tree species (left) within FA, alongside pitcher plant (<i>Nepenthes. sp</i>) (right)	68
Figure 2.19. Remains of a large tree (left) alongside the sparsely vegetated canopy layer (right) within FB.	68
Figure 2.20. Location of the two deforested PSF study sites in relation to the Sebungan and Sabaju estates	69
Figure 2.21. Satellite imagery, obtained from Google earth®, of the two deforested PSF study sites in contrast to the Sabaju 4 estate and FA site	70
Figure 2.22. The 3 m drainage ditch within the DF site, approximately 3 m wide and 2 m deep	71
Figure 2.23. Protruding islands of mineral soil in distance; newly-established drainage ditches in the foreground of site R-DF (photo taken 2 months after deforestation)	72
Figure 2.24 Example of newly established drainage ditch within R-DF alongside newly planted oil palm seedlings (photo taken August 2016, 6 months after deforestation)	72
Figure 2.25. Abundant woody debris covering the R-DF peat surface, with evidence of stacking into windrows.	73
Figure 2.26. Schematic diagram of dipwell tube	74
Figure 2.27 Example of an NPOC calibration curve (0 – 100 mg L ⁻¹) alongside the calibration coefficient (r^2) and equation of the line.	82
Figure 2.28 Example of a planation drainage channel rating curve, alongside the goodness of fit (r^2) and equation used to describe the relationship between stage height and discharge	84
Figure 2.29. Example of gauge posts installed in a plantation channel	85

	Page
Figure 2.30. Conceptual diagram of the key water transport pathways in the model	89
Figure 3.1A. Average DOC concentrations and absorbance at 254 nm for the two storage methods in Experiment 1. Error bars indicate the standard error of the mean. The degree of statistical significance between the two methods (paired two tailed, t-test) is also shown ($n=10$).	103
Figure 3.2A. Relationship between SUVA of the refrigerated samples and DOC concentration differences between the two storage techniques, in Experiment 1. The regression was significant ($P \leq 0.05$). The large numerical constants look implausible but are correct. They result from counterbalancing the x- multiplier and the constant over the very small x-range involved.	104
Figure 3.3A. Changes in absorbance values at 270 nm (A_{270}), 350 nm (A_{350}) and 700 nm (A_{700}), of samples kept in cold storage (4 °C) for approximately 12 weeks, from the same samples analysed immediately after collection, in Experiment 2. Positive values are increases. There are two sets of 17 samples, Set 1 collected on 3 rd August 2015; Set 2 on 5 th October 2015.	105
Figure 3.4A. Average normalised % differences in DOC observed before and after approximately 12 weeks of cold storage (4 °C) for the same sample for both sample sets, in Experiment 2. DOC concentrations were calculated using the two-wavelength approach (Carter et al., 2012). Error bars show the standard error of the mean. The significance of differences is also shown (unpaired, two-tailed, t-tests, $n=17$).	106
Figure 3.5A. Changes in absolute absorbance values at 270 nm (A_{270}), 350 nm (A_{350}) and 700 nm (A_{700}), following freeze/thaw, in Experiment 2. Positive values are increases. There is one set of 17 samples.	107
Figure 3.6A. Comparison of DOC concentrations before and after freeze/thaw, in Experiment 2. DOC concentrations were calculated using the two-wavelength approach (Carter et al., 2012). Error bars show the standard error of the mean ($n=17$).	108

	Page
Figure 3.1B. Location of the Sebungan and Sabaju oil palm estates in Sebauh Bintulu district Sarawak. The estates are bordered by a network of rivers (grey and white lines) namely the Batang Kemena, S. Sebungan, S. Batang and S.Pandan. Arrows indicate direction of water flow.	116
Figure 3.2B. Regression relationships between measured DOC concentrations from Campaign A and absorbance at 270nm (a) and 350 nm (b) along with (c) modelled DOC concentrations from Campaign B derived using the equation generated in (a) and (d) equation generated in (b). Dashed lines show 1:1 relationship	123
Figure 3.3B a) Original model calibration (constructed from April 2015 data/ Campaign A). Regression of modelled DOC concentrations (n=47) against respective measured DOC concentrations. Extinction coefficients were derived independently from the same data used for calibration (calibrated extinction coefficients): $E_{A, \lambda 1} = 74.32$, $E_{A, \lambda 2} = 30$, $E_{B, \lambda 1} = 15$, $E_{B, \lambda 2} = 0$ b) Regression of DOC concentrations from the independent data set ($2\lambda_{\text{calibrated}}$ model) (collected from Campaign B), against respective measured DOC concentrations. Model DOC concentrations generated using the calibrated extinction coefficients c) Regression of 2λ modelled DOC concentrations for validation samples against respective measured DOC concentrations using 'universal calibration coefficients' (Carter et al., 2012). Dashed lines show 1:1 relationships.	125
Figure 3.4B Regression analysis between DOC concentrations derived from the spectrophotometer (using the 2λ -calibrated approach) and the TOC analyser (a), along with an illustration of the corresponding S_0 values (b)	134
Figure 4.1 Flow chart to illustrate the sequence of approaches (blue boxes) taken to determine the area specific TOC fluxes for both the plantation and forest landcover classes. A brief summary of the approach details (black boxes) is provided alongside the problems encountered (red box) which caused the method to be discarded. The shaded boxes (blue and orange) indicate the final approaches taken.	137

	Page
Figure 4.2 Comparison between chloride concentrations obtained using the ion specific electrode and Dionex machine, along with the correlation coefficient (r^2) and line equation. The ion specific electrode slightly over estimated Cl^- concentrations but overall the average concentration differences between the two techniques was small (1.3 mg L^{-1}).	139
Figure 4.3 Soil retention curves for a range of different n values including the optimum model value of 2.8	141
Figure 4.4 Visual relationship between the volumetric water content of the peat and evapotranspiration	142
Figure 4.5 Time series of area specific runoff (mm hr^{-1}) for all flow monitored plantation drains, for an 8-month period across the SE (a), SA 1 (b), SA 3 (c) and SA 4 (d). The areas used to derive run off rates were obtained using the area estimates from manual flow direction mapping and delineation	146
Figure 4.6 Discharge, measured (solid line) and modelled (dashed line) for the SE 1 calibration site (a) along with a regression of the measured and modelled discharge data (b). Dashed line shows 1:1 relationship	149
Figure 4.7 Modelled and predicted discharge in catchments (a) SE 2, (b) SE3, and (c) SE4	150
Figure 4.8. Modelled and predicted discharge in catchments (a) SA 1.2, (b) SA 1.4, and (c) SA 4.1 (d) SA 4.4	152
Figure 4.9 Map of the Sebungan estate, including the location of the four sampling point locations and their approximate catchment areas, arrows indicate the direction of water flow	154
Figure 4.10 Map of the Sabaju 1 estate, including the location of the four sampling point locations and the approximate catchment areas for SA 1.2, SA 1.3 and SA 1.4, arrows indicate the direction of water flow	155

	Page
Figure 4.11 Map of the Sabaju 3 estate, including the location of the five sampling point locations and the approximate catchment areas for SA 3.1, SA 3.3 and SA 3.5, arrows indicate the direction of water flow. Note there is no SA 3.4	156
Figure 4.12 Map of the Sabaju 4 estate, including the location of the four sampling point locations and the approximate catchment areas for SA 4.1, SA 4.2 and SA 4.4, arrows indicate the direction of water flow	157
Figure 4.13. Monthly rainfall data (August 2015 to August 2016) compiled from a combination of data obtained from the rainfall gauge at the Sebungan plantation base (1 st August 2015 – 5 th January 2016) and manual measurements made by the plantation estate offices (August 2015 – 2016). Site monthly rainfall values were derived by averaging rainfall records collected from the rain gauge and the plantation offices, for the respective months. The shaded areas indicate the timing of a distinct wet period (light grey; November to December 2015, inclusively) and dry period (light orange; January to June 2016, inclusively).	158
Figure 4.14 Runoff data (mid-September 2015 to mid-August, 2016) across the plantation sites instrumented with mini-divers in a) SE b) SA1 and c) SA4. Data presented are the mean daily runoff for the different drain types; calculated by averaging all daily runoff data for the respective drain type within each respective plantation. The shaded areas indicate the timing of a distinct wet period (light grey; November to December 2015, inclusively) and a dry period (light orange; January to June 2016, inclusively).	160
Figure 4.15 Mean TOC concentrations during the study period for all landcover classes (August 2015-2016; R-DF = February-August 2016), across a chronosequence of plantation ages. Where: M= main, C= collection, 6 and 9 = age of plantation in years and letters a to c denote statistically significant differences ($p < 0.05$) between study sites (Kruskal-Wallis test). Error bars display the standard error of the mean.	162
Figure 4.16. Mean TOC concentration data for the individual plantation study sites, split into main (dark grey) and collection (light grey) drains.	163

	Page
Figure 4.17. Mean TOC concentrations during the study period for sites split into components of DOC (grey) and POC (white), expressed as percentages. The plantation sites are further subdivided into the different drain types; main (m) and collection (c), and are positioned in time order since forest clearance.	164
Figure 4.18. Weekly TOC concentration data for the different landcover classes, alongside monthly rainfall (mm). Data presented are mean weekly TOC concentrations from all drains within each landcover class. Monthly rain data were obtained from the rainfall gauge at the Sebungan plantation base (1 st August 2015 – 5 th January 2016) and manual measurements made by the plantation estate offices (August 2015 – 2016).	166
Figure 4.19. Weekly TOC concentration data for different landcover classes, alongside daily rainfall (mm day ⁻¹) from 3 rd August, 2015 until 15 th December, 2016 when the onsite rain gauge was in operation.	167
Figure 4.20 Weekly TOC concentration data for (a) the forest sites and (b) the plantation estates, alongside monthly rainfall (mm month ⁻¹). Data presented are mean weekly TOC concentrations from all drains within each site. Monthly rainfall data were obtained from the rainfall gauge at the Sebungan plantation base (1 st August 2015 – 5 th January 2016) and manual measurements made by the plantation estate offices (August 2015 – 2016).	169
Figure 4.21. Solute rating curves for the Sebungan (a, n=132) and Sabaju (b, n=347) plantation estates, along with goodness of fit metrics (r^2) and line equations. Note different x axis scales.	171
Figure 4.22. Solute rating curves displaying hysteresis curves in weekly solute concentrations against stream discharge, for a high discharge period during the wet season (event from November, 2015 – January, 2016; a and b) and the dry season (event from April-June, 2016; c and d). The data presented are the mean weekly discharge and TOC concentrations from the main (a,c) and collection (b,d) drains for each plantation estate. Discharges were taken at the time of water sample collection. The collection drain for SA4 has been omitted from graph (d) due to low/no flow data. Arrows indicate the direction of hysteresis for each high discharge period.	172

	Page
Figure 4.23. Watertable depths for the plantation and forest study sites across the study period (August 2015-September 2016). Box plots show mean watertable depth from all watertable monitored areas (central horizontal line), along with the minimum and maximum heights recorded over the entire study period (bars). Box = 75 th and 25 th percentiles. Negative numbers denote distance below peat surface.	173
Figure 4.24. Weekly watertable depths measured in dipwells for the individual study sites. Date presented are the mean weekly watertable depths from all monitored areas within each study site. Negative numbers denote distance below peat surface. Blue dashed lines indicate the recommended RSPO watertable depth range for OPPs on peat (between – 40 to – 60 cm)	174
Figure 4.25 Relationships between average weekly watertable depth (cm) and average weekly TOC concentration (mg L ⁻¹) for all monitored areas. Significant correlations were observed for FA ($r^2 = 0.21$ **, n= 32) and SA 3 ($r^2 = 0.18$ ****, n=33); where * = the level of significance (*= $P \leq 0.05$; ** = $P \leq 0.01$; ***= $P \leq 0.001$; ****= $P \leq 0.0001$)	176
Figure 4.26 Time series of weekly mean TOC concentrations (grey) and concurrent weekly mean watertable depths (black) taken at the time of sample collection, for the four plantation estates.	177
Figure 4.27 Time series plots of weekly mean TOC concentrations (grey) and concurrent weekly mean watertable depths (black) for the forest sites.	178
Figure 4.28 Correlation between TOC concentrations with a) pH and b) EC, across the different landcover classes. The r^2 values are displayed alongside the level of significance (*) (ns= no significance $P > 0.05$; *= $P \leq 0.05$; ** = $P \leq 0.01$; ***= $P \leq 0.001$; ****= $P \leq 0.0001$). All data is presented including outliers.	180
Figure 4.29 Mean annual TOC fluxes during the study period for the plantation estates split into components of DOC (grey) and POC (white). Percentage contributions of DOC and POC are also given. The plantation sites are subdivided into the different drain types; main (M) and collection (C), and are positioned in age order.	183

	Page
Figure 4.30 Weekly fluvial TOC yield (August 2015 – 2015; 54 weeks) for the plantation main (a) and collection (b) drains, alongside monthly rainfall totals.	185
Figure 4.31 Relationship between weekly TOC fluxes and (a-b) TOC concentrations and (c-d) weekly discharge for the Sebungan (a and c) and Sabaju (b and d) plantations.	186
Figure 4.32 Daily discharge (mm day^{-1} ; grey lines) and corresponding weekly fluxes ($\text{g C m}^{-2} \text{ week}^{-1}$; black dots) for a selection of plantation study sites instrumented with mini divers (a) SE1, (b) SE4, (c) SA 1.4 and (d) SA 4.1.	187
Figure 4.33 Diagram to illustrate the effect of high and low watertables on the hydraulic conductivity and TOC supply, within a peatland. The black line represents the K_{sat} and labile TOC profiles (i.e. decreasing values with increased peat column depth)	192
Figure 4.34. Diagram to illustrate the impact of plantation drainage channels on adjacent forest reserves	195
Figure 4.35 Schematic diagram to show NEE (black arrows; $\text{g C m}^{-2} \text{ yr}^{-1}$) and fluvial organic carbon loss estimates (dark blue arrow; $\text{g C m}^{-2} \text{ yr}^{-1}$) across the conversion gradient, including: (a) intact PSF, (b) degraded PSF, (c) OPP. *Net ecosystem exchange for the intact and degraded PSF are derived from Hirano et al., (2012) using tower based (eddy covariance) gas measurements, and the TOC fluxes obtained from Moore et al., (2013). **Net ecosystem exchange for the OPP obtained from IPCC (2014) and the TOC fluxes from this study. A net carbon gain is estimated from the intact PSF of $111 \text{ g C m}^{-2} \text{ yr}^{-1}$ ($-174 + 63 = -111$; net carbon sink) whereas there is a net carbon loss from the degraded and OPP of $596 \text{ g C m}^{-2} \text{ yr}^{-1}$ ($+499 + 97 = +596$) and $1,204 \text{ g C m}^{-2} \text{ yr}^{-1}$ ($+1,100 + 104 = +1,204$), respectively.	202
Figure 5.1 ^{14}C (%modern) levels of organic carbon photosynthesized from 1850-2000. Light shaded areas represent dateable carbon (pre-1955). Dark shaded areas represent bomb-enriched carbon, fixed between 1957 and 2000 (Evans et al, 2007)	206

	Page
Figure 5.2 Approximate location of the main (red) and collection (blue) drains sampled for the intensive DOC collection experiment.	210
Figure 5.3 Outline of the radiocarbon dating method used on the DOC water samples	212
Figure 5.4 (a) Radiocarbon DO^{14}C levels (% modern) from the DOC samples analysed across the Sebungan (SE) and Sabaju 3 (SA 3) estates. Solid black line (104% modern) represents the current atmospheric $^{14}\text{CO}_2$ levels. Dashed line (100% modern) represents the atmospheric composition in 1950, prior to nuclear testing. (b) Radiocarbon DO^{14}C levels reported as conventional radiocarbon years (yrs BP, relative to 1950). Mean ^{14}C levels >100% modern cannot be assigned an age and are subsequently referred to as 'modern'. Vertical grey line divides the Sebungan and Sabaju 3 sample sites.	214
Figure 5.5. Mean watertable values plotted against ^{14}C (%modern) for all six sites, alongside the line equation and regression metric (r^2). Minus numbers denote distance in relation to the peat surface. Coloured circles illustrate the clustering of sites with high (blue) and low (red) mean watertables.	215
Figure 5.6. Modelled down-profile of DO^{14}C , as estimated from the age attribution model for all radiocarbon dated sites ($n=6$)	217
Figure 5.7. Modelled down-profile of DO^{14}C , as estimate from the age attribution model for all six radiocarbon dated sites grouped into their respective plantation estates (a) Sebungan and (b) Sabaju 3	218
Figure 5.8. Mean (a) SUVA_{254} data and (b) % aromaticity data during the study period for all landcover classes, along the conversion gradient. Error bars display the standard error of the mean.	220

	Page
<p>Figure 5.9. Mean SUVA₂₅₄ and % aromaticity data separated into the individual plantations, August 2015 – August 2016. Where: the dashed line represents the division between the young and old plantations and bars display the standard error of the mean. Main and collection drains are denoted by the dark grey and white bars, respectively. Letters a-c and (*) denote significant differences (Kruskal-Wallis test, <i>post-hoc</i>) between estates and drain types, respectively. Ns= no significant difference ($P > 0.05$).</p>	222
<p>Figure 5.10 Weekly SUVA₂₅₄ data for the different landcover classes. Data presented is average weekly TOC concentrations from all drains within each landcover class. Weekly data for the P, F and DF landcover classes totals 54 weeks with the R-DF site totalling 25 weeks. The shaded areas indicate the timing of a distinct wet period (light grey; November to December, inclusively) and dry period (light orange; January to June, inclusively).</p>	224
<p>Figure 5.11. Temporal dynamics in mean (a) daily discharge and (b) DOC concentrations (blue line) and SUVA (orange line) for the Sebungan (SE) plantation. Red circles indicate periods of increased discharge and carbon quality metrics. Daily discharge readings are an average of the SE plantation sites installed within mini-divers.</p>	226
<p>Figure 5.12. Temporal dynamics in mean (a) daily discharge and (b) DOC concentrations (blue line) and SUVA (orange line) for the Sabaju 1 (SA 1) plantation. Red circles indicate periods of increased discharge and carbon quality metrics. Daily discharge readings are an average of the SA 1 plantation sites installed within mini-divers.</p>	227
<p>Figure 5.13 Weekly variability in mean values for all three E ratios (a) E2:E3, (b) E2:E4, (c) E4:E6, across the four landcover classes, during the study duration.</p>	229
<p>Figure 5.14 Correlation between % aromaticity and (a) E2:E3 ratio and (b) E4:E6 ratio. The correlation of fit (r^2) is displayed on (b) alongside the equation of the line.</p>	230

	Page
Figure 5.15 Mean (a) DOC concentrations, (b) % aromaticity and (c) SUVA ₂₅₄ data from the intense DOC collection experiment. Bars displayed the standard error of the mean	231
Figure 6.1 Comparison of TOC flux data from a range of peatland studies. Blue bars indicate the plantation fluxes from this study. Solid black line indicates the division between tropical and temperate peat fluxes.	242
Figure 6.2 Summary graph comparing the SUVA, TOC concentration and TOC flux data for the main (grey) and collection (white) drains	243
Figure 6.3 Comparison of mean watertable depth across the radiocarbon dated sites with the % of carbon greater than 1000 years (BP), as constructed from the age attribution model. Dashed lines indicate the RSPO watertable guidelines for OPP.	244
Figure 6.4 Principal component analysis from TD-PTR-MS for the forest and oil palm plantation samples.	247
Figure 6.5 Boxplots of the fraction of semi-volatile (%) DOC normalised to the total DOC concentration. Horizontal lines; central = mean, upper = maximum and lower = minimum; Box = 75 th and 25 th percentiles.	247
Figure 6.6 Van Krevelen plots displaying the (a) atomic ratio of O/C and H/C and (b) number of carbon atoms (nC) and oxidative carbon state (OSc) for the individual plantation and forest DOC samples. Red circle indicates three anomalous forest samples (see text above for further detail).	249
Figure 6.7 Boxplots of the fraction of semi-volatile (%) DOC normalised to the total DOC concentration for the Sarawak forest site and oil palm plantations, alongside the selectively logged (KI) and extensively drained (KD) Kalimantan sites. Horizontal lines; central = mean, upper = maximum and lower = minimum; Box = 75 th and 25 th percentiles.	250
Figure 6.8 Schematic diagram to illustrate the role of the watertable in governing fluvial organic carbon dynamics within a peatland oil palm plantation	252

Tables

	Page
Table 1.1. Estimated carbon storage in tropical peatlands, on a regional scale (Page et al., 2011b; Dargie et al., 2017)	3
Table 1.2. Estimated carbon storage of tropical peatlands in Southeast Asia, by country (adapted from Page et al., 2011b)	4
Table 1.3. Peat cover (ha) in Malaysia by region (Wetlands International, 2010)	5
Table 1.4. Overview of studies that project future oil palm expansion (adapted from Valin et al., 2014)	18
Table 1.5. Area of oil palm on all soil types and peat soil in Malaysia	19
Table 1.6. Overview of GHG emissions from oil palm plantations on tropical peatlands	21
Table 1.7. Summary of CO ₂ emissions from oil palm plantations on peatlands, using chamber based methods	22
Table 1.8. Summary of CO ₂ emissions from oil palm plantations on peatlands, using subsidence monitoring	23
Table 1.9. Emission factors from draining organic soils, as a consequence of biological oxidation, from a variety of land uses and ecosystem types	30
Table 1.10 Estimated global DOC fluxes from riverine systems into the global ocean	34
Table 1.11. Comparison of DOC fluxes from peatlands across different climatic zones	35
Table 1.12. Factors influencing DOC production and input	37

	Page
Table 2.1. The former land use of the study area before conversion to oil palm (EIA Report, 2006)	51
Table 2.2. Advantages and disadvantages of filters used for DOC analysis, with corresponding references	77
Table 2.3. Techniques used to determine DOC concentrations from peatland catchments, along with their advantages and disadvantages	80
Table 2.4 Individual plantation study sites alongside the drain type (M = main, C= collection) and gauge method for channel water height	85
Table 3.1B. Values of the extinction coefficients used by Carter et al., (2012) and those generated from the calibrated data set, where $\lambda_1 = 270$ nm and $\lambda_2 = 350$ nm.	119
Table 3.2B. Mean concentration and percentage differences between modelled and measured DOC concentrations (mg L^{-1}) for the four different models using the validation data set (collected during Campaign B). Positive and negative values indicate that modelled DOC concentrations overestimate and underestimate measured DOC concentrations, respectively. n= number of samples.	126
Table 3.3B. Summary of goodness of fit metrics for all development and validation models. R^2 values and slope of regression lines between modelled and measured DOC for the model approaches, along with NSE and RMSE values. n= number of samples.	126
Table 4.1 Model parameters with the adjustable components highlighted in grey. Full model details and a description of the parameters are described in Chapter Two, Section 2.8.2.2	141
Table 4.2 Evapotranspiration estimates for forest sites	145
Table 4.3. Evapotranspiration estimates from Southeast Asia across OPP and forest land cover classes	147

	Page
Table 4.4. Model performance statistics for the goodness of fit between the measured and modelled discharges, for the Sebungan catchments, along with the resulting catchment sizes.	151
Table 4.5 Model performance statistics for the goodness of fit between the measured and modelled discharges, for the Sebungan catchments, along with the resulting estimated catchment sizes.	151
Table 4.6 Comparison of original catchment area estimates, derived from manual flow mapping (original), and new area estimates (updated) using volume weighted TOC concentrations. Grey shaded rows represent the point locations where only water samples were taken.	153
Table 4.7. Summary of fluvial carbon data (+/- SEM) for different landcover classes	162
Table 4.8. Results of Kruskal-Wallis test (<i>post-hoc</i> ; <i>Dunn's Multiple Comparison test</i>) for the TOC concentration data across the individual plantation study sites and drain types. Where ns = no significant difference and * = the level of significance (* = $P \leq 0.05$; ** = $P \leq 0.01$; *** = $P \leq 0.001$; **** = $P \leq 0.0001$)	164
Table 4.9. Period of time, expressed in percentages, when the watertable was within a certain depth range. Bold and underlined figures highlight the most common depth range.	175
Table 4.10. Mean pH and EC readings for all water samples across the different landcover classes, along with number of samples (n) and errors are given as +/- SEM	179
Table 4.11 Annual TOC flux estimates across the four plantation estates presented alongside upper and lower uncertainty bounds resulting from uncertainties in DOC concentrations. Sites where discharge readings could not be recorded due to changing hydrological conditions, resulting from management efforts (i.e. ditch blocking) are shaded in grey.	182

	Page
Table 4.12. Results of a one-way ANOVA (<i>post-hoc</i>) for the TOC concentration data across the individual plantation study sites and drain types. (*) denotes the level of significance (ns= no significance $P > 0.05$; * = $P \leq 0.05$; ** = $P \leq 0.01$; *** = $P \leq 0.001$; **** = $P \leq 0.0001$)	183
Table 4.13 Annual TOC flux estimates for the forest sites presented alongside the upper and lower flux bounds in response to the uncertainty in DOC concentrations and annual runoff.	188
Table 5.1 Various wavelengths and ratios used to determine specific properties relating to DOC, adapted from Peacock et al. (2014b).	205
Table 5.2. Mean and standard errors for radiocarbon DO^{14}C expressed as %modern and in conventional radiocarbon years (years BP, relative to AD 1950), expressed at $\pm 1\sigma$ level, for individual samples sites across the Sebungan and Sabaju estates. Mean ^{14}C levels $>100\%$ modern cannot be assigned an age and are subsequently referred to as 'modern'. Mean annual watertable data for each site is also presented, alongside the maximum and minimum watertables recorded. Negative numbers indicate distance from the peat surface.	213
Table 5.3. Sampling sites, together with conventional and modelled radiocarbon age estimates. As two solutions were possible for 'modern' samples (i.e. similar ^{14}C values occur before and after the bomb peak) the decay constant (k) was modelled using a high (1.0) and low (0.0001) value. However, ^{14}C values could only be reproduced using the 'low k' model suggestive of a predominately prebomb carbon content, as highlighted in bold.	216
Table 5.4. Summary of SUVA_{254} and % aromaticity data for the landcover classes	221
Table 5.5. Results of Kruskal-Wallis test (<i>post-hoc</i>) for SUVA_{254} and % aromaticity applied to the different landcover classes. Where ns = no significant differences and * = the level of significance. Identical trends in significance were displayed between the two parameters	221

	Page
Table 5.6 Mean and standard errors for the three E ratios examined. n = the number of samples.	228
Table 6.1 Estimated depth of DOC source (cm), alongside maximum watertable drawdown, for the dated samples. Where +/- number represent a DOC source from higher/lower down the peat column, relative to the maximum watertable.	246
Table 6.2 Estimated fluvial organic carbon fluxes for the plantation estates based on the main drain TOC flux and total plantation area	252
Table 6.3 Predicted future OPP expansion in Sarawak and associated TOC flux estimates	253
Table 6.4 Impact of Sarawak peatland OPPs on river outgassing, assuming 53% of DOC is decomposed and emitted as CO ₂ into the atmosphere.	254
Table 6.5 Regional annual TOC fluxes for all peatland area covered by OPPs within Peninsular Malaysia, Borneo and Sumatra. Area estimates are taken from Miettinen et al., (2016) for the year 2008.	255
Table 6.6. Peatland land cover estimates by Miettinen et al. (2016) and Moore et al. (2013), across Peninsular Malaysia, Borneo and Sumatra, for the years 2015 and 2008, respectively.	256
Table 6.7 TOC flux estimates from PSF areas accounting for industrial oil palm plantations across Peninsular Malaysia, Borneo and Sumatra, for the year 2015. Area estimates are taken from Miettinen et al. (2016).	256
Table 6.8 TOC flux estimates from all degraded PSF areas accounting for all industrial peatland plantations across Peninsular Malaysia, Borneo and Sumatra, for the year 2015.	257
Table 6.9 Total carbon emissions for the Sebungan and Sabaju oil palm plantations	258
Table 6.10 Total carbon emissions from peatlands within Peninsular Malaysia, Borneo and Sumatra	258

List of abbreviations and acronyms

Abbreviation	Meaning
A	Catchment area
A_{unknown}	Catchment area unknown
BAU	Business as usual
BD	Bulk density
BP	Before present
C	Collection drain
C_{est}	Estimated channel discharge using the water storage model
CMB	Chloride mass balance approach
C_{meas}	Measured discharge
C_{mean}	Mean discharge
C_p	Mean concentration of Cl ⁻ in a rain sample
C_Q	Mean concentration of Cl ⁻ in water discharge
CO ₂ -eq	Carbon Dioxide equivalent
CV	Coefficient of variance
D/DBPR	Disinfectant/Disinfection By-Products Rule
DEM	Digital Elevation Models
DF	Deforested
DIC	Dissolved inorganic carbon
DO ¹⁴ C	Radiocarbon dated DOC
DOC	Dissolved organic carbon
EC	Electro conductivity
EIA	Environmental Impact Assessment

ET	Evapotranspiration
ET _A	Actual Evapotranspiration
ET _o	Reference Evapotranspiration
ET _p	Potential Evapotranspiration
F	Forest sites combined (FA + FB)
FA/FB	Forest sample sites
GF	Glass fibre
GHG	Greenhouse gases
GPP	Gross primary productivity
GtC	Gigatonne of Carbon
HTCO	High temperature catalytic oxidation
IC	Inorganic Carbon
IPCC	International Panel on Climate Change
$J_{a.s}$	Area specific flux
K_c	Resistance factors
KFCP	Kalimantan Forests and Climate Partnership
Kn	Hydraulic conductivity
K_{sat}	Saturated hydraulic conductivity
LUC	Land use change
M	Main drain
Mha	Million hectares
MPOB	Malaysian Oil Palm Board
MW	Molecular weight
nC	Number of carbon atoms per sample
NEE	Net ecosystem exchange

NEP	Net ecosystem productivity
NPK	Nitrogen, Phosphorus and Potassium
NPOC	Non-purgeable organic carbon
NSE	Nash-Sutcliffe efficiency
OLF	Overland flow
OPP	Oil palm plantation
OSc	Oxidative state of carbon
P	Plantation (SA + SE)
POC	Particulate organic carbon
POM	Particulate organic matter
PSF	Peat swamp forest
q	Vertical drainage of water out of soil
Q	Discharge
Q _A	Annual discharge
R-DF	Recently deforested
R_E	Annual flow volume
RMSE	Root mean square error
RSPO	Roundtable on sustainable palm oil
SA	Sabaju
SA1/3/4	Sabaju estates
SE	Sebungan
SEM	Standard error means
SMH	Smallholder
SUVA ₂₅₄	Specific Ultra-Violet Absorption
THM	Trihalomethane
TOC	Total organic carbon

UV	Ultra-violet
VBA	Visual Basic for Applications
VWM	Volume weighted mean
WaSIM	Water Balance Simulation Model
WCO	Wet chemical oxidation
WMB	Water mass balance
Yr ⁻¹	Per year

Chapter One: Introduction

1.1 General overview

Tropical peatland is a significant terrestrial carbon sink and covers a total area of 440,000 km² (Page et al., 2011). Its greatest extent (248,000 km²) and carbon reserve (57 Gt C) is found within Southeast Asia (Dargie et al., 2017), which supports biologically diverse peat swamp forests (PSFs). However, this ecosystem is being economically exploited which is driving land conversion by deforestation, drainage and fire (Hansen et al., 2009; Miettinen et al., 2012b; 2016; 2017). Consequently, only 6% of PSFs in Peninsular Malaysia, Borneo and Sumatra are considered pristine (Miettinen et al., 2016). This conversion significantly contributes to global anthropogenic greenhouse gas (GHG) emissions (Couwenberg et al., 2010; Hirano et al., 2012), with managed landcover types contributing 78 % of Southeast Asia's total peat oxidation emissions (146.2 Mt C yr⁻¹; Miettinen et al., 2017). Central to this has been the expansion of oil palm plantations (OPP) across Peninsular Malaysia, Borneo and Sumatra (Wicke et al., 2008; 2011; SarVision, 2011; Schrier-Uijl et al., 2013; Gandaseca et al., 2014; Cole et al., 2015; Miettinen et al., 2016). This form of conversion is responsible for 16% and 32% of total emissions from peat oxidation in Indonesia and Malaysia, respectively (Agus et al., 2013) and is ultimately converting the peatland carbon sink into a significant carbon source.

Previous research has largely focused on the direct atmospheric carbon losses from peatland conversion (Germer & Sauerborn, 2008; Hooijer et al., 2012), with alternative carbon loss pathways, and specifically fluvial pathways, largely overlooked. At present, no study has quantified the effect of peatland OPP development on fluvial organic carbon losses, and only one study (Moore et al., 2013) has reported on the considerable losses of dissolved organic carbon (DOC) from drained tropical peatlands. This fluvial component provides an important carbon transport pathway, connecting terrestrial and marine ecosystems (Evans et al., 2012). Once in transit, fluvial organic carbon has the

potential to directly feedback into the atmosphere as carbon dioxide (CO₂) and methane (CH₄) through biological and photo-chemical induced degradation (Muller et al., 2016). Moore et al. (2013) show that overall carbon losses from disturbed peatlands are underestimated by 22% if this aquatic component is not included. Consequently, failure to account for fluvial organic carbon could lead to significant underestimations in ecosystem carbon budgets as well as the impact of anthropogenic land-use change on tropical peatland carbon dynamics.

This thesis will provide the first robust and detailed study focused on fluvial organic carbon export from peatland OPPs. This will help to build a fuller picture of the temporal dynamics of fluvial organic carbon and potentially provide the basis for changes in plantation management in support of carbon conservation.

1.2 Tropical peatlands

Peatlands cover around 3% of the global land mass (Zinck & Huber, 2011) and store approximately 600 Gt of carbon (GtC; 1 Gt = 1 g × 10¹⁵), exceeding that of the global vegetation carbon pool (560 GtC; Turetsky et al., 2015). Peatland extent is dominated by high-latitudes with 49% of peatlands concentrated in North America alone (Chimner & Karberg, 2008; Zinck & Huber, 2011). In contrast, while tropical peatland coverage is smaller (10%) they store almost one fifth (89 GtC, 15%) of the entire peatland carbon pool, making them dense stores of carbon (Page et al., 2011b; Turetsky et al., 2015). The recent discovery of a highly significant peatland area within the Congo (Dargie et al., 2017) has elevated the tropical peatland area and carbon stores, increasing the magnitude of peat carbon across Africa by five times (Dargie et al., 2017; 7.82 GtC to 34.4 GtC). Taking this into account a revised and more contemporary best estimate for tropical peat carbon stocks is 105 GtC (Table 1.1; Dargie et al., 2017). Of this, an estimated 57 GtC is stored within the peatlands of Southeast Asia (Page et al., 2011b; Dargie et al., 2017), equivalent to 54% of total tropical peat carbon stocks (Table 1.1).

Table 1.1. Estimated carbon storage in tropical peatlands, on a regional scale (Page et al., 2011b; Dargie et al., 2017)

Carbon storage (GtC)		
Region	Revised best estimate¹	% (Revised best estimate)¹
Africa	34.40 ¹	32.76
Southeast Asia	57.02 ²	54.30
Asia (other)	0.43	0.41
Central America	3.05	2.90
Pacific	0.01	0.01
South America	9.67	9.21
TOTAL	105	100

¹ Revised carbon stock estimates incorporating newly discovered Congo peatland (Dargie et al., 2017).

² Updated carbon stock estimates for Southeast Asia accounting for carbon stock losses of 0.5 GtC yr⁻¹ since original data collection (23 years x 0.5 = 11.5 Gt C total loss) (Dargie et al., 2017)

1.2.1 The tropical peatlands of Southeast Asia

Most of Southeast Asia's peatlands are distributed across Indonesia (206,950 km², 84%) and Malaysia (25,889 km², 10%) which comprise the majority share in total peat volume (Page et al., 2011b; Figure 1.1). Similar trends in magnitude are also reflected in the proportions of the peat carbon store (Table 1.2), with Indonesia and Malaysia accounting for 84% and 13% of Southeast Asia's total carbon pool, respectively. Within Malaysia, the province of Sarawak supports the largest extent of peat coverage (69%), followed by Peninsular Malaysia and Sabah (Table 1.3; Wetlands International, 2010). The distribution of peat soils within Sarawak is heavily concentrated along coastal margins (Figure 1.2), with an estimated peat thickness of between 3m (Hooijer et al., 2006) and 7m (Page et al., 2010).

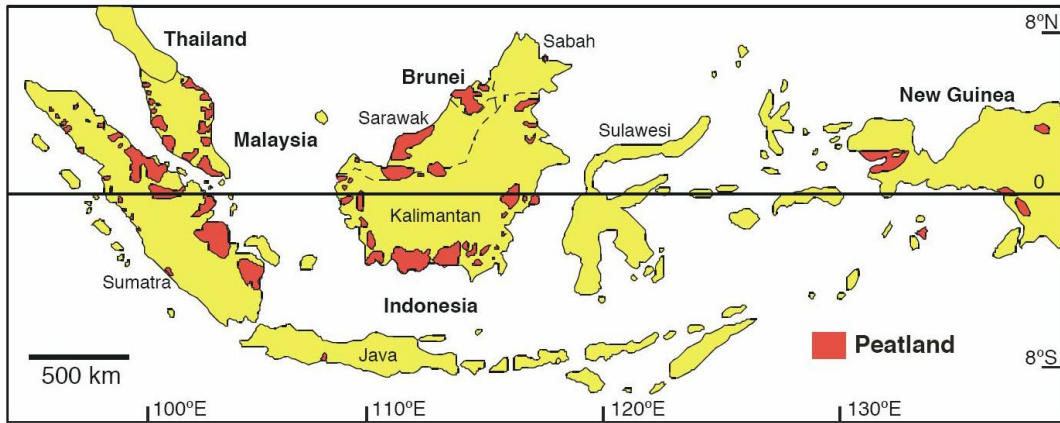


Figure 1.1. Distribution of tropical peatlands found throughout Southeast Asia (Page et al., 2004)

Table 1.2. Estimated carbon storage of tropical peatlands in Southeast Asia, by country (adapted from Page et al., 2011b)

Country	Carbon storage (GtC)			% (best estimate)
	Minimum	Best	Maximum	
Brunei	0.32	0.32	0.32	0.47
Indonesia	57.37	57.37	58.33	83.75
Malaysia	7.93	9.13	9.16	13.33
Burma (Myanmar)	0.04	0.09	0.13	0.13
Papua New Guinea	0.63	1.38	1.67	2.01
Philippines	0.02	0.17	0.2	0.25
Thailand	0.03	0.03	0.03	0.04
Vietnam	0	0.01	0.03	0.01
TOTAL	66.34	68.5	69.87	100

Table 1.3. Peat cover (ha) in Malaysia by region (Wetlands International, 2010)

Region	Area (ha)	% of peat
Sarawak	1,697,847	69.08
Peninsular Malaysia	642, 918	26.16
Sabah	116, 965	4.76

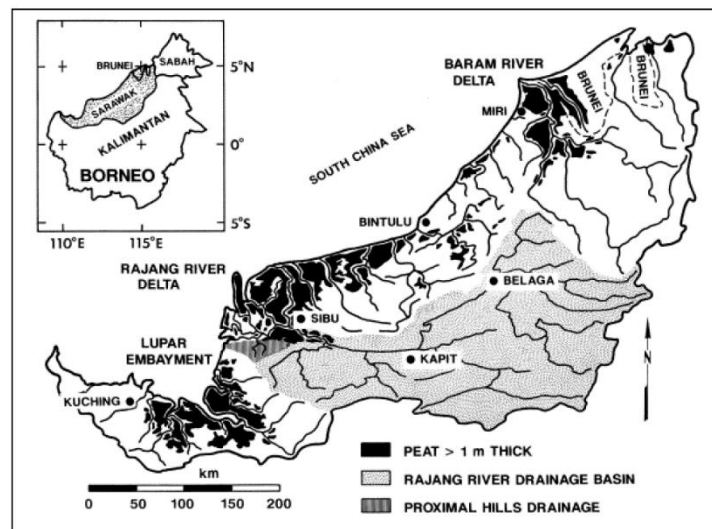


Figure 1.2. Distribution of peat soils within Sarawak (Sa'don et al., 2015)

1.3 Tropical peatland characteristics

Tropical peatlands can be grouped into three main categories depending upon their origin: i) coastal, ii) sub-coastal and iii) high interior (Page et al., 1999; 2004; 2011a). Much of the lowland peatlands, throughout Malaysia, have formed along coastal margins, on marine sediments and behind accreting mangrove forests (Page et al., 2010; Wetlands International, 2010). However, some have formed further inland (sub-coastal), along former coastal margins, such as those in Marudi, Sarawak (Anderson & Muller, 1975; Wetlands International, 2010).

1.3.1 *Dome structure*

Tropical peatlands form due to a combination of topographic relief, high organic matter input and waterlogged conditions, which promotes the prevalence of anoxic conditions and build-up of undecomposed organic matter (Page et al., 2010). These areas often receive high effective rainfall and have impermeable substrates (Page et al., 2010; Schrier-Uijl et al., 2013). Peatlands typically form between two rivers, or stream channels, leading to the formation of their characteristic elliptical dome shape, with freshwater swamp forests at their riverine margins (Figure 1.3; Alongi et al., 1998; Page et al., 2004; Wetlands International, 2010; Adon et al., 2012).

The developmental stages of a peat dome are outlined in Figure 1.4. This begins with a flat area of land between two rivers. Frequent flooding of this area causes the river channels to overflow leaving behind a strip of alluvium, supporting a transitional freshwater swamp forest (Wetland International, 2010; Dommain et al., 2015). As flooding continues the river levees start to build up, eventually creating a shallow basin, with poor drainage (Rais, 2011). Any organic matter input into the basin, will be submerged and partially decomposed, leading to the accumulation of peat, with average accumulation rates of between 1.3 and 1.5 mm yr⁻¹ (Page et al., 2004; Murdiyarso et al., 2010). Peat can also accumulate behind an outer mangrove belt where sediment and organic matter becomes trapped in the mangrove root system.

These areas, in time, support the development of PSFs, further increasing the input of organic matter (Dommain et al., 2015). Overtime this will cause the peat to become thicker, increasing hydraulic resistance, creating a hydraulic gradient (Rais, 2011). Consequently, the watertable tends to be higher at the peat swamp centre and lower at the fringes, creating differential decomposition rates, leading to the formation of a distinct convex dome shaped surface (Figure 1.4; Wetlands International, 2010; Page et al., 2011a).

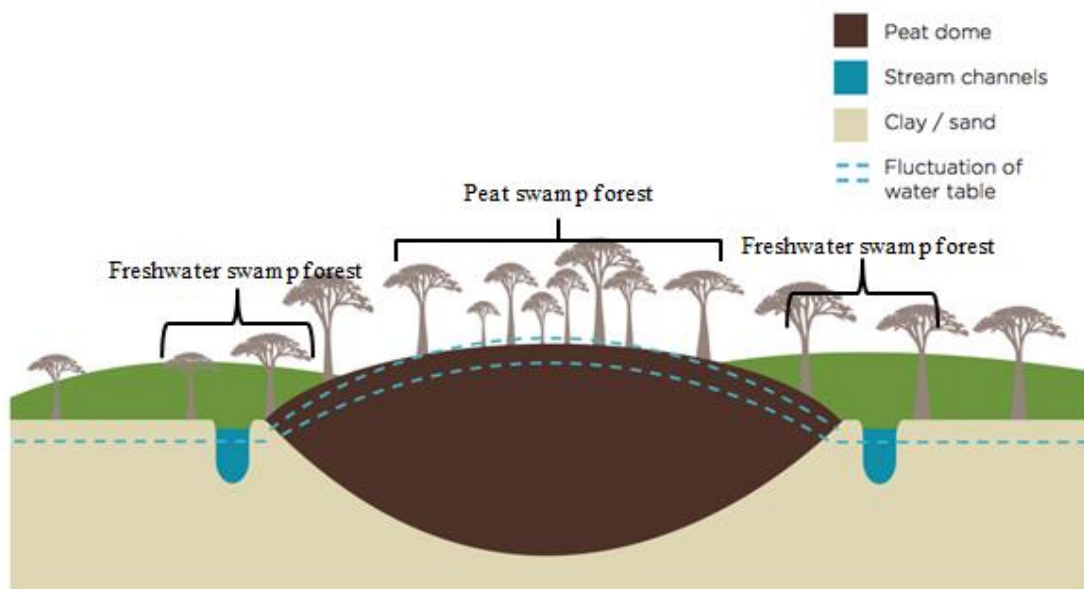


Figure 1.3. Representation of a highly developed inland peat dome, with peat swamp forest and freshwater swamp forests at margins (Page et al., 2011a)

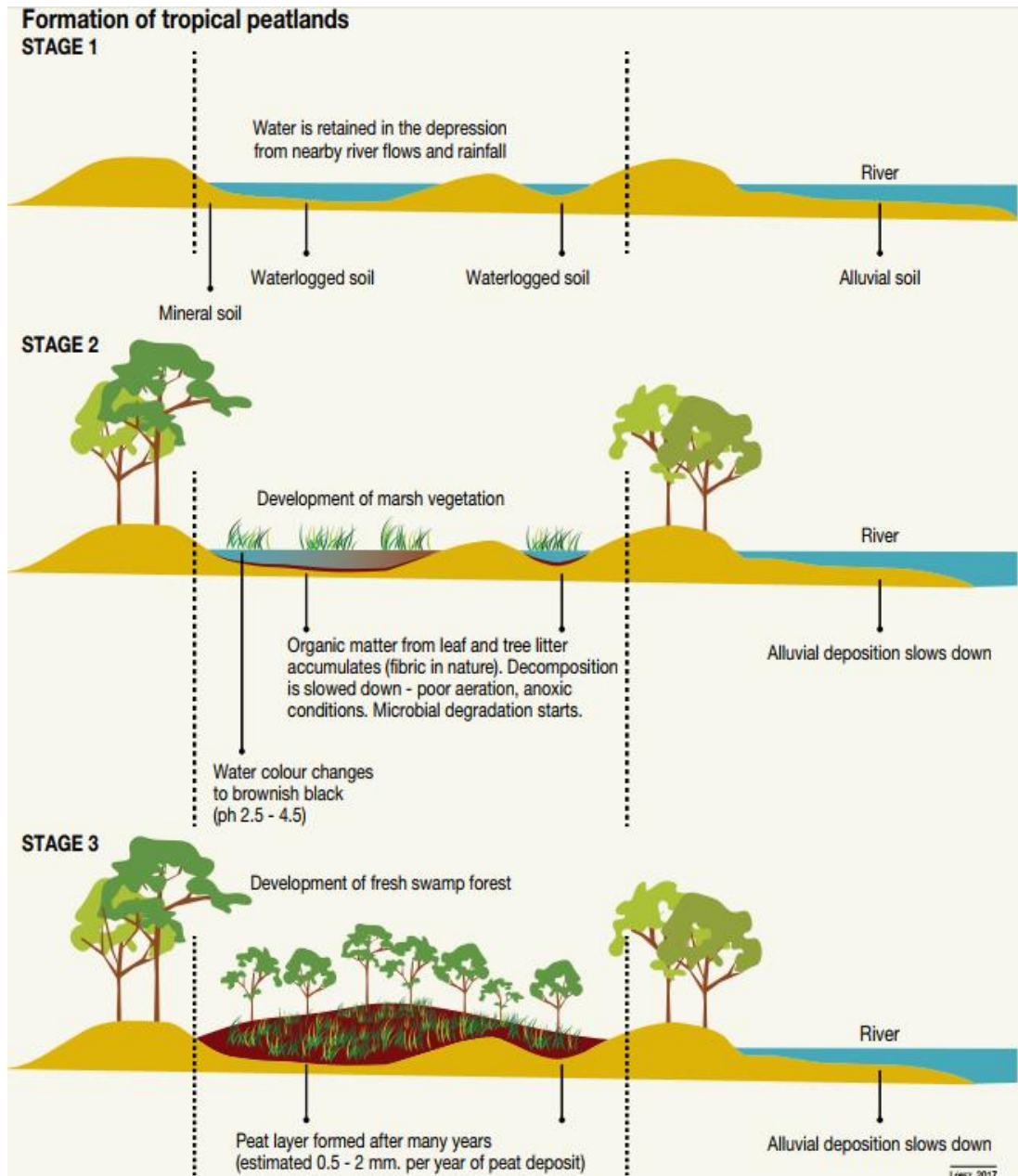


Figure 1.4. Basic schematic diagram outlining the development of a peat dome (ASEAN, 2011 cited in Crump, 2017)

1.3.2 Hydrology

Tropical peat domes are discrete hydrological units (Wetlands International, 2010) as the accumulating peat isolates the surface from the underlying mineral rich groundwater (Page et al., 2011a). This makes them entirely dependent upon precipitation inputs for their nutrient and water supplies, making them ombrotrophic in nature (Page et al., 2004; 2010). The lack of mineral input coupled with leaching of organic compounds makes the surrounding water extremely acidic (<pH 4; Posa et al., 2011). Sustaining the peat dome structure requires continuous water saturation, allowing anoxic conditions to prevail, inhibiting decomposition (Dommain et al., 2010; 2011). This environment is hard to maintain due to high evapotranspiration rates and distinct dry seasons, typical of tropical climates in Southeast Asia (Dommain et al., 2010). In addition, the dome shape promotes gravity induced run-off, forming its own watershed, causing water to naturally drain from the top of the peat dome into the surrounding rivers (Figure 1.5; Dommain et al., 2010; 2011). Consequently, tropical peatlands contain many hydrological self-regulating mechanisms to sustain these permanent waterlogged conditions, including: depressions between hummocks and spreading buttress roots (Page et al., 2004; Dommain et al., 2015; Baird et al., 2017). Another unique feature includes 'tip-up-pools', whereby storm events cause trees to become uprooted, creating a cavity (Dommain et al., 2015). This can become infilled with water and leaf litter creating a localised 'hot spot' for peat and therefore carbon accumulation (Dommain et al., 2015).

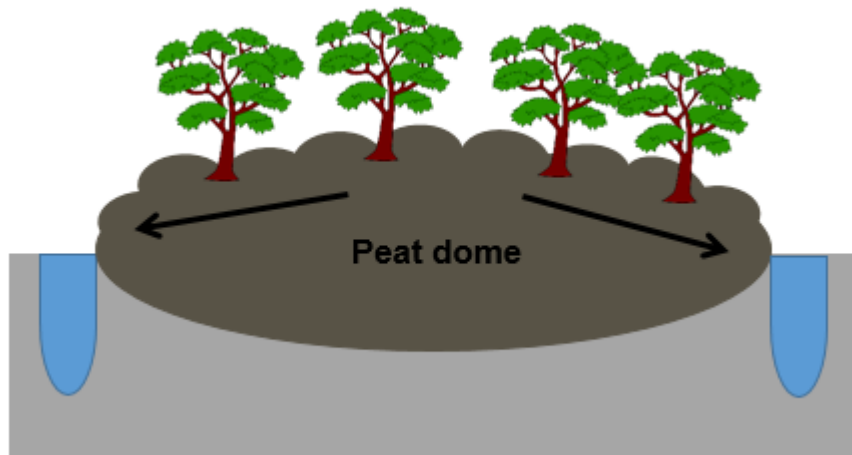


Figure 1.5. Diagram to show the natural drainage system (black arrows) within tropical peatlands, with water retention features i.e. hummocked topography and large buttress rooted trees

1.3.3 Vegetation communities

The hummocked topography of the peat dome surface causes changes in elevation and associated changes to abiotic and biotic conditions (Page et al., 1999). These often coincide with shifts in vegetation species composition, referred to as phasic community transition zones (Page et al., 1999). Anderson (1963, cited in Schrier-Uijl et al., 2013) describes six phasic communities typically present on Sarawak peat domes:

1) *Mixed swamp forest*: located within the river's flooding area and consists of a mixed community with important species such as *Gonystylus bancanus*, *Copaifera palustris* and *Shorea sp.* found here. Dense middle and lower storeys. Heights range from 40-45m (Wetlands International, 2010; Schrier-Uijl et al., 2013).

2) *Alan forest*: dominated by a single species (*Shorea albida*). Dense middle and lower storeys. Heights range from 40-45m (Wetlands International, 2010; Schrier-Uijl et al., 2013).

3) *Alan bunga forest*: the highest stratum is associated with the *Shorea albida* species. Canopy is very uneven with lots of broken gaps, usually caused by lightning strikes. Absent middle storey, with a dense understorey dominated by a single species. Heights range from 50-60m (Wetlands International, 2010; Schrier-Uijl et al., 2013).

4) *High pole forest*: species dominated by *Litsea palustris*, *Parastemon spicatum* and *Tristaniopsis*. Canopy is even and mostly unbroken. Heights range from 35-40m (Wetlands International, 2010; Schrier-Uijl et al., 2013).

5) *Low pole forest*: narrow transitional zones which resembles the high pole zone but with shorter and densely distributed tree species. The most abundant species are *Palaquim* species. Heights range from 15-20m (Wetlands International, 2010; Schrier-Uijl et al., 2013).

6) *Padang Paya*: Very open zone found in the centre of the peat dome and the least fertile area. Common species include *Cyperaceae*, herbaceous flora and other small trees. Heights up to 7m (Wetlands International, 2010; Schrier-Uijl et al., 2013).

1.3.4 Carbon balance on tropical peatlands

Under natural conditions with no anthropogenic influence intact PSFs function as effective carbon sinks (Page et al., 2004; Dommain et al., 2015). However, increasingly, due to disturbance, these ecosystems are rapidly becoming large carbon sources. The carbon balance within an intact PSF involves several vertical and lateral carbon transport pathways (Figure 1.6). It is principally dictated by the uptake of carbon via photosynthesis (gross primary productivity, GPP) and the release of carbon, in the form of CO₂ and CH₄, from autotrophic (root respiration) and heterotrophic respiration (decomposition of organic matter via microbes) (Page et al., 2011a; Page & Baird, 2016). This set of processes is collectively referred to as net ecosystem productivity (NEP; Page et al., 2011a). In addition, a proportion of carbon is naturally lost via

leaching through the fluvial export of dissolved (DOC) and particulate (POC) organic carbon (Page et al., 2011a; Page & Baird, 2016).

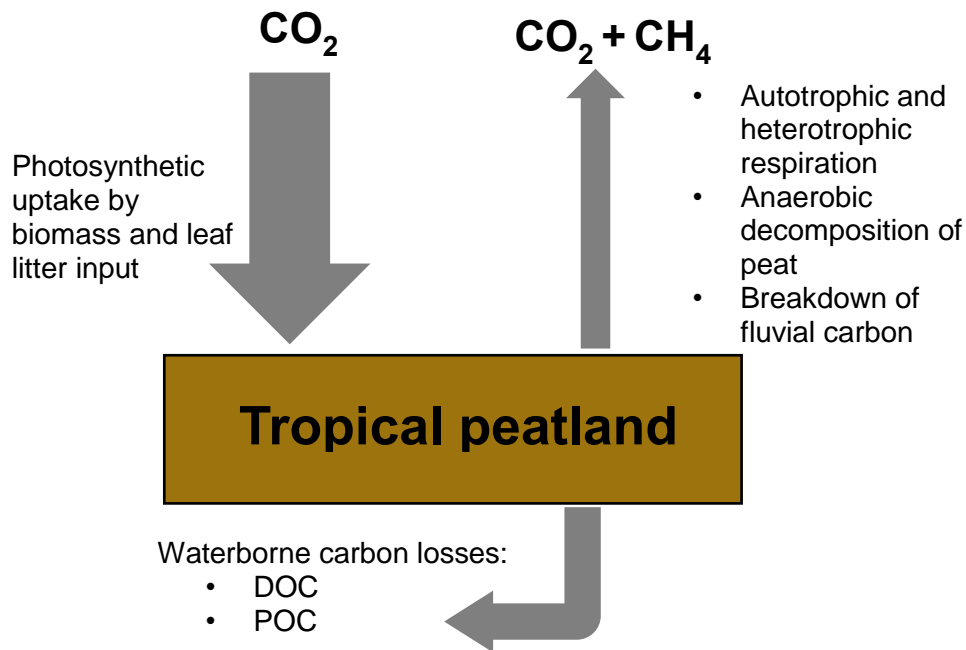


Figure 1.6. Simplified schematic diagram to highlight the main carbon inputs and output pathways on an intact tropical PSF

CO₂ is actively fixed into the PSF biomass through the process of photosynthesis (GPP), with PSF biomass estimates of 179.7 ± 38.2 t C ha⁻¹ (Murdiyarso et al., 2010). Some of this GPP is returned back into the atmosphere as CO₂ (Page et al., 2011a). In addition, a proportion of GPP is sequestered into the below-ground biomass which contributes to the accumulation of peat (1.3 and 1.5 mm yr⁻¹) equivalent to 0.75 ± 0.25 Mg C ha⁻¹ (Page et al., 2004; Murdiyarso et al., 2010). During the dry season, when the watertable is at its lowest, the peatland will experience oxic conditions within the top surface layer (upper ~ 40 cm). Under these conditions (Figure 1.7a), aerobic decomposition prevails and any organic matter deposited on the peat surface, will be actively decomposed by microbes (heterotrophic respiration) and liberated as CO₂, N₂O and CH₄ (Page et al., 2011a; Jauhainen et al., 2014).

For most of the year, the peatland watertable is close to or above the surface and operates under anoxic conditions (Figure 1.7b), associated with anaerobic processes (Page et al., 2011a). Under this scenario organic matter decomposition is suppressed and any accumulating organic matter inputs, will be incorporated into the peat (Hooijer et al., 2010; Page et al., 2011a; Jauhiainen et al., 2012). Organic matter decomposition, by aerobic processes, will still take place but at a much-reduced rate, with organic matter input exceeding the rate of organic matter breakdown. Under anoxic conditions decomposition is facilitated by methanogenic bacteria, liberating CH₄ from waterlogged areas within the peat profile (Page et al., 2011a). This CH₄ can, in turn, be reduced at the anoxic-oxic interface as it transitions from an anoxic layer through to an aerobic peat layer, converting it into CO₂ (Page et al., 2011a). Furthermore, CH₄ can be released into the atmosphere via vascular plant structures, providing a key carbon transport pathway (Jauhiainen et al., 2005). This is reinforced by Pangala et al. (2013) who established that the trunks of certain PSF tree species, within the Sebangau catchment in Indonesia, contributed 62-87% of the total ecosystem's methane flux.

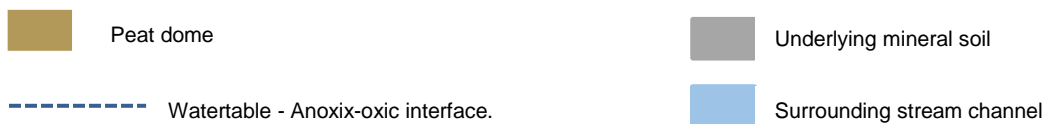
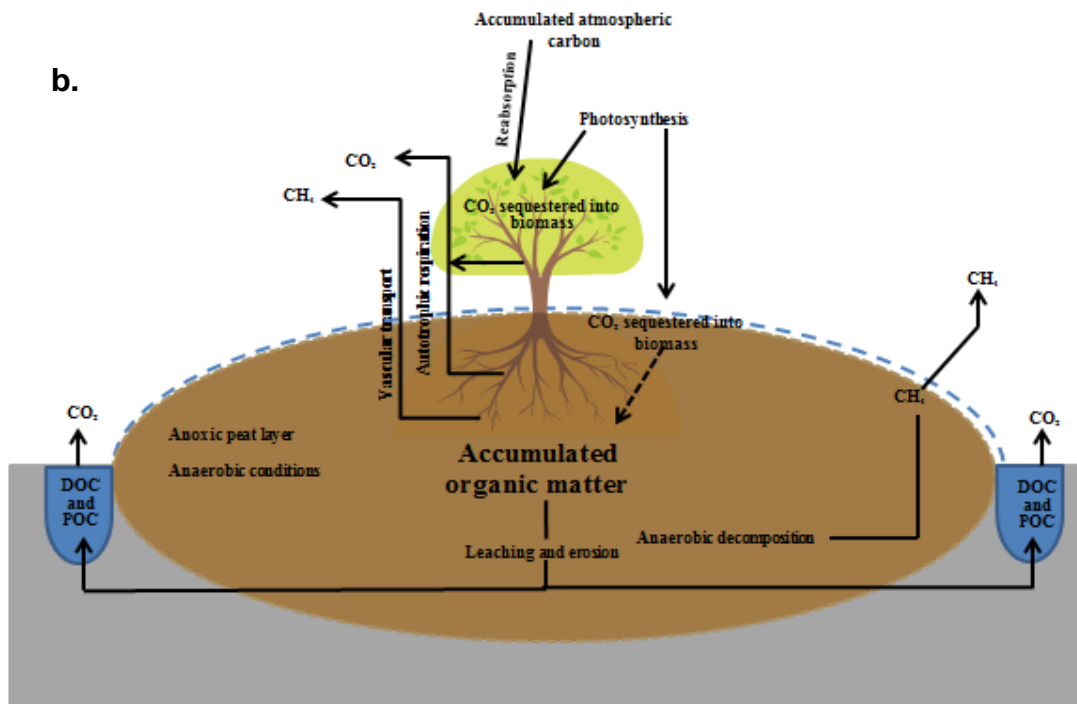
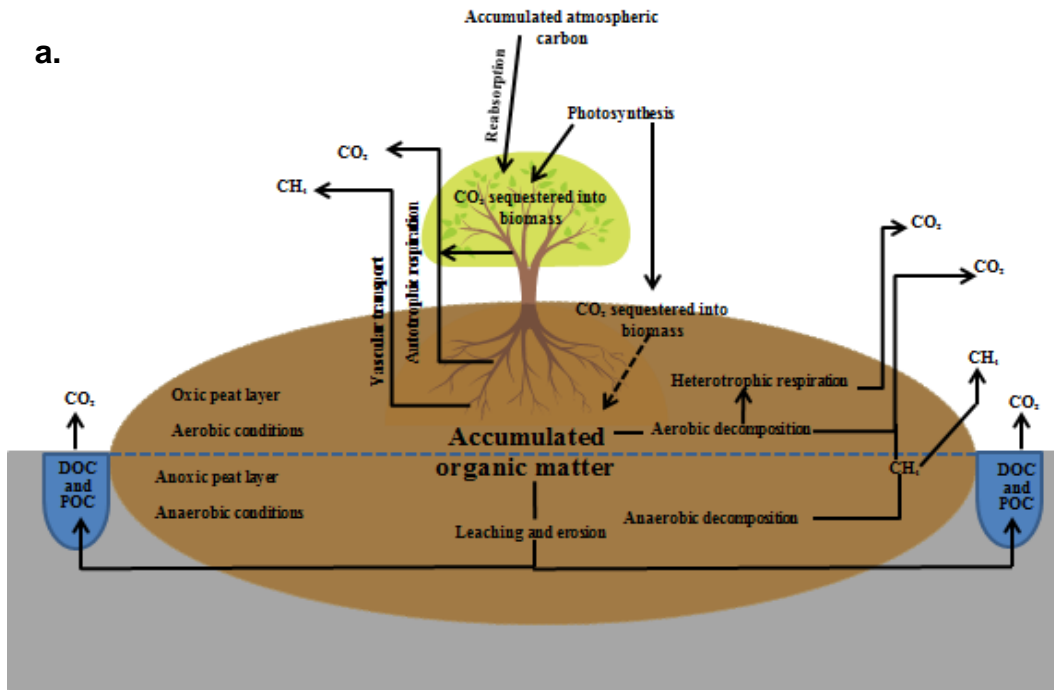


Figure 1.7 Schematic diagram outlining the basic processes involved in the carbon cycle of an intact peatland, under a low watertable, dry season (a) and high watertable, wet season (b).

The difference between the amount of carbon sequestered, via GPP, and that lost, is often reabsorbed by the surrounding PSF into the tree's biomass and accumulating organic matter (Jauhiainen et al., 2012). Consequently, under natural conditions these ecosystems function as effective net carbon stores (Page et al., 2011b; Turetsky et al., 2015). Their carbon storage capacity is dictated by their ability to maintain a positive net imbalance between a high GPP and low rates of organic matter decomposition (Hooijer et al., 2010; Page et al., 2011a; Jauhiainen et al., 2012). This, in turn, is dependent upon the prevalence and maintenance of anoxic and acidic conditions, which inhibit decomposition (Dommain et al., 2010). In addition, GPP is strongly controlled by the structure of the forest vegetation itself (density, height and stem diameter), which changes throughout the peat dome in response to variable abiotic and biotic factors (Page et al., 1999; Page et al., 2011a). Furthermore, heterotrophic CO₂ emissions are dependent upon microbial dynamics, controlled by temperature (Jauhiainen et al., 2014), watertable fluctuations (Mishra et al., 2014) and the availability of labile organic matter. The interdependence between the vegetation and peat dome structure makes these ecosystems extremely fragile to change, with small system perturbations largely impacting on their overall functionality.

The remaining flux component consists of the fluvial export of carbon, which is naturally leached from the surrounding organic matter. This component is sensitive to land-use related disturbances (Moore et al., 2013; Butman et al., 2015; Rixen et al., 2016) and has been extensively studied within temperate and boreal peatland ecosystems (Freeman et al., 2001a; Hullatt et al., 2014 a,b; Leach et al., 2016). As such, losses from tropical peatlands are poorly understood (Moore et al., 2013; Evans et al., 2014), and have yet to be quantified from tropical peatland OPPs.

1.4. Tropical peatland disturbance

PSF conversion into other land uses is common throughout Southeast Asia (Figure 1.8) and contributes significantly to global anthropogenic GHG emissions (Couwenberg et al., 2010; Hirano et al., 2012). Oil palm has played a central role in observed land-use changes within Indonesia and Malaysia over the last few decades, driven by global consumer needs for vegetable oil based products (Wicke et al., 2008; 2011; SarVision, 2011; Schrier-Uijl et al., 2013; Gandaseca et al., 2014; Cole et al., 2015). In 2007, it was estimated that industrial plantations covered approximately 2.3 million ha (Mha) of peatland distributed across Peninsular Malaysia, Borneo and Sumatra (Miettinen et al., 2012a). However, more recent figures show that this has now increased to 4.3 Mha (Miettinen et al., 2016), with 50 % of PSFs in this region now covered by 'managed land' (22.4 % smallholders; 27.4 % industrial; Miettinen et al., 2016; 2017). Of this, industrial OPPs cover 3.1 Mha on peat, nearly doubling their extent in less than 10 years (Miettinen et al., 2016; 2017).

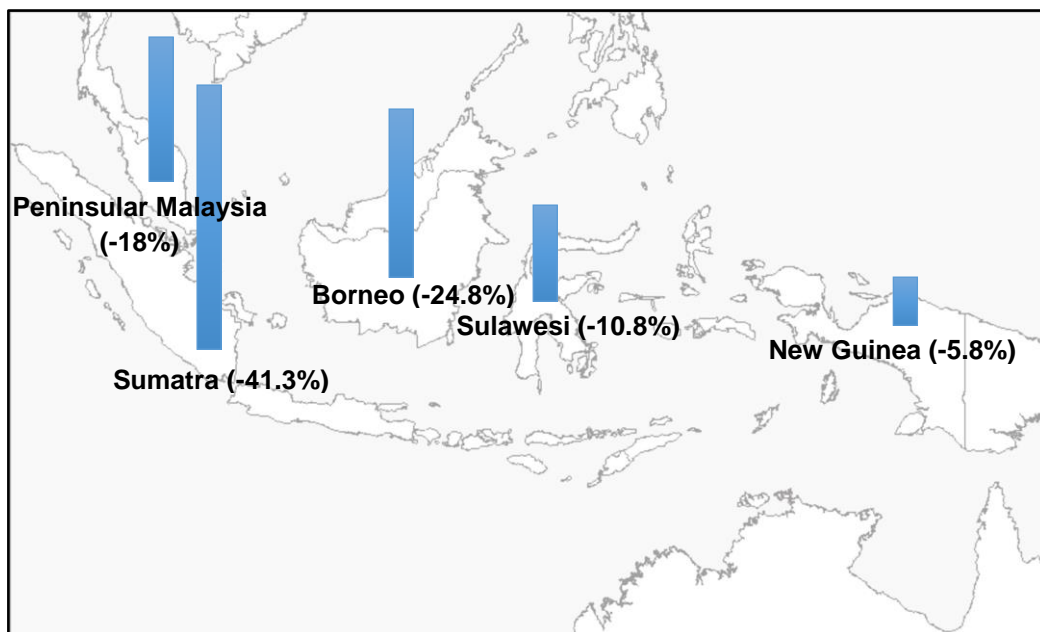


Figure 1.8. Land cover change on peatland from 2000-2010, figures taken from Miettinen et al., (2011)

1.4.1 Oil palm plantation expansion

OPP expansion on peatland has been quantified using various methods resulting in a range of estimates (Table 1.4; Omar et al., 2010; Miettinen & Liew, 2010b; Koh et al., 2011; Carlson et al., 2012; Miettinen et al., 2012a; 2016). For Indonesia, projections of OPP on peat soils by 2020, range from 16% (Carlson et al., 2012) to 28% (Miettinen et al., 2012b), whereas for Malaysia estimates range from 14%, following a business as usual (BAU) approach (Harris et al., 2013), to 42% (Miettinen et al., 2012b). Based on the values presented in Table 1.4, the average share of the area of OPP on peat by 2020 is estimated at 21% and 23%, for Indonesia and Malaysia, respectively. These projected increases in area are comparable to historical growth averages with Malaysian peatland OPPs increasing from 8% to 13% between 2003 and 2008 (Miettinen et al., 2012b). However, large uncertainties exist relating to these trends with changing policies amongst countries and provinces and opposition to palm oil regulation likely to impact the rate of future expansion (Valin et al., 2014). Nevertheless, Miettinen et al. (2012b) state that if there are no constraints to expansion approximately 93% of Malaysian peat could be under OPPs by the year 2030.

Table 1.4. Overview of studies that project future oil palm expansion (adapted from Valin et al., 2014)

Study	Projection methods/model assumptions	% of oil palm plantations on peat in 2020	
		Indonesia	Malaysia
Miettinen et al. (2012b)	Extrapolated trends based on 2007 to 2010 period, assuming a linear projection.	28%	42% ¹
Carlson et al. (2012)	Assumed that areas currently under allocated oil palm lease would be developed in the future.	16%	No data
Harris et al. (2013)	Identified areas most suitable for oil palm expansion (suitability criteria) (Valin et al., 2014) along with two approaches: i) historical average; assuming a constant rate of expansion on peat using a 20year average, following a business as usual approach (BAU) ii) policy intervention e.g. peat moratorium (Valin et al., 2014)	22% (BAU approach)	14% ² (BAU approach)
		19% (Peat moratorium)	13% (Peat moratorium)

¹ Miettinen provides a breakdown of oil palm expansion on peat by region for Malaysia: Peninsular Malaysia (9%), Sabah (2%), Sarawak (82%)

² After spreadsheet examination by Valin et al., (2014) on the data produced by Harris et al., (2013) a cell error was found where 7% was used instead of 14%, thus, the corrected value has been used.

OPP expansion on peat is highly prevalent within the Malaysian province of Sarawak (Table 1.5; MPOB, 2012; Kho & Jepsen, 2015; Page & Hooijer, 2016). This is attributed to the hilly topography of the area, limiting land availability and forcing peatland conversion in the flat coastal lowlands. From the year 2000-2010 it was estimated that 0.42 Mha of Sarawak peatlands were developed for palm oil production. By early 2016, nearly half (46%) of the total peatland area in Sarawak was under industrial plantations (Wetlands International., 2016), with 96% of this area used for the cultivation of oil palm. By 2020 it is expected that between 1.2 Mha to 2 Mha will be opened for OPP

establishment, resulting in 84% of Sarawak’s peatland under oil palm (Miettinen et al., 2012b). As a result, Sarawak has some of the highest OPP development rates on peat, with annual deforestation rates of around 7.8% (SarVision, 2011), 12 times greater than those experienced across other parts of Asia (Cole et al., 2015).

Table 1.5. Area of oil palm on all soil types and peat soil in Malaysia

Year	Peninsular Malaysia (ha)	Sabah (ha)	Sarawak (ha)
Area of oil palm on all soil types (figures taken from MPBO, 2008, cited in Wetlands International, 2010)			
2000	2,045,500	1,000,777	330,387
2001	2,096,856	1,027,328	374,828
2002	2,187,856	1,068,973	414,260
2003	2,202,166	1,135,100	464,774
2004	2,298,608	1,165,412	508,309
2005	2,298,608	1,209,368	543,398
2006	2,334,247	1,239,497	591,471
2007	2,362,057	1,278,244	664,612
Areas of oil palm on peat soils (2003 figures taken from Tropical Peatland Research Institute, 2009, cited in Wetlands International; 2009 figures taken from Omar et al., 2010)			
2003	200,000	10,000	100,000
2009	207,458	21,406	437,174

1.4.2 Disturbance effects on the carbon balance

The development of peatland OPPs encompasses the major disturbances experienced by PSFs, including: i) deforestation, to remove the original PSF ii) fire, to clear the remaining debris and iii) drainage, to create the optimum soil moisture conditions for cultivation (Hooijer et al., 2010; Page et al., 2011b; Schrier-Uijl et al., 2013). Consequently, peatland OPPs significantly contribute to global GHG emissions through peat oxidation and combustion (Table 1.6),

with estimates ranging from 36.2 to 100 Mg CO_{2-eq} ha⁻¹ y⁻¹, over a typical 25-year OPP lifecycle (Germer & Sauerborn, 2008; Hooijer et al., 2012).

The relative contribution of peat derived carbon to overall OPP GHG emissions is presented in Tables 1.7 to 1.8, with values varying depending upon plantation age and drainage depth. Most of the studies presented (Tables 1.7 and 1.8) assume constant emissions over the course of plantation development (Reijnder & Huijbregt, 2008; Murdiyarso et al., 2010). However, Hooijer et al. (2012; 2014) distinguishes two distinct phases of carbon loss and subsidence following drainage. Carbon losses are initially very high for 5 years following initial conversion when there is high availability of labile carbon residues, after which rates significantly decrease and become more constant (Hooijer et al., 2014). Consequently, the long-term average CO₂ emissions projected by Hooijer et al. (2012) tend to be much larger than those from other sources, with values of 178 to 86 Mg CO_{2-eq} ha⁻¹ yr⁻¹, for 5 to 50 years following conversion, respectively.

Table 1.6. Overview of GHG emissions from oil palm plantations on tropical peatlands

Study	Description	Key findings
Germer & Sauerborn (2008)	Using literature data to quantify GHG emissions from oil palm plantations on forests on both peat and mineral soils along with grassland. Considered both zero burning and burning scenarios for land clearance.	GHG emissions of 32.6 ± 16 Mg CO _{2-eq} ha ⁻¹ yr ⁻¹ or 816 ± 393 MgCO _{2-eq} ha ⁻¹ over a 25 year production cycle
Reijnder & Huijbregts (2008)	Gaseous carbon emissions from oil palm production chain. Focused on the conversion of tropical forests to oil palm and used values published from within the literature.	GHG emissions of 36.7-55 Mg CO _{2-eq} ha ⁻¹ yr ⁻¹ over a 25 year cycle
Murdiyarso et al. (2010)	Accounted for all ecosystem fluxes (gaseous and fluvial) from an oil palm plantation over a 25-year cycle, using published literature values	Land use conversion from PSF to oil palm plantations equates to: Carbon losses of around 405 Mg C ha ⁻¹ over a 25 year cycle (16.2 ± 2.8 Mg C ha ⁻¹ yr ⁻¹). These carbon losses are attributed to: ceasing peat accumulation in forest (18.8 Mg C ha ⁻¹), burning peat from land clearance (100 Mg C ha ⁻¹), change in biomass carbon stocks (155.5 Mg C ha ⁻¹), peat carbon loss in oil palm plantation (soil outputs-inputs) (131 Mg C ha ⁻¹) GHG emissions of 59.4 ± 10.2 Mg CO _{2-eq} ha ⁻¹ yr ⁻¹ over 25 year cycle, with 61.6% attributed to CO ₂ emissions from peat decomposition and 25% from the clearance of land by fire.
Hooijer et al. (2012)	Subsidence monitoring on Acacia plantations (Riau) and mature oil palm plantations established on peat (Jambi)	GHG emissions of 100 Mg CO _{2-eq} ha ⁻¹ yr ⁻¹ over 25 year cycle. Separates oxidation and compaction components of subsidence.

Table 1.7. Summary of CO₂ emissions from oil palm plantations on peatlands, using chamber based methods

Study	Age	Location	Total respiration Mg CO ₂ ha ⁻¹ y ⁻¹	Peat respiration Mg CO ₂ ha ⁻¹ y ⁻¹	Drainage depth (m)	Comments
Melling et al. (2007)	5	Sarawak, Malaysia	56.5	40.9	unknown	Measurements taken during the day and over short time scale
						Did not separate heterotrophic and autotrophic respiration
Comeau et al. (2013)	7	Sumatra, Indonesia	28.4		0.5-1	Slightly different microtopographies were experienced across the three sites, which might have impacted on the soil fluxes recorded.
Jauhiainen et al. (2012)	8-10	Sumatra, Indonesia	102.5± 27.8	80-94±17.2	0.8	Acacia plantation*
	1		40.9 ± 18.0	24.3 ± 9.7		Limited spatial extent and spatial biases
Agus et al. (2010)	5	Nanggroe Aceh Darussala Province, Indonesia	27.3 ± 15.6	18.2 ± 11.1	0.7-1.5	Limited sampling duration October-November 7-10am
	10		32.9 ± 20.7	19.3 ± 16.6		
	1		54**			Limited information about the plantation sites. Method section is limited and does not outline how autotrophic and heterotrophic respiration were separated but yet states that heterotrophic respiration was similar at all locations.
Melling et al. (2014)	5	Mukah, Sarawak, Malaysia	60		0.7-1.75	
	7		68			
	4	Riau and Jambi		66±25		Values are likely to be overestimated as data was only collected during the day
Husnain et al. (2014)	6	Provinces, Sumatra, Indonesia		38±2	0.5-0.7	
	15			34±16		

* study not conducted on an oil palm plantation but on an *Acacia* plantation. Emissions are likely to represent an overestimate as acacia plantations are managed on shorter rotations (5-7 years vs 25 years) promoting more regular soil disturbance.

**values originally published in units of Mg C ha yr⁻¹ were converted to Mg CO₂ ha⁻¹ yr⁻¹ using a conversion factor of 3.67 as recommended by Page et al. (2011a)

Table 1.8. Summary of CO₂ emissions from oil palm plantations on peatlands, using subsidence monitoring

Study	Drainage depths (m) and associated CO ₂ emissions Mg CO ₂ -eq ha ⁻¹ yr ⁻¹						Comments
	50	60	70	80	90	100	
Couwenberg et al. (2010)	45	54	63	72	81	90	For every 10cm of drainage 0.9 Mg CO ₂ -eq ha ⁻¹ yr ⁻¹ is released assuming 40% contribution of decomposition to subsidence and bulk carbon density of 0.068 g C cm ⁻³
	67	80	93	106	120	133	For every 10cm of drainage 1.330 Mg CO ₂ -eq ha ⁻¹ yr ⁻¹ is released assuming 60% contribution of decomposition to subsidence and bulk carbon density of 0.068 g C cm ⁻³
Hooijer et al. (2012)			86 to 100 [*]				Empirical CO ₂ emissions as a result of drainage at a depth of 70cm, assuming 92% contribution of decomposition to subsidence. Emissions are given over a period of 25-50 year plantation cycle.

*while Acacia (young) and oil palm (mature) were both measured, the subsidence rates over the first 5years, for the Acacia, were applied to the oil palm as both displayed similar characteristics

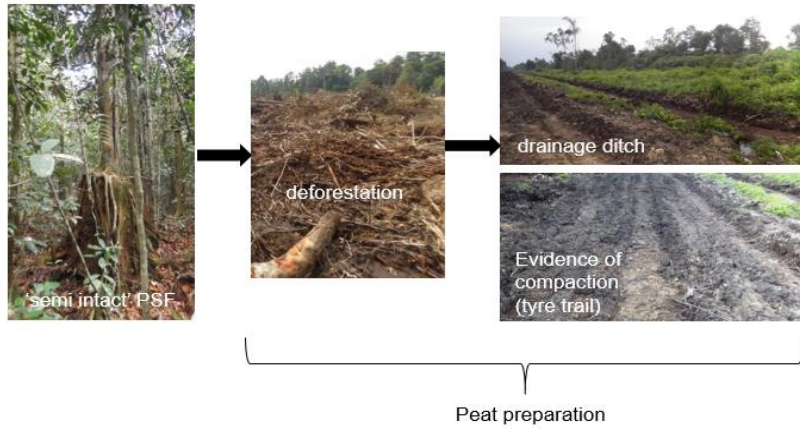
Photographs, along with descriptions to illustrate the main sequences involved in PSF to OPP conversion are presented in Figure 1.9. The first stage of PSF conversion involves land clearance and preparation. During deforestation, living biomass is destroyed causing GPP to decrease and the net ecosystem exchange (NEE) to increase (Schrier-Uijl et al., 2013). This is highlighted by Hirano et al. (2012) reporting average NEE values of 174 ± 203 and 499 ± 72 g C m⁻² yr⁻¹, for a relatively intact and drained/burnt PSF, respectively. The carbon lost from the destruction of the forest exceeds that contained within the biomass of the OPP (Murdiyarso et al., 2010; Tonks et al., 2017). Kho & Jepsen (2015) report an average standing biomass stock of 28 Mg C ha⁻¹ and 58 ± 10.7 Mg C ha⁻¹ for a peatland OPP and PSF, respectively. Consequently, the carbon lost from forest conversion exceeds the potential fixation of carbon by the established OPP (Schrier-Uijl et al., 2013), with a considerable proportion transferred to the atmosphere. In addition, fires are often used to clear the biomass debris, resulting in both biomass and peat combustion and additional carbon losses of around 100 ± 50 Mg C ha⁻¹ (Murdiyarso et al., 2010).

The next stage of development involves drainage of the waterlogged soils to make the land available for agricultural use (Page et al., 2011a; Schrier-Uijl et al., 2013; Figure 1.9). This is achieved through the installation of ditches, causing the peat to dry out and increase in bulk density. Heavy machinery (i.e. excavators) are then able to access the area for land preparation (i.e. stacking of the PSF debris and creation of plantation drainage channels). In some plantations machinery is used to compact the peat surface (resulting in increased peat bulk density) in order to improve palm rooting stability and anchorage.

Stage one:

Involves land clearance and drainage to make the peat agriculturally suitable for cultivation.

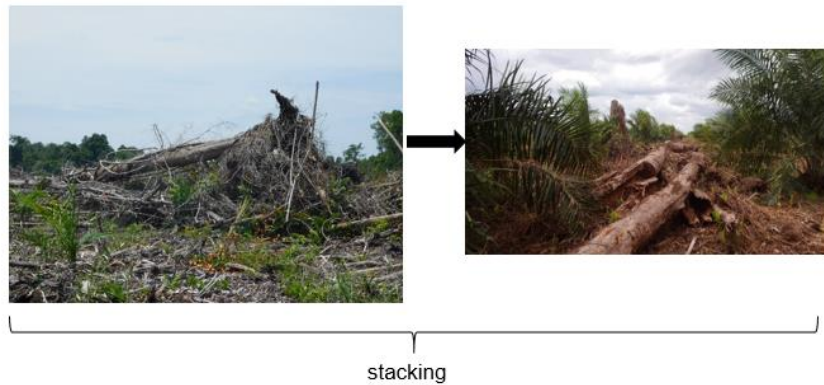
Drainage is carried out through the installation of drainage ditches. This is subsequently compacted by large industrial machines, which drive up and down the peat surface, evident by tyre makings.



Stage two:

Woody debris, remnant from the PSF, is stacked to form divisions between the plantation inter-rows.

This decomposes overtime but is still often visible within the older plantation stands.



Stage three:

The drainage channel infrastructure is developed forming a dense network of interconnecting drains throughout the estate

Palm oil seedlings are planted which often required further peat compaction around stem base.



Stage four:

The crop is harvested after 5-years (the time taken to reach maturity)



Figure 1.9 Photos to illustrate the sequence of peatland preparation for oil palm plantation development

Networks of high-density drainage channels are installed throughout plantations to ensure the watertable is maintained at an optimum depth (i.e. -60 to -85 cm below the peat surface; Page et al., 2011a). The size of the drainage channels varies depending upon their purpose but collectively they make up a network of interconnecting field, collection and main drain systems (Mutret, 1999; MPOB, 2010; MPOB, 2011). The response of a tropical peatland ecosystem to the on-going process of drainage is outlined in Figure 1.10. Drainage of the peat dome results in immediate peat subsidence. This is attributed to watertable drawdown and the exposure of previously saturated peat layers to aerobic conditions, promoting rapid microbial biodegradation (Page et al., 2010; Mishra et al., 2014). Subsidence is also a physical process with peat drainage often causing the supporting pore water pressure, within the peat, to collapse (Hooijer et al., 2012). This will physically modify the peat by decreasing the structural integrity of the column (Couwenberg & Hooijer, 2013), whilst reducing the volume and buoyancy, increasing bulk density (Hooijer et al., 2012, Couwenberg & Hooijer, 2013). Rapid subsidence occurs during the first 5 years following drainage, bringing the watertable back up to the peat surface (Page et al., 2011a; Hooijer et al., 2012). To counter this, drainage efforts are further intensified to re-stabilize the watertable at a lower level (Page et al., 2011a). Consequently, while natural forest conversion represents a one-off carbon emission from the loss of biomass, at the time of conversion, the emissions resulting from the long-term drainage requirements for a peatland OPP are continuous (Schrier-Uijl et al., 2013).

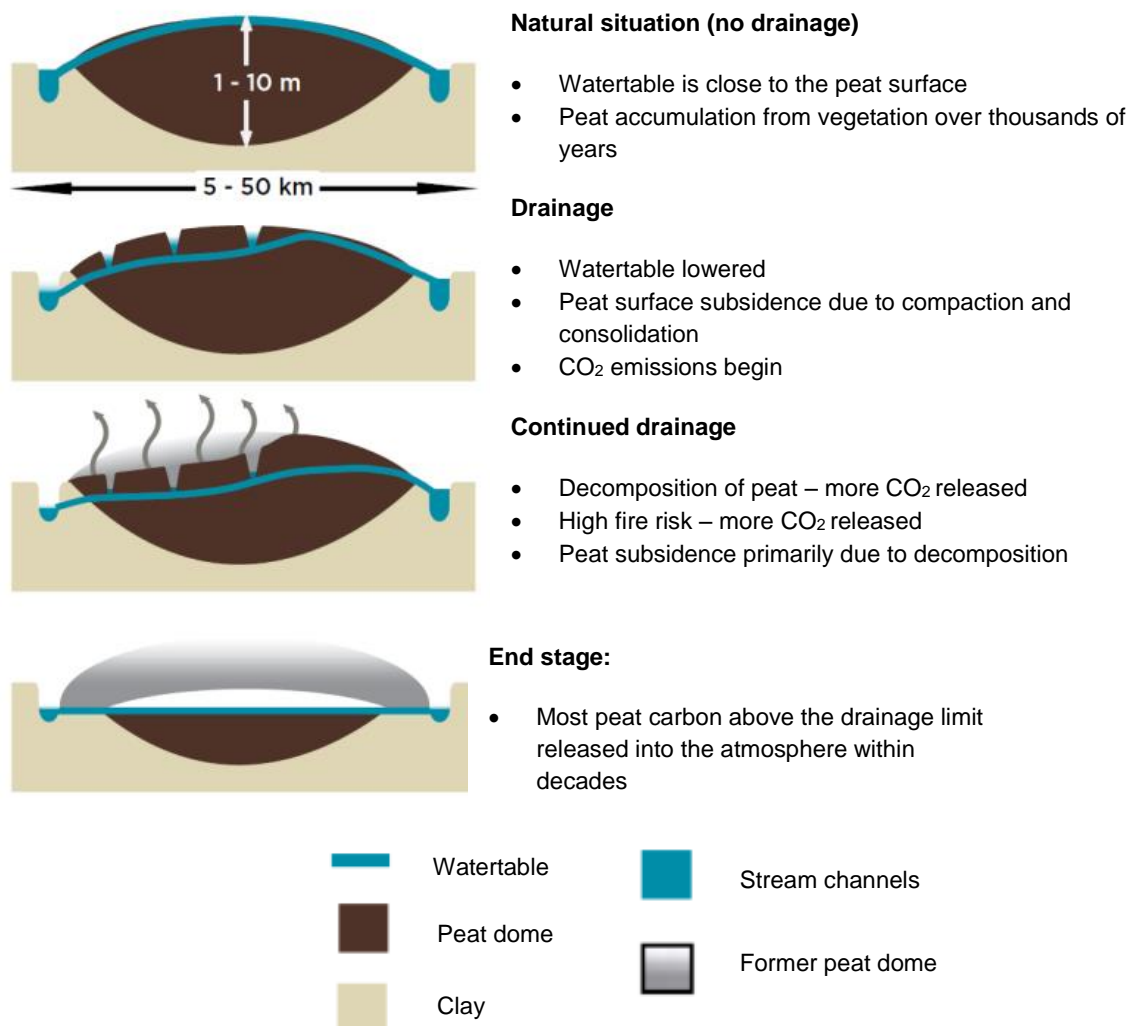


Figure 1.10 Schematic diagram outlining the effect of drainage on a peat dome (Hooijer et al., 2010; Page et al., 2011a)

Frequent and intense fires are often used to initially clear the land, which may spread from the surrounding landscape into the OPP if the watertables are very low (Langner et al., 2007; Page et al., 2009; Konecny et al., 2015; Turetsky et al., 2015; Page & Hooijer, 2016). In addition, large increases in peat surface temperature are often experienced during the initial stages of plantation development, due to a more open canopy, exposing the peat surface to direct solar radiation (Jauhiainen et al., 2012; Schrier-Uijl et al.,

2013). This temperature increase will enhance peat oxidation further and the breakdown of fresh labile carbon compounds (Page et al., 2011a).

Following these initial stages (> 5 years) GHG emissions will start to reduce and eventually stabilize (Hooijer et al., 2012). The bioavailability of the remaining carbon pool will have declined, leaving behind refractory carbon compounds, more resilient to microbial breakdown (Page et al., 2011a). Consequently, organic matter breakdown is lower leading to smaller carbon emissions and a reduction in carbon surface water concentrations (Moore et al., 2013).

1.4.3 Summary of emissions factors from drained organic soils under different land-uses

Recent insights into PSF to OPP conversion emissions are reflected in the IPCC (2014) report guidelines and the Kalimantan Forests and Climate Partnership (KFCP) study (Hooijer et al., 2014). Emission factors from several peatland land-cover types are now available (Table 1.9). Emissions from drained tropical PSFs are an order of magnitude greater than those from drained boreal peatlands ($0.25\text{-}0.93\text{ Mg C ha}^{-1}\text{ yr}^{-1}$ vs $5.3\text{-}7.9\text{ Mg C ha}^{-1}\text{ yr}^{-1}$) with carbon losses from drained temperate peatlands approximately half those in tropical peatland regions ($2.6\text{ Mg C ha}^{-1}\text{ yr}^{-1}$). The impact of converting degraded tropical PSFs into plantations doubles, and in some instances, triples the carbon emissions from $4.5\text{ - }7.9\text{ Mg C ha}^{-1}\text{ yr}^{-1}$ to $15\text{ Mg C ha}^{-1}\text{ yr}^{-1}$ (Hooijer et al., 2014). The KFCP study also reports higher emissions peaks of $80\text{ Mg C ha}^{-1}\text{ yr}^{-1}$ from locations 50 m from plantation canals, following the initial drainage (Hooijer et al., 2014). This is equivalent to $294\text{ Mg CO}_2\text{ ha}^{-1}\text{ yr}^{-1}$ and is comparable to the emissions values reported in Hooijer et al. (2012; $178\text{ Mg CO}_2\text{ ha}^{-1}\text{ yr}^{-1}$). However, this figure is not representative of the wider plantation landscape, where drainage impact away from main canals will be lower (Hooijer et al., 2014) thus, this value is replaced with a more conservative estimate of $178\text{ Mg CO}_2\text{ ha}^{-1}\text{ yr}^{-1}$ or $49\text{ Mg C ha}^{-1}\text{ yr}^{-1}$.

The general emissions factor for industrial plantations (15 Mg C ha⁻¹ yr⁻¹; 55 Mg CO₂ ha⁻¹ yr⁻¹) translates into an average yearly subsidence rate of 3.5 cm yr⁻¹ (Hooijer et al., 2015). The long-term consequences of such intense drainage efforts are reinforced by Hooijer et al. (2015) for an area of western Sarawak (400,000 ha). Within 50 years, 52% of the study area will be at risk of frequent flooding as a result of peat subsidence, with 68% of the area unable to support agriculture. Within 100 years, subsidence will have caused peat elevation to drop so significantly that 81% of the area will be at high flood risk with 93% of the area predicted to be agriculturally redundant (Hooijer et al., 2015).

Table 1.9. Emission factors from draining organic soils, as a consequence of biological oxidation, from a variety of land uses and ecosystem types

Ecosystem	Land use	Condition/ degree of human modification	Emissions factor (Mg C ha ⁻¹ yr ⁻¹) > 5 years following drainage	CO ₂ emissions (Mg CO ₂ -eq ha ⁻¹ yr ⁻¹) *	Emissions factor (Mg C ha ⁻¹ yr ⁻¹) first 5 years following drainage	CO ₂ emissions (Mg CO ₂ -eq ha ⁻¹ yr ⁻¹)
Boreal	Forest land	Drained	0.25-0.93 (IPCC)	0.92-3.41		
	Forest land, including shrub land and land that may not be classified as forest	Drained	0.37 (IPCC)	1.36		
Temperate	Grassland	Drained	5.7 (IPCC) 2.6 (IPCC)	20.92 9.54		
	Forest land	Drained				
	Grassland, nutrient poor	Drained	5.3 (IPCC)	19.45		
	Grassland nutrient rich	Deeply drained	6.1 (IPCC)	22.39		
Tropical	Primary peatland forest	No human modification (i.e. drainage)	0 (KFCP)	0	0 (KFCP)	0
		Slightly drained, selectively logged, no large canals within 1500m and no burning	3.95 (KFCP)	14.50	3.95 (KFCP)	14.50
		Moderately drained, selectively logged and drained by large canals at 1000-3000m intervals. Not burnt	5.3 (IPCC) 7.9 (KFCP)	19.45 - 29.0	26 (KFCP)	95.42
		Fully degraded, burnt at least twice, drained by large canals 1000-3000m. Usually burnt at least twice	4.5 (KFCP) 5.3 (IPCC)	16.52- 19.45	26 (KFCP)	95.42
	Plantation	Drained, large canals less than 1km and/or field drains less than 400m apart	15 (IPCC)	55	49 (Hooijer et al., 2012)	178

* Values were converted to Mg CO₂ ha⁻¹ yr⁻¹ using a conversion factor of 3.67 as recommended by Page et al., (2011a)

1.5 Fluvial carbon overview

Riverine systems play an integral role in the transport of fluvial carbon (Pawson et al., 2012), with 1000 to 1800 teragrams (1 Tg = 10^{12} grams) discharged into the ocean annually, via these systems (Ludwig et al., 1996; Raymond et al., 2013). Of this, 60% is transported in an inorganic form (i.e. dissolved inorganic carbon, DIC) and 40% transported organically as DOC and POC (Degens et al., 1991; Meybeck et al., 1993). The relative proportions of these fractions carried by aquatic environments vary depending upon water type, location and land-use, with amounts of DIC from tropical peatland catchments considered negligible (Figure 1.11; Moore et al., 2012; 2013).

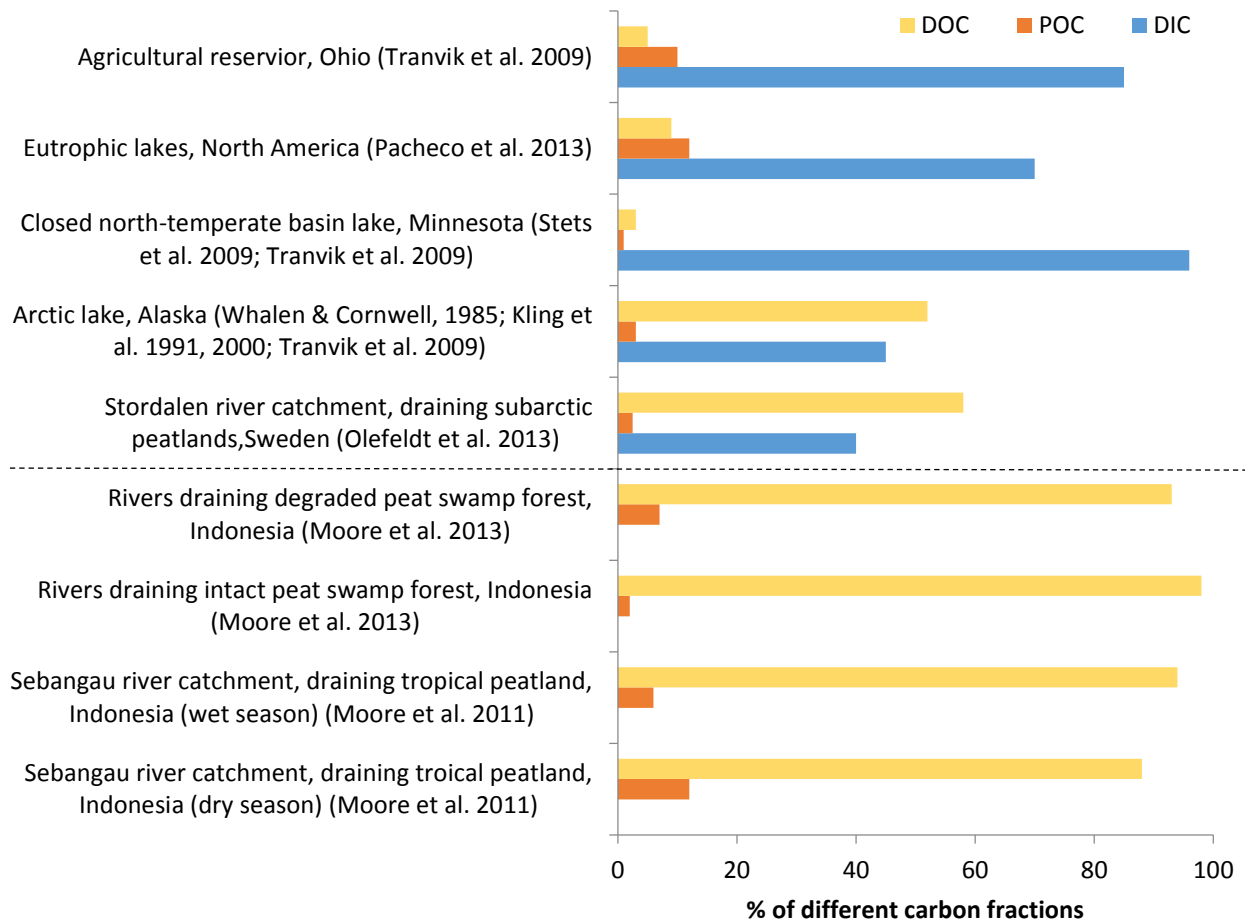


Figure 1.11. Percentage of the different carbon fractions found in contrasting fluvial systems, along with supporting references. Dashed line indicates division between temperate and tropical peat.

1.5.1 Peatland fluvial carbon components

Inorganic: weathering, and the subsequent dissolution of carbonate and silicate rocks, drives DIC formation (Field & Raupach, 2004). During this process carbonate and silicate ions dissolve into the water system and atmospheric CO₂ is drawn-down and sequestered, altering water alkalinity (Field & Raupach, 2004). The dominant inorganic dissolved ions in surface waters include HCO₃⁻, Ca²⁺ and SO₄²⁻ (Bianchi, 2007; Tammooh et al., 2013).

Organic: derived from the erosion and solubilisation of organic matter and can be grouped into three main categories depending upon origin (Degens 1982, cited in Hope et al., 1994):

1. *Allochthonous*, derived from terrestrial organic matter (Hope et al., 1994)
2. *Autochthonous*, derived from in-situ biological matter (Hope et al., 1994)
3. *Anthropogenic*, composed from matter derived from agricultural, domestic and industrial activities (Hope et al., 1994)

In terms of its composition, fluvial organic carbon can be divided into two main fractions, namely humic and non-humic. The non-humic component includes simple sugars, proteins, cellulose, waxes and oils, which tend to be more biologically labile than the humic component (Reddy & DeLaune, 2008). The humic fraction is a heterogeneous mixture of coloured compounds (Reddy & DeLaune, 2008) and can be subcategorised into humic acids, fluvic acids and humin (Figure 1.12). These contain both aromatic and aliphatic carbon-rich compounds as well as several oxygenated functional groups, such as carboxyl (COOH) and phenolic hydroxyls (OH) (Hope et al., 1994; Pango et al., 2014). The distinction between DOC and POC is generally made on the relative size of their particles with DOC able to pass through a 0.45-µm filter, and POC retained (Thurman, 1985; Moore et al., 2011).

Total organic: DOC and POC combine to form TOC (total organic carbon; $DOC+POC= TOC$) with DOC making up the greatest proportion (90%) within tropical peatland ecosystems (Reddy & DeLaune, 2008; Moore et al., 2011; Figure 1.12).

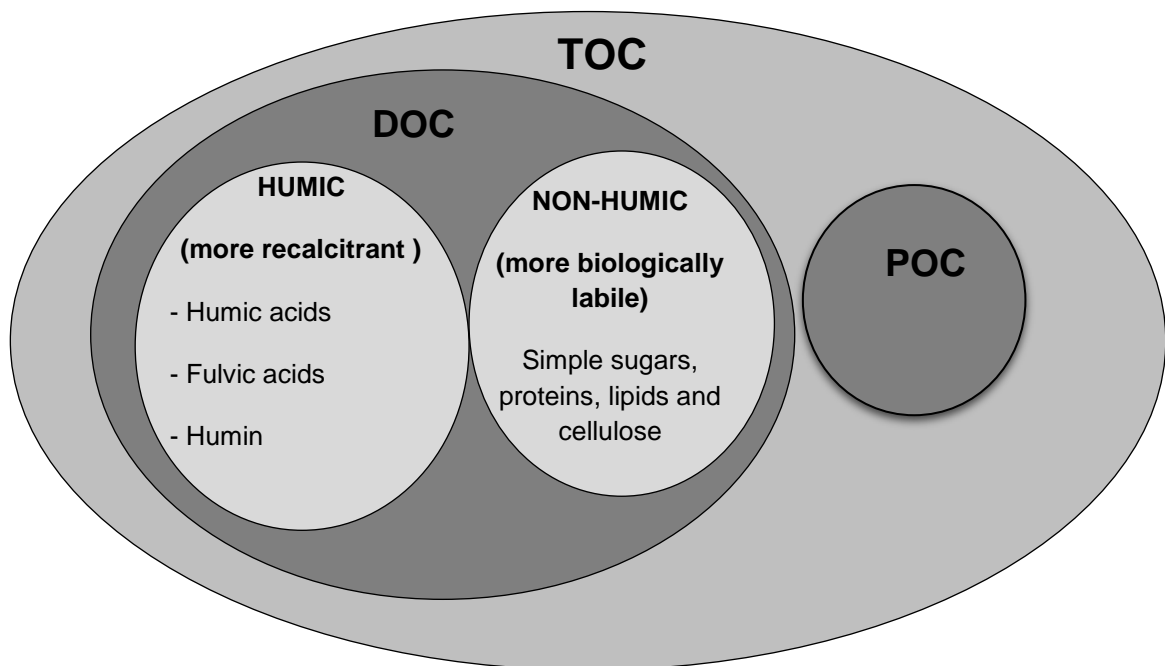


Figure 1.12. Diagram to illustrate the relationship between DOC, POC and TOC

1.5.2 Peatland fluvial carbon fluxes

In temperate peatland ecosystems, most of the DIC is in the form of CO_2^{aq} , which typically evades into the atmosphere (IPCC, 2014). Dinsmore et al. (2010) report DIC fluxes from within a Scottish peatland catchment of $0.12-0.16 \text{ t C ha yr}^{-1}$. In contrast, the DIC content of pore and surface waters, from tropical peatlands is limited, due to the low pH found within these ecosystems (Moore et al., 2011; 2013). Subsequently, DIC fluxes from tropical peatland ecosystems are negligible and thus, tend to be excluded from tropical peatland

carbon budgets (Moore et al., 2011; 2013). In terms of global DOC export, estimates are wide ranging (Table 1.10) with DOC fluxes from rivers ranging from 170 Tg C yr⁻¹ (Harrison et al., 2005) to 360 Tg C yr⁻¹ (Aitkenhead & McDowell, 2000).

Table 1.10 Estimated global DOC fluxes from riverine systems into the global ocean

Flux Tg C yr ⁻¹	Reference	
170	Harrison et al. (2005)	Used Global Nutrient Export from watershed model (NEWS-DOC)
170	Dai et al. (2012)	Used DOC concentrations from 118 river systems worldwide coupled with long-term discharge rates and considered the removal of DOC during estuarine transport
210	Ludwig et al. (1996)	Relationship between organic carbon fluxes coupled with the river basin characterizing features: climate, biome and geomorphology
250	Cauwet (2002)	Used DOC fluxes from large rivers and 1990 data from arctic rivers
360	Aitkenhead & McDowell (2000)	Used DOC fluxes from 164 watersheds grouped into biome and found a link between mean annual DOC fluxes and the mean soil C:N ratio within each biome classification

Tropical peatland ecosystems are inherently more vulnerable to DOC losses in comparison to temperate systems (Table 1.11) for several significant reasons. Firstly, tropical peatlands are exposed to warmer climatic conditions, usually 20°C greater than average annual European temperatures (Evans et al., 2014). This thermal exposure accelerates the decomposition of organic matter (Wang et al., 2014) and availability of carbon that can be incorporated into DOC. Secondly, tropical peat has a high saturated hydraulic conductance (K_{sat}), with ranges of 276 mm day⁻¹ (Kelly et al., 2014) to 475,200 mm day⁻¹ (Baird et al., 2017). This is in direct contrast to higher-latitude peatlands, such

as blanket bogs (1.68 mm day^{-1}) making the transmittance of water at both the surface and at depth greater within tropical peat (Wosten et al., 2008; Evans et al., 2014; Baird et al., 2017). This hydraulic sensitivity coupled with higher decomposition rates works to accelerate both DOC production and mobility within the peat profile (Evans et al., 2014; Baird et al., 2017; Table 1.11).

Table 1.11. Comparison of DOC fluxes from peatlands across different climatic zones

Climatic zone	Site	Approximate DOC flux t C m² yr⁻¹	Source
Temperate	Auchencorth Moss (Scotland) – semi intact- low intensity sheep grazing	27 25	Billett et al. (2004) Dinsmore et al. (2010)
Temperate	Moor House (UK)	66	Worrall et al. (2009)
Temperate	Mer Bleue (Canada)	40	Roulet et al. (2007)
Boreal	Gkencar (Ireland)	14	Koehler et al. (2011)
Boreal	Stordalen (Sweden)	3.2	Olefeldt et al. (2012)
Tropical	Sebangu catchment (Indonesia)	83	Moore et al. (2011)
Tropical	Intact PSF (Indonesia)	63	Moore et al. (2013)
Tropical	Intact PSF (Sarawak)	64	Muller et al. (2015)
Tropical	Degraded PSF (Indonesia)	97	Moore et al. (2013)
Tropical	Averaged from a range of studies in Sumatra, Kalimantan and Peninsular Malaysia –intact PSF	60	Evans et al. (2015)

DOC losses are further intensified in response to disturbance (Moore et al., 2013), which encompasses many of the factors which regulate and modify DOC production (Table 1.12). For example, the presence of ditch-drainage, a typical feature on cultivated peat, causes steep hydraulic gradients to develop between the peat and nearby drainage ditches (Baird et al., 2017). This modifies the hydraulic behaviour of the system leading to rapid water outflow and lateral carbon export from within the peat. Baird et al. (2017) report carbon losses of $2.86 \text{ kg C m}^{-2} \text{ yr}^{-1}$ and $0.09 \text{ kg C m}^{-2} \text{ yr}^{-1}$ for a modelled ditch drained system and hydraulically intact tropical peat dome, respectively.

A leading study by Moore et al. (2013) reported TOC fluxes from moderately and severely degraded PSF areas, to be 55% greater than those of an adjacent intact PSF. This was attributed to two major drivers: reduced biomass and increased drainage which worked to increase peatland DOC export via several feedback mechanisms (Verwer et al., 2008; Moore et al., 2013; Figure 1.13). Similarly, research by Gandois et al. (2013) found greater pore water DOC concentrations from a deforested but undrained PSF ($79.9 \pm 5.5 \text{ mg L}^{-1}$), within Brunei, compared to that of a neighboring pristine site ($62.2 \pm 2.2 \text{ mg L}^{-1}$). This translated into average DOC fluxes of $81 \pm 28 \text{ g C m}^{-2} \text{ yr}^{-1}$ and $104 \pm 39 \text{ g C m}^{-2} \text{ yr}^{-1}$ for the pristine and deforested sites, respectively, representing a 28% increase in DOC export (Gandois et al., 2013).

Table 1.12. Factors influencing DOC production and input

FACTOR	MECHANISM	EFFECT	EFFECT ON DOC	REFERENCE
Increased hydrological input	Increased run off and overland flow	Increased soil erosion and mineralization	Increased production and input of DOC	Evans et al. (2006)
	Change in dominant terrestrial flow pathway from lower horizons, which absorb DOC, to organic mineral horizons that produce DOC	More DOC mobilized	Increased production and input of DOC	McDowell & Likens, (1988)
Increased temperature	Increase in microbial activity	Increased decomposition	Increased production and input of DOC	Freeman et al. (2001a) Evans et al. (2006)
Increase in vegetation	Increase in biomass and NPP, increasing available carbon	Increase in organic matter input	Increased production and input of DOC	Larsen et al. (2011)
	Increased root exudation			Freeman et al. (2004)
Increased burning	Increased exposure of peat surface	Increased throughflow leading to a 'flushing' out of DOC and removal of the 'enzymatic latch mechanism'	Increased production and input of DOC	Clutterbuck & Yallop (2010)
		Increase in soil temperature, enhancing microbial activity and subsequent decomposition		
Low watertable/ increased drought	Increase in aerobic conditions	Switching on of 'enzymatic latch mechanism'	Increase in organic matter break down, increasing production but also consumption of DOC	Freeman et al. (2001b) Clark et al.(2005)
	Increase in sulphate production, via oxidation, leading to a reduction in pH and increase in ionic strength	Reduction in mobility and solubility of DOC	Decrease in production and input of DOC	Evans et al.(2006)
Increase in sulphur deposition	Increase in soil acidity and ionic strength	Reduction in mobility and solubility of DOC	Decreased production and input of DOC	Freeman et al.(2001b) Clark et al.(2005) Evans et al.(2006)

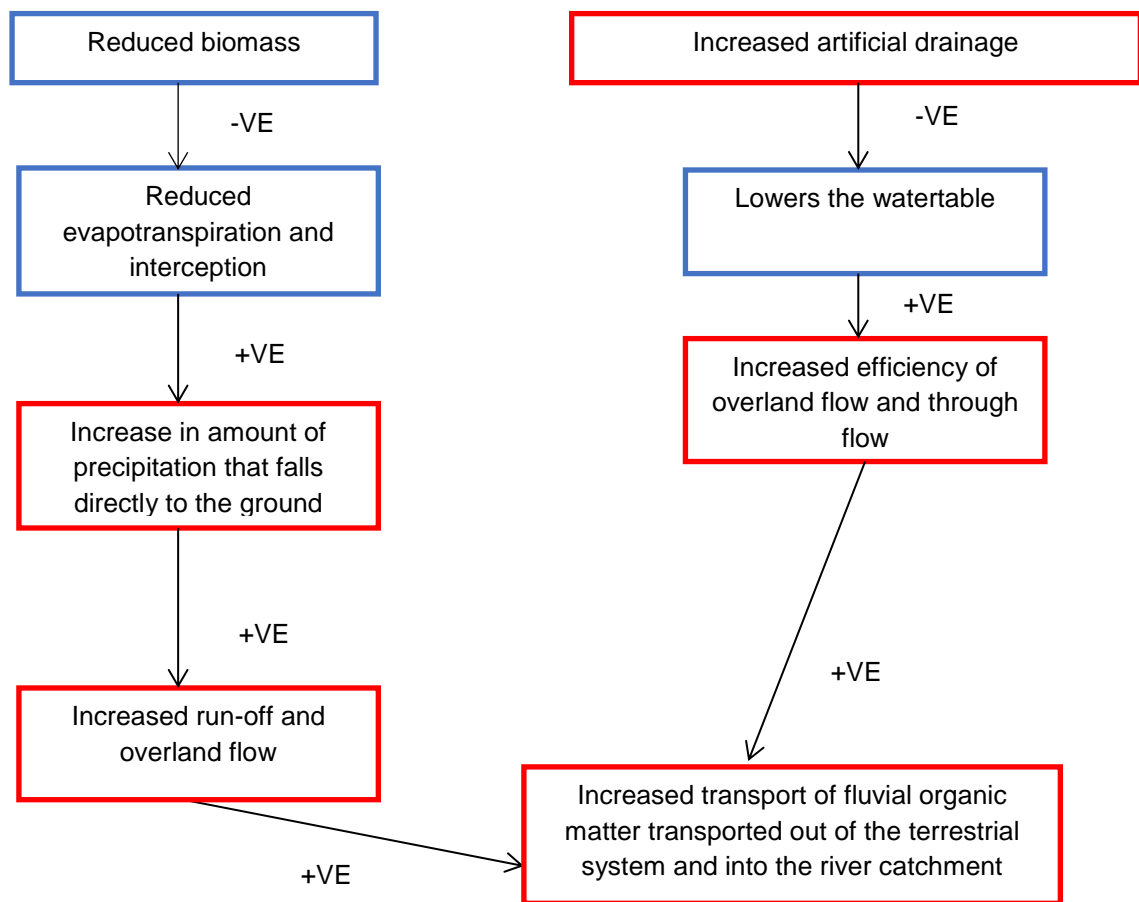


Figure 1.13. Feedback mechanisms responsible for accelerating fluvial organic carbon losses, within tropical peatland catchments, as a result of deforestation and drainage (Verwer et al., 2008; Moore et al., 2013). Where: red box= increase; blue box= decrease

Radiocarbon dating has revealed the consequences of peatland disturbance on the source age of DOC (DO^{14}C) and the implications of this for long-term carbon storage (Moore et al., 2013; Evans et al., 2014; Hulatt et al., 2014a; b). Peatland degradation on both temperate and tropical peatlands has been linked to the mobilization and release of aged carbon (Evans et al., 2007; Moore et al., 2013; Hulatt et al., 2014a; Campeau et al., 2017). Butman et al. (2015) report intensive agriculture (i.e. OPPs) to be the most influential driver governing the export of aged fluvial carbon.

However, DO^{14}C investigations have largely focused on high-latitude peat-dominated catchments (Evans et al., 2007; Raymond et al., 2007; Tipping et al., 2010; Campeau et al., 2017), with limited data from degraded tropical peatlands (Moore et al., 2011; 2013; Evans et al., 2014). A leading study by Moore et al. (2013) revealed DO^{14}C age signatures from waters draining disturbed PSFs that corresponded to ages of 92 to 2,260 years before present (BP; where present means 1950; Moore et al., 2013). Moore et al. (2013) also presented the first radiocarbon dates from two peatland OPPs with DO^{14}C levels corresponding to mean ages of around 4,000 years BP. Together these findings imply a loss in long-term stored carbon, with continued drainage and subsidence causing older stored carbon to be released from further down the peat column (Evans et al., 2014). Furthermore, there is evidence to suggest that degraded tropical peatlands are inherently more susceptible to aged carbon losses, in the form of DOC, compared to disturbed peatlands from higher-latitudes. This is reinforced by Evans et al. (2014) who found some high-latitude peatlands (UK blanket bogs) to have young DO^{14}C (<50 years), despite being drained.

1.5.3 Peatland fluvial carbon as a source of CO_2

The biodegradation of a molecule depends upon its inherent biochemical properties (Benner & Kaiser, 2011). DOC contains both labile and refractory material (Norman & Thomas, 2014). Labile DOC includes glucose, sucrose and acetate and is released from plant roots, soil and aquatic microorganisms (Clark et al., 2010). In contrast, the aromatic constituent is released during the decomposition of soil organic matter and includes lignin derived phenolic compounds. In general, microorganisms have an affinity towards the non-humic substances, such as glucose, carbohydrates and amino acids which are easier to consume (Clark et al., 2010). Consequently, the humic compounds are more recalcitrant, with some phenolic compounds reliant on specialized fungi for their breakdown (Mutabaruka et al., 2007), representing a limiting step in the terrestrial carbon cycle.

The impact of DOC export on GHG emissions ultimately depends upon its fate (Jauhiainen et al., 2016); whether it is returned to the atmosphere as CO₂ or deposited as stable marine sediments (Billett et al., 2004; 2013; IPCC, 2014). There are several potential pathways which fluvial carbon can take:

- i) Fluvial carbon is incorporated into sediment via the process of flocculation (Muller et al., 2016).
- ii) Fluvial carbon is degraded by microbial and photochemical processes causing the release of GHGs including CO₂, CH₄ and CO (carbon monoxide) into the atmosphere (Muller et al., 2016).
- iii) Fluvial carbon remains unprocessed and is transported into the ocean where it contributes to the marine recalcitrant carbon pool.

If the first and third pathway are true then this simply represents a translocation of carbon between stable carbon stores which will have little impact on GHG emissions (IPCC, 2014). However, growing evidence suggests that a large proportion of fluvial organic carbon follows the second pathway whereby it is metabolized and oxidized, returning it to the atmosphere as a GHG emission (Jonsson et al., 2007; Moore et al. 2011; Bastviken et al., 2015; Jauhiainen et al., 2016).

Muller et al. (2016) investigated the fate of peat-derived carbon from two estuaries in western Sarawak. The DOC acted as a substrate for microbes, facilitating aerobic respiration via organic matter breakdown, contributing to CO₂ production (Muller et al., 2016). In addition, carbon monoxide (CO) production exhibited a diurnal cycle with higher production during the day, suggesting DOC also contributes to carbon emissions via photodegradation (Muller et al., 2016). To further this, growing evidence now suggests that DOC from peatland ecosystems may not be as biologically reactive as previously thought and that DOC degradation is more heavily controlled by photochemical rather than biological processes (Cory et al., 2014; Evans et al., 2015; Pickard et al., 2017). This is supported by Moody et al. (2013) reporting very high DOC loss rates of 73% over a period of 10 days in light environments.

Wit et al. (2015) investigated CO₂ outgassing from six peat draining rivers in Indonesia and Malaysia. Their results suggest much higher DOC-CO₂ outgassing with an average of 53.4 % of exported DOC degraded and subsequently converted into CO₂. The inclusion of this DOC-outgassing flux results in a 20 % increase in the net ecosystem carbon loss of disturbed peatlands raising the total to 638 g C m⁻² yr⁻¹ (net source). Interpolating these findings to account for all peatlands in Southeast Asia results in a river outgassing of 66.9 Tg C yr⁻¹.

Taken together the above observations suggest that inland peatland waters could be a major component of local and global GHG emissions, fuelled, in part, by the breakdown of DOC into its gaseous metabolic products whilst in riverine transit. This is supported by Evans et al. (2015) who estimate that an additional 1 - 4 t CO_{2-eq} ha⁻¹ yr⁻¹ of GHG emissions is emitted from waterborne carbon from drained peatlands, equivalent to approximately 15 – 50% of total GHG emissions. The contribution of DOC and POC to the overall waterborne carbon flux varies depending upon the ecosystem, however, in terms of drained tropical peatlands DOC dominates contributing as much as 65% (2.77 t CO_{2-eq} ha⁻¹ yr⁻¹) of the estimated waterborne carbon flux from this ecosystem (4 - 4.5 t CO_{2-eq} ha⁻¹ yr⁻¹; Evans et al., 2015). This implies that it is important to consider the qualitative as well as the quantitative aspects of peat-derived fluvial organic carbon.

1.6 Thesis aims and objectives

Data sets on fluvial carbon losses from degraded peatlands are limited (Moore et al. 2013) but these losses represent an important indirect contributor to GHG emissions. At present no study has investigated fluvial organic carbon losses from peatland OPPs. However, the expansive areas of tropical peat within Sarawak and elsewhere in Southeast Asia, coupled with rapid OPP expansion, make this region likely to be a significant contributor to fluvial organic carbon export. As such, the principal aim of this investigation is to: **quantify fluvial organic carbon losses from oil palm plantations draining tropical peat in Sarawak, Malaysia.**

The specific research objectives are:

1. To quantify and characterize DOC and POC losses from peatland OPP drainage channels and compare losses between OPP and peat swamp forest land-cover classes
2. To derive annual area specific TOC fluxes from peatland OPPs in both the wet and dry seasons and upscale fluxes to the aerial extent of plantations in i) the study area, ii) Sarawak and iii) Peninsular Malaysia, Borneo and Sumatra
3. To establish the drivers responsible for variations in fluvial organic carbon losses between sites and seasons e.g. plantation age and watertable depth
4. To provide better guidance for scientists studying the tropical carbon cycle: specifically, on DOC analysis and sample storage when working at remote field sites

1.7 Thesis outline

This thesis contains six Chapters (Figure 1.14). Chapter One has introduced the research context by outlining key concepts and highlighting current knowledge gaps, which this thesis aims to address. The methodology is split into two Chapters (Two and Three). Chapter Two discusses the general methodology employed to help meet the research objectives, as well as detailed descriptions of the field sites. The methodology is further developed in Chapter Three which describes specific techniques for the i) preservation and ii) quantification of tropical DOC, split into two respective subsections. The principal aim of this investigation is addressed in Chapter Four which quantifies the fluvial organic carbon losses from two Malaysian oil palm plantations, both established on tropical peatland. The derived flux values consider methodological uncertainties, as discussed in Chapter Three. Chapter Five considers the qualitative aspects of tropical DOC using spectrophotometric and radiocarbon dating techniques, which provide an insight into the likely fate of the carbon. Finally, Chapter Six synthesises the data presented in the two

previous Chapters, summarises the main research findings and places the results into a global context. The implications are then discussed with reference to the scale of carbon fluxes presented within Chapter Four. Chapter Six concludes with a discussion of research limitations as well as recommendations for further work.

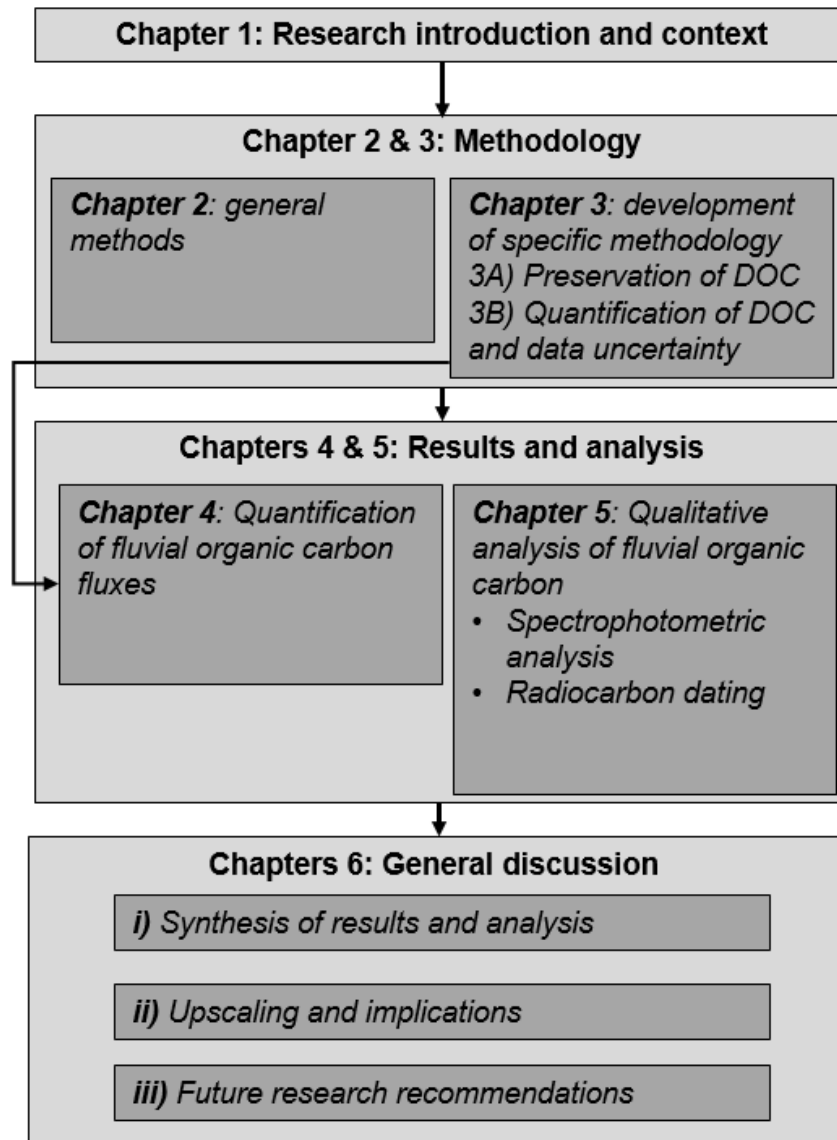


Figure 1.14 Thesis Chapters and subsections, alongside interlinks between the separate Chapters

Chapter Two: Methodology

2.1 Introduction

Chapter Two describes the climatic region where the fieldwork was conducted and the individual field sites that were continuously monitored for a year (54 weeks). The generic field and laboratory methodologies are also discussed, alongside justifications for each of the methods and the statistical analyses performed. Some of the methods discussed within this Chapter are subsequently referred to within the specific results Chapters in which they are employed.

Methods described within this Chapter include those for: determination of DOC and POC concentrations, sample preservation, in-situ measurement of environmental parameters (i.e. water table depth, discharge, water pH and electrical conductivity), and calculation of fluvial carbon flux.

2.2 Study sites

2.2.1 Location

All study sites were located in the coastal lowland of the Malaysian province of Sarawak, northern Borneo, situated in Southeast Asia (Figure 2.1). This region is characterized by an equatorial climate with high, even temperatures (mean 26°C) throughout the year and heavy rainfall (~ 3000 mm received annually), without a distinct dry season (Melling et al., 2005). The study sites were situated within two adjacent oil palm plantation (OPP) estates: Sebungan (SE) and Sabaju (SA; 1 – 4; formerly Lavang-estate). These estates are situated east (~70 km) of the coastal town of Bintulu (Figure 2.2), within the Lavang-Sabauh region and are located between Latitudes 3°07.81' N and 3°14.91'N and Longitudes 113°18.72' E and 113°32.19'E (Figure 2.3).

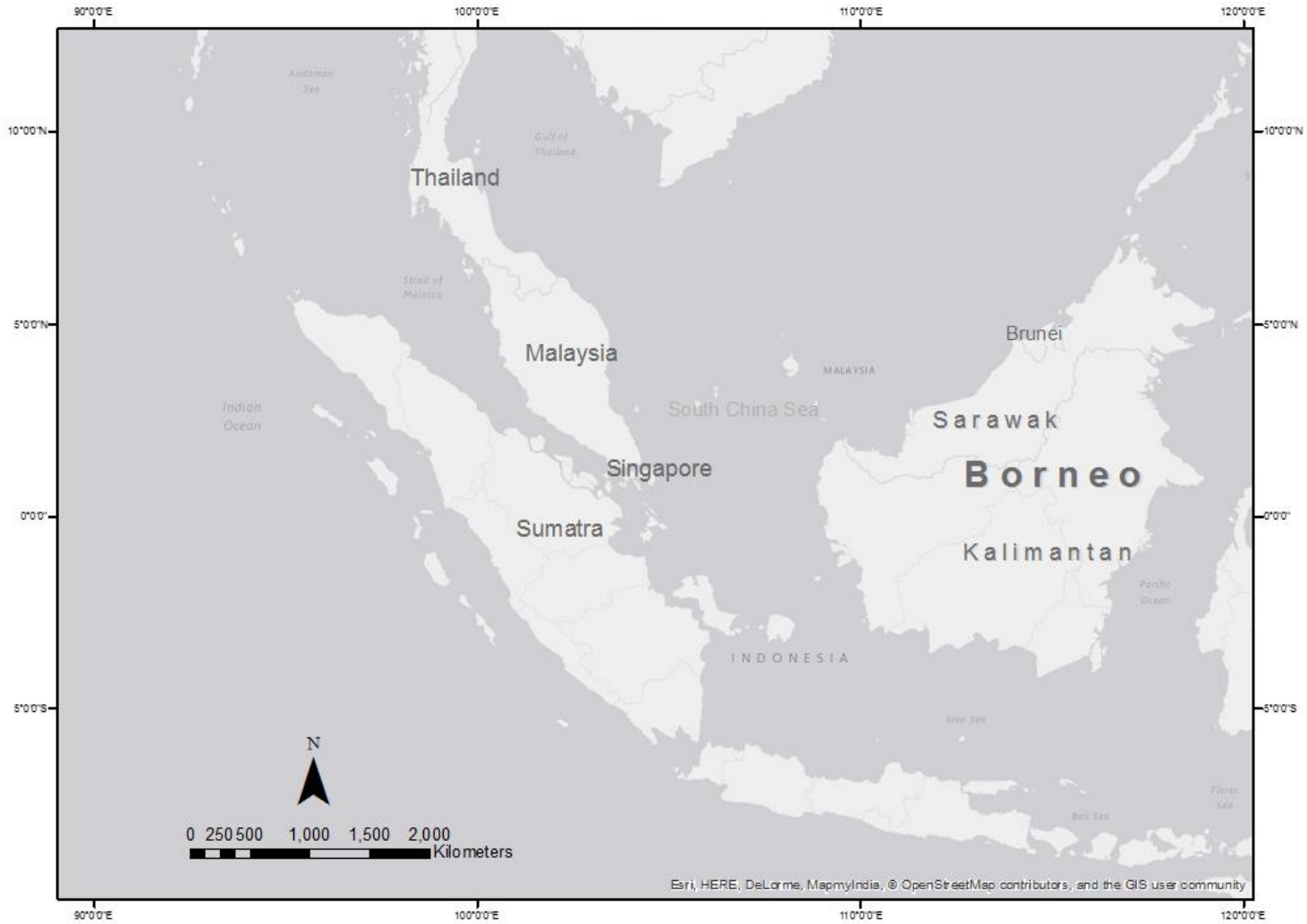


Figure 2.1. Location of Sarawak State Malaysia.

Maps throughout this thesis were created using ArcGIS® software by Esri. ArcGIS® and ArcMap™ are the intellectual property of Esri and are used herein under license. Copyright © Esri.

All rights reserved. For more information about Esri® software, please visit www.esri.com.'

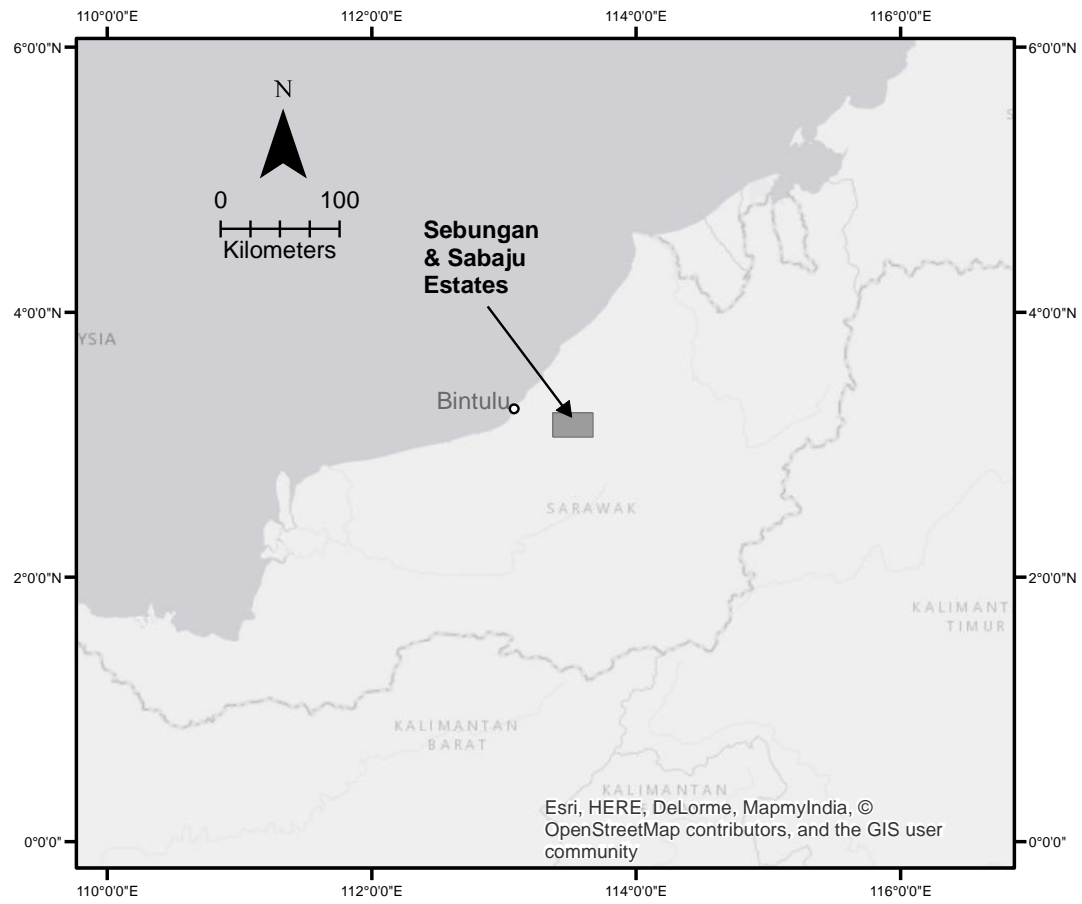


Figure 2.2 Location of the oil palm plantation study sites (Sebungan and Sabaju Estates) in relation to the coastal town of Bintulu.

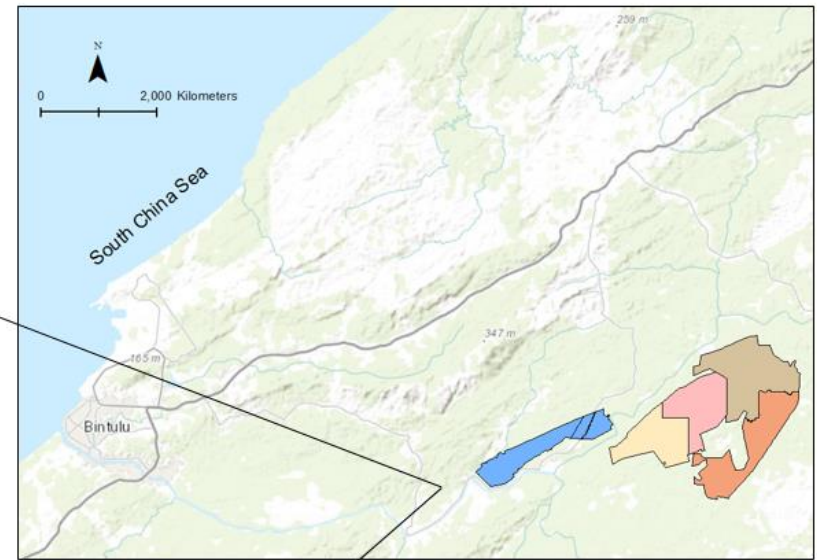
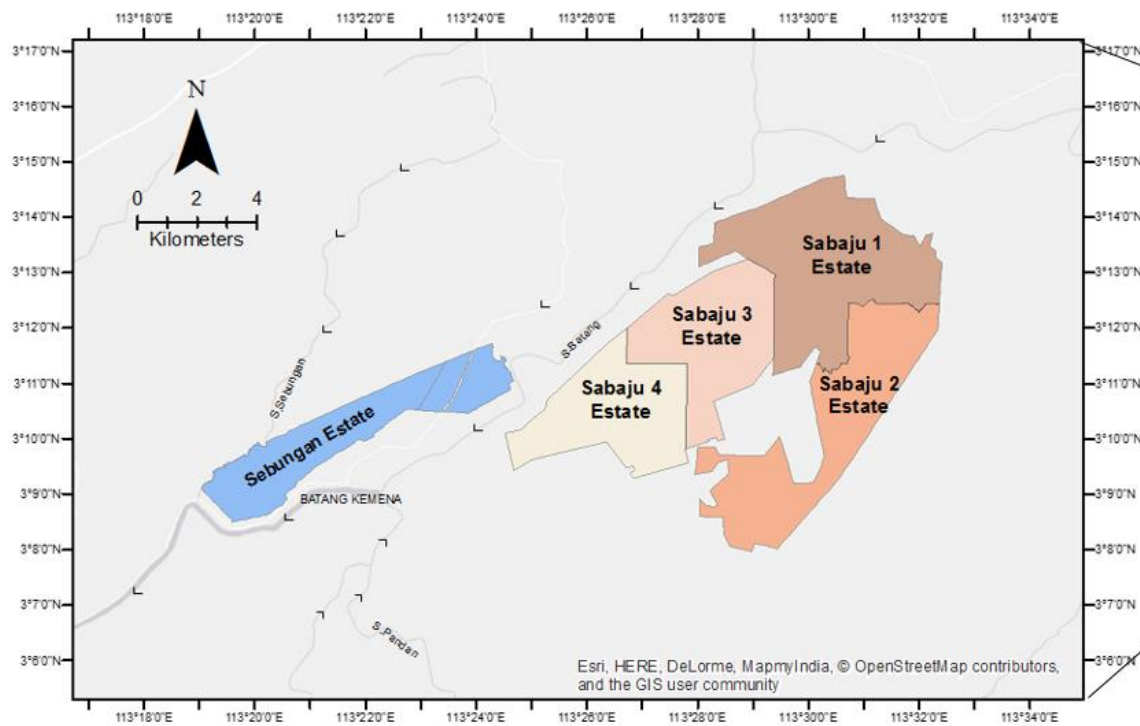


Figure 2.3 Location of the Sebungan and Sabaju oil palm estates in Sebauh Bintulu district Sarawak. The estates are bordered by a network of rivers (left map: grey and white lines; right map: blue lines) namely the Batang Kemena, S. Sebungan, S. Batang and S.Pandan. Arrows indicate direction of water flow.

2.2.2 Climate

Mean annual temperatures are around 26°C with annual precipitation of between 3,000 – 3,200 mm (Environmental Impact Assessment Report, EIA, 2006; Figure 2.4). The area is under the influence of both the Northeastern (October-January) and the Southwestern monsoon (May-August); the former is responsible for contributing 41-43% of the area’s annual rainfall, making this period the wettest, with the latter contributing 26-27% of annual rainfall (EIA Report, 2006). During the transitional months between monsoon seasons the precipitation varies unpredictably (EIA Report, 2006). In terms of evaporation, the mean ranges from 111-133 mm per month with the highest amounts occurring during the drier season, mid-year (EIA Report, 2006). Drought can occur in the months of June to August, if evaporation exceeds rainfall, but tends not to last for more than two consecutive months (EIA Report, 2006). Monthly rainfall during the dry season usually exceeds 100-150 mm.

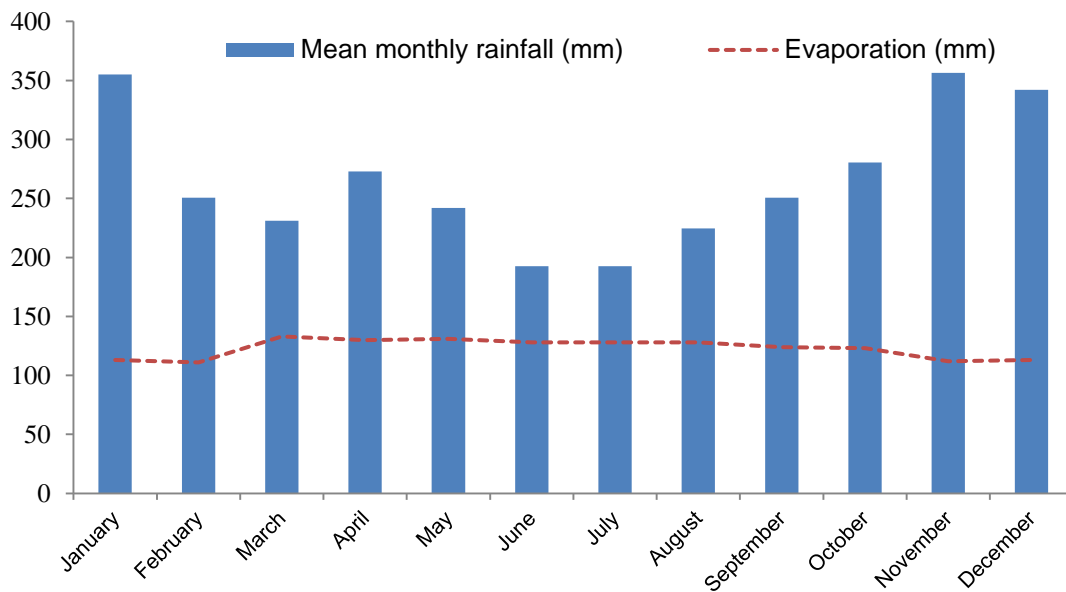


Figure 2.4. Average annual rainfall and evaporation for the Lavang-Sabauh region over a 30-year record (1969-1998) and 35 year record (1964-1998), respectively. Rainfall data was collected from the Sebauh DID rainfall station no. 3132023 and Lavang DID rainfall station no. 3234022, with evapotranspiration data taken from Bintulu Airport Station no. 3130302 (EIA Report, 2006)

2.2.3 Geology and topography

OPP development in the study location started in 2007/2008 with the establishment of the Sebungan and Sabaju 1 estates. Prior to development the majority of vegetation cover was mixed peat swamp forest (PSF; Table 2.1), which had been subject to intense logging. Vegetation also comprised of hill forests, found on steeper sloping mineral soil facets, and Alan and Padang paya forests on the peat dome. Alan forests are found on the shoulder of the peat dome on woody peat, with Padang paya forests found on the flatter peat dome plain associated with more fibrous peat (Sangok et al., 2017).

The topography of the region in which the estates are located is relatively flat consisting of 0 – 4% slopes and undulating 4 – 12% slopes (Param Agricultural Soil Survey, 2013). Peat dominates 83% of the area and is believed to have accumulated over the Quaternary period (last 4,819 years; Dommain et al., 2011), with 73% of the area's peat considered to be very deep (> 250 cm) (EIA Report, 2006). These peatlands are ombrogenous (i.e. precipitation is the only source of water and nutrients to the peat surface) and form shallow gradient convex domes.

The study estates are located on peat domes formed between the Batang Kemena and Sebungan Sungai and between the Batang Kemena and Pandan rivers (EIA Report, 2006) (Figure 2.3). The peat gradually rises away from these rivers, forming a dome shaped morphology, with the highest elevation of 7.5 m recorded in the dome center (EIA Report, 2006).

Table 2.1. The former land use of the study area before conversion to oil palm (EIA Report, 2006)

Land use/vegetation	Area (ha)			Percentage (%)
	Sebungan	Sabaju	TOTAL	
Mixed swamp forest (logged)	1,633	2,073	3,706	56.6
Hill forest (logged)	23	866	889	13.6
Alan forest	0	636	636	9.7
Padang paya forest	0	146	146	2.2
Areas affected by cultivation	11	1,159	1,170	17.9
TOTAL	1,677	4,880	6,547	100

2.3 Descriptions of the plantation experimental sites

An initial field visit was undertaken in April 2015. A 4 x 4 vehicle was used to drive around the different plantation roads (Figure 2.5). A set of detailed plantation maps (courtesy of the Sarawak Oil Palms Berhad GIS and cartography unit) were then used to understand the hydrology and layout of the area, which was necessary to determine sampling locations. Water flow directions and drainage layout were manually mapped onto the paper drainage maps using the field observations. These were then digitally generated using ArcGIS so that catchment areas could be determined.

Plantation management was typical of other peatland OPPs in this region. An artificial drainage network has been established to maintain optimum peat watertables for crop growth (i.e. in the range of -60 cm to -40 cm below the peat surface). This drainage network consists of a grid of interconnecting drains (Figure 2.5 and 2.6). The edges of the planting blocks (approximately 19 - 50 ha in area) are defined by a set of roads that provide complete access to individual blocks (Figure 2.5). Each planting block is drained by multiple field drains which feed into a central collection drain (Figure 2.6). These

collection drains subsequently feed into a system of main drains, which run parallel to the edge of the planting blocks. The water from the main drains then feeds into the surrounding perimeter drain, where it is eventually discharged into the nearby river network (Figure 2.6). The hydrology within these agro-landscapes is intensively managed throughout the year. Channel water depths and flow directions are monitored and controlled via channel alterations (i.e. the use of sand bags and barge boards to narrow and slow the flow of water) and the installation of weirs. This enables the flow conditions to be artificially controlled in order to contend with the prevailing environmental conditions e.g. drought and flooding.

The selection of sampling sites was based on the following criteria:

1. Samples from plantation estates of different ages
2. Inclusion of main and collection drains, in order to represent different spatial scales (i.e. collection represented a small sub-catchment of an individual planting block; main drains encompassed multiple planting blocks representing a larger catchment area).
3. Drains with good water flow and direction, with clear channels (i.e. little overgrown vegetation to disrupt flow).
4. Dominance of peat within the draining and nearby plantation blocks (i.e. no mineral soil present)

Based on the initial field visit (April 2015), four plantation estates were selected for investigation: Sebungan (SE), Sabaju 1 (SA 1), Sabaju 3 (SA 3) and Sabaju 4 (SA 4). Four to five sample points were selected within each estate. Sabaju 2 was excluded from the study due to the abundance of mineral soil within this estate. For the purposes of this study, SE and SA 1 were classified as 9-year-old plantations since they had palms that had been planted in 2007 and 2008, respectively, while SA 3 and SA 4 were classified as 6-year-old plantations with palms planted between 2010 and 2011.

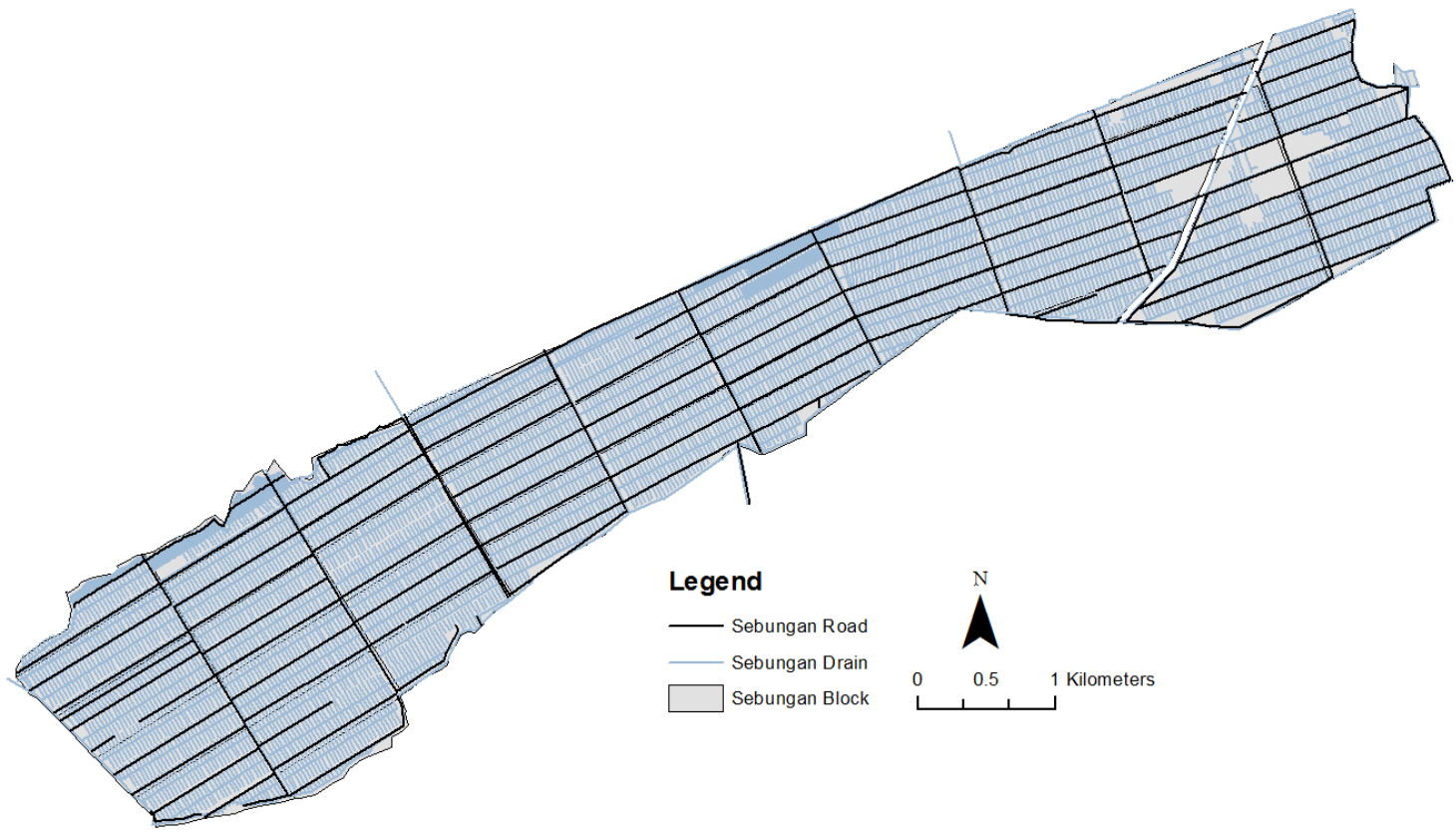


Figure 2.5 Example of a peatland oil palm plantation (Sebungan estate) layout with the planting blocks, drains and roads highlighted

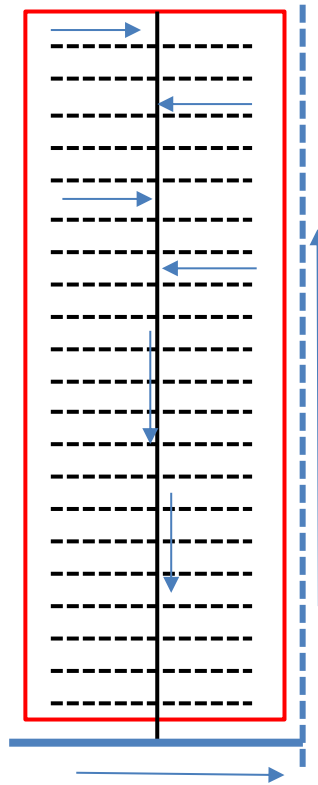


Figure 2.6. Schematic of typical drainage set up on a peat OPP planting block. Where: red box = planting area, black dashed line = field drains, solid black line = collection drain, solid blue line = main drain, blue dashed line = perimeter drain and arrows show the direction of water flow.

2.3.1 Sebungan Estate

The SE estate was established and is managed by Sarawak Oil Palms Berhad (SOPB), Bintulu Division on an elliptical-shaped peat dome formed between two rivers (Batang Kemena and S. Sebungan) which provide the main drainage for the plantation. The maximum peat depth is 5.6 m (EIA Report, 2006). SE was planted with oil palm in 2007, making it the oldest plantation within this study. The total planted area is approximately 1,648 ha and is divided into several elongated planting blocks which range in area from 19.39 ha – 48.73 ha. In comparison to the SA estates, the surface peat in this plantation was more heavily compacted prior to planting. Compaction is

achieved by running caterpillar-tracked vehicles over the peat surface in order to provide greater rooting stability for the palms. This difference in site preparation is supported by peat bulk density (BD) measurements (Appendix A); the average BD for the upper 1 m of peat in the SE estate was 0.2 g m^{-3} , compared to an average BD value for the SA estates of 0.1 g m^{-3} . Due to the age of the plantation the semi-mature palms provided a partially closed canopy setting (70% closed) and some shade for the peat surface (Figure 2.7).



Figure 2.7. Photographs to illustrate the height of the oil palm trees and the semi-closed canopy structure in the SE plantation estate.

Four sample points were chosen for investigation in the SE estate (Figure 2.8); these included one main drain and three smaller collection drains. From the initial visit the area drained by the main drain was estimated at $800,000 \text{ m}^2$, with the areas drained by the collection drains ranging from $210,000$ to $250,000 \text{ m}^2$ (Figure 2.8). The approximate dimensions of the channels varied; the main drain measured 3.6 m wide and 2 m deep with the collection drains ranging from 1 to 2 m wide, and never exceeding 2 m in depth. The water depth of the main drain varied along its length due to the presence of weir structures, designed to artificially modify channel water volumes (Figure 2.9). Channel water depth was particularly low during October-November 2015 and April-May 2016, causing some of the collection drains to completely dry out (Figure 2.10).

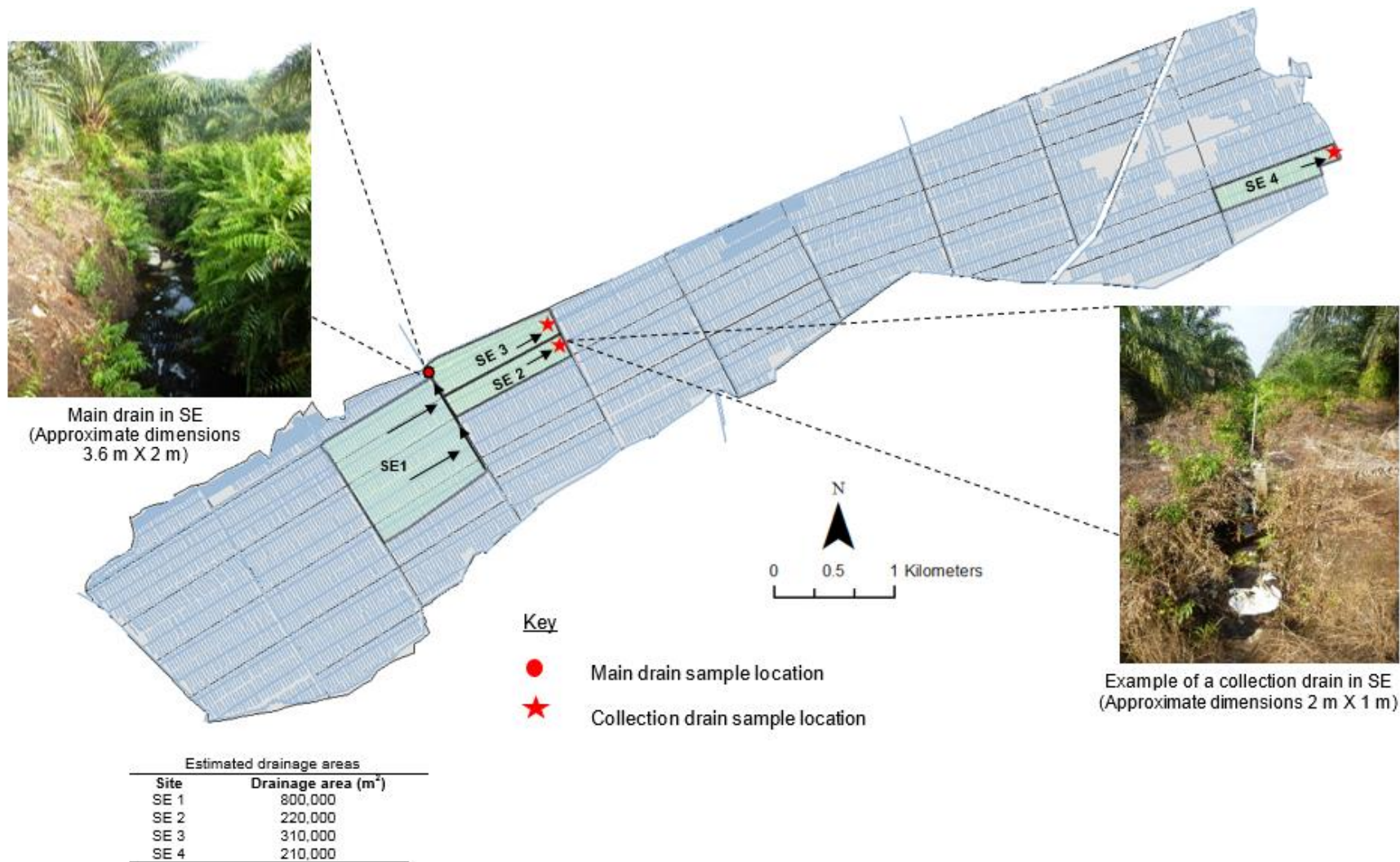


Figure 2.8 Map of the Sebungan estate, including the location of the four point locations and their approximate catchment areas (shaded), arrows indicate the direction of water flow



Figure 2.9. Example of wooden weir structures located in the SE main drain, used to artificially modify water channel heights.



Figure 2.10. Photograph to illustrate the dry collection drains encountered during October 2015

2.3.2 Sabaju Estates

The SA estate is divided into four individual OPP sub-estates (SA 1-4). The estates are located on an irregularly shaped peat dome, with some mineral 'islands' protruding above the peat surface; the average peat depth across the whole SE estate is 4.2 m (EIA Report, 2006). Peat coring throughout SA revealed very deep peat (8 m+) within SA 4, followed by deep peat deposits within SA 3 (4 m) and shallower peat within SA 1 (2 m). The estate can be accessed via the SE estate using a ferry to cross the S. Batang, which separates the two plantation areas (Figure 2.3). The internal road network is then used to travel to and from the four sub-estates. As with the SE estate, the SA estates are owned and managed by SOPB. Of the three sub-estates under investigation (SA 1, 3 and 4), the youngest palms were in SA 4 (1,638.2 ha) which was planted in 2011, followed by SA 3 (1,714.2 ha) planted in 2010, with the oldest palms found within SA 1 (2526.2 ha) planted in 2008.

The younger palm ages in SA 3 and SA 4 result in a low canopy coverage (20 %) and higher exposure of the peat surface to direct radiation (Figure 2.11). In contrast, SA 1 has a more developed canopy coverage (65 %) and, as a result, the peat surface is more shaded, similar to conditions found within the SE estate (Figure 2.7). Large islands of mineral soil (up to 49.63 ha) can be found distributed across SA but are mainly concentrated to the east of SA 1. In addition, undecomposed woody debris from the former PSF can be found on the peat surface along the crop windrows, and is particularly prominent within SA 4 (Figure 2.12).



Figure 2.11 Photographs to illustrate the exposed peat surface in SA 3 (a) and SA 4 (b) and limited canopy coverage in 6 year old plantation stands.



Figure 2.12 Large woody PSF debris on the peat surface in SA 4. The debris is stacked into windrows which were observed across the Sabaju plantation estates (photograph taken from SA 4)

Within SA 1 four sample point locations were chosen (Figure 2.13); one main drain and three collection drains. From the initial field visit the drainage areas were estimated to range from 240,000 to 1,120,000 m². The main drain measured 6 m wide and 2 m deep, with the three collection drains ranging from 2 to 3 m wide, not exceeding depths of 2 m. During the sampling period, the watertable depth within SA 1 ranged from -53 cm to - 6 cm, below the peat surface, with an average depth of -31 cm. The lowest watertable levels were recorded in April 2016 and peaked during December 2015.

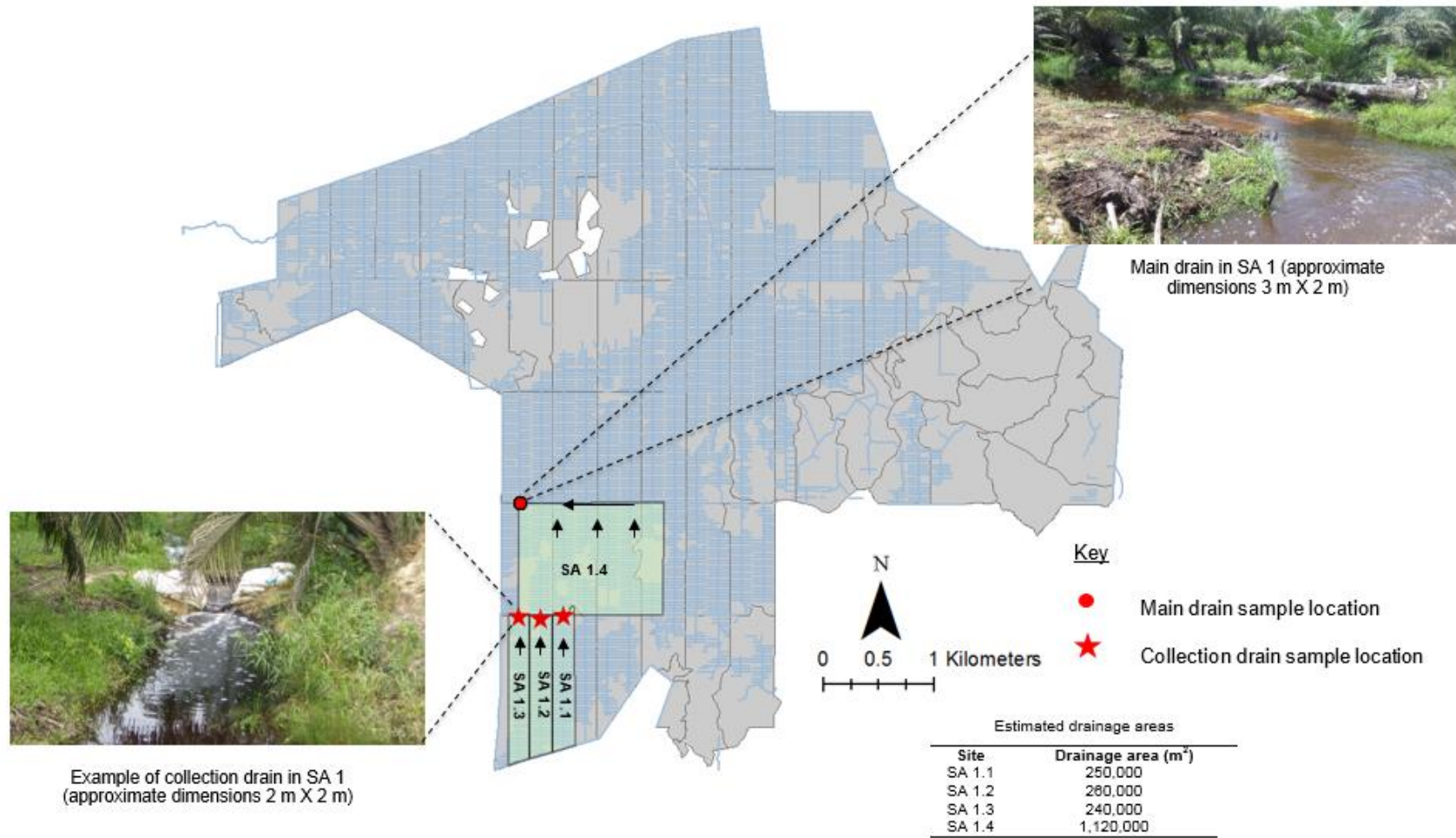


Figure 2.13 Map of the Sabaju 1 estate, including the location of the four point locations and their approximate catchment areas (shaded), arrows indicate the direction of water flow

Five point locations were selected in SA 3 (Figure 2.14); one main drain and four collection drains. From the initial field visit the areas drained by the collection drains were estimated to range from 170,000 to 350,000 m², with the main drain catchment estimated at 6,030,000 m². The main drain measured 5 m wide and 3 m deep with the collection drains ranging from 2 to 5 m wide, with a maximum depth of 2 m. The watertables within SA 3 varied throughout the year and ranged between -82 cm to +4 cm, in comparison to the peat surface, with the lowest readings recorded in October 2015 and April 2016 and the highest within November and December 2015. This, in some instances caused the channel's maximum water capacity to be exceeded resulting in overland flow and flooding on several occasions (September 2015; Figure 2.15).

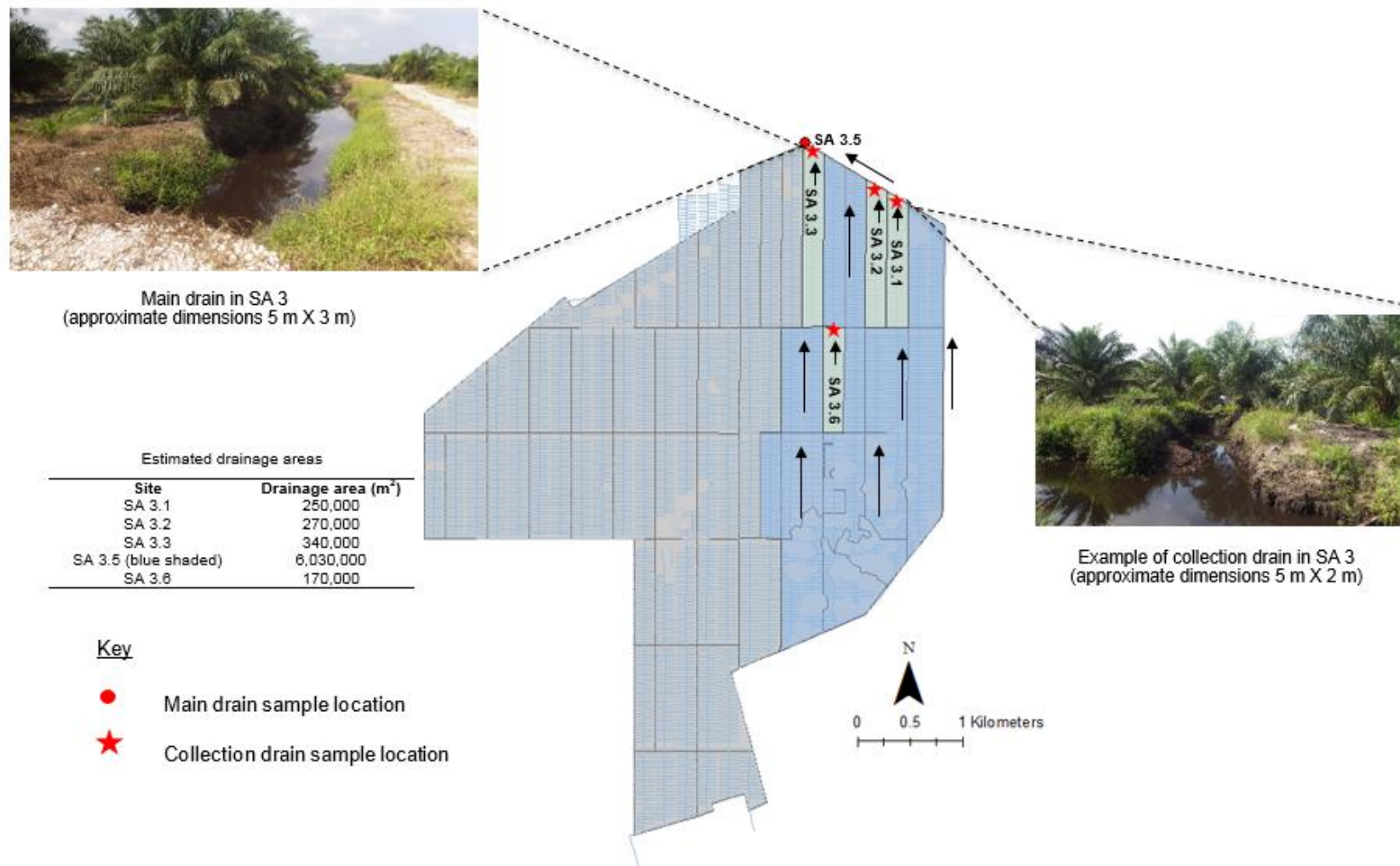


Figure 2.14 Map of the Sabaju 3 estate, including the location of the five point locations, and their approximate catchment areas (shaded), arrows indicate the direction of water flow. Note there is no SA 3.4 location.



Figure 2.15 Example of the flooding experienced in SA 3

Four sample point locations were selected in SA 4; this consisted of two main drains and two collection drain sites (Figure 2.16). From the initial field visit the drainage areas were estimated to range from 220,000 to 4,190,000 m². The main drains ranged from 2.5 to 4 m wide with depths of 3 to 4 m. The width of the collection drains ranged from 1 to 5 m and did not exceed more than 3 m in depth.

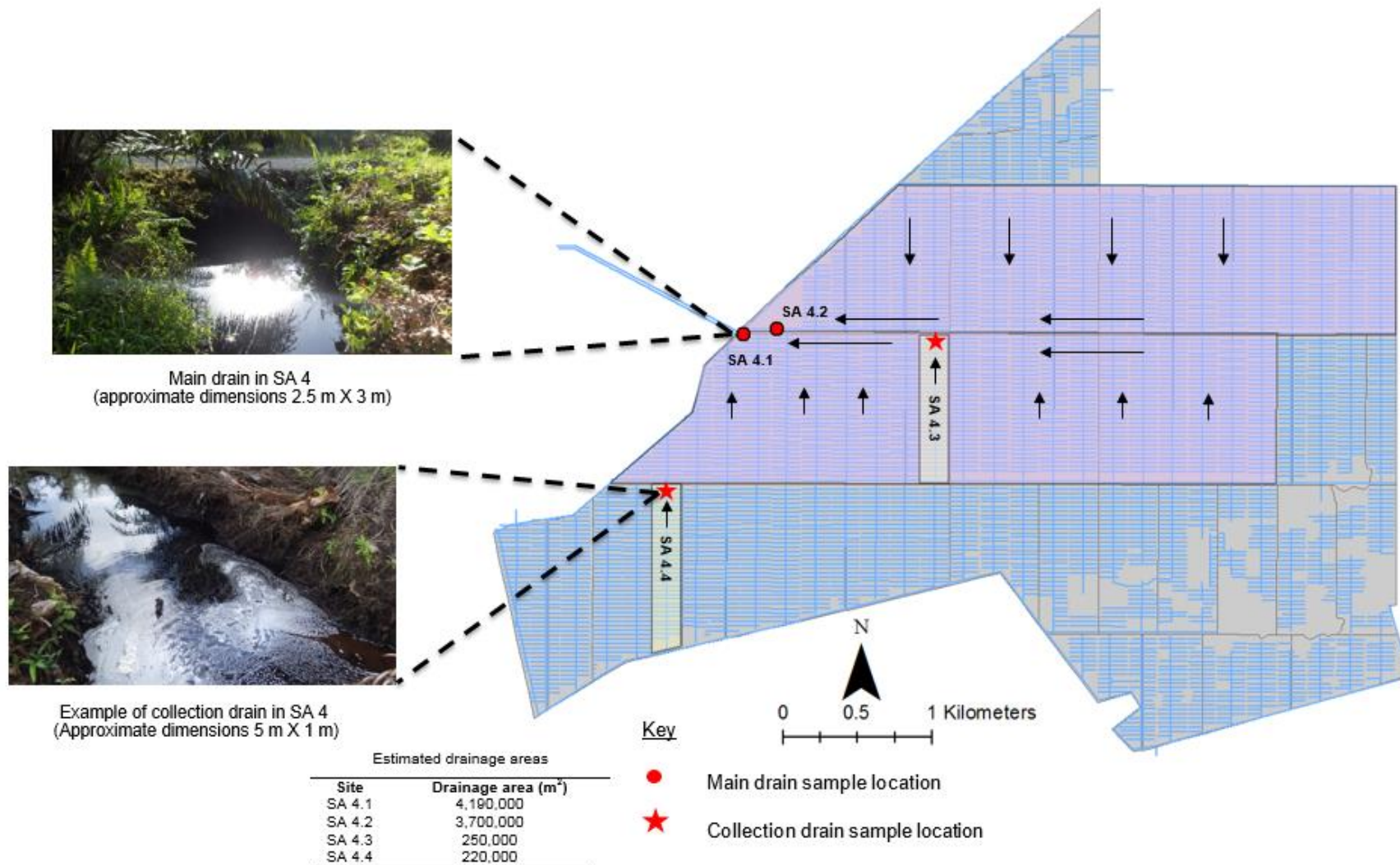


Figure 2.16 Map of the Sabaju 4 estate, including the location of the four point locations and their approximate catchment areas (shaded), arrows indicate the direction of water flow

2.4 Descriptions of the forest experimental sites

2.4.1 Peat Swamp Forests

In addition to the plantation (P) estates, two PSF sites (FA and FB; collectively referred to as F, Forest) were chosen as reference/control sites enabling a comparison to be made between the two ecosystems (F vs P). The forest stands chosen were located along the perimeter of the SA 4 (FA) and SE (FB) estates, where the forest blocks act as a 'buffer zone' between the plantation and surrounding river network. These specific sites were selected because they had clear access into them from the plantations. Both forest sites have been subjected to various disturbances (e.g. logging and drainage), and therefore cannot be classed as 'pristine'. However, they are representative of the current state of most of the remaining PSFs in Borneo, and particularly those within Sarawak.

Two PSF sites (FA, FB) were selected for study. These were situated along the western boundaries of the SE (N 03°10.101, E 113°20.490) and SA 4 estate (N 03°10.082, E 113°24.375; Figure 2.17). Both forest fragments had been subjected to selective logging to remove important timber species such as *Gonystylus bancanus* and *Shorea sp.* This had resulted in a reduced canopy height (< 25m) with just the middle, lower and understory layers remaining.

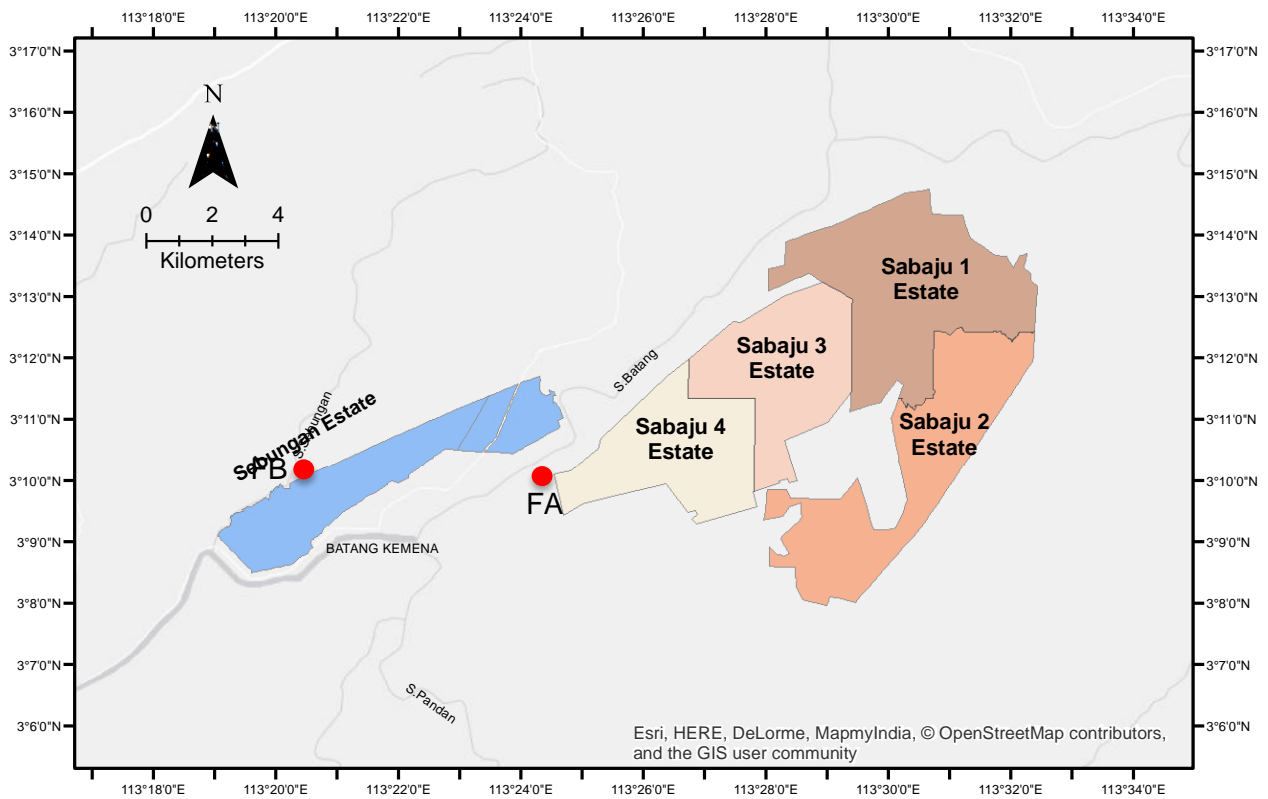


Figure 2.17. Location of the two PSF study sites in relation to the Sebungan and Sabaju estates

FA was observed to be in a better general condition with a greater canopy density compared to FB (Figure 2.18). This is reflected by a more closed canopy (80%) with some tall tree species still present throughout the site (Figure 2.18, left image). A 4 m deep plantation perimeter drain bordered FA, causing direct drainage. Consequently, the watertable never rose above the peat surface, with recorded watertable depths ranging from - 5.3 to - 66 cm, below the peat surface.

FB has experienced greater levels of disturbance resulting in a sparse canopy, with significant light penetration to the forest understory (Figure 2.19). The perimeter drain surrounding FB is also much deeper (10 m) resulting in a more significant drainage effect. As a result, watertable depths ranged from - 52 to - 109.3 cm below the peat surface. At both F sites, peak watertable depths

were recorded during November to December 2015 and the lowest depths between September and October 2015.



Figure 2.18. Closed canopy and tall tree species (left) within FA, alongside pitcher plant (*Nepenthes. sp*) (right)



Figure 2.19. Remains of a large tree (left) alongside the sparsely vegetated canopy layer (right) within FB.

2.4.2 Deforested peat swamp forest areas

Two areas of recently deforested PSF (DF and R-DF) were also sampled, situated along the western (N 03°10.070, E 113°24.540) and southeastern borders of SA 4 (Figure 2.20 and 2.21) in order to capture this stage in the plantation conversion process. DF was cleared in March 2015 and was sampled in parallel with the plantation water samples over a full year (3rd August 2015 – 8th August 2016). The more recently deforested site (R-DF) was not cleared until early February 2016 and thus had a shorter sampling regime over 25 weeks (22nd February 2016 - 8th August 2016).

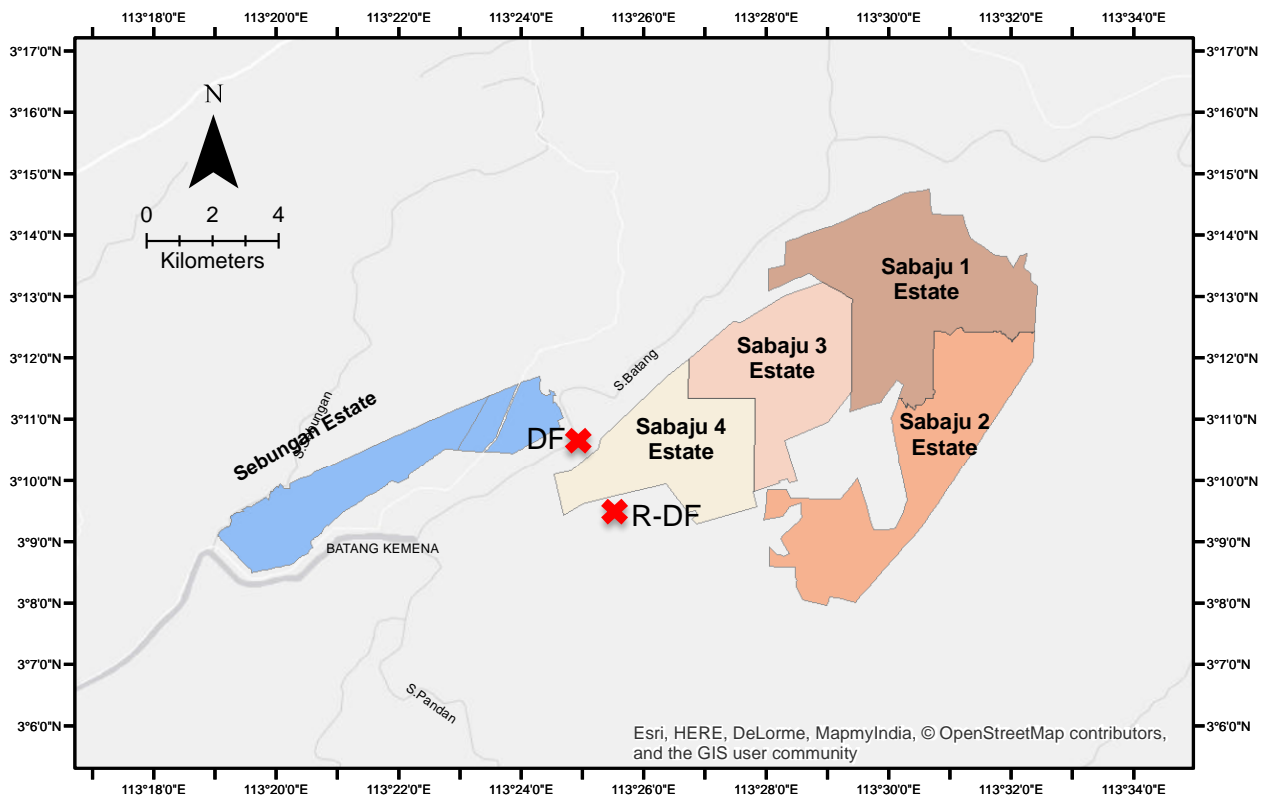


Figure 2.20. Location of the two deforested PSF study sites in relation to the Sebungan and Sabaju estates

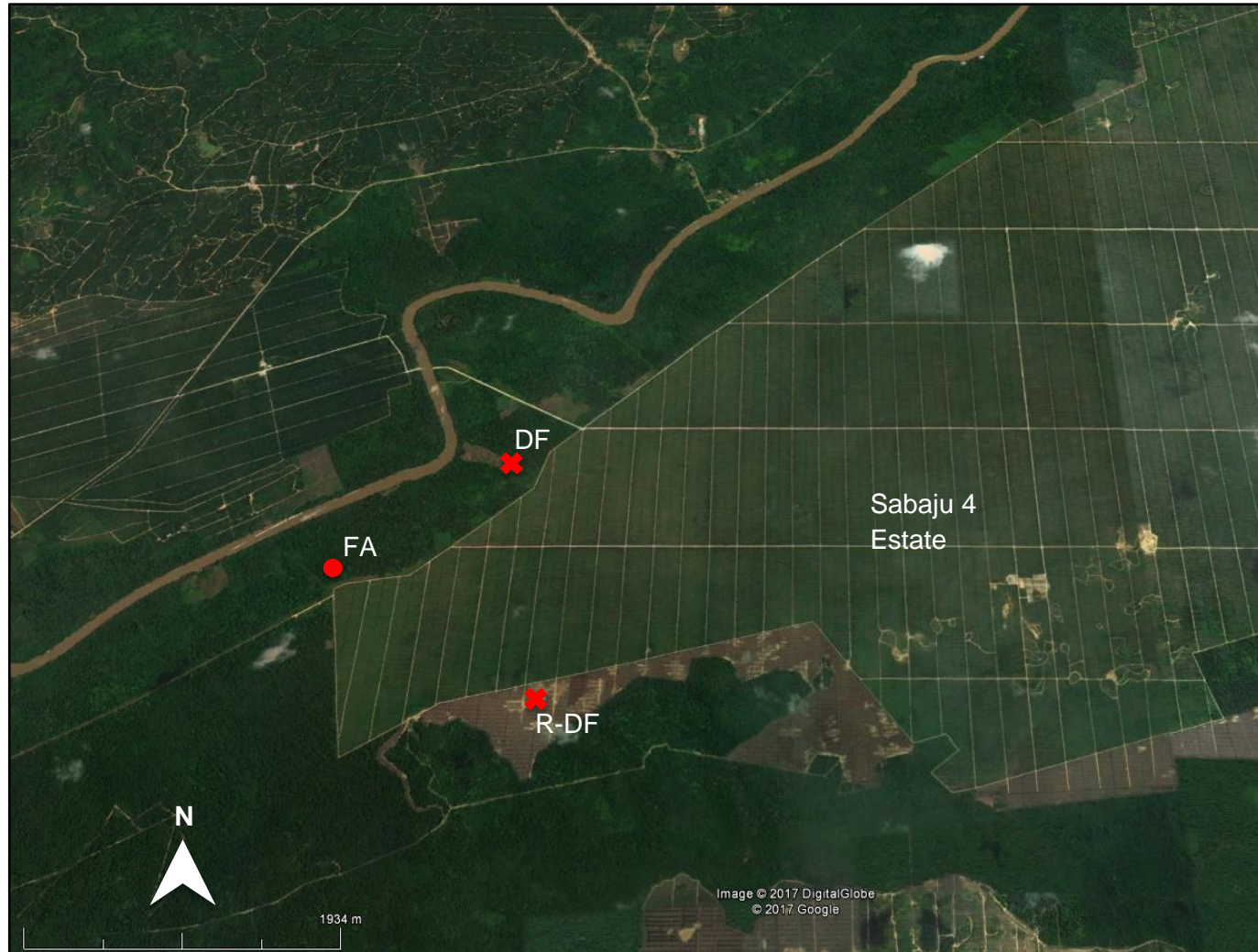


Figure 2.21. Satellite imagery, obtained from Google earth®, of the two deforested PSF study sites in contrast to the Sabaju 4 estate and FA site

The area cleared for DF represents a small (1 ha) strip of land adjacent to the SA 4 estate (Figure 2.21). A 3 m wide drainage ditch runs parallel to the site, draining the water from the cleared area into the nearby S. Batang (Figure 2.22).



Figure 2.22. The 3 m drainage ditch within the DF site, approximately 3 m wide and 2 m deep

The R-DF site was deforested in February 2016 prior to the establishment of the Sabaju 5 estate. This area has a mixture of both peat and mineral soils with large mineral islands protruding through the peat surface (Figure 2.23). Several large (2m wide) drainage ditches were established within this site to provide initial peat drainage (Figure 2.24). At the time of sampling, the woody debris from the PSF had not been removed and was abundant on the peat surface (Figure 2.25), although there was also evidence of stacking to form windrows (Figure 2.25).



Figure 2.23. Protruding islands of mineral soil in distance; newly-established drainage ditches in the foreground of site R-DF (photo taken 2 months after deforestation)



Figure 2.24 Example of newly established drainage ditch within R-DF alongside newly planted oil palm seedlings (photo taken August 2016, 6 months after deforestation)



Figure 2.25. Abundant woody debris covering the R-DF peat surface, with evidence of stacking into windrows.

2.5. Sampling methods

2.5.1 Sample collection

DOC and POC (TOC) water samples were collected, from the OPP, F, DF and R-DF land-cover classes. This resulted in an average of 46 samples per week. All water samples for DOC determination were collected using pre-rinsed (with sample) polypropylene 60 ml Nalgene wide-neck bottles, as recommended for DOC collection and analysis (Norrman, 1993). Water samples for POC determination were collected using 500 ml plastic bottles to ensure enough sample was collected for analysis. After collection the samples were transported back to the plantation base before being immediately filtered.

In the OPPs, water samples were collected from a combination of collection (C) and main (M) drains. In each instance the samples were collected at a point immediately upstream from where the channel discharged (Moore et al., 2011; 2013). The sampling location was marked with a GPS and visually identified. When sampling, the point of collection was approached from a downstream position to ensure minimal disturbance.

Water samples from F (FA and FB) were collected from 3 clusters of dipwell tubes, within each site, which acted as 'pseudo ditches' as no clear forest drainage outlet could be found (Figure 2.26). Dipwells were 2 m in length and inserted 1.5 m into the peat surface, at half meter intervals from one another. Water samples were extracted by lowering a test tube into the dipwell using a wire, until enough water had been collected. Dipwells were constructed from 32 mm diameter PVC tubes cut to 2 m in length (Figure 2.26). 5 mm holes were drilled down the tubes, spaced at 35 mm intervals. A hand drill was used to drill completely through the tube creating two holes directly opposite each other. The tube was then rotated through 90° and the same done again, resulting in four holes positioned next to each other. The top of the tube was fitted with a removable cap allowing access to the tube but preventing rain and debris entering the tube in-between measurements. The bottom of the tube was fitted with a glued PVC plug to prevent sediment encroachment.

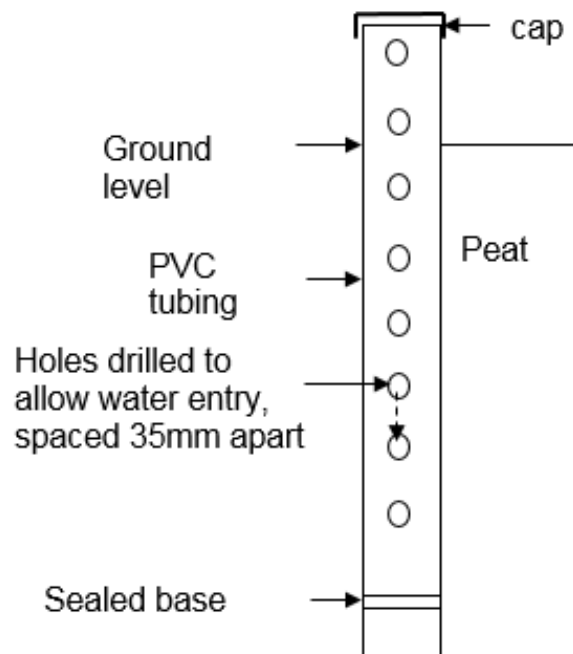


Figure 2.26. Schematic diagram of dipwell tube

Within the deforested sites (DF and R-DF) water samples were collected from the 3 m wide drainage ditch within DF and one of the main drainage ditches within R-DF, selected based upon its location away from large mineral deposits. Water samples were extracted using the same method within the plantations.

Sample locations were monitored from 3rd August 2015 until 8th August 2016 (54 weeks), with the exception of R-DF which was sampled 22nd February 2016 - 8th August 2016 (25 weeks). Weekly sampling was carried out by myself during three intense fieldwork campaigns (3rd August 2015-11th October 2015; 15th February 2016-1st May 2016; 15th August 2016-15th September 2016). During the remaining weeks, sampling was carried out by a member of staff from the Malaysian Palm Oil Board (MPOB), using the same methodology described above with a sampling frequency of every 1-3 weeks.

2.5.2 Sample filtration

Filtration is an essential step in the determination of DOC (Horowitz et al., 1996; Khan & Subramina-Pillai, 2006) and is primarily used to separate the suspended sediment (POC) from the dissolved (DOC) fraction (Sharp et al., 1993; Khan & Subramina-Pillai, 2006; Moore et al., 2011).

There are several filter options available for DOC determination (Table 2.2) but there are no specific requirements for filter selection (Karanfil et al., 2002). Glass fibre (GF) filters are common for DOC processing due to their high-flow rate and ability to be made relatively 'organic free' via combustion at high temperatures (450°C; Sharp et al., 1993). Research by Karanfil et al. (2003) has emphasized the importance of this in relation to DOC analysis, with certain filter types leaching both water-soluble organic carbon and other compounds, and thereby interfering with DOC concentrations. Two of the most common filters used for DOC analysis are cellulose acetate and cellulose nitrate membranes (Kolka et al., 2008), which have been utilized in a wide range of environmental studies (Moore et al., 2011; Xu et al., 2012; Moore et al., 2013;

Li et al., 2014; Marvin-DiPasquale et al., 2014). The major advantage of using these filter types is that they do not release DOC during filtration and thus, reduce sample contamination (Kolka et al., 2008).

DOC is operationally defined as being able to pass through a 0.45- μm filter, whereas POC is retained (Thurman, 1985; Moore et al., 2011). Consequently, as cellulose acetate and cellulose nitrate membranes have an absolute pore size of 0.45- μm they can adequately separate the DOC from the POC fraction (Moore et al., 2011). This is in contrast to GF filters which tend to exhibit slightly larger pore sizes ($>0.45\text{-}\mu\text{m}$), permitting POC contamination, and aluminum oxide filters ($<0.45\text{-}\mu\text{m}$) which restrict DOC filtration. However, Chow et al. (2005) argue that a pore size of 0.45- μm can still permit the filtration of other organic fractions, resulting in a heterogeneous organic carbon filtrate (Thurman, 1985; Chow et al., 2005). However, the contribution of sub-micrometer particles ($<1\ \mu\text{m}$) to DOC has been estimated at only 10%, so the impact on overall DOC concentrations is minimal (Chow et al., 2005).

For this investigation two types of filter were used. POC was determined using GF (Advantec) with a pore size of 0.4 μm . This filter was chosen as it can be made relatively 'organic free' through various combustion techniques and can also withstand the high temperatures necessary to burn off any carbon on the filter. DOC was filtered using cellulose nitrate membrane filters (Whatman) with a pore size of 0.45 μm . Before DOC filtration, filter papers were pre-rinsed with 10 ml of field sample to flush out any existing organic material present on the filter.

Filtration can be carried out using gravity, pressure or a vacuum (Sharp et al., 1993). In the case of DOC, gravity filtration is too time consuming when using a 0.45- μm filter size, thus, filtration via vacuum and pressure are preferable (Quevauviller, 1995). For pressure filtration, high-purity gases are required which can be expensive and unavailable in remote field locations (Sharp et al., 1993). In contrast, vacuum filtration has been effectively carried out in remote

field site locations (Moore et al., 2011), making this method both transportable and time efficient. Consequently, filtration was carried out using a hand-held vacuum pump (Mityvac, MV8510) immediately after the freshly collected samples were transported back to the plantation base.

Table 2.2. Advantages and disadvantages of filters used for DOC analysis, with corresponding references

Filter	Advantages	Disadvantages	Reference
Glass fibre	<ul style="list-style-type: none"> • High flow rates • Can be made 'organic free' via combustion 	<ul style="list-style-type: none"> • Hard to remove bacteria from the filter • Combustion can modify the filters characteristics • Pore size > 0.45-μm 	Sharp et al., 1993 Karanfil et al., 2003
Silver membrane	<ul style="list-style-type: none"> • Immediate separation of DOC and POC • Less sample handling requires 	<ul style="list-style-type: none"> • Takes time for the sample to filter • Sample must have low quantities of suspended sediment present (<50mg l⁻¹) • High cost 	Malcom & McKinley, 1989
Aluminium oxide	<ul style="list-style-type: none"> • 'organic free' on combustion 	<ul style="list-style-type: none"> • Small pore size 0.2-0.02 μm • Absorbs humic material 	Sharp et al., 1993
Cellulose acetate membrane	<ul style="list-style-type: none"> • Used in a wide range of environmental studies • Does not release DOC during filtration • Absolute pore size of 0.45-μm 	<ul style="list-style-type: none"> • Susceptible to biodegradation over time • Bacteria adhesion to the surface can occur 	Kolka et al., 2008 Moore et al., 2011 Xu et al., 2012 Nguyen et al., 2012
Cellulose nitrate membrane	<ul style="list-style-type: none"> • Available with absolute pore size of 0.45-μm • Insoluble in water • Not affected by dilute acids, alkalies, aliphatic and aromatic hydrocarbons 	<ul style="list-style-type: none"> • Hwang et al., (1979) reported significant amounts TOC and nitrate in distilled water filtrates, when using this filter type 	Hwang et al., 1979 Karanfil et al., 2003

2.5.3 Sample preservation

After filtration, it is vital that the DOC is preserved to conserve the labile organic carbon fraction and reduce alterations to DOC concentrations pre analysis (Sharp et al., 1993; Moore et al., 2011). However, there is only partial guidance concerning sampling and analysis protocols, particularly in relation to DOC preservation (Peacock et al., 2015; Cook et al., 2016). The US Environmental Protection Agency (Disinfectant/Disinfection By-Products Rule, D/DBPR) currently dictates that DOC water samples be analysed within the first 48 hours (Karanfil et al., 2002), while others suggest analysis be carried out no more than one day after sample collection (Wilson et al., 2011). If this is not possible then active measures must be taken to preserve the DOC fraction to limit biological, chemical and physical degradation. A common protocol is to freeze or acidify the water samples (Moore et al., 2011; Peacock, 2014b; 2015; Norman & Thomas, 2014). However, Peacock et al. (2015) warn that this can alter the DOC concentration in both fresh and marine water samples (Fellman et al., 2008) as well as the absorbance and fluorescence properties. Common acids used for preservation are hydrochloric, phosphoric and dilute sulphuric acid (Sharp et al., 1993; Moore et al., 2011). These typically lower the sample's pH to between 2.3 to 3.5, required for the quantitative removal of DIC (dissolved inorganic carbon) and elimination of microbial activity via enzyme denaturation (Sharp et al., 1993). However, changes to the pH of the sample can induce flocculation and coagulation of DOC (Worrall et al., 2006; Peacock et al., 2015) whilst freezing can induce DOC losses via abiotic particle precipitation (Peacock et al., 2015), complicating DOC analysis.

Several investigations by Peacock et al. (2014b; 2015) have sought to address the problems associated with DOC preservation by investigating how DOC concentrations change during storage and the implications of this for analysis. Overall, Peacock et al. (2014b) found little change in DOC properties when samples, from UK ombrotrophic peatlands, were filtered and stored for 12 weeks in the dark at 4°C (Peacock et al., 2014b). Earlier studies had also reported no significant change in DOC concentrations, following the same

storage technique (Ekström et al., 2011; Carter et al., 2012). However, these studies were all conducted on samples from temperate peatland, with limited guidance on preservation techniques for DOC water samples derived from tropical peatland. Therefore, a preliminary storage experiment was designed to determine the effects of cold storage at 4 °C on tropical water DOC concentrations and quality. Based on the results of this experiment, preservation via refrigeration (at 4°C) was found to be an acceptable method for DOC preservation. Further details of this study are presented in Cook et al. (2016) and Chapter Three.

2.6 Sample analysis

2.6.1 In-situ measurements

Before laboratory analysis, samples were subjected to several in-situ measurements. Immediately, following collection, water temperature (°C), pH and electrical conductivity (EC; $\mu\text{s cm}^{-1}$) of the un-filtered water samples were recorded, using a portable pH and EC (Hana) probe. The use of wide neck Nalgene sample bottles meant that probes could be inserted directly into the water sample without the need for transfer into another container. This reduced the risk of sample contamination.

2.6.2 Dissolved organic carbon

A number of methods have been used to quantify DOC concentrations in water samples obtained from peatland catchments (Table 2.3). For this investigation, DOC concentrations were determined using a combination of both UV-visible spectrophotometry and the non-purgeable organic carbon (NPOC) technique.

Table 2.3. Techniques used to determine DOC concentrations from peatland catchments, along with their advantages and disadvantages

Study	Location	Method	Comment
Moore et al., (2011, 2013)	Tropical peatlands, Sebangau River catchment, Central Kalimantan, Indonesia	Measured DOC concentration using high temperature catalytic oxidation (HTCO) , with TOC analyser, and following the non-purgeable organic carbon (NPOC) technique for DOC	Expensive equipment is required, which can limit the number of samples tested, but both are widely used and tested techniques.
Gandios et al., (2013)	Tropical peatlands, Kuala Belait District in Brunei Darussalam on Borneo Island	determined by subtraction, whereby total carbon and inorganic carbon are measured independently and subtracted from one another or the inorganic carbon fraction is first chemically removed, leaving only the NPOC fraction remaining for instrument analysis	One of the advantages of HTCO methods over WCO is that low sample volumes are required for analysis (0.05-0.20 vs 2-25ml) allowing a greater number of replicates to be generated for the same sample size (Panetta et al., 2008).
Hulatt et al., (2014)	Kiiminki river catchment, draining peat mires in Finland		
Lou et al., (2014)	Zoige peatland, Tibetan Plateau, China	Used wet chemical oxidation (WCO) to determine TOC and DIC.	
Peacock et al., (2014b)	Two ombrotrophic peatlands in north Wales, UK	UV-visible spectroscopy using 230-800nm	Simpler method and less expensive. Lower wavelengths ($\leq 263\text{nm}$) provide a more robust proxy for DOC determination. However, only provides a proxy for DOC concentrations (Peacock et al., 2014b).
Qassim et al., (2014)	Bleaklow Plateau in the Peak District National Park	Colourimetric analysis	Cheaper alternative to HTCO techniques but requires knowledge of the expected concentration of organic carbon (Bartlett & Ross, 1988)

2.6.2.1 UV-visible spectrophotometry

Spectroscopy methods can be used to quantify DOC concentrations and qualify carbon compounds (Tipping et al., 2009; Carter et al., 2012; Peacock et al., 2014). A detailed description of spectrophotometric techniques are provided in Chapter Three B. The two-wavelength approach is an example of a proxy method that was originally proposed by Tipping et al. (2009) and further advanced by Carter et al. (2012). This technique is model based and, after parameterization, can estimate a sample's DOC concentration based on its absorbance at 270 nm and 350 nm (Carter et al., 2012; Peacock et al., 2014b). Detailed methods are outlined in Cook et al. (2017) in Chapter Three B. UV spectroscopy across a range of wavelengths (254, 270, 350, 400, 600 and 700 nm) has also been used to provide proxy information about the quality of DOC compounds (Peacock et al., 2014b; Peacock et al., 2015), discussed further within Chapter Five.

Whilst in the field, the DOC concentration of water samples was obtained following the two-wavelength approach and using a Cole-Parmer UV/visible spectrophotometer (230 VAC, 50 Hz). This meant that values for DOC concentrations could be generated immediately, whilst also reducing the number of samples that had to be shipped back to the UK.

2.6.2.2 Non-purgeable organic carbon technique

Upon returning to the UK, the DOC concentrations of the filtered water samples were analyzed (as NPOC) using a Shimadzu Total Carbon analyzer. Samples were acidified with 1 M hydrochloric acid (such that $\text{pH} < 3$), via syringe injection, and then sparged with purified air to remove any inorganic carbon (IC) (Sharp, 1993). TOC was then measured using a non-dispersive infrared sensor and subsequently compared to an NPOC calibration curve, with standards ranging from 0-100 mg L⁻¹. The most appropriate ranges for each sample were automatically selected by the instrument to ensure a high level of

accuracy (precision ~ 2 – 5 %; Graneli et al., 1996; Bjorkvald et al., 2008; Shafer et al., 2010). An example of an NPOC calibration curve used during one of the sample runs is presented in Figure 2.27.

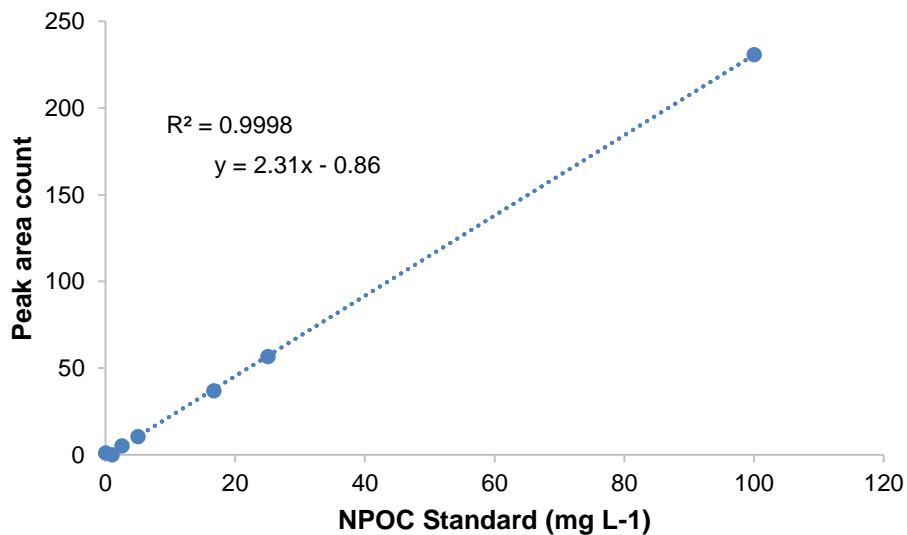


Figure 2.27 Example of an NPOC calibration curve (0 – 100 mg L⁻¹) alongside the calibration coefficient (r^2) and equation of the line.

2.6.3 Particulate organic carbon

To determine POC, 500 ml of deionized water was first passed through Advantec GF filters (0.4 μm), which were placed in a furnace preheated to 550°C for three hours, and the mass determined once cooled. Using the same filters, 500 ml of water sample was passed through and dried for three hours at 105°C, allowed to cool and the mass recorded. The filters were then placed back in a furnace for a further three hours at 550°C, and the mass noted once cooled. The mass difference between the last two heating phases (at 105°C and 550°C) quantified the particulate organic matter (POM) present. This was subsequently converted into POC by assuming that organic matter is 50% carbon (Hope et al., 1994). This method measured the

concentration of POC (mg) in a volume of 500 ml¹ which was subsequently converted into the standard unit of mg L⁻¹.

2.7 Hydrological measurements

Salt dilution gauging was used to calculate the discharge rate (m³ s⁻¹) from the plantation drains over a range of flow conditions, calculated by:

$$Q = \frac{V}{k\Delta t \sum_n [EC(t) - EC_{bg}]} \quad (2.1)$$

where: Q is the stream discharge (m³ s⁻¹), k is the calibration constant, $EC(t)$, is the electrical conductivity measured at a discrete time interval t (e.g. 5 seconds), EC_{bg} is the background electrical conductivity and V is the volume of salt solution injected (e.g 1 kg of salt per litre of water).

Discharge rates were then used to create individual drainage channel rating curves by plotting a series of concurrent measurements of stage height and discharge, across the various stream flow conditions. The relationship between stage height and discharge was subsequently expressed by applying a line of 'best-fit' to the observed measurements (Figure 2.28). Using the respective line equations, stage height could then be converted into discharge measurements, generating continuous flow data for the whole sample period.

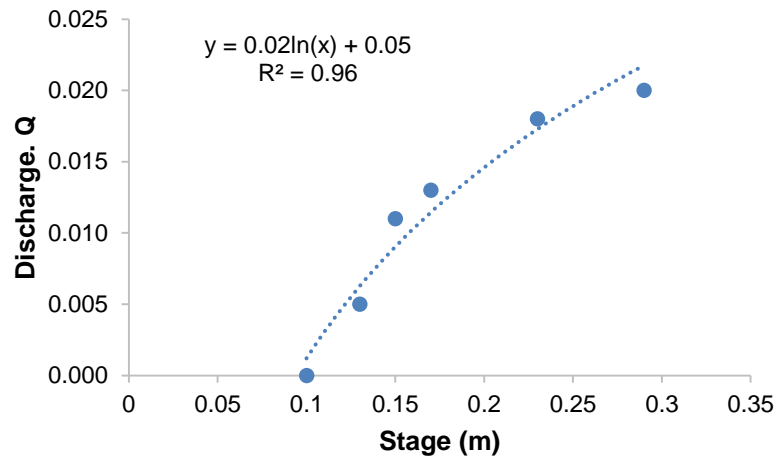


Figure 2.28 Example of a plantation drainage channel rating curve, alongside the goodness of fit (r^2) and equation used to describe the relationship between stage height and discharge

Gauge posts were installed in plantation channels (Figure 2.29), constructed from PVC pipes with measurement markings down the side. When water samples were collected a manual measurement of the channel stage height was noted and plotted onto the corresponding rating curve, generating a discharge measurement for the time of collection. In addition, water levels within some of the drainage channels were ‘continuously’ measured (at 1 hour intervals) using absolute pressure water level loggers (Mini-Divers, Schlumberger, D1501), allowing a continuous record of stage heights and therefore discharge values to be generated throughout the year. Barometric pressure was also monitored, using a Baro-diver® (Schlumberger), to enable the conversion of the raw water pressure data into ‘actual’ water levels. Table 2.4 provides an outline of the method used to monitor in-channel water height, for all the plantation study sites. Mini divers® (Schlumberger, were installed into a total of 8 study sites. The remaining study sites were gauged manually except for SA 1.1, SA 3.2 and SA 3.3, which experienced sporadic changes in their hydrological regime, as a result of plantation management efforts i.e. ditch blocking and channel widening. Overall, there were 14 locations at which flow was monitored.



Figure 2.29. Example of gauge posts installed in a plantation channel

Table 2.4 Individual plantation study sites alongside the drain type (M = main, C= collection) and gauge method for channel water height

Plantation estate	Site	Drain	Gauge method
Sebungan	SE1	M	mini diver
	SE2	C	mini diver
	SE3	C	mini diver
	SE4	C	mini diver
Sabaju 1	SA 1.1	C	water only
	SA 1.2	C	mini diver
	SA 1.3	C	manual stage
	SA 1.4	M	mini diver
Sabaju 3	SA 3.1	C	manual stage
	SA 3.2	C	water only
	SA 3.3	C	water only
	SA 3.5	M	manual stage
	SA 3.6	C	manual stage
Sabaju 4	SA 4.1	M	mini diver
	SA 4.2	M	manual stage
	SA 4.3	C	manual stage
	SA 4.4	C	mini diver

2.8 Carbon flux calculations

Both the channel discharge (Q) and the channel water carbon concentration (C) are required to calculate the instantaneous carbon flux, briefly

$$J=C.Q \quad (2.2)$$

where: J is the annual DOC/POC flux (mg yr^{-1}), C is the concentration of DOC/POC in (mg L^{-1}) and Q is the drain discharge/runoff in mm yr^{-1}

The total yearly flux can then be derived by an integration of the instantaneous fluxes. However, in practice, it is rare that both continuous and exact flow measurements are obtained alongside a continuous record of concentration data (Moatar & Meybeck, 2005). As such, uncertainty can come from the method used to temporally integrate the discrete concentration and flux data (Moatar & Meybeck, 2005). To address this Walling & Webb (1985) propose five interpolation algorithms that can be used to estimate loads, based on the relationship between flow and concentration. An interpolation approach is required when continuous flow data is sparse but where concentration and discharge data, at the time of sampling, are available. The following subsections outline various approaches to estimate fluvial organic carbon fluxes, based on the underlying principals discussed within Walling & Webb (1985).

2.8.1 Catchment area

One approach (Method 3; Walling & Webb, 1985; Littlewood, 1992) can be to multiply the instantaneous DOC/POC concentration by the mean channel discharge over the period (i.e. one week) between samples (Q_p), briefly

$$J_s = C_i.Q_p \quad (2.3)$$

Where J_s is the flux expressed in mg s^{-1} , C_i is the instantaneous DOC/POC concentration (mg L^{-1}) and Q_p is the mean channel discharge over the period between sampling (mm s^{-1}).

J_s can then be upscaled to an appropriate magnitude (weekly) and expressed per unit area (i.e. area specific flux in $\text{g C m}^{-2} \text{ week}^{-1}$) by dividing the carbon flux by the known catchment area, given by

$$J_{a.s.w} = \frac{J}{A} \quad (2.4)$$

where: $J_{a.s.w}$ is the weekly area specific DOC/POC flux ($\text{g C m}^{-2} \text{ week}^{-1}$) and A is the catchment area (m^2).

The $J_{a.s.w}$ data can then be summed together to give the yearly area specific flux ($J_{a.s.y}$; $\text{g C m}^{-2} \text{ year}^{-1}$), briefly

$$J_{a.s.y} = \sum J_{a.s.w} \quad (2.5)$$

2.8.2 Water mass balance approach

The annual water mass balance (WMB) of a closed hydrological system can be used to determine the system's annual flow volume (R_E , m yr^{-1}) via a comparison of system inputs (precipitation, P , m yr^{-1}) and outputs (actual evapotranspiration, ET_a , m yr^{-1}), briefly

$$R_E = P - ET_a \quad (2.6)$$

The WMB assumes a zero change in water storage over time. R_E can then be multiplied by the mean TOC concentration (TOC_{mean} ; mg L^{-1}), for the catchment, to calculate the annual area-specific flux ($J_{a.s.y}$), briefly

$$J_{a.s.y} = (P - ET_a) \times TOC_{mean} \quad (2.7)$$

A WMB approach can be achieved using various methods, including i) chloride (Cl⁻) mass balance (CMB) and ii) soil water balance modelling.

2.8.2.1 Chloride mass balance

Actual evapotranspiration (ET_a) can be calculated using a combination of precipitation values (P) and discharge (Q) briefly:

$$ET_a = P - Q \quad (2.8)$$

The CMB approach is based on a number assumptions i) that all Cl⁻ is derived from atmospheric deposition, with consistent inputs across all sites, ii) there is no storage of Cl⁻ within the catchment and iii) Cl⁻ concentration is not altered during transport throughout the catchment (Auterives et al., 2011; Moore et al., 2013). Subsequently, the rainfall signature is only modified by evapotranspiration rates (Auterives et al., 2011) and thus,

$$C_p \cdot P = C_Q \cdot Q \quad (2.9)$$

where, C_p is the mean concentration of Cl⁻ in a rain sample (mg L⁻¹) and C_Q is the mean concentration of Cl⁻ in water discharge (mg L⁻¹).

Equation 2.9 can be rearranged to determine Q by,

$$Q = \frac{C_p \cdot P}{C_Q} \quad (2.10)$$

Equation 2.10 can be substituted back into equation 2.8 to determine ET_a , using the ratio between C_Q and C_p , briefly,

$$ET_a = P \cdot \frac{C_p - C_Q}{C_p} \quad (2.11)$$

The chloride derived ET_a estimate can then be substituted back into equation 2.6 to determine R_E , which is then multiplied by the mean TOC concentration to determine the flux ($J_{a.s.y}$; equation 2.7).

2.8.2.2 Soil water balancing model

Rainfall runoff modelling is a valuable tool for conceptualizing the water mass balance of a catchment (Whelan & Gandolfi, 2002; Pullan et al., 2016; Najmaddin et al., 2017). Najmaddin et al. (2017) and Pullan et al. (2016) describe a simple yet physically realistic soil-to-water transport model based on the water balance equation (2.10) briefly,

$$\Delta = P - ET_A - q \quad (2.12)$$

where Δ the change in soil water storage over time, P is precipitation as rainfall (mm day^{-1}), ET_A is actual evapotranspiration (mm day^{-1}) and q is the vertical drainage of water out of the system (mm day^{-1}). A visual representation of this model is presented in Figure 2.30

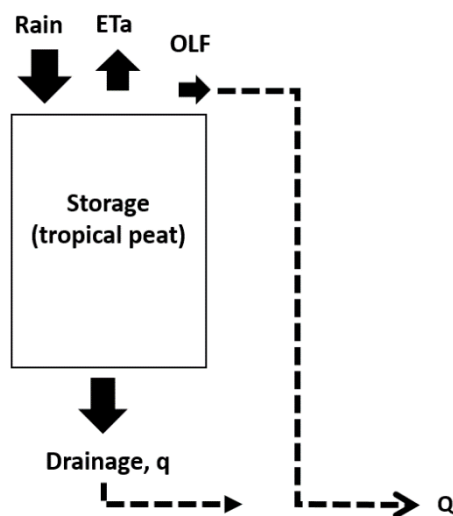


Figure 2.30. Conceptual diagram of the key water transport pathways in the model

ET_A is calculated from reference evapotranspiration (ET_0) which can be calculated using the Penman-Monteith equation, given by

$$\lambda ET_0 = \frac{\Delta (R_n - G) + \rho_a c_p \frac{(e_s - e_a)}{r_a}}{\Delta + \gamma \left(1 + \frac{r_s}{r_a}\right)} \quad (2.13)$$

where: ET_0 = reference evapotranspiration (mm day^{-1}), R_n = net radiation at the crop surface ($\text{MJ m}^{-2} \text{day}^{-1}$), G = soil heat flux density ($\text{MJ m}^{-2} \text{day}^{-1}$), ρ_a = air density (kg m^{-3}), c_p = specific heat of dry air ($\text{MJ kg}^{-1} \text{ }^\circ\text{C}^{-1}$), e_s = saturation vapour pressure (kPa), e_a = actual vapour pressure (kPa), $e_s - e_a$ = saturation vapour pressure deficit (kPa), D = slope vapour pressure curve ($\text{kPa } ^\circ\text{C}^{-1}$), γ psychrometric constant ($\text{kPa } ^\circ\text{C}^{-1}$), r_a = bulk surface aerodynamic resistance for water vapor (s m^{-1}), r_s = the canopy surface resistance (s m^{-1}).

Using the ET_0 estimate it is also possible to calculate the potential evapotranspiration (ET_p ; mm d^{-1}) using resistance factors (K_c), to account for specific vegetated surfaces (i.e forest or crop surfaces), thereby giving an insight into water stresses within the different ecosystems (Ward & Robinson, 2000; Allen, 2003; Liu et al., 2017), briefly

$$ET_p = ET_0 \cdot K_c \quad (2.14)$$

The vertical drainage of water from the soil (q) is estimated by assuming a unit hydraulic gradient ($\text{grad } \theta = -1$) and unsaturated hydraulic conductivity ($K(\theta)$). The flux is therefore proportional to $K(\theta)$ briefly,

$$q = K(\theta) \quad (2.15)$$

where $K(\theta)$ is the unsaturated hydraulic conductivity (mm day^{-1}) at an average profile volumetric water content (θ , $\text{cm}^3 \text{ cm}^{-3}$).

$K(\theta)$ is predicted using the Mualem-Van Genuchten model (Najmaddin et al., 2017) given by,

$$K(\theta) = K_{sat} \cdot \theta_*^{0.5} \cdot \left[1 - \left(1 - \theta_*^{\frac{1}{m}} \right)^m \right]^2 \quad (2.16)$$

where K_{sat} is the saturated hydraulic conductivity (mm day^{-1}), m is an empirical shape factor parameter of the soil water retention curve and θ_* is the dimensionless water content.

The shape factor parameter m relates to the van Genuchten parameter n and is given by,

$$m = 1 - \left(\frac{1}{n} \right) \quad (2.17)$$

The model can then be calibrated on a site where detailed flow data and an approximation of catchment size are known. Assuming the calibrated parameters are applicable to all sites, the calibrated model can then be applied to other catchments where detailed flow data is available but where catchment area is unknown. The area can then be derived from the model and used to calculate the area specific flux as outlined in equation 2.4.

2.8.3 Flow weighted TOC concentrations

This approach involves multiplying flow-weighted TOC concentrations by the annual flow volume. A worked example of this method is outlined in Appendix B. It is also referred to as the Method 5 algorithm within Littlewood (1992) and has been shown to perform well for many empirical studies using infrequent concentration and discharge data (Moatar and Meybeck, 2005; Littlewood and Marsh, 2005; Birgand et al., 2011). It is given by,

$$J_{a.s.y} = \frac{\sum(C_i \cdot Q_i)}{\sum Q_i} \cdot R_E \quad (2.18)$$

where, $J_{a.s.y}$ is the area-specific flux ($\text{g C m}^{-2} \text{ yr}^{-1}$), C_i (g C m^{-3}) is the instantaneous (sampled) concentration of TOC (DOC+POC; mg L^{-1}) on sampling date i , Q_i is the corresponding discharge at the time of sampling on date i ($\text{m}^3 \text{ s}^{-1}$) and R_E is the annual flow volume ($\text{m}^3 \text{ yr}^{-1}$).

R_E can be calculated by dividing the measured annual discharge data (Q_A , $\text{m}^3 \text{ yr}^{-1}$) by the catchment's known area (A , m^2), briefly

$$R_E = \frac{Q_A}{A} \quad (2.19)$$

In the case of the plantations, R_E was assumed to be the same for all plantation sites. This allows for the flux ($J_{a.s.y}$) to be estimated even in the absence of a catchment area for all sites.

Equation 2.19 can be rearranged to calculate an unknown catchment area ($A_{unknown}$, m^2), assuming an equal value for R_E , by dividing the annual measured discharge (Q_A , m^3) by the area specific runoff depth (R_E):

$$A_{unknown} = \frac{Q_A}{R_E} \quad (2.20)$$

2.9 Environmental parameters

2.9.1 Rainfall

An automated rainfall gauge (Davis Vantage Pro 2) was set up at the Sebungan plantation base to monitor rainfall (mm) at half hourly intervals. In addition, monthly rainfall data was also acquired from the estate plantation offices (Sebungan and Sabaju) who provided manual rain gauge readings (August 2015 - August 2016). Due to equipment failure, daily rainfall data from the automated gauge could only be obtained from 1st August 2015 until the 6th January, 2016. As a result, a value for annual rainfall was derived by averaging the data from the automated records, when available, and the manually derived data.

2.9.2 Watertable height

Peatland watertable heights were determined using dipwells (Figure 2.26). Clusters of three dipwells (0.5m apart) were installed throughout the plantation and forest sites. Within the plantations, dipwells were established within the center of the planting blocks and marked with tape to avoid destruction during plantation harvesting. Before installation an auger was used to create an appropriate hole, preventing excessive peat smearing during dipwell installation, which could cause the holes to become blocked, restricting water flow. Measurements of water table height were made during each field sampling visit and at the same time as water samples were collected,. First the height of the dipwell above the peat surface was recorded (H). Then using an automated dipmeter (In-situ Rugged Water Level TAPES) the depth of the water inside the tube was measured (D). These two readings were then subtracted from one another (H-D) to give the overall height of the watertable below the peat surface.

2.10 Statistical analyses

Statistical analysis was performed using GraphPad Prism, version 7. The level of statistical significance was set at a probability of 0.05 but greater significance was also noted. For multiple comparisons, one-way ANOVAs were performed, based on the assumptions that the data adhered to normality and homogeneity of sample variance. If significant differences between the group means were identified then a *post-hoc* test was carried out. Normality was tested using the Shapiro-Wilk normality test and homogeneity using the Bartlett test. Where Shapiro-Wilk was $p > 0.05$ the Bartlett test was then performed. If the result for the Bartlett test was $p > 0.05$ then parametric statistics were employed on the data set. Where the Bartlett test was $p < 0.05$, data was log transformed and if these variables were still $p < 0.05$ then the data was subjected to non-parametric testing. The non-parametric Kruskal-Wallis test was performed on non-normally distributed data and *post-hoc* test carried out as above. In addition, the relationship between variables was tested using linear regression models.

Chapter Three: The preservation and quantification of dissolved organic carbon (DOC)

3.1 Introduction

This Chapter is divided into two methodology subsections. Chapter 3A focuses on the effects of cold storage (4°C) as a preservation method for tropical DOC water samples. This work was undertaken in order to develop an acceptable storage method for preserving both the collected DOC water sample concentrations and optical absorbance properties, in between analysis in Malaysia and the UK. Chapter 3B evaluates the use of UV-visible spectroscopy for determining tropical DOC concentrations. This was undertaken in order to provide tropical researchers with better guidance on analysis techniques for DOC water samples which can be undertaken at remote field sites allowing immediate post collection analysis. Chapter 3B concludes with a discussion on the uncertainties associated with the spectroscopy derived DOC concentrations and how this was factored into the calculation of fluvial carbon fluxes.

Chapter 3A Cold storage as a method for the long-term preservation of tropical dissolved organic carbon (DOC)

This chapter is published in Mires and Peat: **Cook, S.**, Peacock, M., Evans, C.D., Page, S.E., Whelan, M., Gauci, V., Khoon, K.L, 2016. *Cold Storage as a method for the long-term preservation of tropical dissolved organic carbon (DOC)*. Mires and Peat 18: 1-8, DOI: 10.19189/MaP.2016.OMB.249

3.1A Abstract

Fluvial fluxes of dissolved organic carbon (DOC) may represent an important loss for terrestrial carbon stores in the tropics. However, there is currently limited guidance on the preservation of tropical water samples for DOC analysis. Commonly employed preservation techniques such as freezing or acidification can limit degradation but may also alter sample properties, complicating DOC analysis. We examined the effects of cold storage at 4 °C on DOC concentration and quality in water samples collected from a tropical peat catchment. Samples were stored in the dark at 4 °C for periods between 6 and 12 weeks. Freeze/thaw experiments were also made. Mean DOC concentrations in samples stored for 6 weeks at 4 °C were 6.1 % greater relative to samples stored at ambient room temperature (33 °C) over the same period. Changes in DOC concentrations, in two sample sets, during cold storage were found to be $2.25 \pm 2.9 \text{ mg L}^{-1}$ (8 %) to $2.69 \pm 1.4 \text{ mg L}^{-1}$ (11 %) over a 12-week period. Freeze/thaw resulted in alterations in the optical properties of samples, and this in turn altered the calculated DOC concentrations by an average of 10.9 %. We conclude that cold storage at 4 °C is an acceptable preservation method for tropical DOC water samples, for moderate time periods, and is preferable to freezing or storage at ambient temperatures.

3.2A Introduction

Dissolved organic carbon (DOC) is becoming increasingly recognised as an important component of the global carbon cycle (Cole et al., 2007). The fluvial transport of DOC provides an important pathway for carbon transfer from terrestrial to aquatic ecosystems (Kalbitz et al., 2000; Freeman et al., 2004). DOC is biologically and chemically reactive (Cauwet, 2002; Benner, 2004; Moore et al., 2011), leading to important emissions of carbon dioxide to the atmosphere (Evans et al., 2012; Muller et al., 2015; Evans et al., 2015).

The susceptibility of DOC to microbial and photochemical degradation makes the long-term storage of DOC water samples challenging, with guidance suggesting analysis take place within 48 hours of sampling (Karanfil et al., 2002). Where this is not possible, attempts are often made to preserve samples i.e. to limit biological, chemical and physical degradation, allowing them to be stored and analysed later. Common preservation practices include freezing and acidification (Moore et al., 2011; Peacock et al., 2014). However, these can alter both the concentration of DOC and its absorbance and fluorescence properties, influencing specific UV absorbance (SUVA, at 254 nm) and E ratios (Spencer et al., 2007; Fellman et al., 2008; Peacock et al., 2015). These ratios can give a valuable insight into the specific structural and compositional properties of DOC (Thurman, 1985; Peacock et al., 2014). The E2:E3 ratio (254 nm: 350 nm), is often used as an indication of aromaticity and the molecular weight of humic substances (Peuravuori and Pihlaja, 1997). Similarly SUVA₂₅₄ is also a measure of aromaticity: high SUVA₂₅₄ values indicate high recalcitrance (Weishaar et al., 2003). The E2:E4 ratio (254 nm: 400 nm) is frequently used to indicate the degree of humification (Park *et al*, 1999) whereas the E4:E6 ratio (400 nm; 600 nm) is a measure of the molecular weight (Thurman, 1985). Acids used for preservation include hydrochloric, phosphoric and dilute sulphuric (Sharp et al., 1993; Moore et al., 2011) which typically lower sample pH to below 3.5. This ensures the quantitative removal of DIC (dissolved inorganic carbon) and suppression of microbial activity via enzyme denaturation (Sharp et al., 1993). However, pH changes can induce

flocculation and coagulation of DOC (Worrall et al., 2006), complicating or vitiating analyses.

Peacock et al., (2014; 2015) have investigated the effectiveness of cold storage at 4 °C as an alternative DOC preservation method. Peacock et al., (2014) reported little change in the absorbance properties of DOC in water samples collected from a UK ombrotrophic peatland when filtered and stored in this way for a period of 12 weeks. A second study found that only 5 % of DOC was lost in cold storage over a similar period (Peacock et al., 2015). Additional studies found no significant changes in DOC concentrations in samples stored at 4 °C for periods of 2 weeks and 7-17 weeks, respectively (Ekström et al., 2011; Carter et al., 2012).

Taken together, these investigations suggest that storing filtered water samples in the dark, at 4 °C is viable for medium-term (e.g. 2-17 weeks) preservation of DOC and that this storage method does not hinder subsequent DOC analyses. However, these studies were all focused on water samples collected from temperate peatlands. We know of no published study of the effectiveness of cold storage on the quality and quantity of DOC in samples collected from tropical peatlands. Recently there has been a strong interest in DOC losses from tropical peatland catchments (Sjogersten et al., 2014; Muller et al., 2015) particularly in relation to anthropogenic disturbance (Moore et al., 2011; 2013). This has been driven, in part, by a realisation that losses of carbon from tropical peatlands to 'blackwater' rivers may be substantial (Evans et al., 2014), coupled with the recognition that these areas function as significant long-term carbon stores (Page et al., 2011). Investigations of tropical systems tend to be carried out in remote places with limited on-site laboratory facilities. Robust sample preservation methods are therefore paramount.

The two aims of our investigation were:

- (1) To quantify the effect of cold storage on the concentration and quality of tropical DOC;
- (2) To assess whether quantitative and qualitative DOC changes during the storage of samples from tropical peatlands differ from those in samples from high-latitudes.

3.3A Methods

The study sites for this investigation were in the Malaysian province of Sarawak, northern Borneo, Southeast Asia. This region is characterized by an equatorial climate with high, temperatures (mean 26 °C) throughout the year and heavy rainfall (3000 mm yr⁻¹), without a distinct dry season (Melling et al., 2005). Water samples were collected from the Sebungan and Sabaju oil palm estates, east of the coastal town of Bintulu (from 3°07.81' N to 3°14.91'N, and 113°18.72' E and 113°32.19'E). The estates belong to the Sarawak Oil Palms Berhad (SOPB), Bintulu division and cover a total area of 9,614 ha.

All water samples were collected and stored in 60 ml transparent polypropylene Nalgene® bottles. Electrical conductivity ($\mu\text{S cm}^{-1}$), pH and temperature (°C) were measured on the unfiltered samples as they were collected. The bottled samples were transported immediately back to the field laboratory. There, samples were filtered through 0.45 μm cellulose nitrate membrane filters, using a hand-held vacuum pump. Two preservation experiments were conducted.

In Experiment 1, DOC concentrations in refrigerator-stored samples were compared to those in samples stored at ambient temperature, for a period of six weeks.

In Experiment 2, DOC concentrations were determined on samples a short time (within 5 days) after collection and compared with concentrations determined on the same samples after cold storage (4 °C) for approximately 12 weeks.

Details of these experiments follow.

3.3.1A Experiment 1. Effect of cold storage on DOC quantity and quality

Ten 60 ml water samples were collected from drainage ditches within the Sebungan oil palm plantation estate on 14th April 2015. Average water sample pH was 3.7, with temperature and electrical conductivity averaging 26 °C and 167 $\mu\text{S cm}^{-1}$, respectively. After filtration each sample was divided, resulting in two sets of identical samples. The 30 ml subsamples were stored in 60 ml bottles (30 ml of sample + 30 ml of air). One set was placed in a refrigerator set at 4 °C and the other was stored at ambient temperature (*ca* 33 °C) in a dark cabinet, for a period of 6 weeks, after which samples were transported in polystyrene boxes, by courier, back to the UK. Total transport time took no more than 4 days, during which samples were kept in air-conditioned facilities (< 18 °C).

Upon return to the UK, samples were analysed using the non-purgeable organic carbon (NPOC) method (Sharp, 1993) on a Shimadzu Total Carbon analyser. Samples were acidified with 1 M hydrochloric acid so pH < 3, via syringe injection, and then sparged with purified air to remove any inorganic carbon (IC) (Sharp, 1993). Total organic carbon was then measured using a non-dispersive infrared sensor and subsequently compared to an NPOC calibration curve, with standards ranging from 0-100 mg L⁻¹. In addition, UV-visible absorbance of the filtered water samples was also measured using a Helios Gamma spectrophotometer at wavelengths of 254, 270, 350, 400, 600 and 700 nm. This allowed the quality of the DOC to be quantified by calculating the E2:E3, the E2:E4 and the E4:E6 ratios, along with SUVA₂₅₄. SUVA₂₅₄ values were calculated using Equation 3.1.

$$\text{SUVA}_{254} = 100 \cdot \left(\frac{A_{254}}{C_{\text{DOC}}} \right) \quad (3.1)$$

where: SUVA₂₅₄ has units of L mg-C⁻¹ m⁻¹, A₂₅₄ is the absorbance at 254 nm and C_{DOC} is the DOC concentration (mg L⁻¹).

3.3.2A Experiment 2. DOC changes during cold storage and the effect of freeze/thaw

An additional 34 water samples were collected from drainage ditches within both the Sebungan and Sabaju oil palm estates, on 3rd August 2015 (sample set 1) and on 5th October 2015 (sample set 2). Average pH ranged from 3.6 to 4.4 for sample sets 1 and 2, respectively. Average temperatures for sample set 1 was 29 °C and 30 °C for sample set 2, with average electrical conductivity values of 200 $\mu\text{S cm}^{-1}$ and 196 $\mu\text{S cm}^{-1}$, for sample set 1 and 2, respectively. Samples were filtered in the same way as those collected on 14th April 2015 (see Experiment 1, above) and stored at 4 °C for an average of 12 weeks (73 to 101 days constrained by availability of analysis equipment; cold storage time represents total cold storage time both in the UK and tropics). During this time, the samples were analysed on a portable Cole-Parmer UV/visible spectrophotometer at wavelengths of 270, 350, 400, 600 and 700 nm, within 5 days of collection. DOC concentrations were determined using a two-wavelength approach (Tipping et al., 2009; Carter *et al*, 2012) and the universal calibration parameters outlined in Carter et al., (2012). Samples were transported back to the UK as described in Experiment 1.

Upon return to the UK samples from set 1 ($n=17$) were reanalyzed on a spectrophotometer (Cole-Parmer UV/visible spectrophotometer, across the same spectrum of wavelengths, on 11th November 2015 (i.e. 101 days after sample collection). The same procedure was carried out on samples from set 2 ($n=17$), on 16th December 2015 (ie.73 days after sample collection). Similarly, DOC concentrations were determined using the same two-wavelength approach (Tipping et al., 2009; Carter *et al*, 2012), as described above.

DOC concentrations determined at the field laboratory were compared with the post-storage concentrations determined in the UK in order to estimate changes in DOC concentration occurring during cold storage (4 °C) and transport (< 18 °C).

After analysis, samples from sample set 1 ($n=17$) were frozen at $-20\text{ }^{\circ}\text{C}$ for 48 hours and then left to melt at ambient laboratory temperature in the dark. These samples were then re-analysed for absorbance at 270, 350 and 700 nm.

3.3.3A Statistical analyses

Quantitative data analysis was performed using parametric statistical tests when appropriate (GraphPad Prism, version 6). Normality was tested using the Shapiro-Wilk test and homogeneity using the Bartlett test. Differences between samples were then assessed using t-tests (paired and un-paired) and ANOVAs. Where data were not normally distributed, Mann-Whitney, Wilcoxon, Kruskal Wallis and Friedman tests were used.

3.4A Results

3.4.1A Experiment 1. Effect of cold storage on DOC quantity and quality

In Experiment 1, DOC concentrations in the refrigerated samples were significantly greater ($P \leq 0.0001$) than those stored at room temperature (Figure 3.1A). Differences in concentrations ranged from 0.26 mg L^{-1} (0.7 % difference) to 3.79 mg L^{-1} (9.9 % difference). The mean DOC concentration from the refrigerated samples was 6.1 % ($2.4 \pm 0.4\text{ mg L}^{-1}$) greater than that from samples stored at ambient temperature. Similarly, absorbance at 254 nm was significantly greater ($P \leq 0.001$) in refrigerated samples than those stored at room temperature (Figure 3.1A), by an average of 0.11 ± 0.02 .

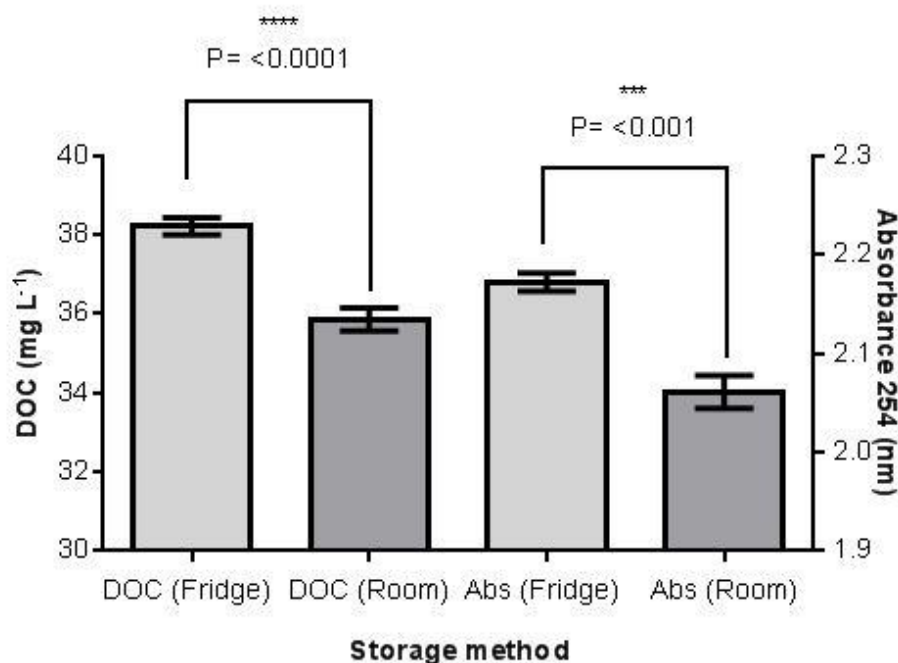


Figure 3.1A. Average DOC concentrations and absorbance at 254 nm for the two storage methods in Experiment 1. Error bars indicate the standard error of the mean. The degree of statistical significance between the two methods (paired two tailed, t-test) is also shown ($n=10$).

SUVA₂₅₄ values ranged between 5.6 - 5.9 L mg-C⁻¹ m⁻¹ for all samples in Experiment 1. These values are high compared to river systems, both northern (1.3 – 4.5 L mg-C⁻¹ m⁻¹) and tropical (3.7 - 4.1 L mg-C⁻¹ m⁻¹) latitudes (Spencer et al., 2008; Moore et al., 2013). A statistically significant negative relationship (Figure 3.2A) was found between SUVA₂₅₄ and differences in DOC concentrations ($R^2= 0.452$; $P \leq 0.05$). This demonstrate that high SUVA₂₅₄ values, an indicator of recalcitrance, correlate with low DOC differences between storage techniques and thus, suggests recalcitrant DOC in samples stored at room temperature maybe less susceptible to biodegradation over time. However, due to the small range in our SUVA₂₅₄ values these findings cannot conclusively support SUVA₂₅₄ as an indicator for DOC aromaticity.

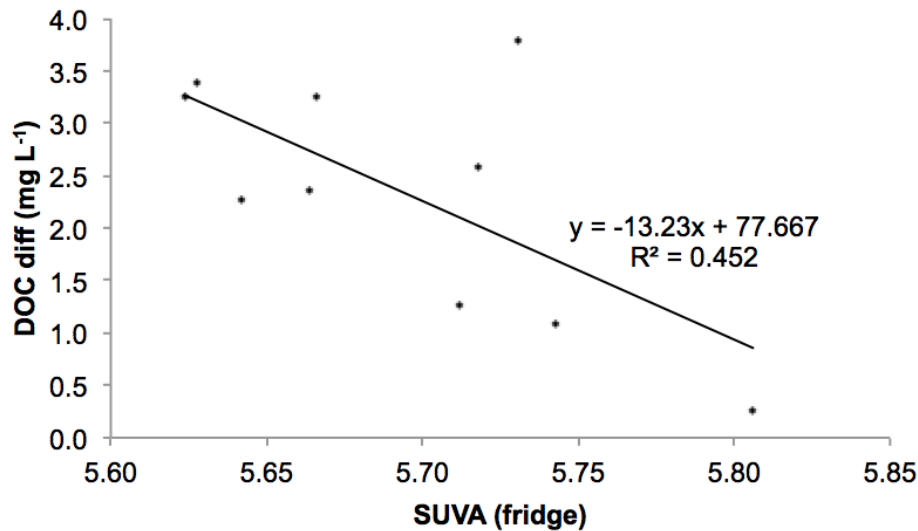


Figure 3.2A. Relationship between SUVA of the refrigerated samples and DOC concentration differences between the two storage techniques, in Experiment 1. The regression was significant ($P \leq 0.05$). The large numerical constants look implausible but are correct. They result from counterbalancing the x- multiplier and the constant over the very small x-range involved.

3.4.2A Experiment 2. DOC changes during cold storage

Absorbance changes

Differences in absorbance measured immediately after sampling and after approximately 12 weeks of cold storage are shown in Figure 3.3A. In sample set 1, absorbance gains were displayed in 9 samples and losses in 8 samples, at wavelengths of both 270 nm and 350 nm. At a wavelength of 700 nm absorbance gains were recorded in 10 samples and losses in three samples, whilst four samples showed no change. In contrast, sample set 2 exhibited gains in all samples at 270 nm, and only two losses out of the 17 samples at both 350 nm and 700 nm.

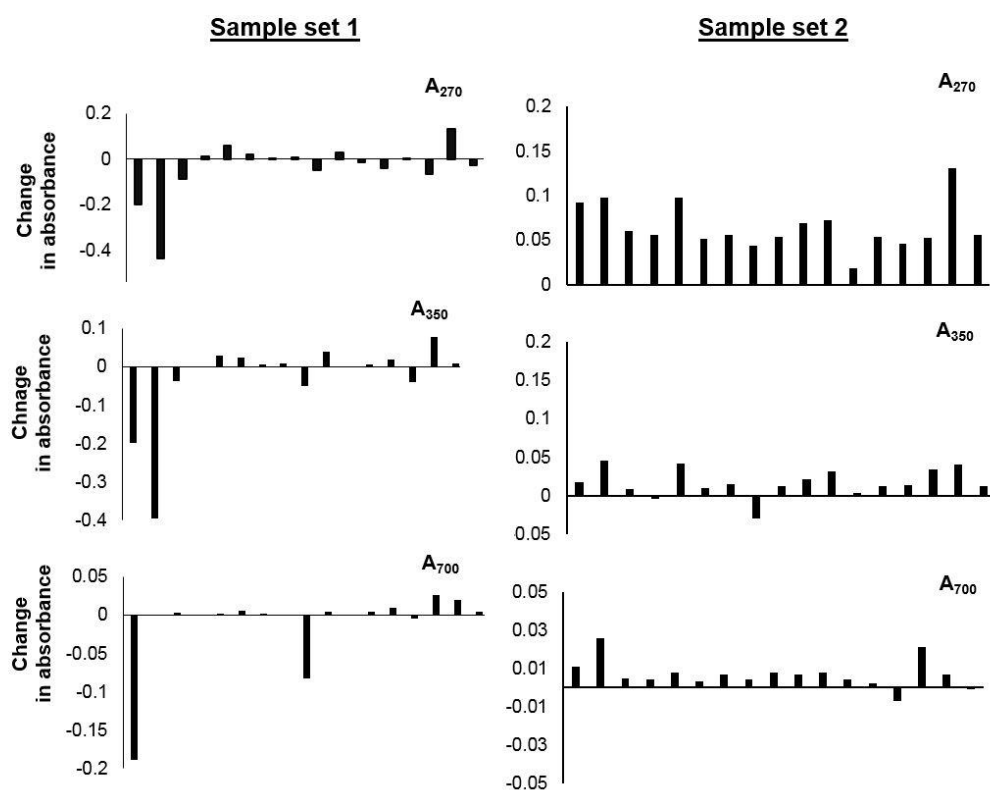


Figure 3.3A. Changes in absorbance values at 270 nm (A_{270}), 350 nm (A_{350}) and 700 nm (A_{700}), of samples kept in cold storage (4 °C) for approximately 12 weeks, from the same samples analysed immediately after collection, in Experiment 2. Positive values are increases. There are two sets of 17 samples, Set 1 collected on 3rd August 2015; Set 2 on 5th October 2015.

Mean absolute absorbance changes at 270 nm were 0.07 ± 0.03 and 0.065 ± 0.006 , for sample sets 1 and 2, respectively. For both sample sets, absorbance values at 270 nm after cold storage, were statistically significant ($P \leq 0.05$) from the original absorbance values before cold storage. Mean absolute absorbance changes at 350 nm were notably higher in sample set 1 (0.06 ± 0.02) compared with sample set 2 (0.024 ± 0.004). However, absorbances at 350 nm before and after cold storage, for both sample sets, did not differ significantly ($P > 0.05$). Changes in absolute absorbance at 700 nm were 0.02 ± 0.01 and 0.009 ± 0.002 for sample sets 1 and 2, respectively, resulting in significant differences ($P \leq 0.01$) between the absorbance values recorded before and after cold storage at 700 nm, for both sample sets.

DOC changes

The overall average absolute % difference in DOC concentration before and after cold storage was 9.6 % ($2.5 \pm 0.5 \text{ mg L}^{-1}$). In sample set 1 the average normalised difference in DOC concentration was $2 \pm 1 \text{ mg L}^{-1}$ (i.e. 8 %) and in sample set 2 it was $2.7 \pm 0.4 \text{ mg L}^{-1}$ (i.e. 11 %) (Figure 3.4A). Percentage changes in DOC concentrations were significantly greater in sample set 2 compared with sample set 1 ($P \leq 0.05$) (Figure 3.4A).

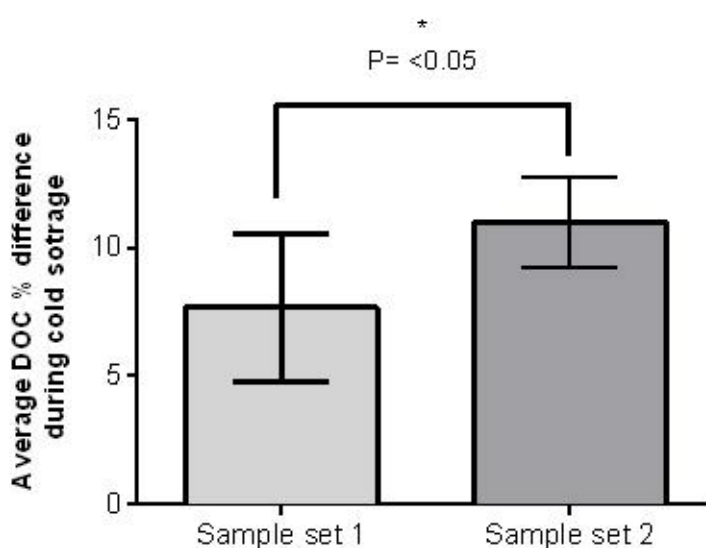


Figure 3.4A. Average normalised % differences in DOC observed before and after approximately 12 weeks of cold storage ($4 \text{ }^{\circ}\text{C}$) for the same sample for both sample sets, in Experiment 2. DOC concentrations were calculated using the two-wavelength approach (Carter et al., 2012). Error bars show the standard error of the mean. The significance of differences is also shown (unpaired, two-tailed, t-tests, $n=17$).

3.4.3A Experiment 2. Effect of freezing and thawing on DOC quality

Following freeze/thaw, absorbance losses were observed for all samples at both 270 and 350 nm (Figure 3.5A). At 700 nm, there was a reduction in absorbance in ten samples and an increase in absorbance in six samples with

no change in one sample (Figure 3.5A). The average change in absolute absorbance at 270, 350 and 700 nm, before and after freeze/thaw, was 0.07 ± 0.02 , 0.034 ± 0.008 and 0.003 ± 0.001 , respectively. Absorbance values after freeze/thaw in comparison to the original absorbances were found to be significantly different ($P \leq 0.0001$) at wavelengths of 270 nm and 350 nm, but not at 700 nm ($P > 0.05$).

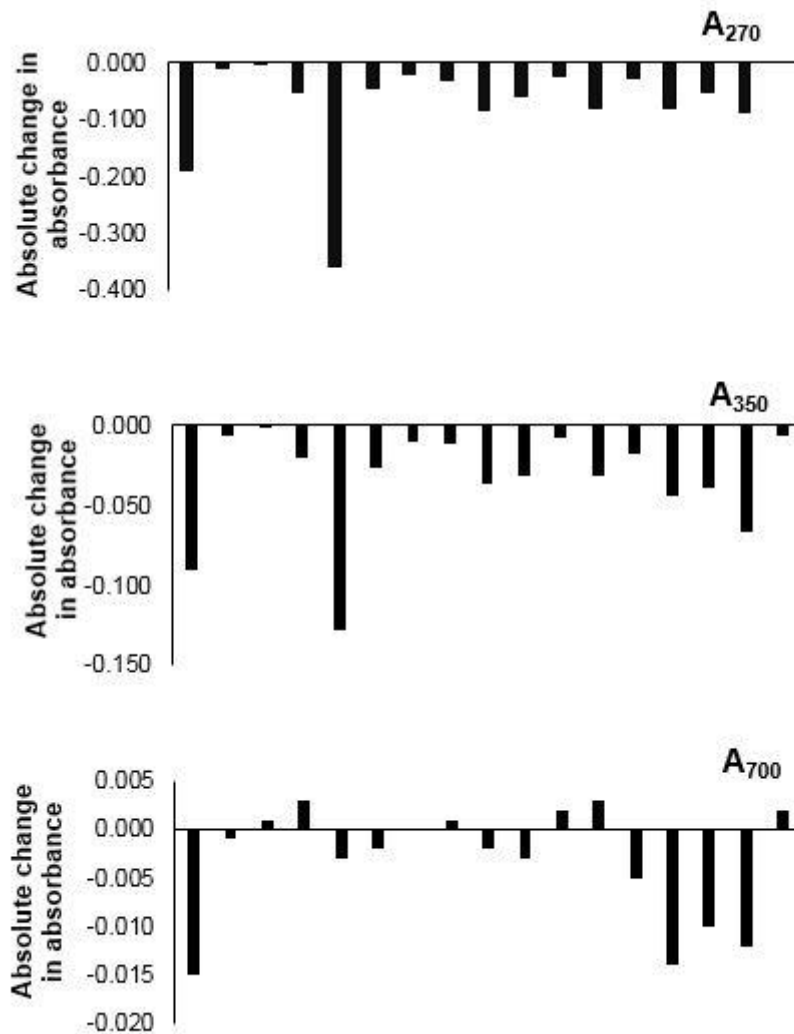


Figure 3.5A. Changes in absolute absorbance values at 270 nm (A_{270}), 350 nm (A_{350}) and 700 nm (A_{700}), following freeze/thaw, in Experiment 2. Positive values are increases. There is one set of 17 samples.

Average calculated DOC concentrations, using the two-wavelength approach, before and after freeze/thaw are shown in Figure 3.6A. The freeze/thaw process resulted in a small loss in overall calculated DOC concentrations, which was not significant compared to the original DOC concentration recorded in August 2015. Absolute changes in DOC concentrations after the freeze/thaw process ranged from 0.12 to 18.5 mg L⁻¹ across the sample set, with an average change of 3 ± 1.1 mg L⁻¹. This represents a 10.9 % difference compared to the original DOC concentrations recorded in August 2015. However, because the freeze/thaw process resulted in significant ($P \leq 0.0001$) alterations to the DOC spectra at 270 nm and 350 nm (Figure 3.5A), this will probably have resulted in the miscalculation of DOC concentrations following freeze/thaw. Therefore, the observed changes in DOC concentrations following freeze/thaw probably represent changes to the DOC absorbance spectra rather than actual losses in DOC concentrations.

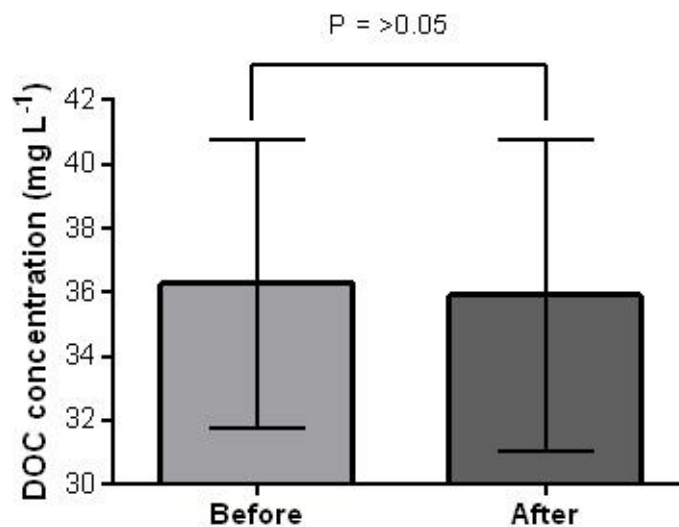


Figure 3.6A. Comparison of DOC concentrations before and after freeze/thaw, in Experiment 2. DOC concentrations were calculated using the two-wavelength approach (Carter et al., 2012). Error bars show the standard error of the mean (n=17).

3.5A Discussion

In Experiment 1, loss rates of DOC in samples kept at an ambient temperature of 33 °C were high (6.1 % over six weeks) relative to those stored at 4 °C, suggesting that tropical DOC concentrations could experience decreases of about 1 % per week. This is not surprising considering the temperature that these samples were exposed to during storage, which will have enhanced microbial activity and associated degradation of DOC (Kalbitz et al., 2000). These differences in DOC concentrations are also reflected in the significant differences ($P \leq 0.001$) in absorbance at 254 nm observed between the two storage methods (Figure 3.1A).

Higher sample SUVA values indicate the presence of humic and fulvic acids, including phenolic compounds, which remain biologically intact in the environment for long periods of time (Clark et al., 2010; Benner & Kaiser, 2011). A significant negative relationship was observed between SUVA and the difference between the two storage methods in DOC (Figure 3.2A). High SUVA values are indicative of recalcitrant DOC compounds, thus this observation suggests that even with prolonged exposure to high temperatures, more of the aromatic DOC remains relatively resistant to degradation (Weishaar et al., 2003). But the small range in $SUVA_{254}$ values presented in Figure 3.2A limits the support for $SUVA_{254}$ as a proxy for DOC bioavailability.

In terms of cold storage effects on DOC quality (Experiment 2), changes in absorbance occurred across the DOC spectra (270 nm, 350 nm and 700 nm) for both sample sets. These observed changes, before and after cold storage, were significant at wavelengths of 270 nm and 700 nm. Interestingly, in sample set 2 the majority of the absorbance observed at all wavelengths increased. This could be a reflection of DOC flocculation with storage time, resulting in a shift in the absorbance properties of the samples. However, absorbance corrections at 700 nm were made when calculating all DOC concentrations in order to adjust for turbidity and thus, sample flocculation, as suggested by Carter et al., (2012). Consequently, it is more likely that the differences in absorbance responses

between the two sample sets is a reflection of the different months in which the two samples sets were collected (August vs October) and thus reflect differences in both water chemistry and perhaps DOC composition.

Overall, the water samples in Experiment 2 showed relatively small changes in DOC concentrations ($2 - 2.7 \text{ mg L}^{-1}$ corresponding to between 8 and 11 %), when stored for approximately 12 weeks at $4 \text{ }^{\circ}\text{C}$. This suggests that if water samples are collected, filtered immediately and refrigerated then DOC losses in water samples from tropical peatlands may be acceptable. From a fieldwork perspective the practical implications of this finding are significant: samples can be stored and shipped back (at a temperature below $20 \text{ }^{\circ}\text{C}$) for analysis when convenient, negating the complex logistical issues associated with immediate analysis in remote locations.

The average variance in DOC loss over the 12 weeks in cold storage was 9.5 mg L^{-1} , however, this was skewed by one data point indicating a large change in DOC concentration during cold storage (50 %). Removal of this single outlier results in an average difference of 2 mg L^{-1} suggesting that losses of DOC during cold storage are low and somewhat predictable.

The data from the freeze/thaw experiment demonstrates that whilst overall changes in DOC concentrations before and after freeze/thaw are small (losses of 10.9 % compared to 9.6 % under cold storage; Experiment 2) significant changes in the absorbance spectra at 270 nm and 350 nm were observed, even after only 48 hours of frozen storage. This suggests that although changes in total DOC concentration may be relatively minor, changes in the quality of the DOC may also be occurring. This may be a consequence of the stability of the different fractions that comprise the DOC molecule that are altered during the freeze/thaw process (Spencer et al.,2007). In addition, as samples were not re-filtered after freezing it is possible that this process caused aggregation, leaving suspended particles of DOC, further contributing to the modifications observed in the optical properties of the DOC. Taken together these observations suggest that freezing may be a suitable preservation method only if bulk DOC measurements are of interest, but could be unsuitable if DOC quality is the main focus of interest,

directly supporting findings by Peacock et al., (2015). However, further experimentation into the effects of freezing samples would need to be undertaken to confirm this observation.

Chapter 3B Quantifying tropical peatland dissolved organic carbon (DOC) using UV-visible spectroscopy

This chapter (sections 3.1B to 3.6B) is published in Water Research: **Cook, S.**, Peacock, M., Evans, C.D., Page, S.E., Whelan, M., Gauci, V., Kho, L.K, 2017. *Quantifying tropical peatland dissolved organic carbon (DOC) using a UV-visible spectroscopy*. Water Research 115: 229-235, DOI: 10.1016/j.watres.2017.02.059

3.1B Abstract

UV-visible spectroscopy has been shown to be a useful technique for determining dissolved organic carbon (DOC) concentrations. However, at present we are unaware of any studies in the literature that have investigated the suitability of this approach for tropical DOC water samples from any tropical peatlands, although some work has been performed in other tropical environments. We used water samples from two oil palm estates in Sarawak, Malaysia to: i) investigate the suitability of both single and two-wavelength proxies for tropical DOC determination; ii) develop a calibration dataset and set of parameters to calculate DOC concentrations indirectly; iii) provide tropical researchers with guidance on the best spectrophotometric approaches to use in future analyses of DOC. Both single and two-wavelength model approaches performed well with no one model significantly outperforming the other. The predictive ability of the models suggests that UV-visible spectroscopy is both a viable and low cost method for rapidly analyzing DOC in water samples immediately post-collection, which can be important when working at remote field sites with access to only basic laboratory facilities.

3.2B Introduction

Dissolved organic carbon (DOC) is derived from the solubilisation of organic matter, and can be leached from the terrestrial landscape into freshwater ecosystems (Thurman, 1985). It plays a crucial role in peatland carbon budgets (Cole et al., 2007; Hulatt et al., 2014; Abrams et al., 2015; Muller et al., 2015) because it represents a carbon loss from the peat itself and, once in the aquatic system can be degraded, both biologically and photo-chemically, liberating CO₂ (carbon dioxide), CH₄ (methane) and CO (carbon monoxide) into the atmosphere (Cole et al., 2007; Clark et al., 2010; Fellman et al., 2014).

Interest in DOC losses from tropical peatlands has increased in recent years, fuelled in part by the realization of how vulnerable this carbon loss pathway is to land-use related disturbance (Moore et al., 2011; 2013; Evans et al., 2014; Rixen et al., 2016). Furthermore, the controls governing DOC mobility and export, along with their wider local and international implications, in the context of the global carbon cycle, still remain uncertain (Evans et al., 2012; 2014).

Measuring DOC directly in the laboratory requires specialised analytical equipment (e.g. a TOC analyser), which may hinder researchers with limited funds and laboratory equipment or those working in remote locations. An alternative and cheaper method is UV-visible spectrometry and spectroscopy, which relies on establishing relationships between DOC quantity and quality (Weishaar et al., 2003), and absorbance values and ratios (Peuravuori and Pihlaja, 1997), along with the ability to derive DOC compositional information based upon spectral slopes and ratios (Helms et al., 2008; Spencer et al., 2012). As such, UV-visible spectroscopy has been shown to be effective for determining DOC concentrations in temperate freshwater systems (De Haan et al., 1982; Tipping et al., 2009; Carter et al., 2012; Peacock et al., 2014b; Causse et al., 2016) as well as tropical catchments (Yamashita et al., 2010; Pereira et al., 2014). Spectrophotometric absorbance over a wide range of wavelengths has been used as a proxy for DOC, ranging from 250 nm (De Haan et al., 1982) to 562 nm (Carpenter and Smith. 1984). Peacock et al.,

(2014b) investigated the effectiveness of a range of single wavelengths between 230-800 nm as a proxy for DOC in waters draining two temperate upland catchments in the UK. The strongest correlations between absorbance and DOC were at 230 nm, 254 nm and 263 nm (Peacock et al., 2014b). The correlation between absorbance and DOC was observed to decline with increasing wavelength, a finding also noted by Asmala et al., (2012) and Grayson and Holden (2016),.

A further spectrophotometric approach is to use an empirical model based on two or more wavelengths to calculate DOC concentrations (e.g. 270 nm and 350 nm; Tipping et al., 2009; Carter et al., 2012). This proxy technique is based on the ratio of optical absorbance of a DOC molecule at a given wavelength (nm) to DOC, referred to as the extinction coefficient (E ; units $l\ g^{-1}\ cm^{-1}$; Tipping et al., 2009) otherwise known as SUVA (specific UV absorbance) . Developing this further Tipping et al., (2009) describe a two-component model that can predict DOC based on the linear sum of two components A and B (Carter et al., 2012). Both components have different features giving them distinct spectra; component A absorbs UV light strongly whereas component B absorbs it weakly (Carter et al., 2012). The model uses these optical absorbance properties as well as differing E coefficients, at two different wavelengths, to estimate DOC concentrations using a number of steps (Carter et al., 2012). A more detailed description of the model and parametrization, as outlined by Carter et al., (2012), is presented in Section 3.3.2B

A set of universal extinction coefficients ($EA_{\lambda 1}$; $EA_{\lambda 2}$; $EB_{\lambda 1}$; $EB_{\lambda 2}$) for the model, at wavelengths 270 and 350 nm, were generated by Carter et al., (2012) using a large number ($n=1700$) of surface water samples collected from the UK and Canada. In principle, any pair of wavelengths can be used (Carter et al., 2012) but 270 and 350 nm have been found to provide particularly robust DOC estimations. For a higher degree of accuracy the universal extinction coefficients can be adjusted for individual sites to produce a calibrated dataset. Carter et al., (2012) found that their two-wavelength method improved the fit between modelled and measured DOC concentrations compared to a single wavelength approach. The practicality and wide applicability of this two-

wavelength approach has also been demonstrated by Peacock et al., (2014b) who used the universal parameters to measure DOC in surface water, but found that the model had to be re-parameterised to calculate DOC in pore water. It would be useful if the same parameterization could be used to calculate DOC concentrations for other systems, including samples from tropical peatlands. Due to the differing environmental conditions and peat chemistry experienced between temperate and tropical regions, the composition of DOC from these systems is likely to vary. It is, therefore, important that these models are validated on tropical samples, particularly given the increased interest in tropical peat dynamics in recent years

At present we are unaware of any studies in the literature that have investigated the suitability of UV-vis spectroscopy methods for measuring DOC concentrations in water samples from tropical peatland catchments and, specifically, from oil palm plantations. While other research has explored tropical DOC concentrations and composition using this method (Johnson et al., 2006; Waterloo et al., 2006; Spencer et al., 2010; Yamashita et al., 2010; Pereira et al., 2014), previous studies have focused on mineral soil-dominated forest catchments, within the Congo (Spencer et al., 2010), Guiana Shield (Yamashita et al., 2010; Pereira et al., 2014) and Amazon basin (Johnson et al., 2006; Waterloo et al., 2006), with only one referencing the presence of peat within their study site (Yamashita et al., 2010). In addition, of these studies only one (Pereira et al., 2014) has applied the original Carter et al., (2012) model in the context of a tropical catchment. In view of the potentially wide applicability of this method, the cost-saving benefits and its potential to produce accurate results without the need for specialised laboratory facilities (particularly valuable for sample analyses at remote field sites), it is important to properly evaluate it. The aims of this investigation are, therefore, three-fold:

- 1) To investigate the suitability of different wavelength absorbance proxies for tropical DOC determination;
- 2) To develop a calibration dataset and a set of parameters that can be used to calculate tropical DOC concentrations indirectly;

- 3) To provide guidance for other tropical researchers on the best UV-vis spectrophotometric approaches to take when analyzing similar samples.

3.3B. Methods

3.3.1B Site descriptions and sampling

Water samples for this investigation were collected from the Sebungan and Sabaju oil palm estates, located in the Malaysian province of Sarawak, northern Borneo (between 3°07.81' N and 3°14.91'N and 113°18.72' E and 113°32.19'E; Figure 3.1B). Both estates are established on tropical peat soils and cover a collective area of nearly 10,000 ha. Air temperatures within this region are high (mean 26°C) and there is heavy rainfall throughout the year (~3000 mm received annually: Melling et al., 2005).

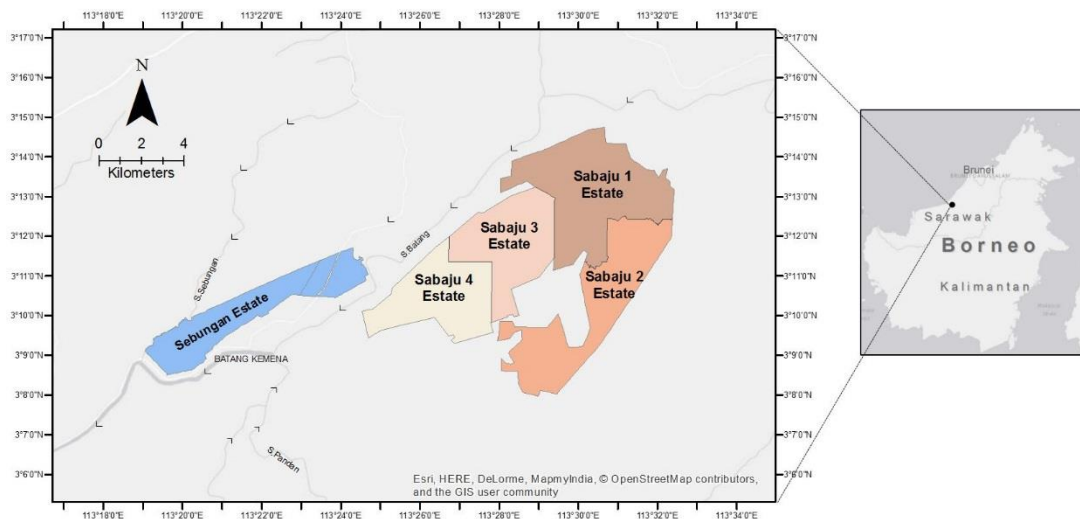


Figure 3.1B. Location of the Sebungan and Sabaju oil palm estates in Sebauh Bintulu district Sarawak. The estates are bordered by a network of rivers (grey and white lines) namely the Batang Kemena, S. Sebungan, S. Batang and S.Pandan. Arrows indicate direction of water flow.

Water samples were collected during two field campaigns: (A) 18th to 30th April 2015 and (B) 3rd August to 6th October 2015. All samples were collected in 60 ml Nalgene® bottles and filtered through 0.45 µm cellulose nitrate membrane filters, using a hand-held vacuum pump within 24 hours of collection. As there was no spectrophotometer present on site during Campaign A filtered samples were subsequently stored in a fridge at 4°C for 6-12 weeks, until shipment back to the UK for analysis. However, an onsite Cole-Parmer UV/visible spectrophotometer was present during Campaign B allowing immediate sample analysis. All samples, regardless of campaign, were subjected to cold storage which has been shown to ensure reasonable preservation of DOC between sampling and analysis (Cook et al., 2016). Subsequently, significant alterations to DOC concentrations and spectrophotometric properties would not be expected in between sampling and DOC analysis back in to the UK.

Upon return to the UK, samples collected during Campaign A were analyzed in June 2015 and those from Campaign B in November 2015 on a Total Organic Carbon (TOC; Shimadzu) analyser (precision ~ 2 – 5 %; Graneli et al., 1996; Bjorkvald et al., 2008; Shafer et al., 2010) as non-purgeable organic carbon (NPOC), to generate measured DOC concentrations. Prior to analysis, samples were acidified (pH < 3) and sparged with purified air to remove inorganic carbon. Measured DOC concentrations were subsequently calculated using a calibration curve ranging from 0 to 100 mg l⁻¹. Additional standards with concentrations close to those expected in the samples were analysed to check for drift. In parallel, samples were also analyzed on a Helios Gamma spectrophotometer to measure UV-vis absorbance at different wavelengths. A set of filtered blanks were analysed in the same manner as the water samples to ensure the suitability of the cellulose nitrate filters for SUVA analysis. Filters leached 0.008 absorbance at 254 nm, and 0.4 mg L⁻¹ DOC. However, considering the relatively high DOC concentrations and absorbance values for the majority of water samples, along with the precision of the TOC analyser, leaching was considered negligible.

3.3.2B Two-wavelength model description

The two wavelength model predicts DOC concentrations (C_{DOC}) on the basis of light absorption at two wavelengths (Tipping et al., 2009; Carter et al., 2012). Briefly,

$$C_{DOC} = \frac{(\alpha_{270} - \alpha_{700})}{E_{270}} + C_{NAC} \quad (3.2)$$

where α_{270} is the absorbance at 270nm, α_{700} is the absorbance at 700nm (used to account for instrumental drift, after Hernes et al., 2008), C_{NAC} is a constant concentration of DOC which does not absorb light (assumed here to be the same as the value reported by Carter et al., 2012 i.e. 0.8 mg L⁻¹) and E_{270} is an extinction coefficient (absorbance cm⁻¹ C_{DOC}⁻¹) of the light-absorbing DOC, given by

$$E_{270} = (f_A \cdot E_{A,270}) + (f_B \cdot E_{B,270}) = (f_A \cdot E_{A,270}) + ((1 - f_A) \cdot E_{B,270}) \quad (3.3)$$

where f_A and f_B are fractions of two components of DOC (A and B: each assumed to have different fixed absorbance spectra) and $E_{A,270}$ and $E_{B,270}$ are, respectively, empirically fitted extinction coefficients for components A and B at 270 nm. The fraction f_A is given by

$$f_A = \frac{E_{B,270} - (R \cdot E_{B,350})}{(R \cdot E_{A,350}) - (R \cdot E_{B,350}) - E_{A,270} + E_{B,270}} \quad (3.4)$$

in which $E_{A,350}$ and $E_{B,350}$ are, respectively, empirically fitted extinction coefficients for components A and B at 350 nm and R is the measured absorbance ratio at 270 and 350 nm ($\alpha_{270} / \alpha_{350}$). There are four empirically fitted extinction coefficients: $E_{A,270}$, $E_{B,270}$, $E_{A,350}$ and $E_{B,350}$ but only $E_{A,270}$ and $E_{B,270}$ were adjusted in our calibration with $E_{A,350}$ and $E_{B,350}$ unchanged from those reported by Carter et al., (2012).

3.3.3B Single-wavelength proxy assessment

The performance of a single wavelength (1λ) model for DOC was assessed using non-linear regression between absorbance at individual wavelengths (270 or 350 nm) and measured DOC concentrations in the samples collected in Campaign A. The resulting regression equations were then validated using the samples collected in Campaign B.

3.3.4B Two-wavelength proxy assessment

Absorbance data (at 270 and 350 nm) were combined with the measured DOC concentrations to generate a calibration data set for the two-wavelength model (2λ : Tipping et al., 2009; Carter et al., 2012). Model parameters (extinction coefficients at each wavelength) were adjusted by trial and error so as to maximize the R^2 value and minimize the sum of squared residuals between absorbance-derived DOC concentration and DOC concentrations measured by the TOC analyzer. The calibrated extinction coefficients are displayed in Table 3.1B alongside the universal extinction coefficients proposed by Carter et al., (2012).

Table 3.1B. Values of the extinction coefficients used by Carter et al., (2012) and those generated from the calibrated data set, where $\lambda_1 = 270$ nm and $\lambda_2 = 350$ nm.

Extinction Coefficients	Universal extinction coefficients ($L g^{-1}$)	Calibrated extinction coefficients ($L g^{-1}$)
EA_{λ_1}	69.3	74.32
EA_{λ_2}	30	30
EB_{λ_1}	15.4	15
EB_{λ_2}	0	0

The empirical model was tested on an independent validation data set (water samples collected during Campaign B). These samples were analyzed immediately after filtration (to minimize storage losses of DOC) on a Cole-Parmer UV/visible spectrophotometer, in Malaysia, at wavelengths of 270 nm and 350 nm. These UV-vis absorbance values were subsequently used in the calibrated model to calculate DOC concentrations. DOC concentrations were measured on a TOC analyzer, using the method previously described. As well as the coefficients derived from the calibration using the samples collected during Campaign A, 'universal calibration coefficients' proposed by Carter et al., (2012) were also used to generate DOC concentrations (Table 3.1B). This allowed the general validity of the universal coefficients in the 2 λ model to be evaluated. It should also be noted that a subset of five of the DOC water samples were chosen to cross-check for consistency between the absorbances produced on the UK-based and Malaysian-based spectrophotometers. This comparison showed an average difference in absorbance values of only $0.003 \pm 0.004 \text{ cm}^{-1}$.

3.3.5B Comparisons between approaches

In summary, a total of four approaches were used to estimate DOC concentrations using UV-vis spectrophotometry:

- 1) 1 λ approach using absorbance values at 270 nm (1 λ_{270})
- 2) 1 λ approach using absorbance values at 350 nm (1 λ_{350})
- 3) 2 λ approach calibrated on the April 2015 dataset/ Campaign A (2 $\lambda_{\text{calibrated}}$)
- 4) 2 λ approach using the 'universal calibration coefficients' (Carter et al., 2012) (2 $\lambda_{\text{non-calibrated}}$)

The performance of the four models was assessed using the following metrics:

- a) Actual differences between measured and estimated DOC concentrations (mg l^{-1});

- b) The coefficient of determination (R^2) for the regression between measured and modelled DOC concentrations;
- c) The root mean squared error (RMSE);
- d) The Nash-Sutcliffe efficiency (Nash and Sutcliffe, 1970) which is a measure of goodness of fit between the modelled and actual DOC concentrations i.e.:

$$NSE = 1 - \frac{\sum (C_{meas} - C_{est})^2}{\sum (C_{meas} - C_{mean})^2} \quad (3.5)$$

where C_{meas} is the measured DOC concentration (TOC analyser), C_{est} is the DOC concentration estimated using the various wavelength proxies and C_{mean} is the mean measured DOC concentration. The closer the NSE is to + 1 the stronger the model fit. A value of 0 or lower indicates that the model performs no better than the mean of the data (Nash and Sutcliffe, 1970).

3.3.6B Statistical analyses

Quantitative data analysis was performed using parametric statistical tests when appropriate (GraphPad Prism, version 6; Microsoft Excel 2013). Normality was tested using the Shapiro-Wilk test.

3.4B. Results

3.3.1B Single-wavelength approach

Single wavelength model development

Figure 3.2B shows the results of a series of regression analyses of modelled and measured DOC concentrations using a single wavelength proxy approach. Measured DOC concentrations for Campaign A data are plotted against modelled DOC concentration using absorbance at 270 nm (Figure 3.2B a; $1\lambda_{\text{original-270}}$ model) and 350 nm (Figure 3.2B b; $1\lambda_{\text{original-350}}$ model). Mean pH and electrical conductivity were 3.3 and $173 \mu\text{S cm}^{-1}$, respectively. The equations generated in Figure 3.2B a; b were then used to model the DOC concentrations for the August-October data set using absorbance at 270 nm ($1\lambda_{270}$ model) and 350 nm ($1\lambda_{350}$) and then compared to the corresponding measured concentrations (Figure 3.2B c;d). Goodness of fit metrics between the three models are displayed in Table 3.3B. Measured DOC concentrations ranged between 8.3 and 82.5 mg L⁻¹. Predicted DOC concentrations ranged between 8.1 and 63.0 mg L⁻¹ and between 1.0 and 71.4 mg L⁻¹, for the $1\lambda_{270}$ and $1\lambda_{350}$ models, respectively.

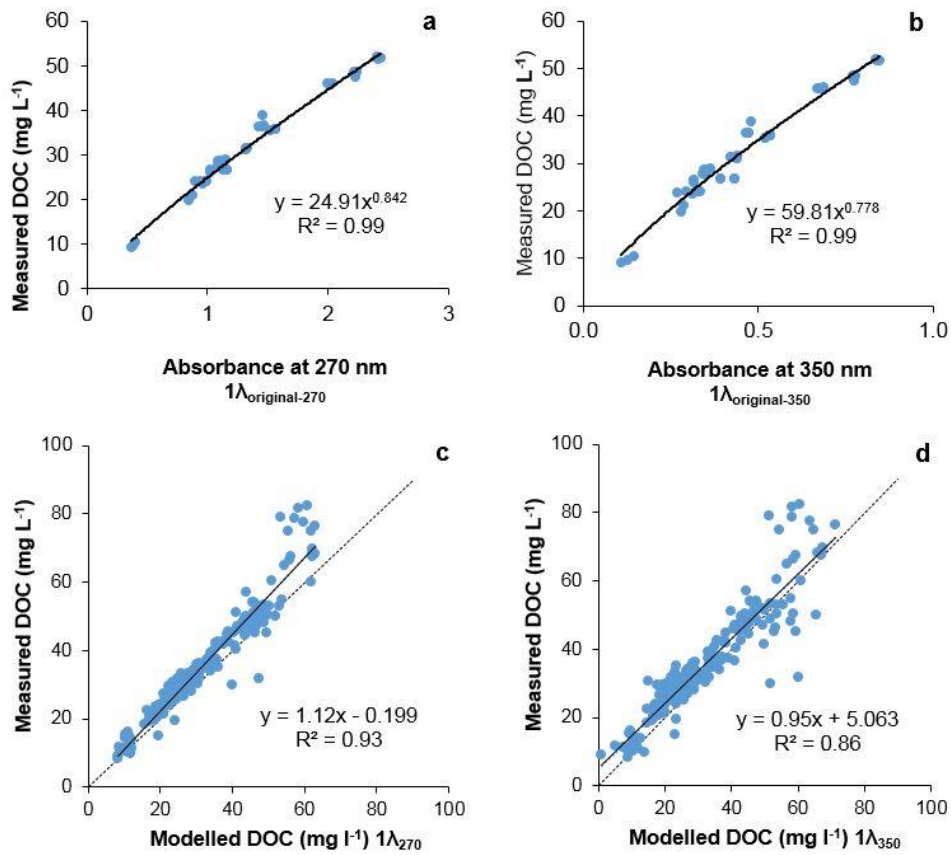


Figure 3.2B. Regression relationships between measured DOC concentrations from Campaign A and absorbance at 270nm (a) and 350 nm (b) along with (c) modelled DOC concentrations from Campaign B derived using the equation generated in (a) and (d) equation generated in (b). Dashed lines show 1:1 relationship.

3.4.2B Two-wavelength approach

Two-wavelength model development and validation

Figure 3.3B shows the results of several regression analyses of modelled and measured DOC concentrations that were used to calibrate the model and validate it. The original calibration ($2\lambda_{\text{original-calibrated}}$ model: Figure 3.3B a) displays the measured DOC concentrations for the April 2015 data set against the modelled DOC concentrations, generated by adjusting the extinction coefficients to maximize the goodness of fit. DOC concentrations ranged from 9.3 to 52.0 mg L⁻¹ and 9.3 to 52.8 mg L⁻¹ for the measured and modelled techniques, respectively. This calibrated model was then validated by testing it on the independent data set ($2\lambda_{\text{calibrated}}$ model: collected during Campaign B), the results of which are displayed in Figure 3.2B. The DOC concentrations from the same data set (Campaign B) were then modelled using the universal extinction coefficients suggested by Carter et al., (2012), as shown in Figure 3.3B c ($2\lambda_{\text{non-calibrated}}$ model). Respective mean pH and electrical conductivity values were 3.7 and 177 $\mu\text{S cm}^{-1}$ for Campaign B samples. Goodness of fit metrics between the three models are displayed in Table 3.3B. Predicted DOC concentrations ranged from 5.5 to 71.7 mg L⁻¹ and from 6.7 to 82.8 mg L⁻¹ for the $2\lambda_{\text{calibrated}}$ and $2\lambda_{\text{non-calibrated}}$ models, respectively. While the DOC concentration ranges within the validation data set (Figure 3.3B b;c) were greater than those observed for the calibrated data (Figure 3.3B a), 92 % of the validation data (190 samples out of 206 samples) fell within the broad range encompassed by the DOC calibration (0 to 60 mg L⁻¹). Accordingly, the majority of the DOC concentration data set was represented.

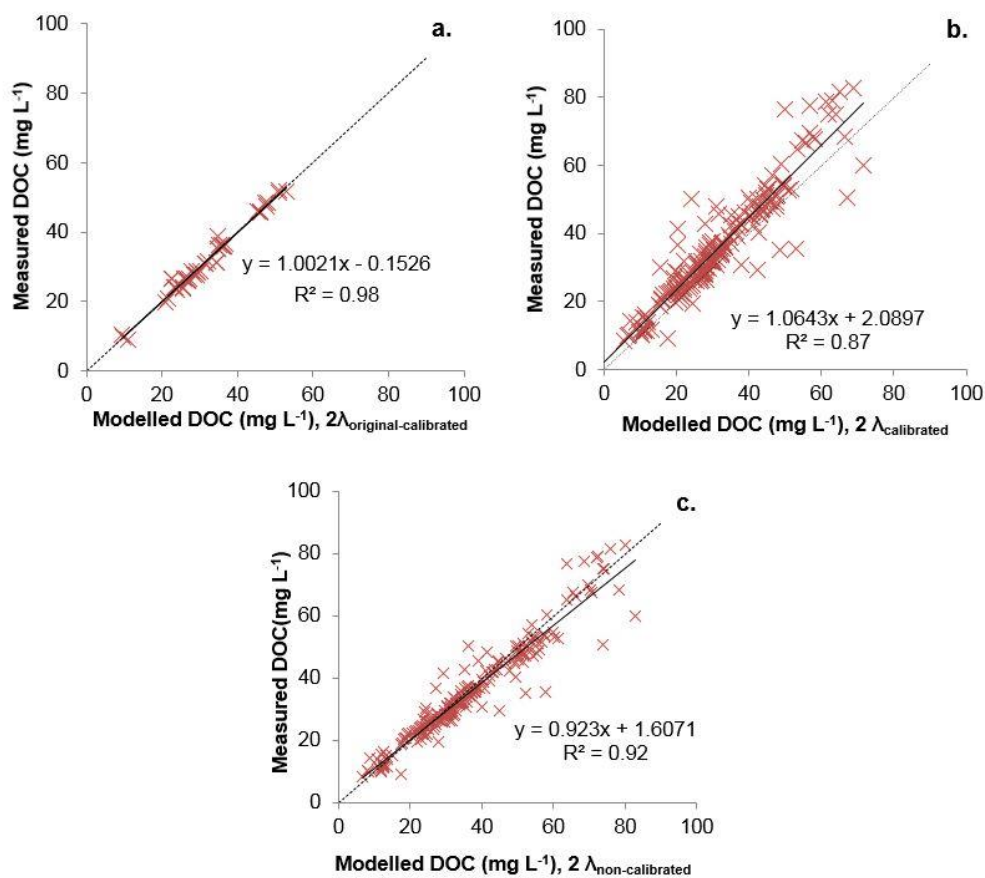


Figure 3.3B a) Original model calibration (constructed from April 2015 data/ Campaign A).

Regression of modelled DOC concentrations ($n=47$) against respective measured DOC concentrations. Extinction coefficients were derived independently from the same data used for calibration (calibrated extinction coefficients): $E_A, \lambda_1=74.32$, $E_A, \lambda_2=30$, $E_B, \lambda_1=15$, $E_B, \lambda_2=0$ **b)**

Regression of DOC concentrations from the independent data set ($2\lambda_{\text{calibrated}}$ model) (collected from Campaign B), against respective measured DOC concentrations. Model DOC concentrations generated using the calibrated extinction coefficients **c)** Regression of 2λ modelled DOC concentrations for validation samples against respective measured DOC concentrations using ‘universal calibration coefficients’ (Carter et al., 2012). Dashed lines show 1:1 relationships.

3.4.3B Overall assessment of models

The overall effectiveness of the four different models to predict DOC concentrations are summarized in Table 3.2B, displaying the concentration and percentage differences between the modelled and measured DOC. The goodness of fit metrics for all four model approaches are present in Table 3.3B; validation data.

Table 3.2B. Mean concentration and percentage differences between modelled and measured DOC concentrations (mg L^{-1}) for the four different models using the validation data set (collected during Campaign B). Positive and negative values indicate that modelled DOC concentrations overestimate and underestimate measured DOC concentrations, respectively. n= number of samples.

	$2\lambda_{\text{calibrated}}$	$2\lambda_{\text{non-calibrated}}$	$1\lambda_{270}$	$1\lambda_{350}$
n	206	206	206	206
Difference between modelled and measured DOC (mg l^{-1})	-4.1 ± 0.4	1.2 ± 0.3	-3.7 ± 0.3	-3.4 ± 0.4
% Difference between modelled and measured DOC	14.4 ± 0.8	9.7 ± 0.8	11.9 ± 0.5	15.5 ± 1.0

Table 3.3B. Summary of goodness of fit metrics for all development and validation models. R^2 values and slope of regression lines between modelled and measured DOC for the model approaches, along with NSE and RMSE values. n= number of samples.

	Model development			Validation data			
	$2\lambda_{\text{original-calibrated}}$	$1\lambda_{\text{original-270}}$	$1\lambda_{\text{original-350}}$	$2\lambda_{\text{calibrated}}$	$2\lambda_{\text{non-calibrated}}$	$1\lambda_{270}$	$1\lambda_{350}$
n	46	46	46	206	206	206	206
R^2	0.98	0.98	0.95	0.87	0.92	0.93	0.86
NSE	N/A	N/A	N/A	0.80	0.91	0.86	0.81
RMSE	1.45	1.51	2.27	6.99	4.82	5.81	6.89

The extinction coefficients for A and B were adjusted to optimize the fit between modelled DOC concentrations and the respective measured values ($R^2 = 0.98$; $p < 0.05$) (Figure 3.3B a). Lower and upper 95% confidence intervals were 0.746 and 1.344, respectively. The optimal extinction coefficients for the 2λ model were: $E_{A,270} = 74.32 \text{ L g}^{-1}$; $E_{A,350} = 30 \text{ L g}^{-1}$; $E_{B,270} = 15 \text{ L g}^{-1}$; $E_{B,350} = 0 \text{ L g}^{-1}$. The $2\lambda_{\text{original-calibrated}}$ model was then tested on an independent validation data set ($2\lambda_{\text{calibrated}}$) (Figure 3.3B b). The model fit was strong ($R^2 = 0.87$; $p < 0.05$, RMSE = 6.99 mg L^{-1} : Table 3.3B). In general, the calibrated model ($2\lambda_{\text{calibrated}}$) tended to underestimate concentrations although on average the mean difference between the modelled and measured values was small ($-4.1 \pm 0.4 \text{ mg L}^{-1}$: Table 3.2B). The lower and upper 95% confidence intervals were -3.3 and -4.9 mg L^{-1} , respectively. The model fit was also strong using the universal extinction coefficients ($2\lambda_{\text{non-calibrated}}$) cited in Carter et al., (2012) ($R^2 = 0.92$; $p < 0.05$) (Figure 3.3B c) with a slightly lower RMSE (4.82 mg L^{-1}). However, this model tended to overestimate DOC concentrations by an average of $1.2 \pm 0.3 \text{ mg L}^{-1}$ (Figure 3.3B). 95% confidence intervals were 1.85 (lower) and 0.57 (upper).

Linear regressions between absorbance at single wavelengths and measured DOC concentrations are shown in Figure 3.2B (a, b).

Modelled DOC concentrations derived using absorbance at 270 nm were a better fit to measured DOC concentrations ($R^2 = 0.93$; $p < 0.05$: Figure 3.2B c) than those derived at 350 nm ($R^2 = 0.86$; $p < 0.05$: Figure 3.2B d). However, both models tended to underestimate DOC concentrations with mean differences between measured and modelled values ranging from $-3.7 \pm 0.3 \text{ mg L}^{-1}$ to $-3.4 \pm 0.4 \text{ mg L}^{-1}$ for the 270 nm and 350 nm models, respectively (Table 3.2B). Confidence intervals at 95% ranged from -4.22 to -4.34 (lower) and -2.57 to -3.11 (upper) for the 350 nm and 270 nm models, respectively. Both single wavelength models displayed a threshold-like behaviour between modelled and measured DOC concentrations (Figure 3.2B c;d). At approximately 60 mg L^{-1} there appears to be a clear decoupling of the absorbance measurements from the measured DOC data, resulting in the majority of modelled DOC concentrations being underestimated (Figure 3.2B c, d). This could be

consistent with findings made by Pereira et al., (2014) and therefore supports their concept of the presence of an “invisible” dissolved organic matter (iDOM) component. This non-humic and, therefore, non-chromophoric constituent is undetectable using conventional spectrophotometric methods yet does contribute to the overall DOC pool (Pereira et al., 2014).

The overall statistical performance of all four models was strong (Table 3.3B). The $2\lambda_{\text{non-calibrated}}$ model performed best in terms of NSE and RMSE (respective values 0.91 and 4.82 mg L⁻¹). This was closely followed by the $1\lambda_{270}$ model, which had a slightly higher R² value (0.93) but lower NSE and RMSE (respective values 0.86 and 5.81 mg L⁻¹). Relative differences (measured - modelled) between the modelled and measured DOC concentrations across all four models ranged from 9.7% to 15.5% (Table 3.2B), with the $2\lambda_{\text{non-calibrated}}$ approach producing the smallest % difference. This trend was also observed for the mean absolute differences (modelled – measured) in DOC concentration (Table 3.2B). The highest NSE was produced by the $2\lambda_{\text{non-calibrated}}$ approach (NSE 0.91). The $2\lambda_{\text{calibrated}}$ approach produced the lowest NSE (0.80). The intercept of the 270 nm proxy ($1\lambda_{270}$) model was closest to zero (0.20 ± 0.74 mg L⁻¹, $p > 0.05$) and the intercept of the 350 nm proxy ($1\lambda_{350}$) was furthest away from zero (5.06 ± 1.04 mg L⁻¹, $p < 0.05$). However, the slope of the $1\lambda_{350}$ regression was closest to unity (0.95 ± 0.03 mg L⁻¹, $p < 0.0001$) and that of the $1\lambda_{270}$ regression was furthest away from 1 (1.12 ± 0.02 mg L⁻¹, $p < 0.0001$). Of the 2λ approaches, the $2\lambda_{\text{non-calibrated}}$ model had a closer intercept to zero (1.61 ± 0.77 mg L⁻¹, $p < 0.05$) than the $2\lambda_{\text{calibrated}}$ model (2.09 ± 0.97 mg L⁻¹, $p < 0.05$) and also had a slope which was closer to unity (0.92 ± 0.02 mg L⁻¹, $p < 0.0001$).

3.5B Discussion

All four models performed well statistically suggesting that tropical DOC concentrations in surface waters can be estimated accurately using UV-vis spectroscopy. Both the two-wavelength and single-wavelength approaches exhibited similar statistical performance and were both suitable as DOC concentration proxies, reinforcing findings reported for temperate peatland waters by Peacock et al., (2014b).

Carter et al., (2012) found that a two-wavelength model improved R^2 values by 0.02 and 0.05 compared to 270 and 350 nm UV proxies, respectively. However, our data suggest that the single-wavelength model at 270 nm produced the strongest R^2 value and the second highest NSE, suggesting that it is as robust as a two-wavelength proxy. This is in agreement with other previous studies (Asmala et al., 2012; Peacock et al., 2013; Peacock et al., 2014b) and is explained by both the higher resolution given by a shorter wavelength (i.e. for which optical absorbance is observed to decrease with increasing wavelength (Wang and Hsieh. 2001) and the fact that peatland DOC is largely composed of aromatic humic substances that strongly absorb light in the UV range (Khan et al., 2014; Thurman. 1985). However, the slope of the regression between modelled and measured DOC concentrations was furthest from unity for the $1\lambda_{270}$ model.

Interestingly (and somewhat surprisingly), the universal $2\lambda_{\text{non-calibrated}}$ model (Carter et al., 2012) outperformed the $2\lambda_{\text{calibrated}}$ model in terms of NSE and mean difference between modelled and measured DOC concentrations for the validation dataset. The universal calibration parameters cited by Carter et al., (2012) were generated using a large number of samples ($n=1700$) from high-latitude peatlands collected over a range of different seasons. Consequently, the range of environmental conditions captured by the universal calibration data set and the number of samples collected was higher than the calibration data set employed here and may help to explain this finding, despite the fact that the data used by Carter et al., (2012) were derived from a different climate

zone. In addition, our calibration data were collected in April which is at the tail end of the wet season in Sarawak, whereas the data used for validation (August to October) were collected at the end of the dry season. Seasonal variations in both the quantity and quality of DOC have been observed in other studies (e.g. Peacock et al., 2014b) and may also explain why a wet-season-calibration did not represent dry-season DOC as well as expected. This is further reinforced by both Johnson et al., (2006) and Pereira et al., (2014) who noted distinct seasonal differences in the composition of tropical DOC. In addition, data used to derive the original calibrated model (Campaign A) were applied to a data set analysed much more rapidly after collection (Campaign B). Therefore, some of the overestimations made by the $2\lambda_{\text{calibrated}}$ model could be due to small DOC losses during storage, although an independent assessment of such cold storage losses suggested that they are modest (Cook et al., 2016). As such, this offers further opportunities to improve upon our existing model and the locally-calibrated model may be improved as sampling continues.

The performance of the universal calibration coefficients (Carter et al., 2012) in this tropical surface water system is encouraging. From a practical perspective, this suggests that other tropical researchers may also be able to use these parameters, in the absence of their own calibration data set. This would allow DOC concentrations to be determined soon after sampling without having to ship samples from remote field locations to the laboratory for site-specific calibrations (although this is always the preferred practice).

There will always be a need for quality control checks on proxy DOC determinations, but the fact that UV-vis spectroscopy is able to predict tropical DOC concentrations accurately and rapidly is extremely promising because it offers the ability to generate *in-situ* data which may improve both the spatial and temporal range of DOC measurements. This may be particularly important for research groups working in remote locations which lack immediate access to specialized (and often expensive), analytical equipment. DOC concentrations and quality (absorbance and fluorescence properties) can change in stored water samples over time even after acidification and or

freezing (Spencer et al., 2007; Fellman et al., 2008; Peacock et al., 2015; Cook et al., 2016), so the possibility of immediate post-collection analysis is attractive.

3.6B Conclusions

The concentrations of DOC in tropical water samples collected from peat-dominated catchments can be determined accurately using both single- and two-wavelength spectrophotometric techniques. This offers researchers the potential to analyse samples rapidly post-collection using an inexpensive method and could be invaluable when working in remote tropical field sites.

3.7B Data uncertainty

Chapter 3B has focused upon the predictive ability of UV-visible spectroscopy for determining tropical DOC concentrations, through a comparison with concentrations determined via a TOC analyser (i.e. difference between modelled and measured DOC concentrations). This method assumes linearity i.e. that the uncertainties in the TOC analyser concentrations (x variable) are negligible compared to those produced by the spectrophotometer (y variable). However, in reality this is not necessarily the case with uncertainty associated with i) the calibration line itself, with the scatter of the points influencing both the gradient and slope, therefore, translating into uncertainty in ii) the y variable (Miller, 2006; Waldron et al., 2014). However, these complex interactions of error were not considered when originally assessing the overall performance of this calibration based technique (i.e. Table 3.2B). As a result the uncertainties surrounding the modelled DOC concentrations are unknown.

In this subsection the statistical rigour associated with this technique (specifically the 2 λ -calibrated approach) is discussed through the use of inverse linear calibrations to determine both the precision (standard deviation, S_0) and accuracy (95 % confidence intervals, CI) of an unknown field sample. This is further used to quantify the uncertainty (i.e. half-width of the 95% CI ,

DOC $\pm x$ mg L⁻¹) associated with the modelled DOC concentrations, which can then be accounted for within the overall fluvial organic carbon flux (Chapter Four).

3.7.1B Inverse confidence limits

The precision or ‘uncertainty’ can be quantified by estimating the S_0 of an unknown sample (equation 3.6), using the error associated with a given x value from a given y value, and vice versa, $s_{y/x}$ (Miller, 2006; Waldron et al., 2014). This approach assumes that the direction of error is equal for both the x and y values, briefly

$$S_0 = \frac{s_{y/x}}{b} \left\{ \frac{1}{m} + \frac{1}{n} + \frac{(y_0 - \bar{y})^2}{b^2 \sum (x_i - \bar{x})^2} \right\}^{1/2} \quad (3.6)$$

Where: n is the number of calibrating points, \bar{y} and \bar{x} are the means of the y and x variables, m is how many times the sample was measured giving a mean value of y_0 , b is the gradient of the regression between x and y variables and $s_{y/x}$ is given by

$$s_{y/x} = \left\{ \frac{\sum (y_i - \hat{y}_i)^2}{n - 2} \right\}^{1/2} \quad (3.7)$$

Where: \hat{y}_i are the values of the fitted y values, i.e. the points on the calibration line fitted using the fitted x values from the calibration line. $s_{y/x}$ is also referred to in excel as the ‘standard error’ which can be obtained from the ‘summary output’ of the regression analysis

The accuracy or 95% *CI* can then be determined by multiplying S_0 by the t -value taken at the required probability level (i.e. 95 %) and $n - 2$ degrees of freedom.

Figure 3.4B displays the output of an ordinary least-squares regression between all DOC concentrations determined by the spectrophotometer, using the 2 λ -calibrated approach, and the TOC analyser. This data was then used to calculate the corresponding uncertainty 'S₀' values, for the spectrophotometer derived DOC concentrations, which were then plotted against the respective concentration data (Figure 3.4B). This produced a distinct curved shape, suggesting that the values of S₀ increase with increasing distance from the mean DOC concentration, as the unknown value becomes less-well constrained. A similar trend was observed by Waldron et al., (2014).

Overall the standard deviation/ uncertainty of the unknown (S₀) ranged from 6.9 to 7.4 mg L⁻¹. This resulted in an average calculated 95 % CI of 17.7 mg L⁻¹, with a range of 13.6 to 14.5 mg L⁻¹. The average calculated half-width of the 95% CI ranged from \pm 6.8 to 7.3 mg L⁻¹, with an average of \pm 6.9 mg L⁻¹. This number offers a truer representation of the uncertainty contributions associated with the modelled DOC concentrations, compared to the standard error of the mean. The implications of this are acknowledged in Chapter Four, with upper and lower carbon flux bounds quoted in response to the uncertainty in DOC concentrations.

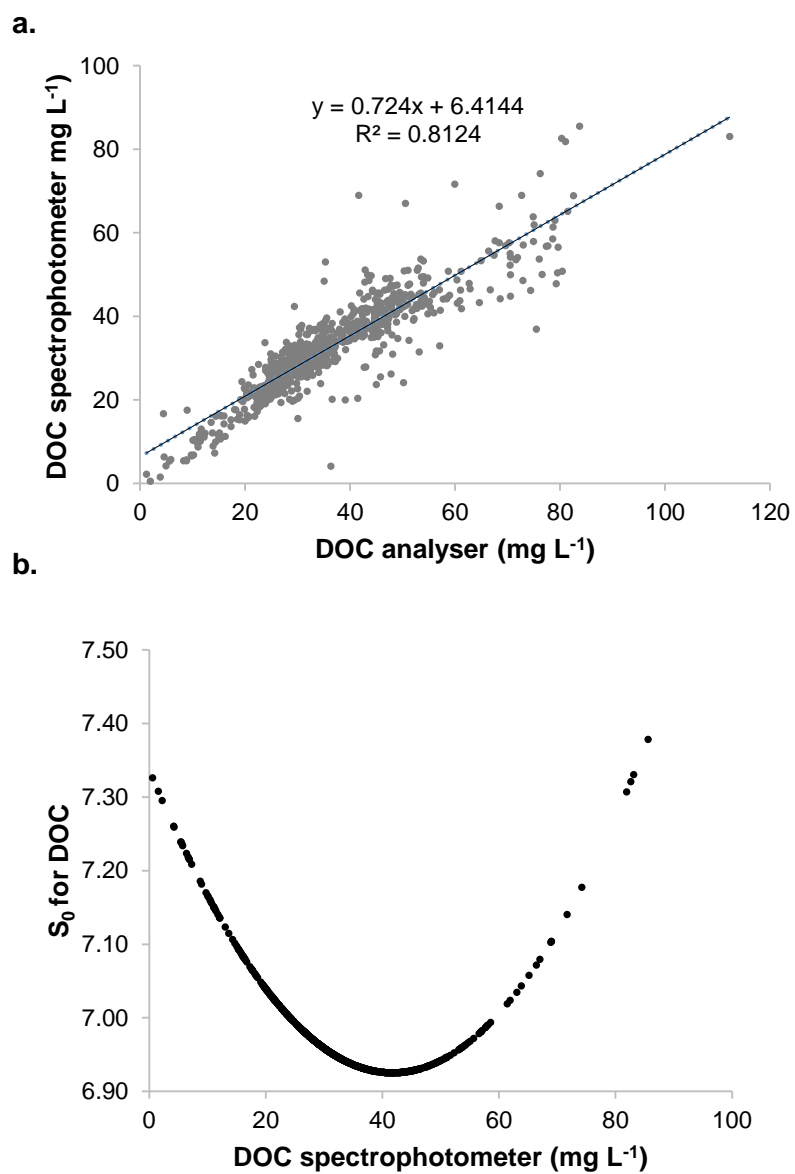


Figure 3.4B Regression analysis between DOC concentrations derived from the spectrophotometer (using the 2 λ -calibrated approach) and the TOC analyser (a), along with an illustration of the corresponding S_0 values (b)

Chapter Four: Fluvial organic carbon losses from oil palm plantations on tropical peat

4.1 Introduction

This chapter tackles the principal aim of the thesis by providing an investigation into fluvial organic carbon losses from across a peatland degradation gradient. The investigation captures the transitional period from 'semi-intact' PSF through to industrial-scale OPP. The climate and hydrology of the study sites are discussed, alongside the fluvial carbon data (i.e. organic carbon concentrations). Several challenges were encountered when calculating the fluvial organic carbon fluxes which led to several hydrological investigations. The methods for these, along with the resulting fluxes are discussed in full within this chapter. Variation in other monitored environmental parameters, including pH, EC and watertable depth, are also examined and explored as possible explanatory variables for patterns in organic carbon concentrations and loads. This chapter concludes with a detailed discussion of the findings. The qualitative carbon properties are discussed in Chapter Five and the implications of these data for peatland management are examined in Chapter Six.

4.2 Methods

Detailed study site descriptions are provided in Chapter Two (Section 2.2, 2.3 and 2.4) along with the methodology, including: sample collection (Section 2.5) and analysis (Section 2.6), overview of carbon flux calculations (Section 2.8) and measurement of environmental parameters (Section 2.9). In brief, water samples were collected from the Sebungan and Sabaju oil palm plantation (OPP) estates, situated ~70 km inland from the coastal town of Bintulu (from 3°07.81' N to 3°14.91'N, and 113°18.72' E and 113°32.19'E). The estates cover a collective area of 9,614 ha. Plantation management is typical of other

peatland OPPs in this region. The stands of oil palm ranged in age from 6 years to 9 years (when sampled in 2015/2016). A mixture of main (M) and collection (C) drains were monitored (with a sampling frequency every 1-3 weeks, over a year-long period of 54 weeks) in four main plantation (P) areas; Sebungan (SE), Sabaju 1 (SA 1), Sabaju 3 (SA 3) and Sabaju 4 (SA 4). In addition to the plantation estates, two 'semi-intact' peat swamp forest (PSF) fragments (FA and FB) adjacent to the plantations and within the same peatland complex, were monitored enabling a comparison to be made between these two ecosystems. The forest (F) fragments were located along the perimeter of the Sebungan (FB) and Sabaju (FA) estates, where they act as a 'buffer zone' between the plantations and the river network. In addition, the opportunity arose to collect organic carbon data from two recently deforested areas (sites DF and R-DF) part way through the study. R-DF was sampled within weeks of initial forest clearance (see Chapter Two, Section 2.4.2, for more details and maps).

4.2.1 Hydrological investigations to determine fluvial organic carbon fluxes

Several challenges were encountered when attempting to derive the fluvial organic carbon fluxes for this investigation. As such, a sequence of different approaches was attempted (Figure 4.1), specifically: i) defining catchment areas, ii) calculating water mass balances and iii) calculating flow weighted TOC concentrations. General method details for each approach are provided in Chapter Two, Section 2.8. A more detailed description of these methods, and associated limitations, are discussed within this sub-section, with the outcomes presented within the Results (Section 4.3.1). The hydrological investigations are divided into those used for the plantation (Section 4.2.1.1) and the forest (Section 4.2.1.2) landcover classes.

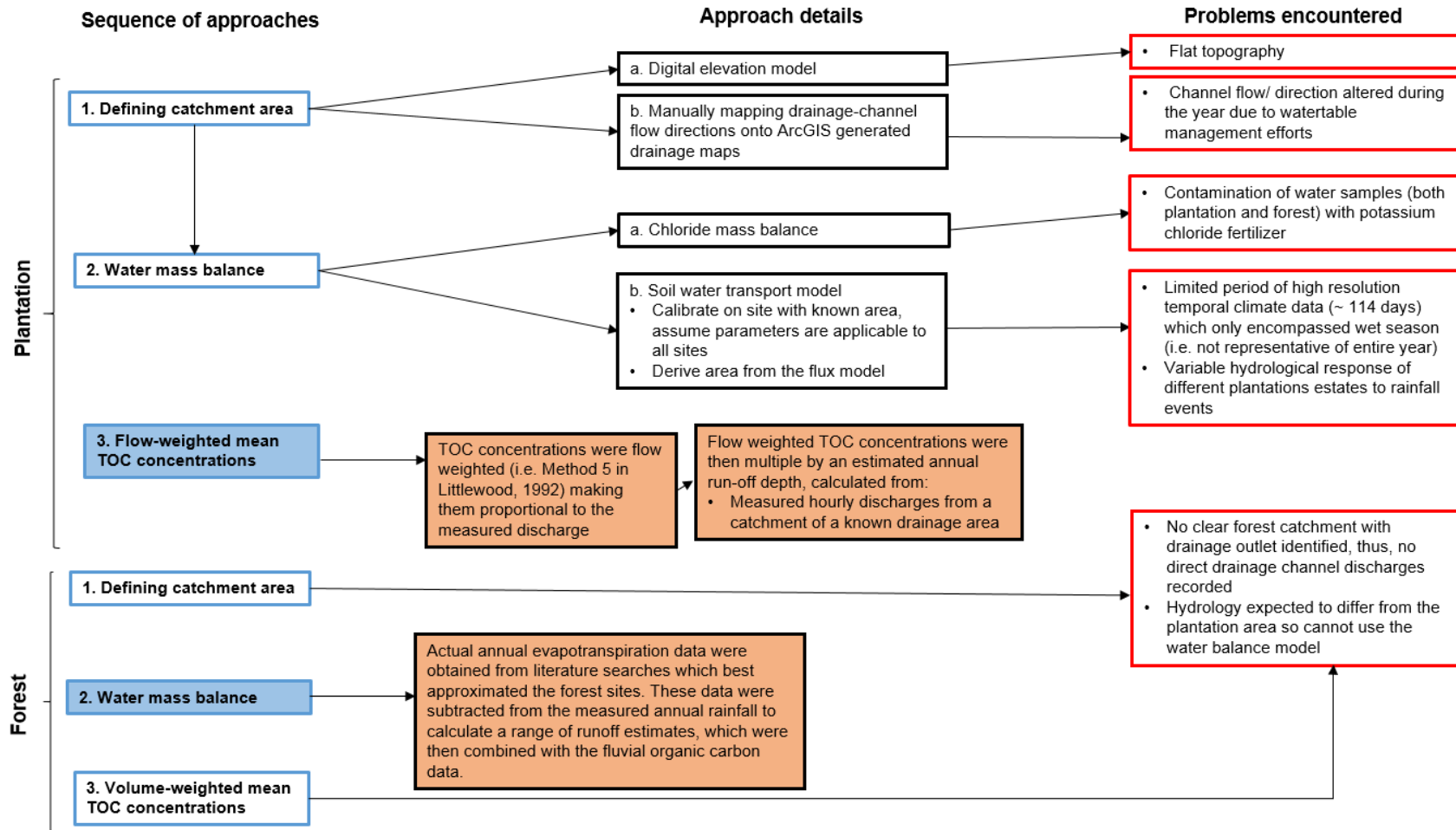


Figure 4.1 Flow chart to illustrate the sequence of approaches (blue boxes) taken to determine the area specific TOC fluxes for both the plantation and forest landcover classes. A brief summary of the approach details (black boxes) is provided alongside the problems encountered (red box) which caused the method to be discarded. The shaded boxes (blue and orange) indicate the final approaches taken.

4.2.1.1 Plantation

The first approach was to define the catchment area (Chapter Two, Section 2.8.1). Hydrological watersheds are commonly delineated using Digital Elevation Models (DEMs; Zhao et al., 2009) (Figure 4.1, Approach 1a). However, problems arise when applying DEMs to flat areas, such as peatlands, due to a lack of flow pathway data and sinks or pits within the DEM data (Pan et al., 2012). This often causes the DEM to fail in accurately capturing both the topographic and hydraulic characteristics of the area (Lindsay & Creed, 2006; Zhao et al., 2009; Pan et al., 2012), leading to miscalculation of watershed extent (Pan et al., 2012). Consequently, plantation channel flow directions were manually mapped using field observations, during an initial field visit in April 2015 (Figure 4.1; Approach 1b). These flow directions were then added on to drainage maps generated using ArcGIS (courtesy of SOPB GIS department) and used to define catchment boundaries, at a range of spatial scales. Full details and maps are presented in Chapter Two (Section 2.3). This approach was only possible within the plantation landcover class for which detailed maps were available. However, this approach was complicated by the fact that, in some locations, the plantation management staff had modified the channel (i.e. by blocking the drains with sand bags or diverting the flow). This affected the channel discharge and ultimately resulted in the miscalculation of some catchment areas.

The second approach was to use a water mass balance method (Figure 4.1, Approach 2; Chapter Two, Section 2.8.2). Annual rainfall was calculated from a combination of on-site manual rain gauge readings and weather station data (Chapter Two, Section 2.9.1). Actual evapotranspiration (ET_a) was first calculated using a chloride mass balance approach (CMB; Chapter Two, Section 2.8.2.1) (Figure 4.1, Approach 2a). Rainwater was collected on the Sebungan plantation in an enclosed plastic container (5 L) equipped with a funnel and positioned in an open area. At the end of each sampling week a 60-ml water sample was extracted from the rainwater collector and placed in

the dark at 4°C until analysis. The rainwater collector was then emptied in preparation for the next week. Upon return to the UK, all rainwater and water samples, collected for fluvial carbon analysis, were analysed for Cl⁻ using an ion-specific electrode and following the manufacturer's procedures (Cole-Parmer combination Chloride selective electrode). This method provided a low-cost alternative to more expensive techniques such as ion chromatography. However, a sub-set of samples were first cross calibrated with a Dionex machine to ensure comparable readings between the two techniques (Figure 4.2).

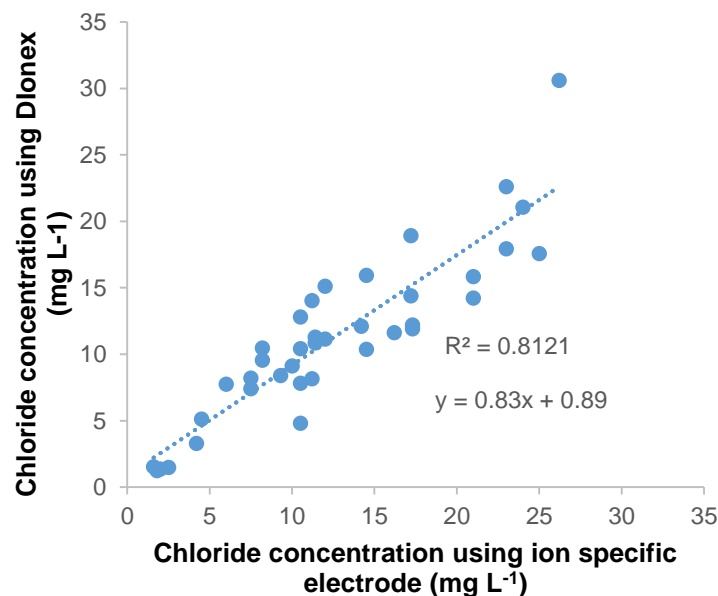


Figure 4.2 Comparison between chloride concentrations obtained using the ion specific electrode and Dionex machine, along with the correlation coefficient (r^2) and line equation. The ion specific electrode slightly over estimated Cl⁻ concentrations but overall the average concentration differences between the two techniques was small (1.3 mg L⁻¹).

Unknowingly, at the time of sample collection, potassium chloride was being used as a fertilizer within the peatland OPPs. Consequently, this was providing an additional source of Cl⁻ into the system, leading to increased ET_a estimates (Appendix C). Traces of this fertilizer were also found within the forest sites, making this approach to ET estimation redundant for both land cover types.

As an alternative a soil water transport model was adapted for the plantation landcover class, as described in Chapter Two, Section 2.8.2.2 (Figure 4.1, Approach 2 b). The model was created using Visual Basic for Application (VBA) within Excel and predicted the hydrological response of a catchment based on three components of the water balance: inputs (precipitation, P), outputs (actual evapotranspiration, ET_A ; discharge, Q ; overland flow, OLF) and storage (i.e. tropical peat). ET_0 values were imported from WaSIM (Water Balance Simulation Model) which were calculated using the Penman-Monteith equation. The climate data required to calculate this algorithm was obtained from available on-site daily meteorological records using an onsite weather station (Davis Vantage Pro2). However, due to equipment malfunction, daily rainfall could only be collected from 1st August 2015 until 6th January 2016, inclusively, making upscaling annual ET_A uncertain.

The model was run using a set of adjustable parameters (Table 4.1) alongside the measured daily plantation rainfall (mm day^{-1}), daily ET_0 (mm day^{-1} ; derived from the Penman-Monteith equation) and available daily measured drainage channel discharge (mm day^{-1}). The adjustable parameters were modified by trial and error to maximize the r^2 value between the measured and modelled discharge data. However, constraints were applied to some of the adjustable parameters, based on literature searches, to ensure that the model adhered to 'reality' as much as possible. For example, K_{sat} of the tropical peat was assumed to be greater than values for temperate peat ecosystems (i.e. blanket bogs; $1.7 - 2.5 \text{ mm day}^{-1}$; Evans et al., 2014; Holden et al., 2004).

The optimum calibration values are presented in Table 4.1. The value for the empirical shape factor n was set at 2.8. This suggested a lag response in the soil's hydraulic conductivity (K_{unsat}/K_{sat}) to an increasing water content, which is more clearly visualised by the soil retention curves outlined in Figure 4.3. The relationship between the optimum water content parameters (i.e. wilting point, threshold and saturated) and the ET metrics are outlined in Figure 4.4. The threshold water content was set at $0.33 \text{ cm}^3 \text{ cm}^{-3}$ after which the water content of the soil becomes low enough to limit ET_A to less than the potential

values (ET_o). This continues until a wilting point of $0.17 \text{ cm}^3 \text{ cm}^{-3}$ is reached, at which point ET metrics are zero. The model was run for the period 15th September 2015 until 6th January 2016 (114 days), where both daily rainfall data and channel discharge were available.

Table 4.1 Model parameters with the adjustable components highlighted in grey. Full model details and a description of the parameters are described in Chapter Two, Section 2.8.2.2

Parameter	Value
van Genuchten parameter n	2.8
Saturated Water Content, θ (cm^3/cm^3)	0.8
Permanent Wilting Point (cm^3/cm^3)	0.17
Soil Depth (cm)	80
Threshold water content when actual evapotranspiration (E_{t_a}) < potential evapotranspiration (E_{t_p}) (cm^3/cm^3)	0.33
Initial Water Content (cm^3/cm^3)	0.3
Saturated hydraulic conductivity (K_{sat}) for soil type (mm/d)	64

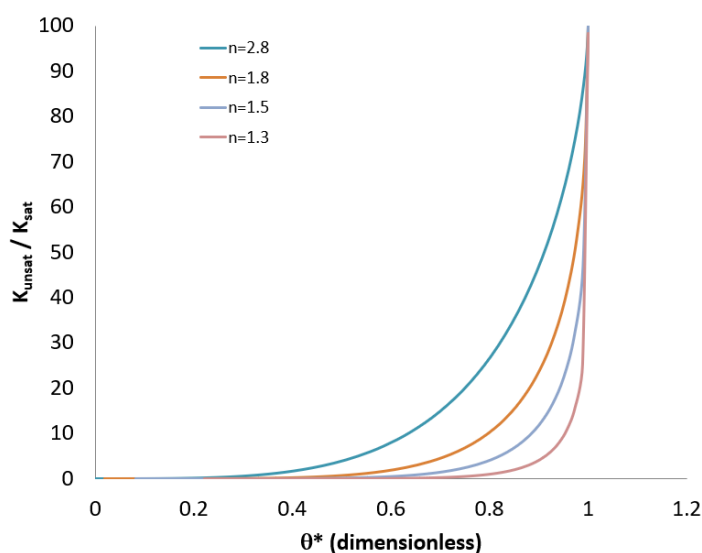


Figure 4.3 Soil retention curves for a range of different n values including the optimum model value of 2.8

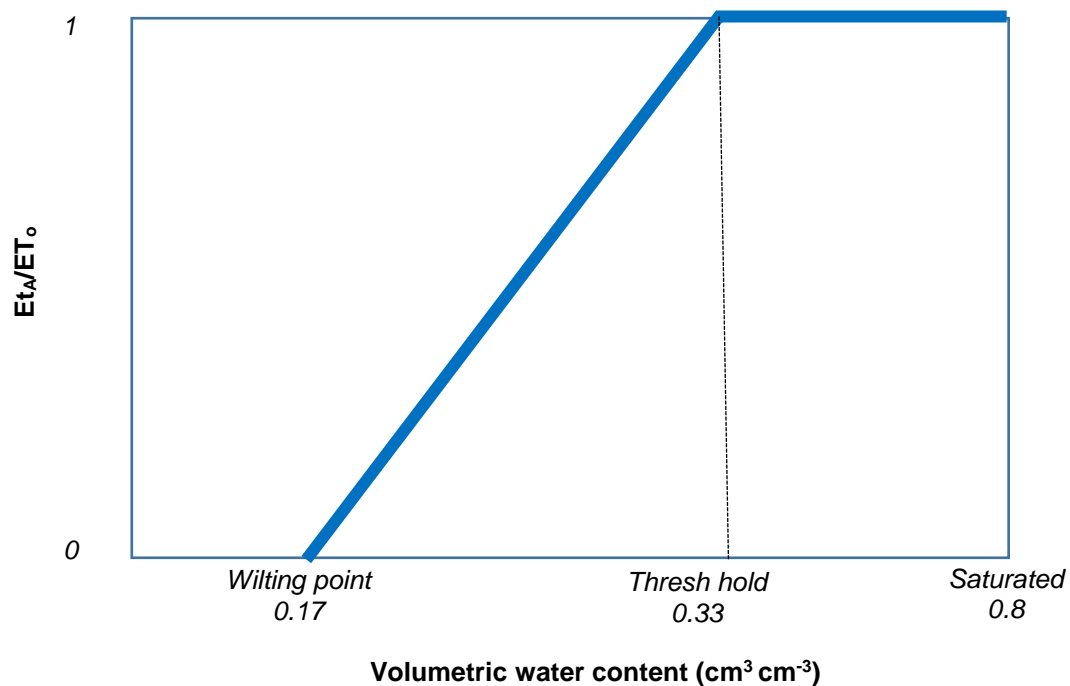


Figure 4.4 Visual relationship between the volumetric water content of the peat and evapotranspiration

The model was initially applied to a sub-catchment of the Sebungan estate (SE 1; area 800,000 m²), where detailed flow data (i.e. discharge, m³ s⁻¹) had been collected and a satisfactory approximation of catchment size was available. The calibrated model was then applied to the other Sebungan study sites (SE2, SE3, SE4) where catchment areas were unknown but where flow data had been continuously recorded. Only drainage area (m²) was adjusted to maximize the 'goodness of fit' between the measured and modelled discharge data. Both the calibrated values (Table 4.1) and the model run time (15/09/2016 – 06/01/2016) were kept constant. The performance of the model in generating the catchment area size was then assessed using the following metrics:

- a) The coefficient of determination (r^2) for the regression between measured and modelled discharge
- b) The root mean square error (RMSE)

- c) The Nash-Sutcliffe efficiency (NSE; Nash & Sutcliffe, 1970) used to quantify the goodness of fit between measured and modelled discharges i.e.:

$$NSE = 1 - \frac{\sum (C_{meas} - C_{est})^2}{\sum (C_{meas} - C_{mean})^2} \quad (4.1)$$

where C_{meas} is the measured discharge, C_{est} is the discharge estimated using the water storage model and C_{mean} is the mean measured discharge. The closer the NSE is to +1 the stronger the model fit. A value of 0 or lower indicates that the model performs no better than the mean of the data (Nash & Sutcliffe, 1970).

However, the wider application of the model was limited by a variable hydrological response of the Sabaju estates to the rainfall events. Furthermore, due to a met station equipment malfunction, the model could only be run for a brief time period (114 days), with its performance unlikely to be representative of the entire sample year.

Due to the limitations associated with manually defining catchment areas and the WMB approaches, the final attempt was to flow weight TOC concentrations (Method Five; Littlewood, 1992) so that TOC was proportional to the measured channel discharge (Figure 4.1; Approach 3). See Chapter Two, Section 2.8.3 for full method details. The annual area specific runoff depth (R_E) was determined by using measured hourly discharge data and the area for a known catchment, which in this case was SE 1. The recorded discharges (mm hour^{-1}) for SE 1 were summed (mm yr^{-1}) and scaled by the known catchment area ($A = 800,000 \text{ m}^2$) to provide an approximate annual flow volume of 2.8 m yr^{-1} (R_E). This value was approximately consistent with the runoff derived from the annual water balance, assuming negligible change in storage (2.0 m yr^{-1}). The value of R_E was assumed to be equal across all the plantation sites and was then multiplied by the flow-weighted TOC concentrations for all the plantation monitored channels, following the

method described in Section 2.8.3 (Chapter Two). The catchment areas for the plantation sample locations were then determined (equation 2.18, Section 2.8.3) and compared with the original catchment areas (i.e. that were manually mapped) and the plantation maps to check they were logical. The new catchment areas were then added onto the drainage maps generated using ArcGIS.

4.2.1.2 Forest

As no clear discharge outlets could be located at the forested sites manual discharge could not be measured. The hydrology was also expected to differ from the plantation area. This made a water balance approach the most appropriate option for determining the yearly fluxes from this landcover class (Figure 4.1). As previous attempts to derive ET_A (i.e. CMB) had proven unsuccessful, literature searches for ET_A values, which best approximated the forest sites, were obtained (Table 4.2). This yearly ET_A data, along with the measured yearly rainfall data, was then used to derive an estimate of annual area specific runoff (R_E). This value was then multiplied by the average TOC concentration data (mg L^{-1}) to calculate the yearly TOC yields for the forest landcover class. As ET_A for this landcover class was not directly measured a range of different estimates were used (Table 4.2; i.e. 1.6 to 1.9 m), to account for this uncertainty, which was then accounted for within the final flux estimates.

Table 4.2 Evapotranspiration estimates for forest sites

Rainfall (mm yr ⁻¹)	ET ₀ (mm yr ⁻¹)	ET _A (mm yr ⁻¹)	Runoff/discharge (mm yr ⁻¹)	Data sources
3167				<ul style="list-style-type: none"> Onsite weather station and plantation office records Supported by EIA Report (2006)
	1207	1219	1948	<ul style="list-style-type: none"> Average ET₀ estimate (Penman Monteith equation) using MET station data 15/09/2015 to 05/01/2016 Average ET_A estimate using <i>K_C</i> value of 1.01 (Liu et al., 2017)
		1242	1925	<ul style="list-style-type: none"> Hourly on-site ET_A data measured (April-September 2017) from the Sebungan Eddy covariance tower. Data was averaged to give mean daily ET_A and upscaled to represent a year.
		1553	1614	<ul style="list-style-type: none"> Eddy covariance variance derived ET data (mean over 4 year period) from a drained PSF, Central Kalimantan, Indonesia (Hirano et al., 2015).

4.3 Results

4.3.1 Hydrological investigation results

A time series of area specific runoff calculated using the areas derived from manual flow mapping are outlined in Figure 4.5. Average rates ranged from 0.18 mm hr^{-1} (SE 2) to 1.4 mm hr^{-1} (SA 3.5). The majority of sites (9 out of 14) displayed average hourly and yearly runoff rates $> 0.40 \text{ mm hr}^{-1}$ and $3,500 \text{ mm yr}^{-1}$, respectively. This was impossible considering mean annual precipitation for this region is *ca.* 3000 mm yr^{-1} , without accounting for the additional water losses from evapotranspiration.

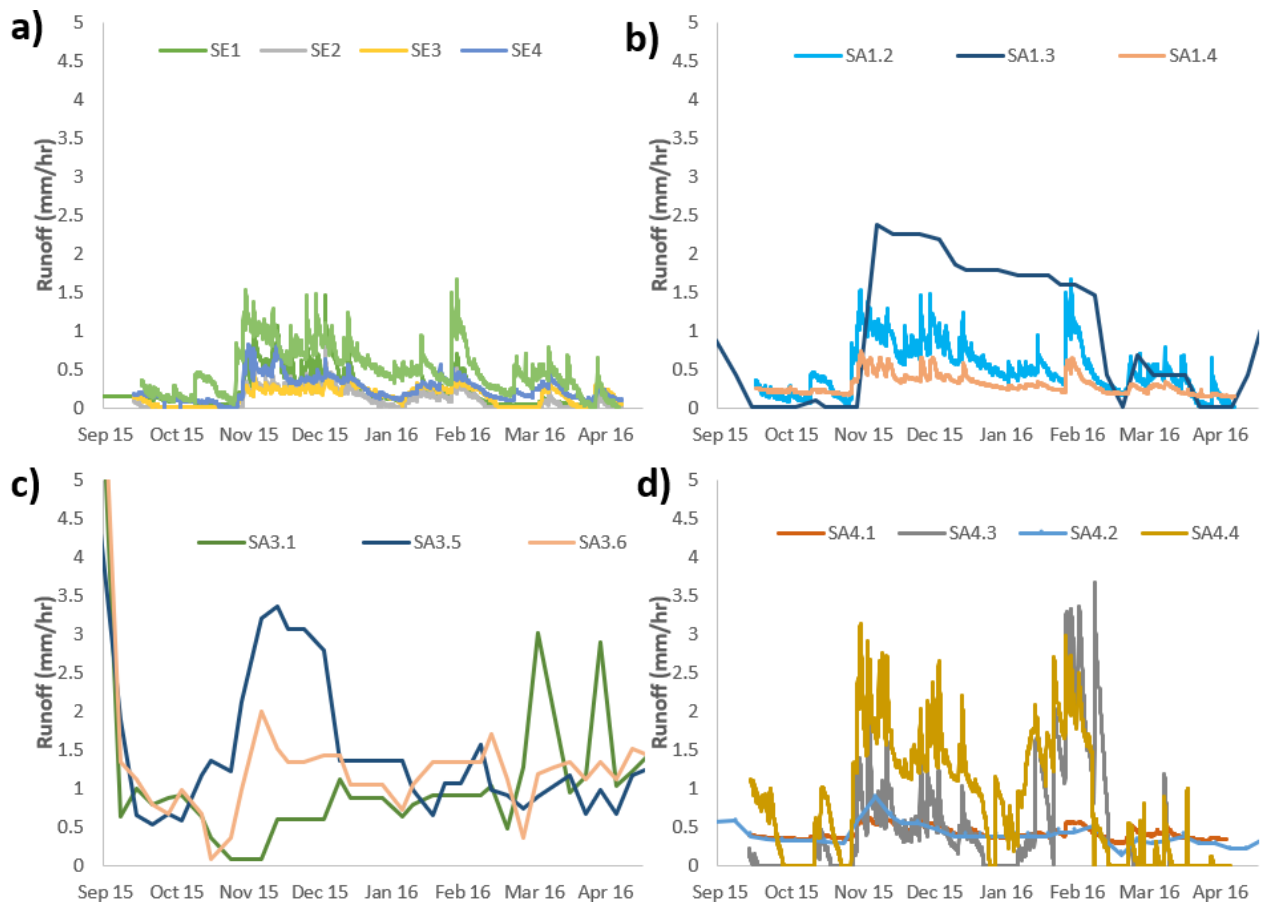


Figure 4.5 Time series of area specific runoff (mm hr^{-1}) for all flow monitored plantation drains, for an 8-month period across the SE (a), SA 1 (b), SA 3 (c) and SA 4 (d). The areas used to derive run off rates were obtained using the area estimates from manual flow direction mapping and delineation

Elevated plantation and forest ET_a (mm day^{-1}) estimates using the CMB approach arising from fertilizer contamination of the water samples, ranged from 4,163 to 5,485 mm year^{-1} . This far exceeded the annual average rainfall of the region (3,000 mm). Daily plantation ET_o (mm day^{-1}) values, derived from the Penman Monteith equation, averaged 3.3 mm day^{-1} . This gave an annual ET_o estimate of 1207 mm year^{-1} , resulting in ET_p values of between 1219 and 1448 mm yr^{-1} . These calculated ET (ET_o/ET_p) estimates are in line with similar values reported across Southeast Asia (Table 4.3). However, none of the literature reported values are from peatland OPPs, as available data from this landcover type is scarce.

Table 4.3. Evapotranspiration estimates from Southeast Asia across OPP and forest land cover classes

	ET_o estimates	Location	Reference
	4 – 5 mm day^{-1}	OPP all around Malaysia	Bakoume et al., (2013)
	3.9 mm day^{-1}	OPP within Peninsular Malaysia	Arshad (2014)
OPP on mineral soil	ET_a estimates	Location	Reference
	2.8-4.7 mm/day	OPP 2-25 years old, Jambi Indonesia	Roll et al., (2015)
	1.3 mm/day (dry season)	OPP 3-4-year-old OPP, North Kedah, Malaysia	Henson & Harun (2005)
	3.3-3.6 mm/day (wet season)		
	2.0-5.5 mm/day	OPP Peninsular India, dry season	Kallarackal et al., (2004)
	3.3-3.6 mm/day	OPP Malaysia, 2-9 year	Yusop et al., (2008)
	1200 mm/year	Average of mature OPP (range of studies)	Dislich et al., (2016)
Tropical forest	1545 mm/year	Borneo tropical forest (Lambir Hills, Sarawak) mineral soil	Kumagai et al., (2005)
PSF	1636 mm/year (intact PSF), 1553 mm/year (drained PSF), 1374 mm/year (drained and burnt PSF)	Southeast Asian PSF	Hirano et al., (2014)

The results from the soil-water transport model are presented in Figures 4.6 to 4.8 and Tables 4.4 and 4.5. Measured and modelled discharge for the calibration site (SE 1) is presented in Figure 4.6, for a catchment size of 800,000 m². The overall performance of the model for predicting discharge was 'excellent' with values of 0.88 for both R² and NSE, respectively (Table 4.4). The model's ability to estimate discharges was also strong for the other three sub-catchments (Table 4.4). In SE2 the model (Figure 4.7 a) was able to strongly reproduce the timing and magnitude of peak discharge events across the 114-day period.

Model performance was weakest within the SE3 and SE4 catchments (Figure 4.7 b and c), reflected by smaller R² and NSE metrics but a greater RMSE (Table 4.4). There was a relatively good agreement between measured and modelled discharges within the SE 3 catchment until the end of November 2015 (Figure 4.7=6 b), after which there was a noticeable discrepancy between the two data sets. In both cases (SE3 and SE4 catchments) the model tended to over-predict a very high magnitude event that occurred on 9th December 2015 (Figure 4.7 b and c). While the model within SE 4 recovered its estimations, with only slight overestimations occurring at the end of December 2015 (Figure 4.7 c), the model continued to deviate from measured discharges within SE3. Marked periods of underestimation occurred throughout mid-December 2015 to early January 2016, within the SE3 catchment. This was intersected by an overestimation in discharge on December 19th, 2015, due to a lagged response of the model to the timing of a measured discharge event which occurred on December 20th 2015.

The underperformance of the model, within SE4, is most noticeable during November 2015. During this month modelled discharges were underestimated by an average of 0.004 m³ day⁻¹ equivalent of 16 % of the respective measured daily discharge for November 2015. This difference is likely explained by the failure of the model to reproduce the timing of some events within November 2015. This resulted in peak discharge events, within the measured data, corresponding to sudden drops in modelled discharge

data. In addition, the model predicted a peak discharge event, on November 8th 2015, which was absent within the measured data set.

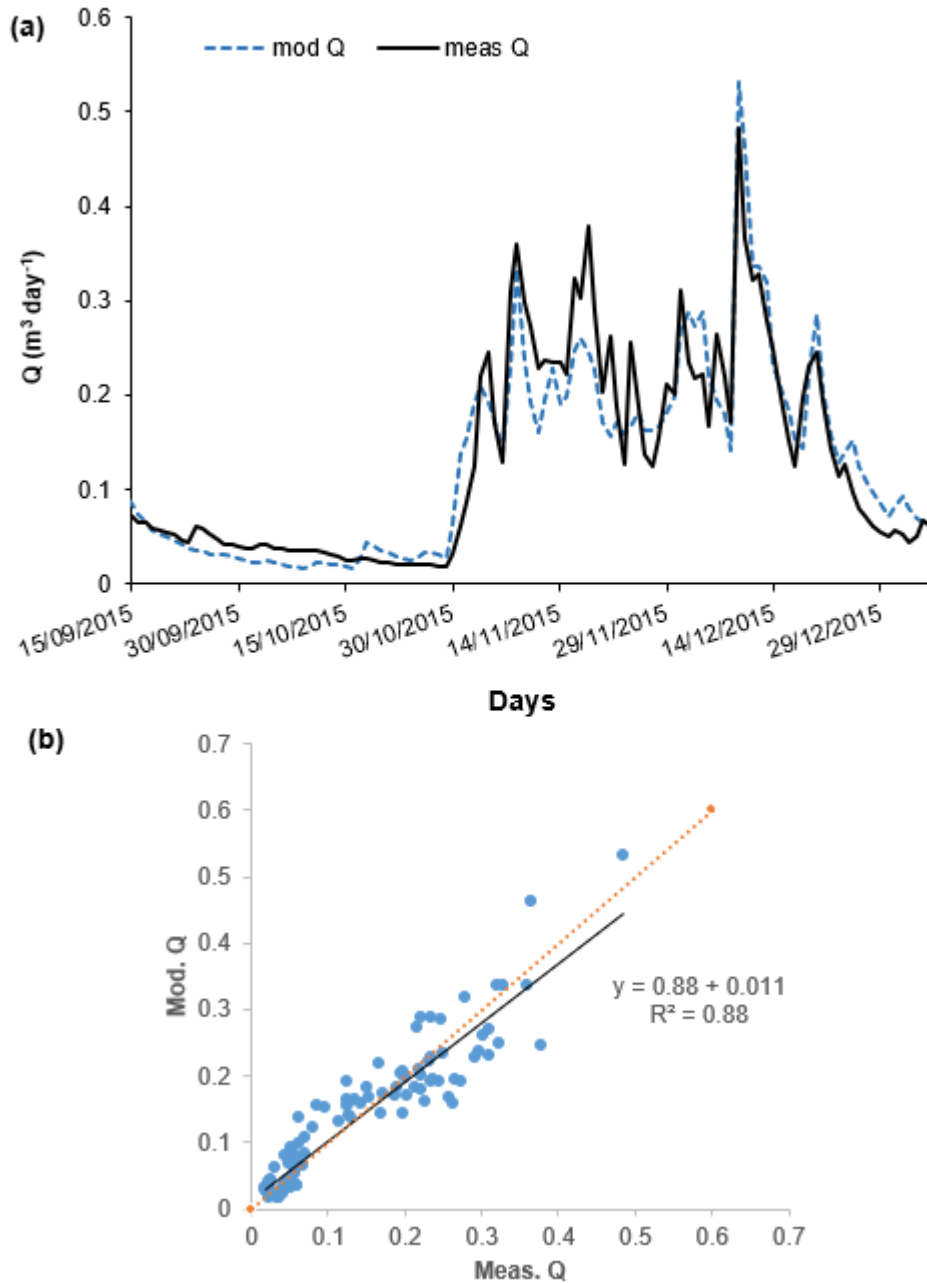


Figure 4.6 Discharge, measured (solid line) and modelled (dashed line) for the SE 1 calibration site (a) along with a regression of the measured and modelled discharge data (b).

Dashed line shows 1:1 relationship

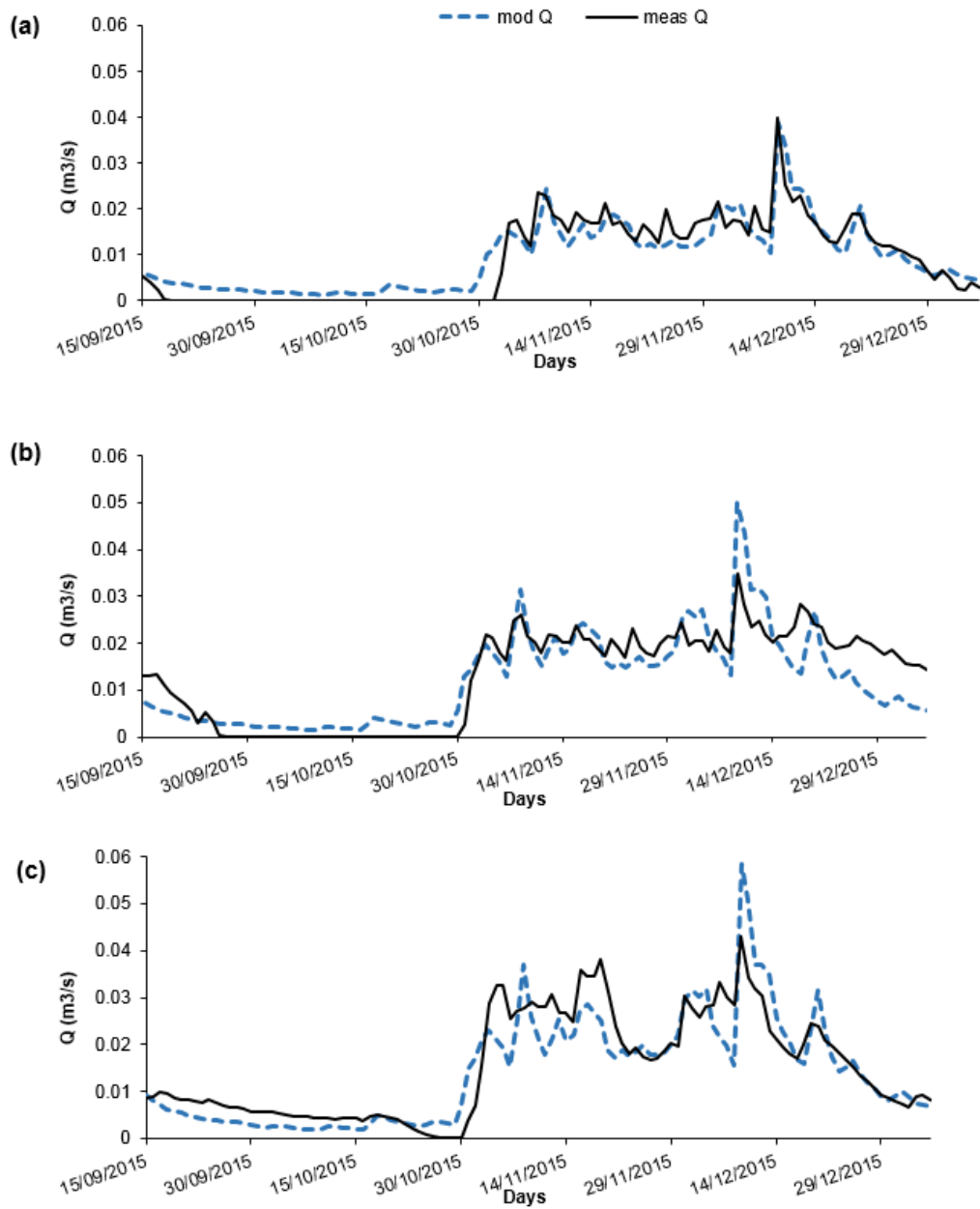


Figure 4.7 Modelled and predicted discharge in catchments (a) SE 2, (b) SE3, and (c) SE4

Table 4.4. Model performance statistics for the goodness of fit between the measured and modelled discharges, for the Sebungan catchments, along with the resulting catchment sizes.

Catchment	R ²	NSE	RMSE	Overall model performance*	Catchment size (m ²)
SE 1	0.88	0.88	0.038	Excellent	800000
SE 2	0.87	0.86	0.003	Excellent	5800
SE 3	0.73	0.70	0.005	Very good	7500
SE 4	0.78	0.75	0.005	Very good	8800

*Overall evaluation criteria based on performance intervals in Henriksen et al., (2003) where: $r^2 > 0.85$ = excellent; r^2 0.65 to 0.85 = very good, r^2 0.50 to 0.65 = good, r^2 0.20-0.50 = poor

When the model was run on the Sabaju sites it did not perform as well (Table 4.5). The model outputs (Figure 4.8) showed distinct discrepancies between the modelled and measured hydrographs, with some peak discharge events absent within the modelled (Figure 4.8 b and d) and measured (Figure 4.8 a and c) data sets. This is also reflected in the lower R² and NEE metrics and the higher RMSE's (Table 4.5).

Table 4.5 Model performance statistics for the goodness of fit between the measured and modelled discharges, for the Sebungan catchments, along with the resulting estimated catchment sizes.

Catchment	R ²	NSE	RMSE	Overall model performance*	Model estimated catchment size (m ²)
SA 1.2	0.67	-0.16	0.021	Very good	250000
SA 1.4	0.43	-0.56	0.042	Poor	480000
SA 4.1	0.68	-2.42	0.125	Very good	1100000
SA 4.4	0.64	0.60	0.027	Good	330000

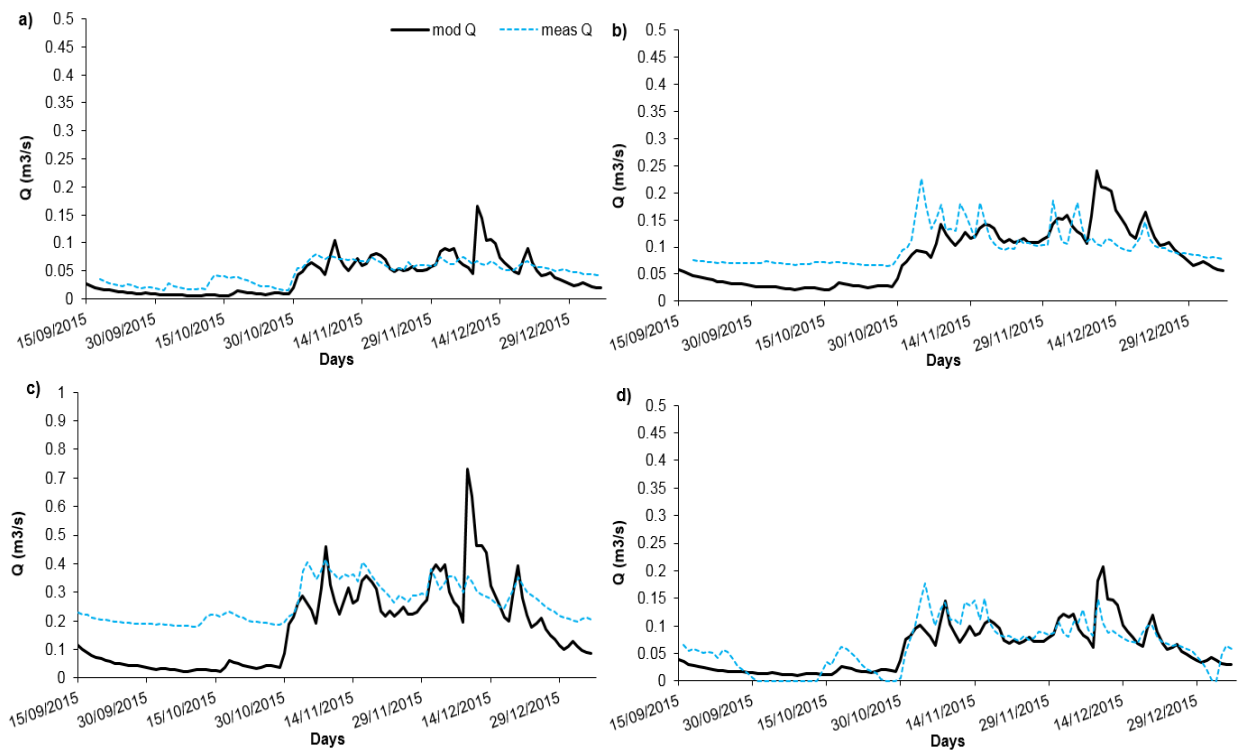


Figure 4.8. Modelled and predicted discharge in catchments (a) SA 1.2, (b) SA 1.4, and (c) SA 4.1 (d) SA 4.4

The catchment areas derived from volume weighting drainage channel TOC concentrations are presented in Table 4.6 (updated), alongside the original areas estimated from manual flow mapping. Updated catchment areas were derived for all sample point locations with the exception of SA 1.1, SA 3.2 and SA 3.3. These three catchments experienced sudden changes in their hydrological regime, throughout the year, as a result of plantation management efforts (i.e. ditch blocking). The updated catchment areas were then plotted on ArcGIS generated maps, and presented in Figures 4.9 to 4.12.

Table 4.6 Comparison of original catchment area estimates, derived from manual flow mapping (original), and new area estimates (updated) using volume weighted TOC concentrations. Grey shaded rows represent the point locations where only water samples were taken.

Site	Drain	Catchment area (m ²)	
		Original	Updated
SE1	M	800,000	800,000
SE2	C	220,000	82,000
SE3	C	310,000	149,000
SE4	C	210,000	146,000
SA 1.1	C	250,000	
SA 1.2	C	260,000	470,000
SA 1.3	C	240,000	380,000
SA 1.4	M	1,120,000	970,000
SA 3.1	C	250,000	1,000,000
SA 3.2	C	270,000	
SA 3.3	C	340,000	
SA 3.5	M	6,030,000	4,727,000
SA 3.6	C	170,000	830,000
SA 4.1	M	4,190,000	2,660,000
SA 4.2	M	3,700,000	1,310,000
SA 4.3	C	250,000	130,000
SA 4.4	C	220,000	450,000

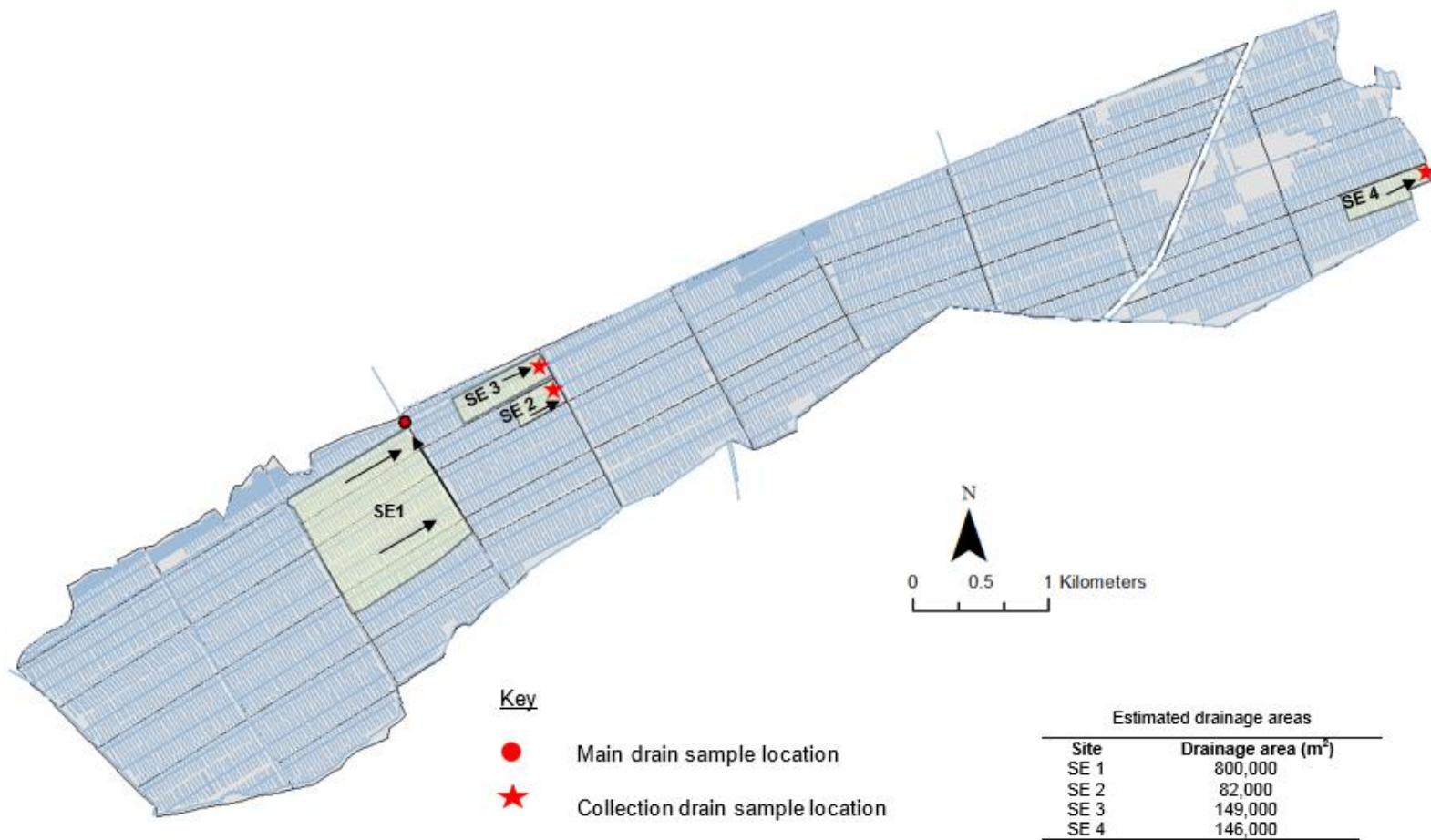


Figure 4.9 Map of the Sebungun estate, including the location of the four sampling point locations and their approximate catchment areas, arrows indicate the direction of water flow

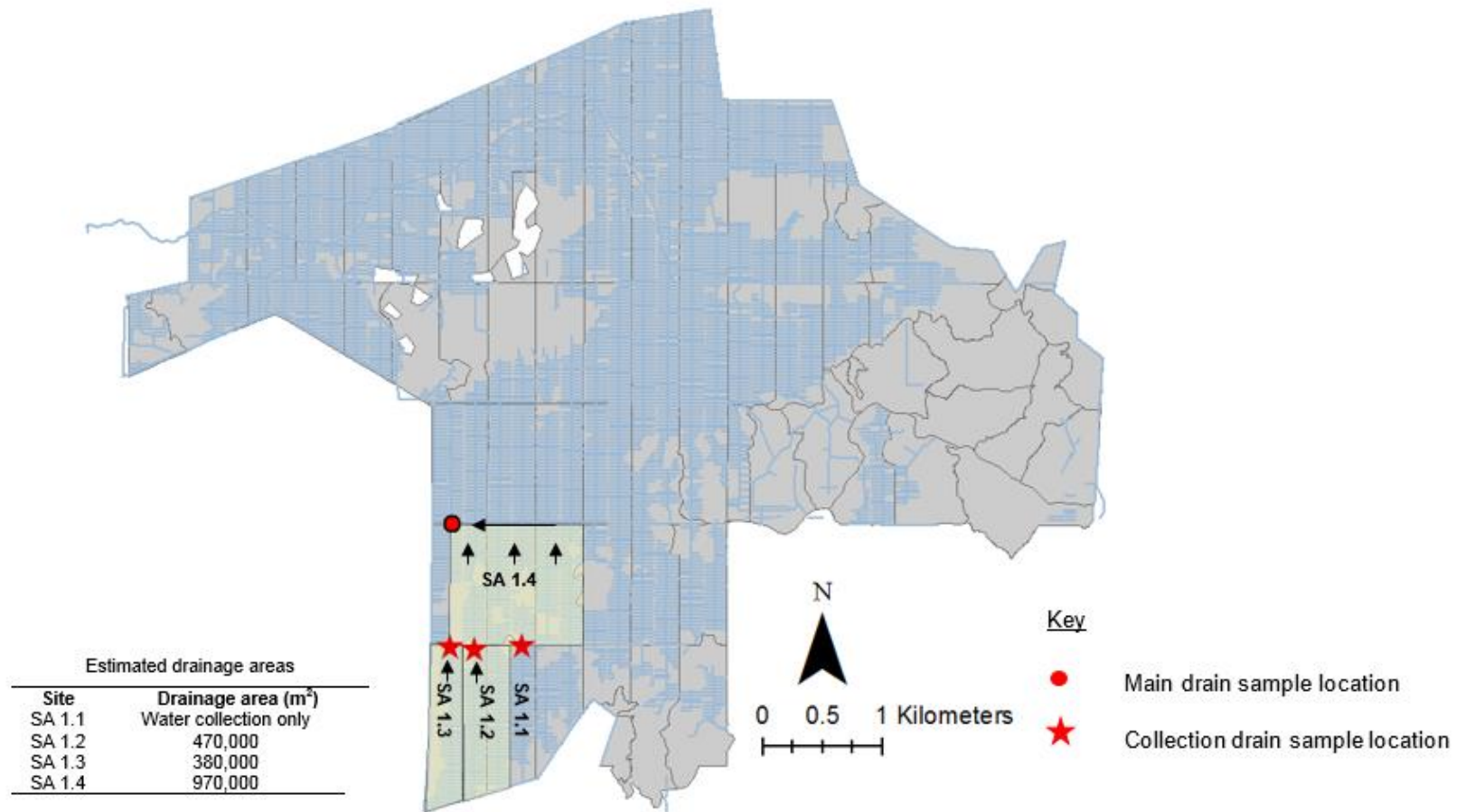


Figure 4.10 Map of the Sabaju 1 estate, including the location of the four sampling point locations and the approximate catchment areas for SA 1.2, SA 1.3 and SA 1.4, arrows indicate the direction of water flow

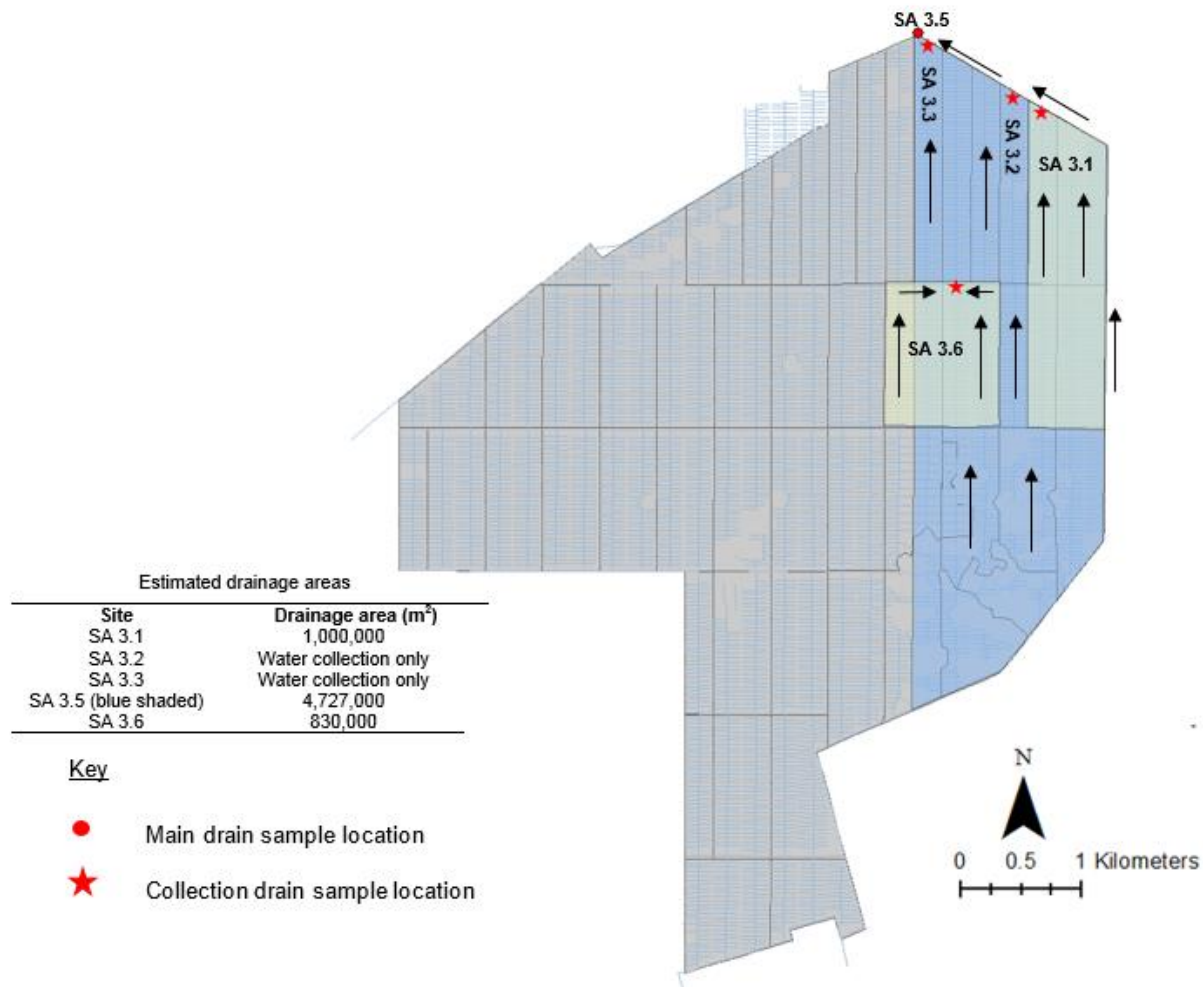


Figure 4.11 Map of the Sabaju 3 estate, including the location of the five sampling point locations and the approximate catchment areas for SA 3.1, SA 3.3 and SA 3.5, arrows indicate the direction of water flow. Note there is no SA 3.4

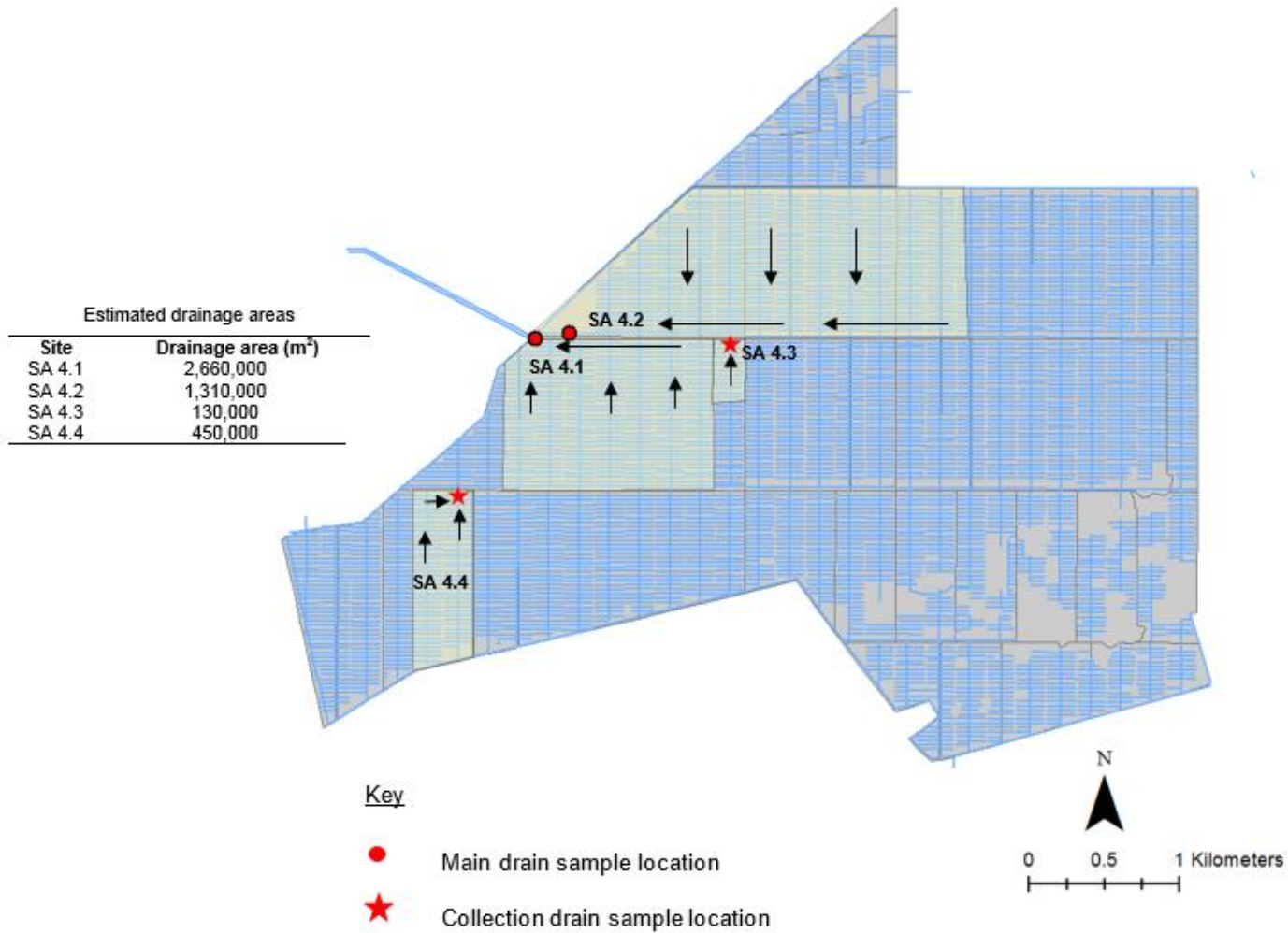


Figure 4.12 Map of the Sabaju 4 estate, including the location of the four sampling point locations and the approximate catchment areas for SA 4.1, SA 4.2 and SA 4.4, arrows indicate the direction of water flow

4.3.2 Rainfall and discharge

Figure 4.13 shows the monthly rainfall pattern during the course of the study measured at the SE plantation base (August 2015 to August 2016). This year was an exceptionally dry year in terms of annual rainfall due to the influence of the El Niño, which affected the area from January 2016 onwards. This effect is particularly clear when August 2015 and August 2016 rainfall totals are compared. Respective values were 337 mm month⁻¹ and 123 mm month⁻¹. In total 3167 mm of annual rainfall was recorded (August, 2015 – August, 2016).

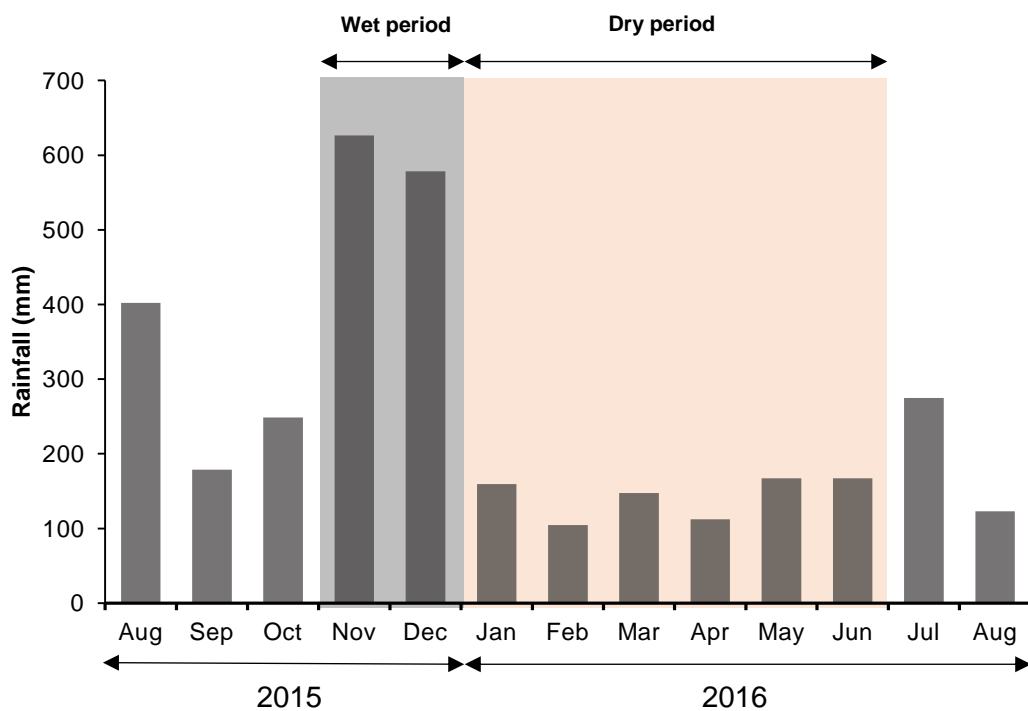


Figure 4.13. Monthly rainfall data (August 2015 to August 2016) compiled from a combination of data obtained from the rainfall gauge at the Sebungan plantation base (1st August 2015 – 5th January 2016) and manual measurements made by the plantation estate offices (August 2015 – 2016). Site monthly rainfall values were derived by averaging rainfall records collected from the rain gauge and the plantation offices, for the respective months.

The shaded areas indicate the timing of a distinct wet period (light grey; November to December 2015, inclusively) and dry period (light orange; January to June 2016, inclusively).

The highest rainfall occurred from November to December 2015, inclusively, with 38 % of annual rainfall received (1205 mm) during these two months alone. The highest daily rainfall recorded was on December 9th 2015 when 6 % of annual rainfall (181 mm) fell in a single day. In contrast, only 27 % of annual rainfall (858 mm) was received during the 6-month period from January to June 2016, inclusively. The driest month recorded was February 2016 in which only 105 mm fell (3 % of annual rainfall).

Catchment corrected discharge data for the eight plantation sites instrumented with mini-divers (as outlined in Table 2.4; Chapter 2) showed a seasonal trend (Figure 4.14), which followed monthly rainfall patterns. In general, SE displayed a flashier hydrological response in comparison to SA with relatively low base flow (0 to 5 mm day⁻¹) and high peak flow > 30 mm day⁻¹ during storm events (e.g. November to December, 2015 and May 2016). In contrast, the hydrographs for SA 1 and the main drain in SA 4 are damped with relatively high base flow (ca. 5 mm day⁻¹) and lower peak flows in the main drains (< 20 mm day⁻¹ for SA 1 and < 15 mm day⁻¹ for SA 4; Figure 4.14 b and c). In contrast runoff in the SA 4 collection drain (Figure 4.14) was flashy throughout the year. This is particularly evident from November 2015 to February 2016 when runoff was approximately double that in the main drains. During the dry period from February 2016 onwards runoff in the SA 4 collection drain was low with smaller peaks in discharge occurring in March, May and July, 2016 between periods of little or no flow. The wet period that occurred from November to December 2015, inclusively, accounted for between 26 % and 41 % of total annual runoff across the study sites, irrespective of drain type. In general, discharges were lowest during the months of February to April 2016, inclusively, with 19 % to 23 % of mean annual discharge occurring at this time.

There was a close match between runoff observed in the SE collection and main drains suggesting very similar catchment composition (i.e. hydraulic properties; Figure 4.14 a). This was also observed for the SA 1 main and collection drains during the wet periods (Figure 4.14 b) but base flow in the collection drains was substantially less than in the main drain.

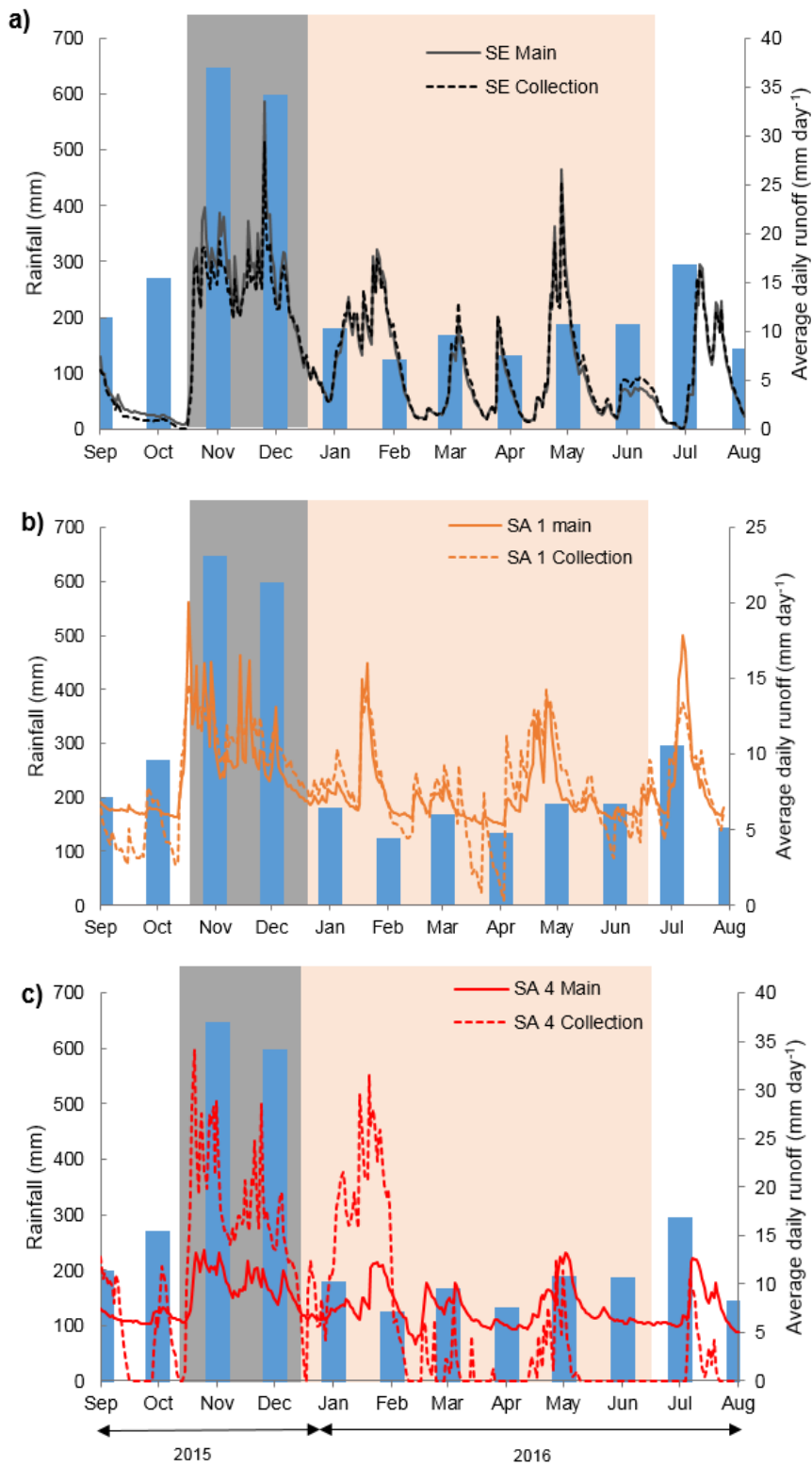


Figure 4.14 Runoff data (mid-September 2015 to mid-August, 2016) across the plantation sites instrumented with mini-divers in a) SE b) SA1 and c) SA4. Data presented are the mean daily runoff for the different drain types; calculated by averaging all daily runoff data for the respective drain type within each respective plantation. The shaded areas indicate the timing of a distinct wet period (light grey; November to December 2015, inclusively) and a dry period (light orange; January to June 2016, inclusively).

4.3.3 Total organic carbon

4.3.3.1 Landcover classes

Mean annual fluvial organic carbon concentrations for different landcover classes are displayed in Figure 4.15 and Table 4.7, alongside the DOC: POC ratios. The highest mean TOC concentrations were observed in R-DF (62.7 mg L⁻¹), followed by FA (51 mg L⁻¹) and DF (46 mg L⁻¹). There was no statistical difference between the mean TOC concentration at R-DF, FA and DF. The lowest concentrations were found within the plantation landcover class with marginally lower concentrations observed within the collection drains compared to the main drains. TOC concentrations were significantly higher in R-DF compared to all plantation drains ($p < 0.001$) and FB ($p < 0.0001$). Interestingly, TOC concentrations at FB were similar to those in the younger (6 years old) OPP. In terms of plantation ages, when grouped into their respective age categories (i.e. SA 3 & SA 4, 6 years old; SE & SA 1, 9 years old), there were highly significant differences in concentrations between drains of the same type but with different plantation ages (M 6 vs M 9, $p < 0.01$; C 6 vs C 9, $p < 0.0001$). The DOC: POC ratios ranged from 5.4 to 16.1 and were generally higher in the older OPP drains. In contrast, there was no difference in TOC concentrations between drains within the same age category (i.e. M 6 vs C 6).

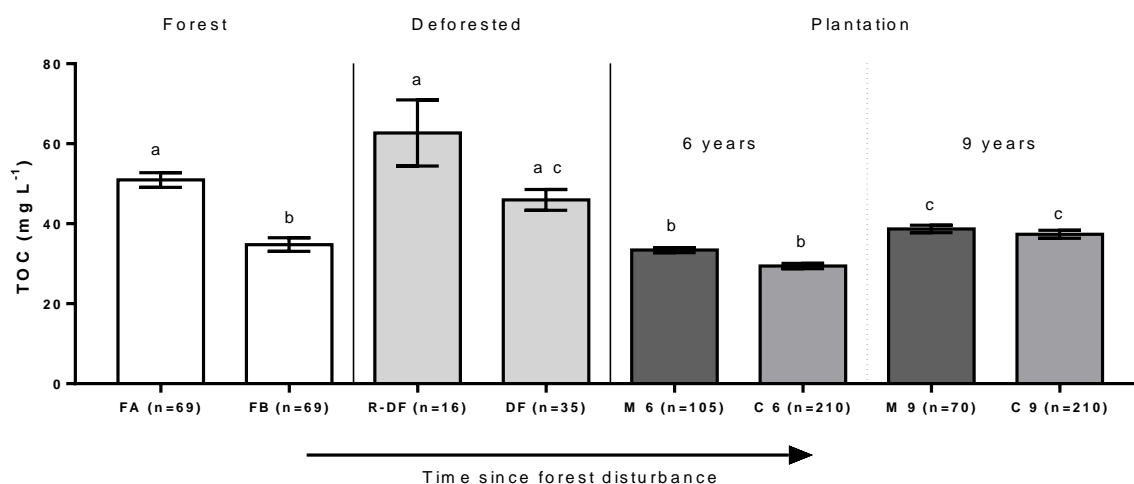


Figure 4.15 Mean TOC concentrations during the study period for all landcover classes (August 2015-2016; R-DF = February-August 2016), across a chronosequence of plantation ages. Where: M= main, C= collection, 6 and 9 = age of plantation in years and letters a to c denote statistically significant differences ($p < 0.05$) between study sites (Kruskal-Wallis test).

Error bars display the standard error of the mean.

Table 4.7. Summary of fluvial carbon data (+/- SEM) for different landcover classes

Landcover class		Mean DOC concentration (mg L ⁻¹)	Mean POC concentration (mg L ⁻¹)	Mean TOC concentration (mg L ⁻¹)	DOC:POC ratio
F	Overall	60.1 ± 1.33	5.8 ± 0.42	65.9 ± 1.42	11.4
FA		45.9 ± 1.67	5.1 ± 0.53	51.0 ± 1.83	10
FB		28.4 ± 1.44	6.4 ± 0.64	34.8 ± 1.69	5.4
R-DF		58.8 ± 8.29	3.9 ± 0.66	62.7 ± 8.27	16.1
DF		41.3 ± 2.44	4.7 ± 0.61	46.0 ± 2.61	9.8
P	Main	32.3 ± 0.61	3.3 ± 0.18	35.6 ± 0.57	10.8
	Collection	30.2 ± 0.60	3.2 ± 0.16	33.4 ± 0.62	10.4
P 6	Main	30.1 ± 0.69	3.3 ± 0.26	33.4 ± 0.65	10.1
	Collection	26.0 ± 0.68	3.4 ± 0.23	29.4 ± 0.66	8.6
P 9	Main	35.5 ± 1.00	3.2 ± 0.25	38.7 ± 0.94	12.1
	Collection	34.5 ± 0.91	2.9 ± 0.22	37.4 ± 0.96	12.9

Mean annual fluvial organic carbon concentrations for the individual plantation study sites are presented in Figure 4.16, with the composition of TOC across all study sites presented in Figure 4.17. Mean annual TOC concentrations ranged from 29.1 to 44.1 mg L⁻¹ and 27.9 to 41.9 mg L⁻¹ in the plantation main drains and collection drains, respectively. The SE plantation sites displayed the highest TOC concentrations with SA 3 exhibiting the lowest. When analysed separately there appeared to be no consistent trends in fluvial carbon concentrations between the individual estates (Table 4.8). Both the main and collection drains at SE were significantly different to all the other plantation sites ($p < 0.0001$) even SA 1, which is of the same age. In addition, TOC concentrations in the two immature plantations were found to differ from one another. The mean concentration in the SA 4 main drain was significantly higher than the mean concentration observed in the SA 3 drains (Table 4.8).

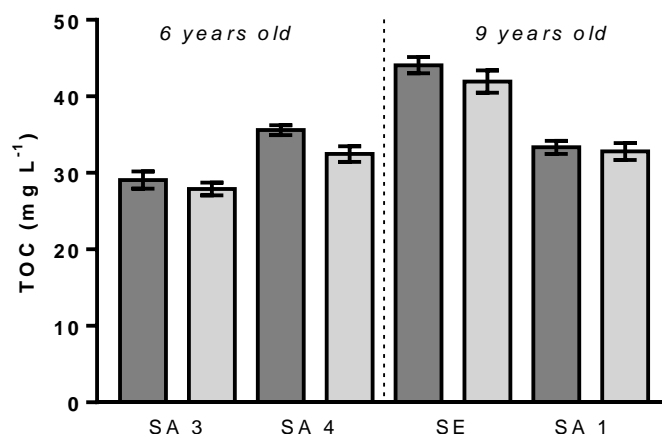


Figure 4.16. Mean TOC concentration data for the individual plantation study sites, split into main (dark grey) and collection (light grey) drains.

Table 4.8. Results of Kruskal-Wallis test (*post-hoc*; *Dunn's Multiple Comparison test*) for the TOC concentration data across the individual plantation study sites and drain types. Where ns = no significant difference and * = the level of significance (* = $P \leq 0.05$; ** = $P \leq 0.01$; *** = $P \leq 0.001$; **** = $P \leq 0.0001$)

	SA3 C	SA3 M	SA4 C	SA4 M	SE C	SE M	SA1 C	SA1 M
SA3 C		ns	ns	****	****	****	ns	ns
SA3 M			ns	**	****	****	ns	ns
SA4 C				ns	****	****	ns	ns
SA4 M					****	****	ns	ns
SE C						ns	****	****
SE M							****	****
SA1 C								ns

DOC is the dominant component of TOC, accounting for between 82 – 94 % of TOC, with POC contributing only 6 – 18 % (Figure 4.17). POC accounted for a greater proportion of TOC at the FB site (6.4 mg L^{-1} ; 18%) resulting in the lowest DOC: POC ratio (5.4; Table 4.7). In contrast, the lowest quantities of POC were found at the most disturbed site (R-DF) with a mean POC concentration of 3.9 mg L^{-1} and the highest DOC: POC ratio (16.1; Table 4.7).

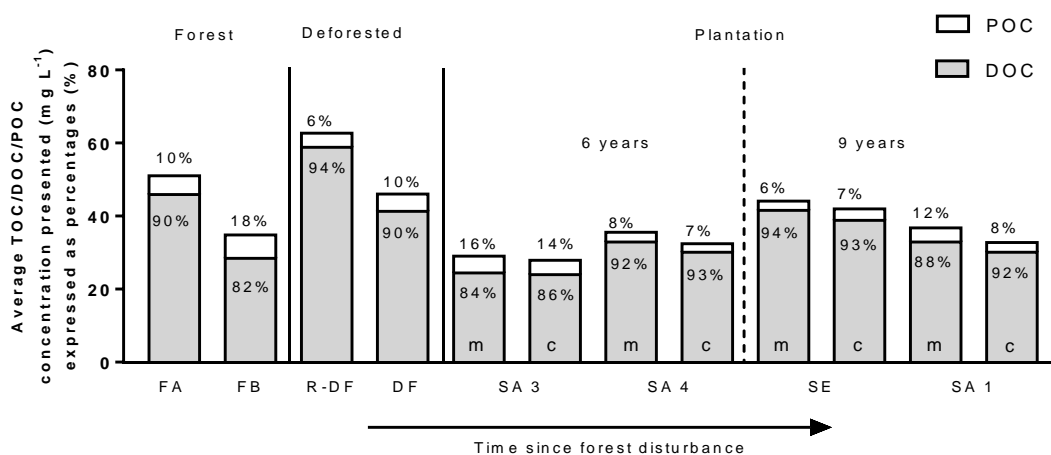


Figure 4.17. Mean TOC concentrations during the study period for sites split into components of DOC (grey) and POC (white), expressed as percentages. The plantation sites are further subdivided into the different drain types; main (m) and collection (c), and are positioned in time order since forest clearance.

4.3.3.2 TOC seasonality

Mean weekly TOC concentration data for different landcover classes over the study duration are presented alongside, i) monthly rainfall (Figure 4.18) and ii) daily rainfall data, where available (Figure 4.19). All landcover classes displayed substantial variability in TOC concentrations throughout the year (Figure 4.18). This variability appeared to be correlated with rainfall events, with some high TOC concentrations occurring during times of increased rainfall. This is more clearly visible in Figure 4.19. However, overall there was no correlation between weekly TOC concentrations and weekly rainfall for any of the landcover classes ($r^2 = 0.01$; $p = 0.19$; coefficient of variance, $CV = 37\%$ $n=242$).

In general, seasonal TOC variability was lowest within the P and F landcover classes, reflected in smaller standard errors (SEM) of 0.73 mg L^{-1} and 2.30 mg L^{-1} , respectively. There was no significant seasonal trend in TOC concentration for P, which remained relatively stable for the duration of the investigation ($\sim 25 \text{ mg L}^{-1}$ to 40 mg L^{-1} ; Figures 4.17 and 4.18). TOC concentration variability was also relatively stable within F. However high concentrations of TOC did occur during the first week of the investigation (Figures 4.18 and 4.16; mean = 82.8 mg L^{-1}). Distinctive peaks in the TOC concentrations in F were also observed during September, November and December, 2015 (Figure 4.18 and 4.19). From January to August 2016, TOC concentrations within F were fairly constant except for two peaks occurring in mid-February and mid-March 2016 (Figure 4.18). The deforested sites (DF and R-DF) displayed the greatest degree of TOC variability, particularly within R-DF as reflected in a high SEM of 8.27 mg L^{-1} . This is clearly demonstrated by four very distinctive peaks in TOC concentrations in mid-March, May, June and July 2016, with mean increases in TOC concentrations of $\sim 70 \text{ mg L}^{-1}$ compared to concentrations observed in the previous weeks.

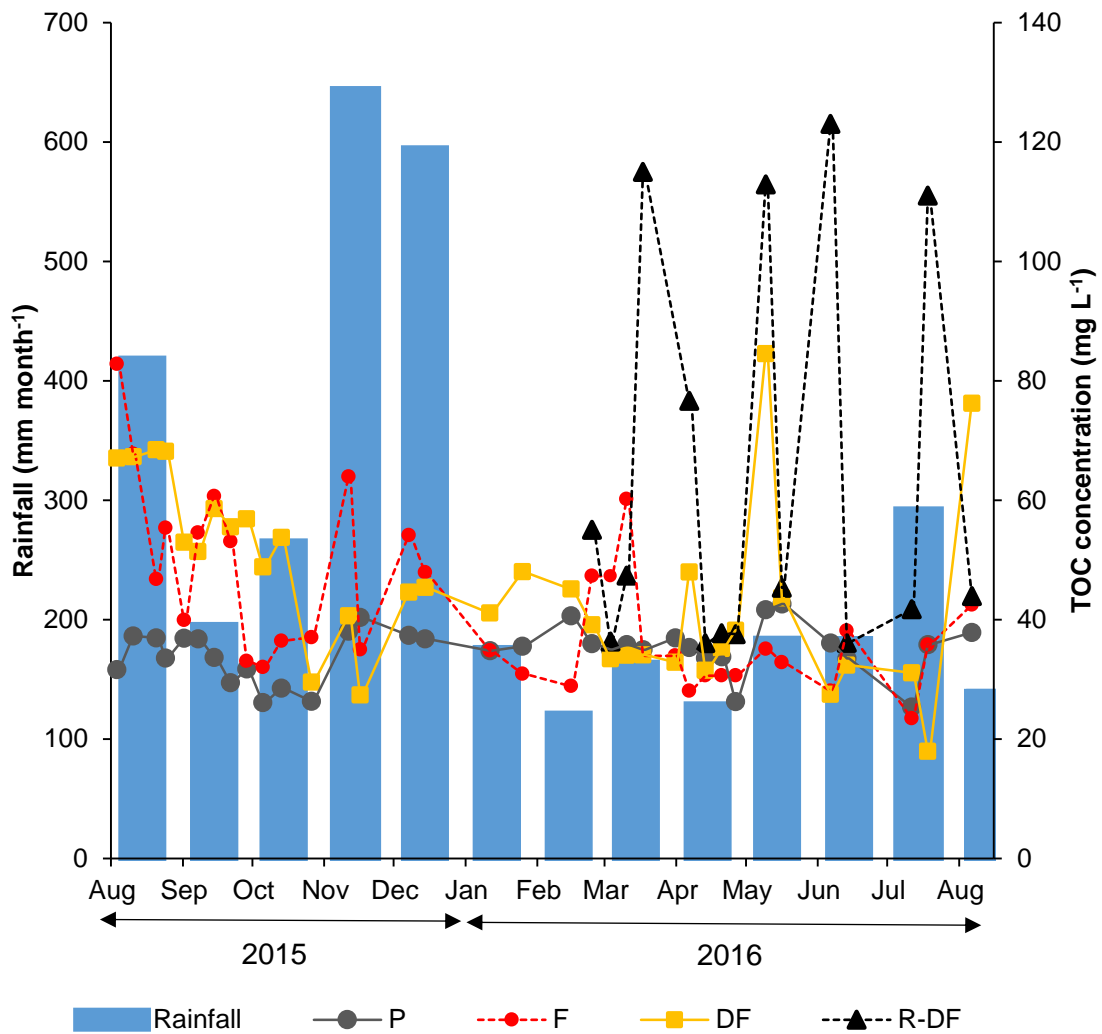


Figure 4.18. Weekly TOC concentration data for the different landcover classes, alongside monthly rainfall (mm). Data presented are mean weekly TOC concentrations from all drains within each landcover class. Monthly rain data were obtained from the rainfall gauge at the Sebungan plantation base (1st August 2015 – 5th January 2016) and manual measurements made by the plantation estate offices (August 2015 – 2016).

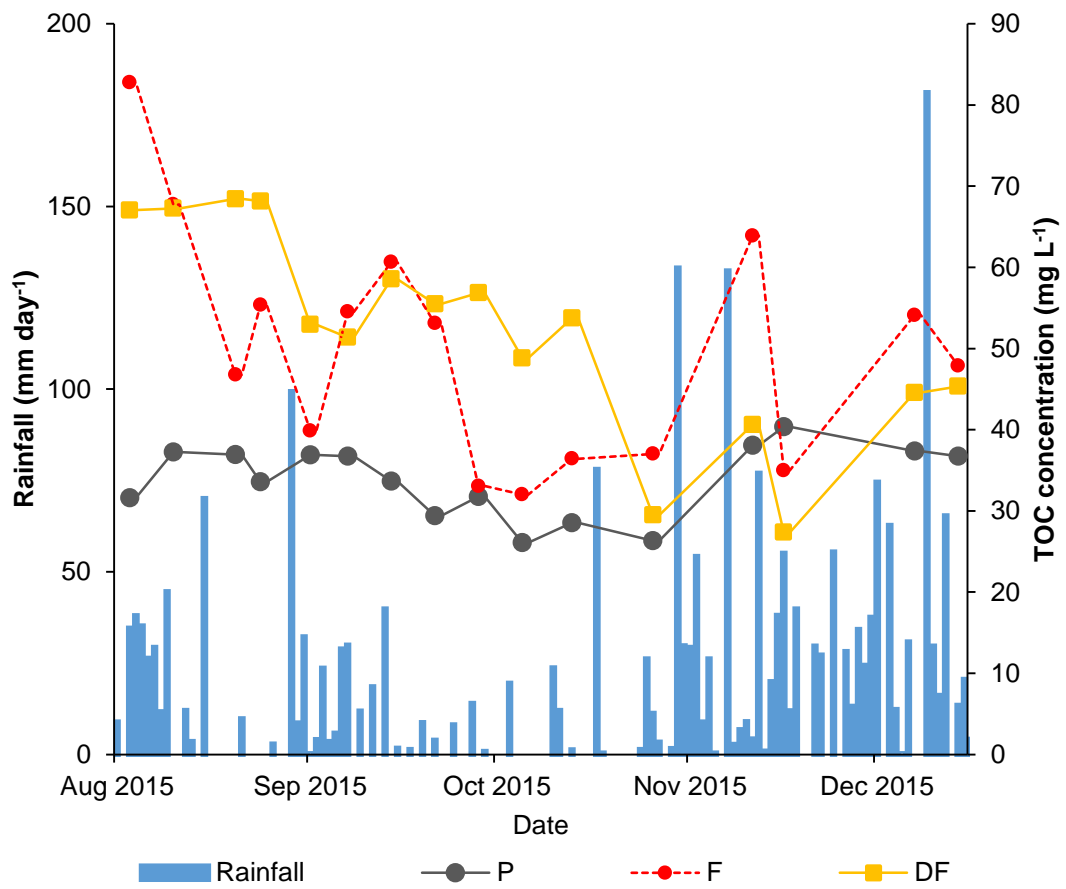


Figure 4.19. Weekly TOC concentration data for different landcover classes, alongside daily rainfall (mm day⁻¹) from 3rd August, 2015 until 15th December, 2016 when the onsite rain gauge was in operation.

A more detailed analysis of TOC variability within the individual forest sites and plantation estates is displayed in Figure 4.20. Both forest sites showed similar trends. However, site FA data were more variable, particularly at the start of the sampling year (i.e. September 2015). The plantation estates displayed comparable trends to one another, despite differences in the magnitude of TOC concentrations. Concentrations in the P sites declined at the start of sampling until November 2015 (Figure 4.20). Concentrations at all P sites increased from November 2015 but then remained relatively constant until February 2016. During this period (which was particularly wet) concentrations within the plantation SE were notably higher than the SA plantations. The variability from February 2016 onwards in the plantation data is less apparent in the forest data, with only one significant increase occurring in February/March 2016.

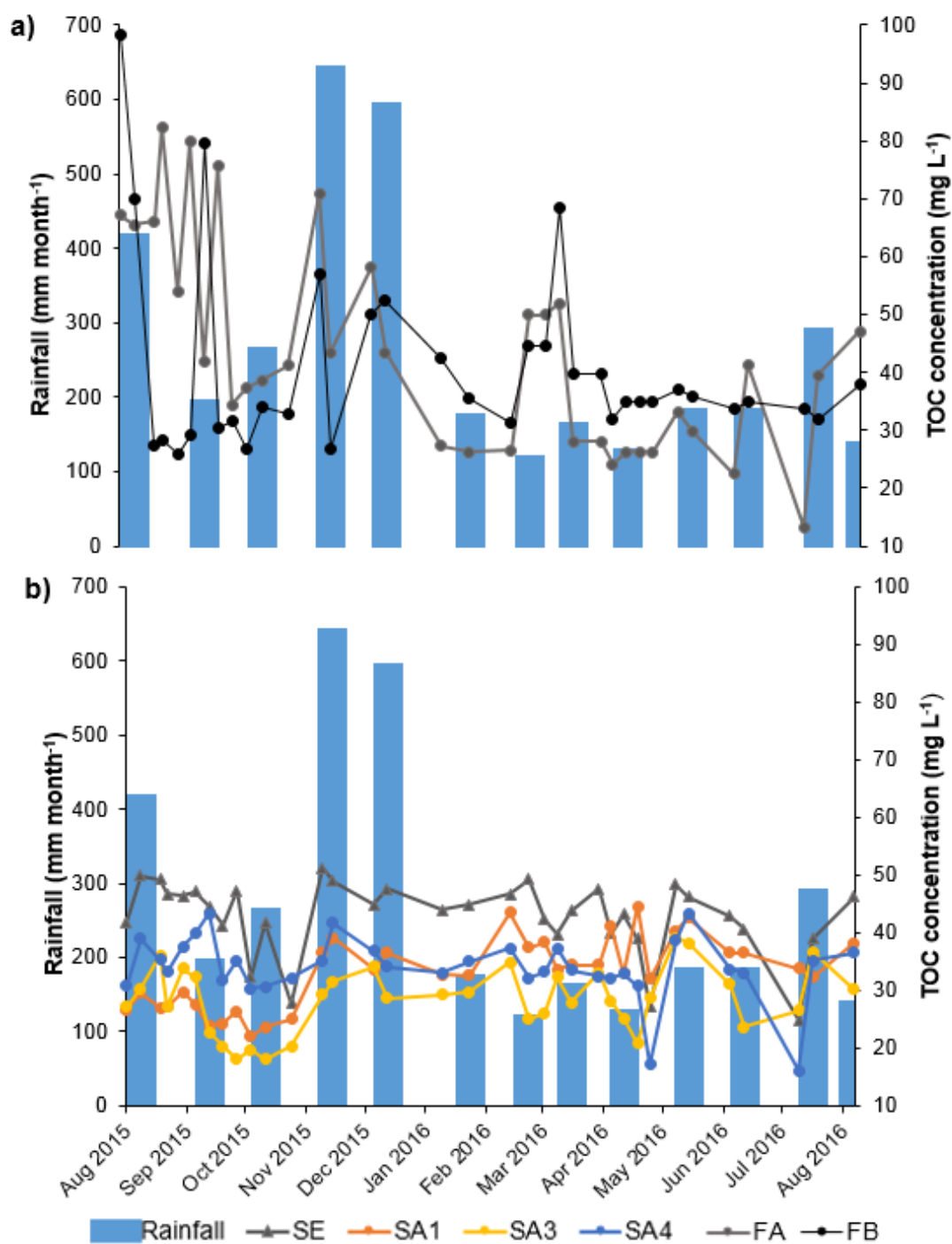


Figure 4.20 Weekly TOC concentration data for (a) the forest sites and (b) the plantation estates, alongside monthly rainfall (mm month⁻¹). Data presented are mean weekly TOC concentrations from all drains within each site. Monthly rainfall data were obtained from the rainfall gauge at the Sebungan plantation base (1st August 2015 – 5th January 2016) and manual measurements made by the plantation estate offices (August 2015 – 2016).

4.3.3.3 Temporal dynamics of TOC

The relationship between weekly TOC concentration and discharge is shown in Figure 4.21 for the entire study period. Similar plots for two high discharge periods during the wet and dry seasons are shown in Figure 4.22 a and b and Figure 4.22 c and d, respectively. The solute rating curves presented in Figure 4.22 are divided according to season and respective drain type.

There was no overall correlation between weekly TOC concentration and discharge (Figure 4.21). However, the hysteresis curves (Figure 4.22) revealed systematic temporal changes in weekly TOC in response to peak discharge events. During the wet season, the SA drains exhibited counter-clockwise hysteresis loops (Figure 4.22 a and b.), with lower TOC concentrations on the rising limb of the hydrograph. In contrast, concentrations in the SE drains exhibited a clockwise loop, with elevated TOC concentrations occurring before peak discharge. The slope of the hysteresis loops varied between estates and drain types. SA 3 (main, wet conditions) exhibited an elongated hysteresis loop with a prolonged period of elevated TOC concentrations during hydrograph recession (Figure 4.22 a). The relationship between TOC and discharge on the rising and falling limbs were also steady and uniform. This suggests a dampened response of TOC to discharge, with large increases in discharge causing only small increases in TOC. A similar pattern was exhibited in the SA 1, SA 3 and SA 4 collection drains (wet conditions; Figure 4.22 b). However, TOC concentrations were more variable on the falling limb, particularly for SA 1 and SA 3. By contrast, the main drains in SA 1 and SA 4 (main, wet conditions) and both SE drains (main and collection, wet conditions) exhibited much steeper solute rating curves suggesting a sensitivity of TOC to small changes in discharge (Figure 4.22 a).

During the dry period all plantation estate drains exhibited a counter-clockwise hysteresis (i.e. higher concentrations on the recession limb than the rising limb; Figure 4.22 c and d). The SA3 and SA1 main drains and, to a lesser extent, SA 1 collections drains displayed a more open and pronounced loop form, suggesting variability in both TOC concentrations and discharge. By contrast,

the gradient on the solute rating curve for the SE main drain was close to zero. This implies low TOC concentration variability despite relatively large changes in discharge. This suggests that the 'availability' of DOC is approximately proportional to flow rate (i.e. the more flow you have the higher TOC concentrations). Conversely, the SE collection drains showed a particularly strong response of TOC to small changes in discharge, with rapid TOC concentration increases on the rising limb (Figure 4.22 d, black line). Similar patterns were also exhibited by SA 3 collection and SA 4 main drains.

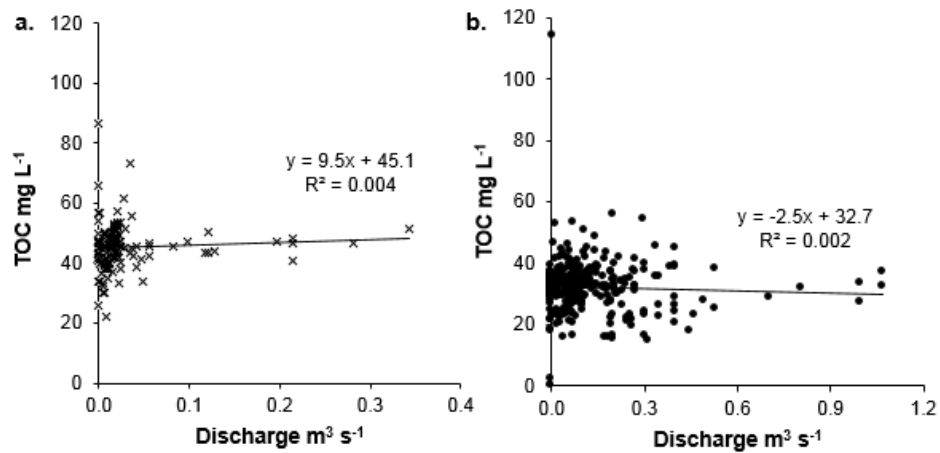


Figure 4.21. Solute rating curves for the Sebungan (a, n=132) and Sabaju (b, n=347) plantation estates, along with goodness of fit metrics (r^2) and line equations. Note different x axis scales.

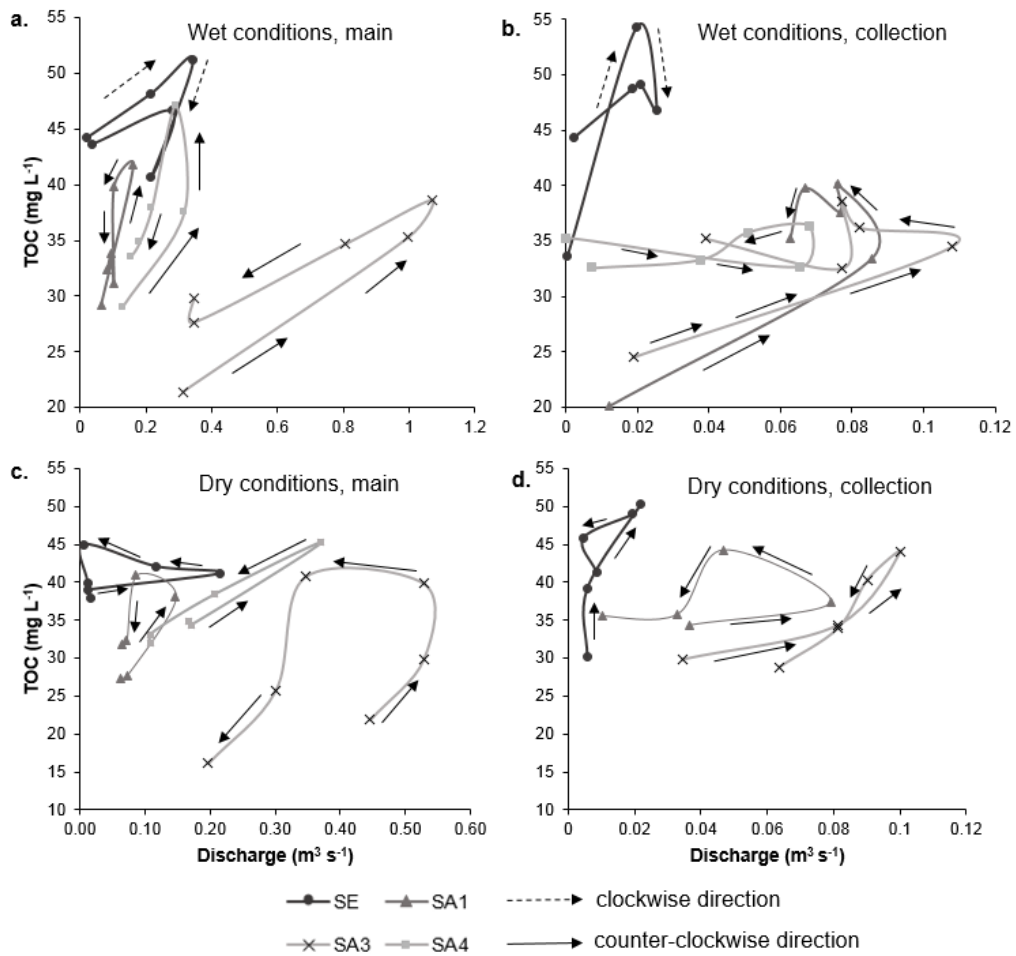


Figure 4.22. Solute rating curves displaying hysteresis curves in weekly solute concentrations against stream discharge, for a high discharge period during the wet season (event from November, 2015 – January, 2016; a and b) and the dry season (event from April-June, 2016; c and d). The data presented are the mean weekly discharge and TOC concentrations from the main (a,c) and collection (b,d) drains for each plantation estate. Discharges were taken at the time of water sample collection. The collection drain for SA4 has been omitted from graph (d) due to low/no flow data. Arrows indicate the direction of hysteresis for each high discharge period.

4.3.4 Environmental parameters

The mean watertable depths for the individual study sites are displayed in Figure 4.23. The lowest mean watertable depth (i.e. furthest from the peat surface) was exhibited in the FB forest site (-75.7 cm) followed by SE (-55.3 cm). The highest watertable (i.e. closest to the peat surface) was observed in SA 1 (-31.3 cm) and FA (-32.7 cm). SE displayed the greatest degree of variability with depths ranging from -128 cm below the peat surface to + 5 cm above it. This was closely followed by SA 3 with watertable depths ranging from -82 cm to + 4 cm. lowest variability was observed at SA 1 where watertable depths varied between -53 cm to -6 cm, below the peat surface.

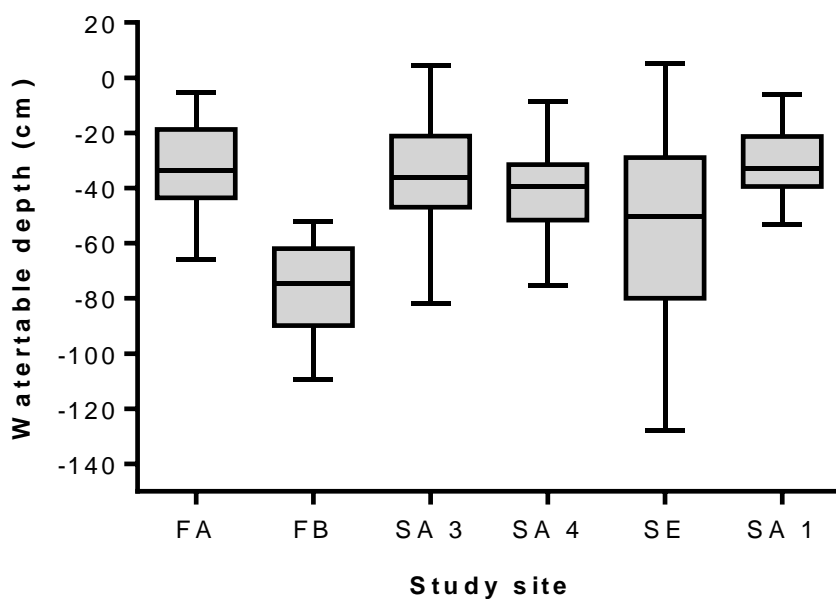


Figure 4.23. Watertable depths for the plantation and forest study sites across the study period (August 2015-September 2016). Box plots show mean watertable depth from all watertable monitored areas (central horizontal line), along with the minimum and maximum heights recorded over the entire study period (bars). Box = 75th and 25th percentiles.

Negative numbers denote distance below peat surface.

The watertable data displayed a degree of seasonality. This was correlated with monthly rainfall (Figure 4.24). As expected, the watertable rose in months with high rainfall (e.g. November and December, 2015) and fell in months with low rainfall (e.g. February, 2016).

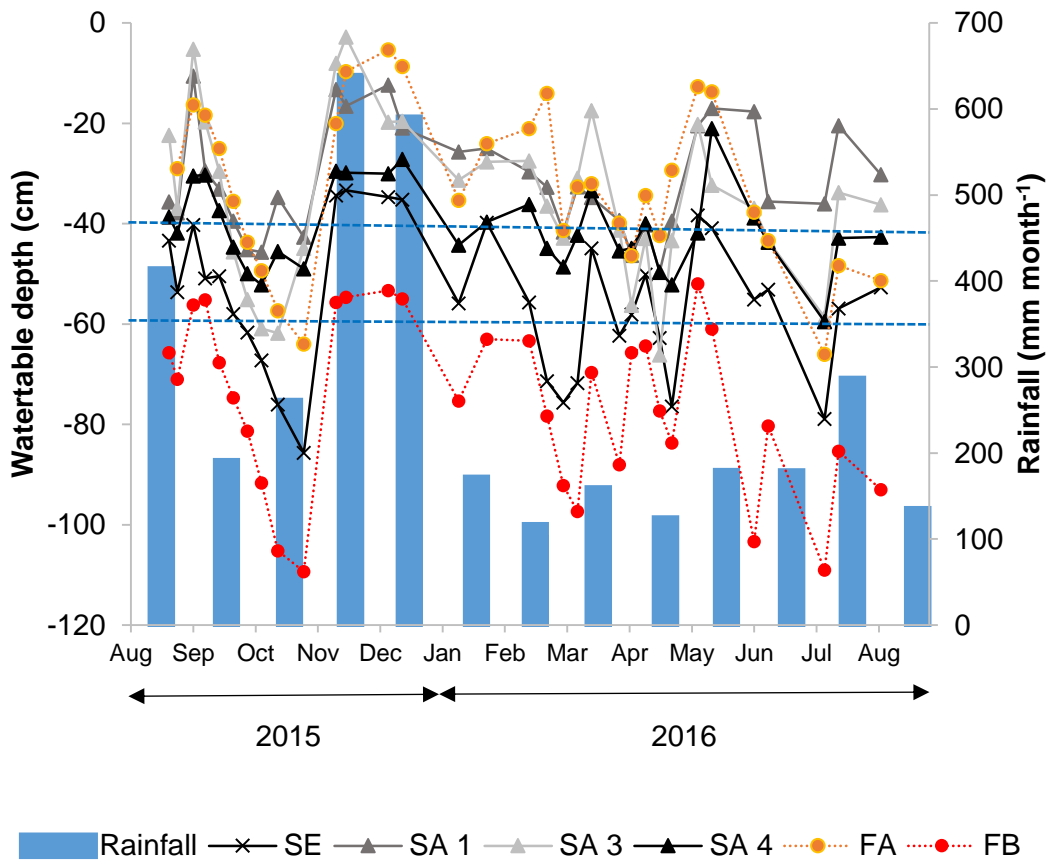


Figure 4.24. Weekly watertable depths measured in dipwells for the individual study sites. Date presented are the mean weekly watertable depths from all monitored areas within each study site. Negative numbers denote distance below peat surface. Blue dashed lines indicate the recommended RSPO watertable depth range for OPPs on peat (between – 40 to – 60 cm)

For much of the study period the watertable depth varied between – 40 and – 60 cm in both SE and SA 4 (Table 4.9), which are within the limits set by the Roundtable on Sustainable Palm Oil (RSPO) for OPP on peat (Lim et al., 2012). However, at other times the SE estate was operating under flooding or drought conditions. In contrast, the watertable depths within SA 1 and SA 3 tended to exceed the upper limit of – 40 cm throughout the year (Figure 4.24, Table 4.9). Watertable depths at the two F study sites were very different. At the FA site watertables were within 40cm of the surface for 66% of the time. By comparison, watertable depths within FB were always more than 40cm from the surface and commonly below 60cm (Figure 4.24, Table 4.9).

Table 4.9. Period of time, expressed in percentages, when the watertable was within a certain depth range. Bold and underlined figures highlight the most common depth range.

	Between - 40 to - 60 cm	40 cm <	60 cm >
SE	<u>48 %</u>	18 %	33 %
SA 1	21 %	<u>79 %</u>	0
SA 3	30 %	<u>61 %</u>	9 %
SA 4	<u>61 %</u>	39 %	0
FA	28 %	<u>66 %</u>	6 %
FB	21 %	0	<u>79 %</u>

There was a weak but statistically significant ($p < 0.05$) relationship between watertable depth and TOC concentration for the P and F sites (Figure 4.25). A high TOC concentration tended to occur when the watertable was closer to the peat surface. Values (r^2) ranged from 0.15 (SA 4.3) to 0.41 (SA 3.3). This trend was also exhibited in Figures 4.26 and 4.27, which show concurrent changes in TOC concentration and watertable depth over time. However, it is also clear that high TOC concentrations also occurred occasionally during periods of watertable decline as illustrated in February and March 2016 within the SE data set (Figure 4.26 a).

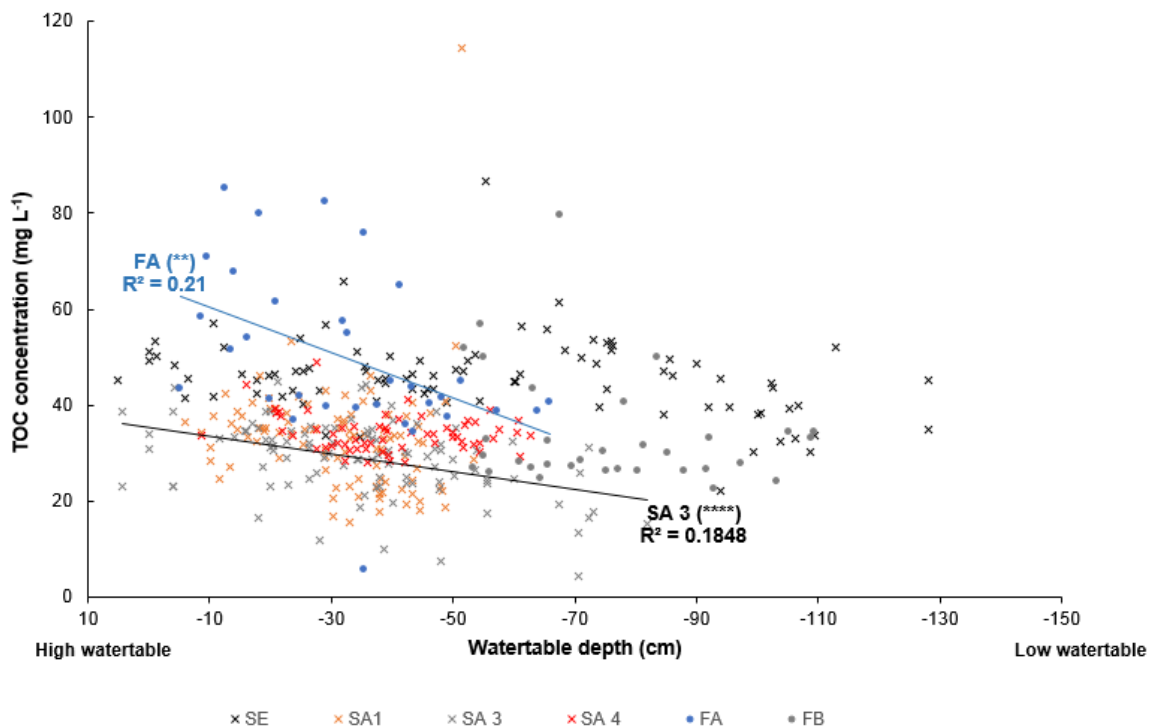


Figure 4.25 Relationships between average weekly watertable depth (cm) and average weekly TOC concentration (mg L⁻¹) for all monitored areas. Significant correlations were observed for FA ($r^2 = 0.21$ **, $n = 32$) and SA 3 ($r^2 = 0.18$ ****, $n = 33$); where * = the level of significance (* = $P \leq 0.05$; ** = $P \leq 0.01$; *** = $P \leq 0.001$; **** = $P \leq 0.0001$)

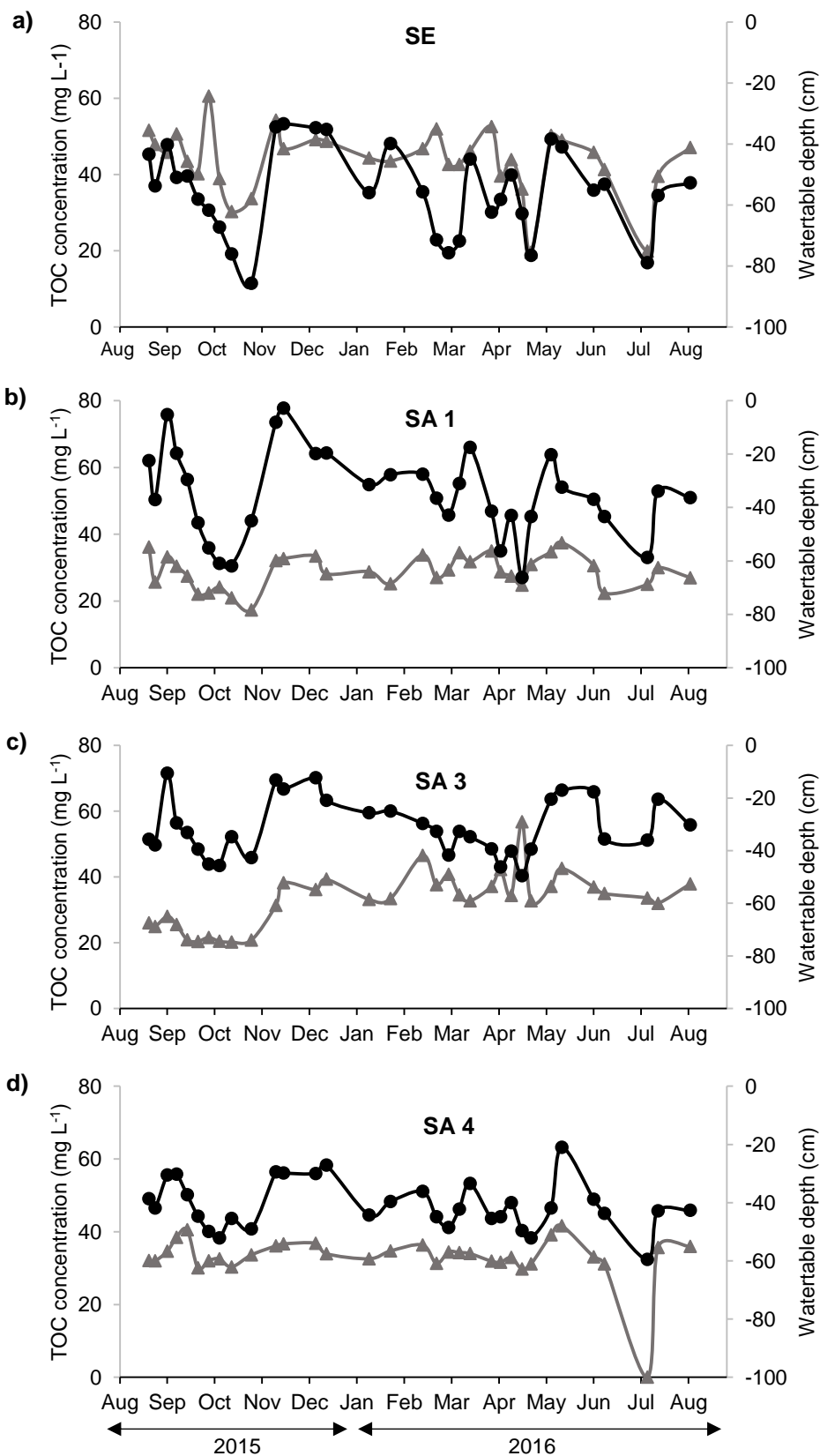


Figure 4.26 Time series of weekly mean TOC concentrations (grey) and concurrent weekly mean watertable depths (black) taken at the time of sample collection, for the four plantation estates.

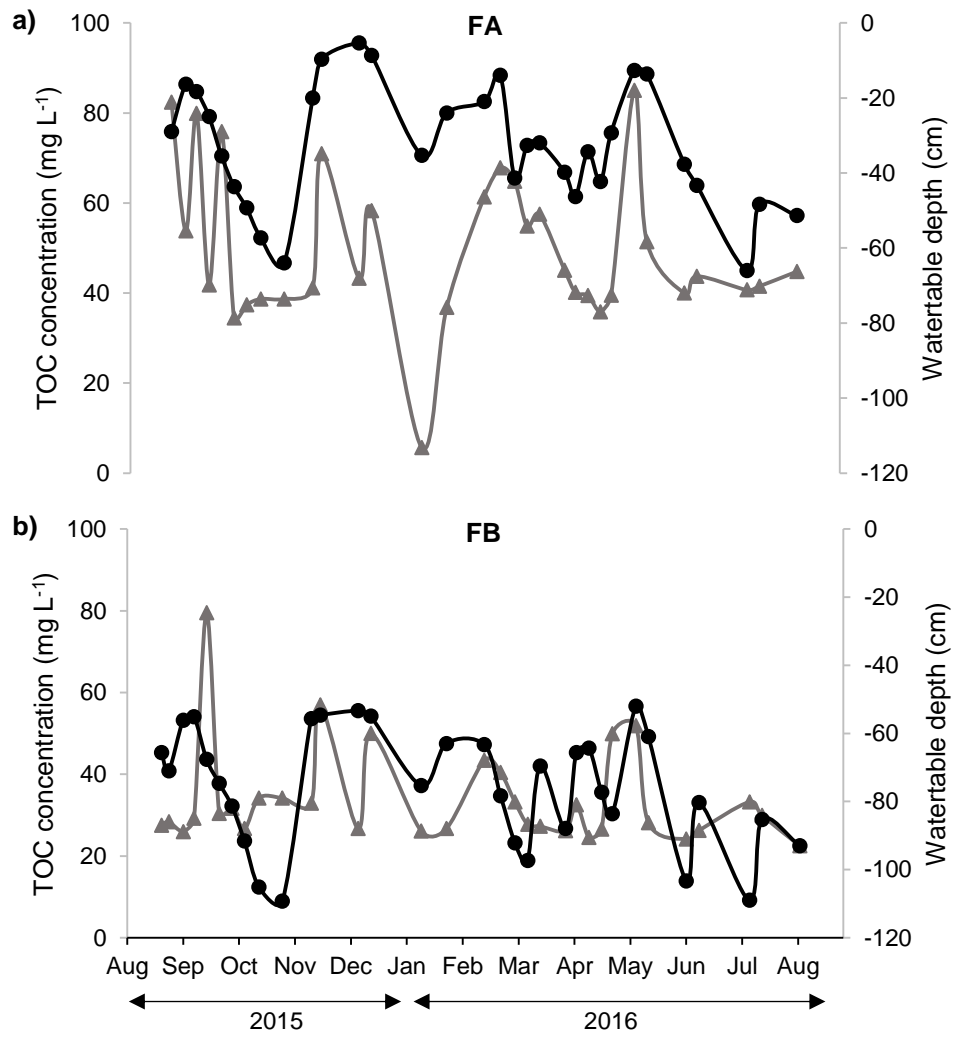


Figure 4.27 Time series plots of weekly mean TOC concentrations (grey) and concurrent weekly mean watertable depths (black) for the forest sites.

The pH and EC ($\mu\text{S cm}^{-1}$) values varied across the different landcover classes (Table 4.10), and overall ranged from 2.5 to 6.6 and $60 \mu\text{S cm}^{-1}$ to $560 \mu\text{S cm}^{-1}$, respectively. In terms of pH and EC, there was no overall correlation between these two parameters and TOC concentration ($r^2 = 0.01$, $p > 0.05$, $n = 1207$; Figure 4.28). However, significant correlations were observed when individual landcover classes were analysed (Figure 4.28). For the F landcover classes the TOC concentration displayed a weak but statistically significant relationship ($p < 0.0001$, $n = 212$) with both pH and EC, with r^2 values of 0.36 and 0.13, respectively (Figure 4.28). In addition, a weak positive relationship was observed between TOC concentrations in the R-DF landcover class and EC ($r^2 = 0.34$, $p < 0.05$, $n = 17$; Figure 4.28 b). However, this relationship was driven by two outlying points which, when removed, resulted in no correlation ($r^2 = 0.001$) between these two variables.

Table 4.10. Mean pH and EC readings for all water samples across the different landcover classes, along with number of samples (n) and errors are given as +/- SEM

	P	F	DF	R-DF
<i>n</i>	576	138	35	16
pH	3.9 ± 0.02	4.8 ± 0.09	3.8 ± 0.09	4.5 ± 0.10
EC	147 ± 3.06	176 ± 9.76	96 ± 7.05	78 ± 16.77

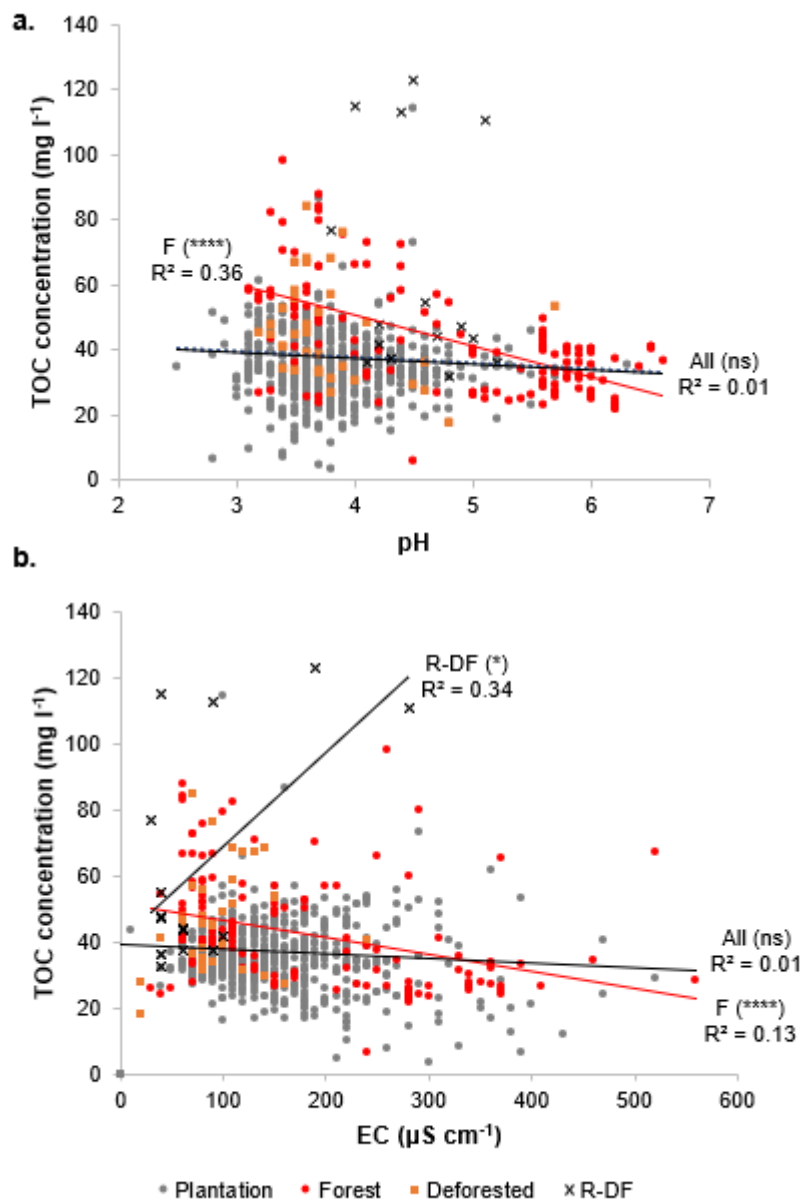


Figure 4.28 Correlation between TOC concentrations with a) pH and b) EC, across the different landcover classes. The r^2 values are displayed alongside the level of significance (*) (ns= no significance $P > 0.05$; * = $P \leq 0.05$; ** = $P \leq 0.01$; *** = $P \leq 0.001$; **** = $P \leq 0.0001$). All data is presented including outliers.

4.3.5 Fluvial carbon fluxes

A combination of both discharge and TOC concentration data were used to calculate weekly TOC yields from the P landcover class. TOC concentrations were volume weighted for each study site, as described in Section 2.8.3. The main and collection drains were separated to avoid pseudo replication. Fluxes were determined for all of the individual P study sites except for three collection drains (SA 1.1, SA 3.2 and SA 3.3), which experienced significant changes in their hydrological regime, as a result of plantation management efforts. This included channel blocking and widening which led to complications in estimating discharge and, therefore, TOC fluxes.

Annual flux data for the plantation landcover classes are presented in Table 4.11 alongside the upper and lower estimates for fluxes taking into account the uncertainty in DOC concentration data (Chapter Three, Section 3.7B). This translates into annual flux estimates of $104 \pm 19.3 \text{ g C m}^{-2} \text{ yr}^{-1}$ and $109 \pm 19.3 \text{ g C m}^{-2} \text{ yr}^{-1}$ for the main and collection drains respectively. The two components of TOC (DOC and POC) contribute a mean of 93 % and 7 %, respectively, to annual TOC yields across all plantation sites (Figure 4.29). This equates to DOC and POC yields of $99 \pm 17.9 \text{ g C m}^{-2} \text{ yr}^{-1}$ and $8 \pm 2.3 \text{ g C m}^{-2} \text{ yr}^{-1}$, respectively, with a slightly higher contribution of TOC derived from DOC in the collection drains (91 % main vs 94 % collection).

In terms of the individual plantations, the highest annual TOC fluxes were displayed by both the main and collection drains of the SE plantation (Figure 4.29). In comparison, the lowest annual fluxes were displayed by SA 3 and SA 1, with higher proportions of POC (mean ~10%; Figure 4.29) contributing to the overall TOC flux. The fluxes from the SE estate were significantly greater ($p < 0.0001$; Table 4.12) than those from the SA estates, irrespective of drain type (Figure 4.29). By contrast, there was no statistical difference in the fluxes from sub-catchments within the SA plantations ($p < 0.05$; Table 4.12).

Table 4.11 Annual TOC flux estimates across the four plantation estates presented alongside upper and lower uncertainty bounds resulting from uncertainties in DOC concentrations. Sites where discharge readings could not be recorded due to changing hydrological conditions, resulting from management efforts (i.e. ditch blocking) are shaded in grey.

Site	Drain	Annual TOC Flux g C m ⁻² yr ⁻¹		
		Flux	Upper	lower
SE1	M	128.8	148.1	109.5
SE2	C	135.7	155.0	116.3
SE3	C	128.1	147.4	108.8
SE4	C	134.0	153.3	114.7
SA 1.1	C			
SA 1.2	C	91.7	111.0	72.4
SA 1.3	C	104.4	123.7	85.0
SA 1.4	M	94.3	113.6	75.0
SA 3.1	C	89.2	108.5	69.8
SA 3.2	C			
SA 3.3	C			
SA 3.5	M	88.6	107.9	69.2
SA 3.6	C	93.7	113.0	74.4
SA 4.1	M	101.2	120.5	81.9
SA 4.2	M	105.3	124.6	85.9
SA 4.3	C	101.4	120.8	82.1
SA 4.4	C	101.6	120.9	82.3
<i>Main drain</i>				
Mean		103.6	122.9	84.3
Difference between flux estimate and upper/lower bounds			19.3	19.3
<i>Collection drain</i>				
Mean		108.8	128.2	89.5
Difference between flux estimate and upper/lower bounds			19.3	19.3

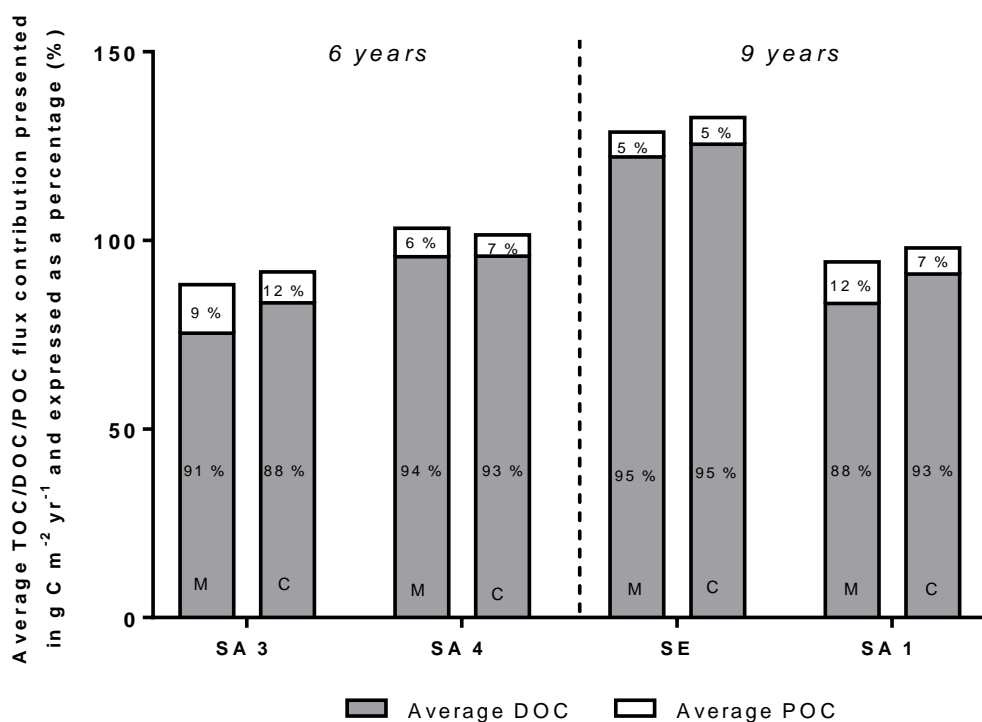


Figure 4.29 Mean annual TOC fluxes during the study period for the plantation estates split into components of DOC (grey) and POC (white). Percentage contributions of DOC and POC are also given. The plantation sites are subdivided into the different drain types; main (M) and collection (C), and are positioned in age order.

Table 4.12. Results of a one-way ANOVA (*post-hoc*) for the TOC concentration data across the individual plantation study sites and drain types. (*) denotes the level of significance (ns= no significance $P > 0.05$; * = $P \leq 0.05$; ** = $P \leq 0.01$; *** = $P \leq 0.001$; **** = $P \leq 0.0001$)

	SA3 C	SA3 M	SA4 C	SA4 M	SE C	SE M	SA1 C	SA1 M
SA3 C		ns	ns	ns	***	**	ns	ns
SA3 M			ns	ns	**	**	ns	ns
SA4 C				ns	*	*	ns	ns
SA4 M					**	*	ns	ns
SE C						ns	**	**
SE M							*	*
SA1 C								ns

The patterns of weekly TOC fluxes, from the P main drains are dominated by discharge and hence, closely mirror the seasonal trends in precipitation (Figure 4.30 a). TOC flux peaks tend to occur with high rainfall totals. This is particularly evident within the SE main drains with 43 % of the annual TOC flux lost during the wet period from November to December 2015. In contrast, the collection drains experienced high variability in TOC fluxes throughout the year with the distinct wet (November – December, 2015) and dry periods (January to June, 2016) accounting for means of 24% and 38% of the annual TOC flux. However, the collection drains did show a degree of sensitivity to rainfall, with increases in monthly rainfall causing some distinctive peaks in weekly TOC fluxes, for example in November 2015 (Figure 4.30 b).

The weekly fluxes from the P landcover class displayed no correlation to TOC concentrations, for either the Sebungan (Figure 4.31 a) or Sabaju estates (Figure 4.31 b). By contrast there was a strong positive correlation observed between weekly TOC fluxes and weekly discharges, in all plantation estates (Figure 4.31 c and d), suggesting that discharge is more important than concentration in controlling the temporal pattern of the flux. This is because discharge varies much more than concentration over time and this variability is systematic (Figure 4.32).

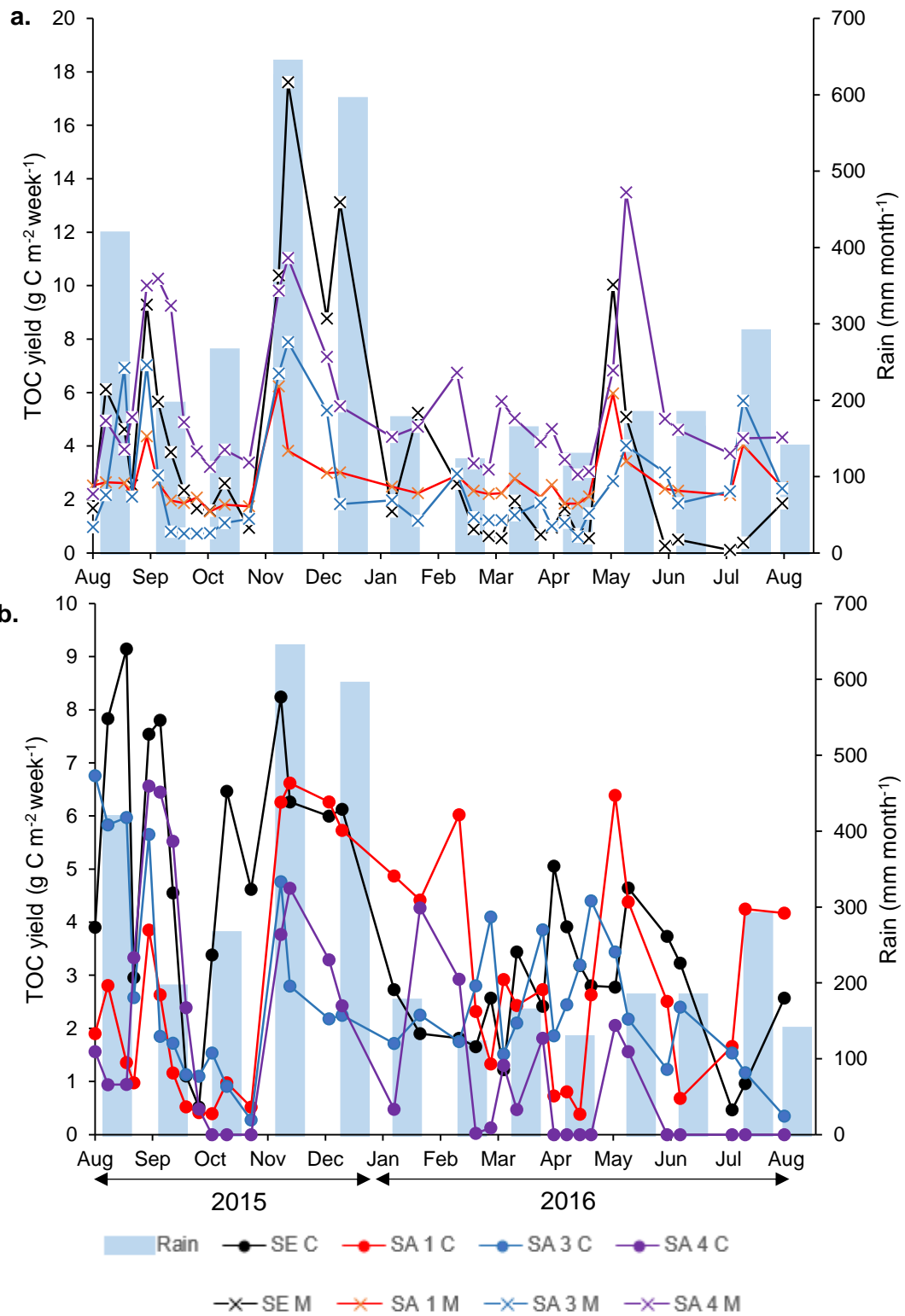


Figure 4.30 Weekly fluvial TOC yield (August 2015 – 2015; 54 weeks) for the plantation main (a) and collection (b) drains, alongside monthly rainfall totals.

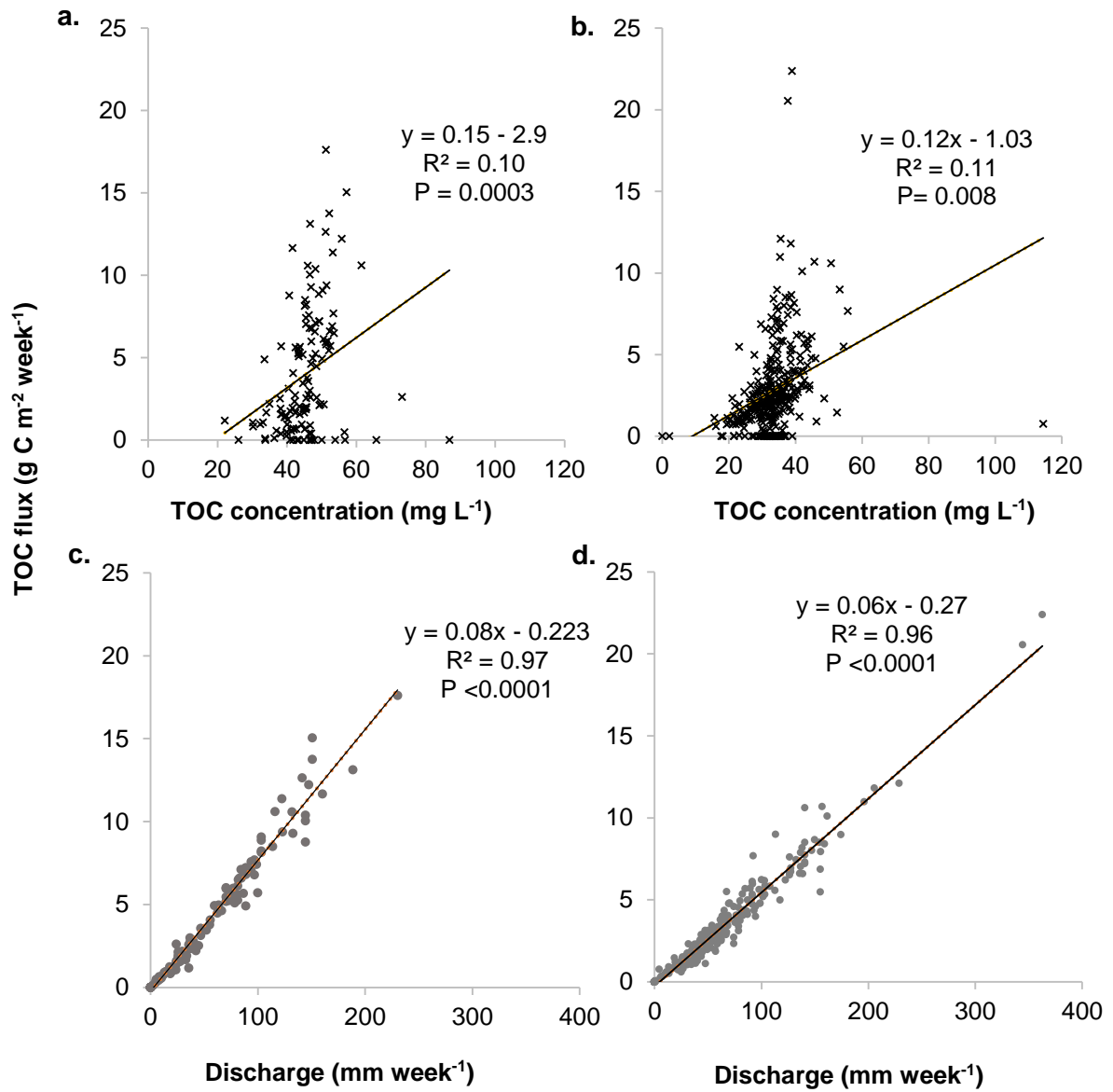


Figure 4.31 Relationship between weekly TOC fluxes and (a-b) TOC concentrations and (c-d) weekly discharge for the Sebungan (a and c) and Sabaju (b and d) plantations.

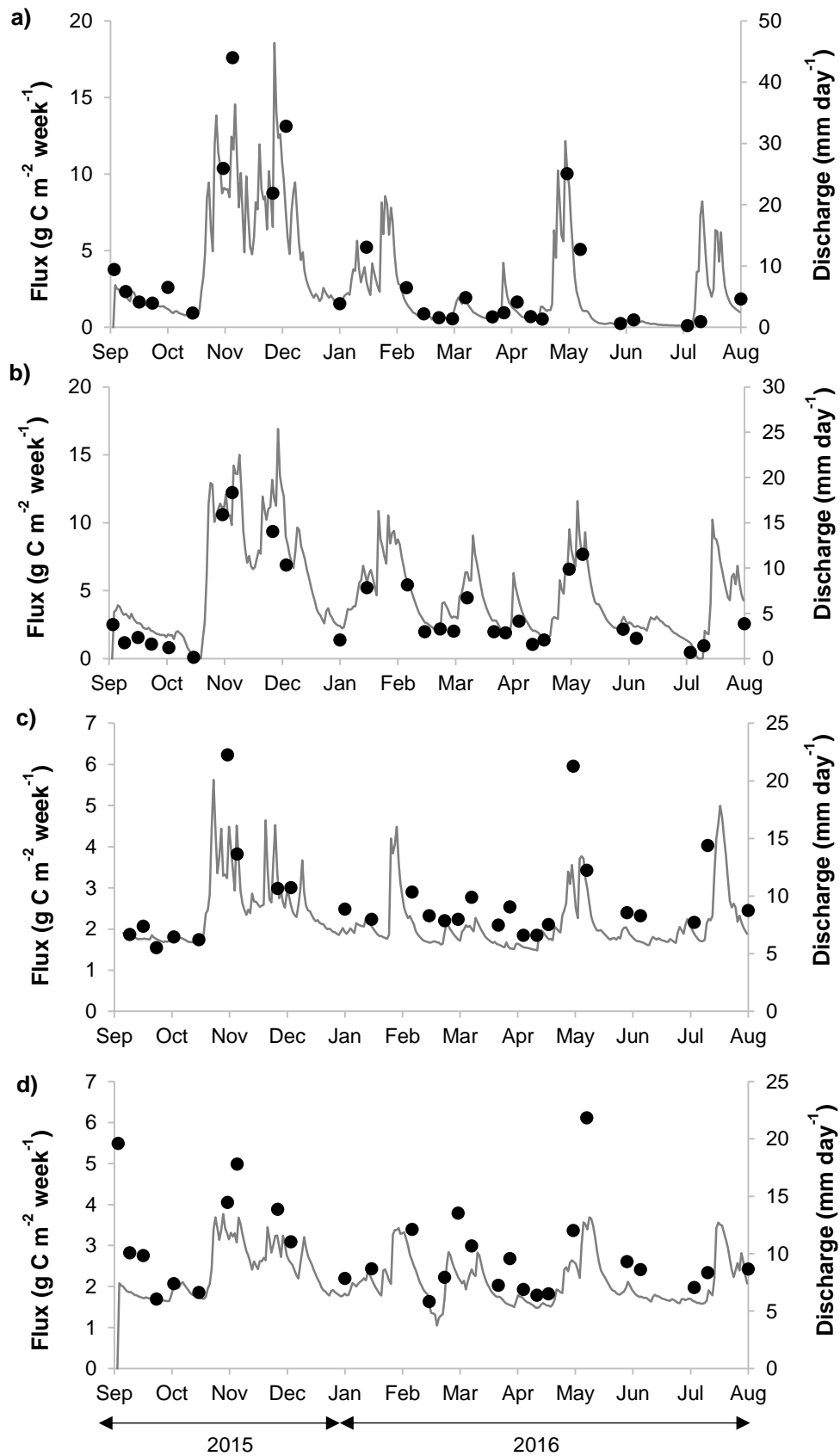


Figure 4.32 Daily discharge (mm day^{-1} ; grey lines) and corresponding weekly fluxes ($\text{g C m}^{-2} \text{ week}^{-1}$; black dots) for a selection of plantation study sites instrumented with mini divers (a) SE1, (b) SE4, (c) SA 1.4 and (d) SA 4.1.

TOC flux estimates for the forest sites are presented in Table 4.13. Upper and lower bands which account for the uncertainty in flux arising from uncertainty in DOC concentrations (Chapter Three, Section 3.7B) and annual runoff (Chapter Four, Section 4.2.1.2) are also shown. The mean fluxes ranged from $71.2 \pm 11.0 \text{ g C m}^{-2} \text{ yr}^{-1}$ to $84.5 \pm 13.1 \text{ g C m}^{-2} \text{ yr}^{-1}$.

Table 4.13 Annual TOC flux estimates for the forest sites presented alongside the upper and lower flux bounds in response to the uncertainty in DOC concentrations and annual runoff.

Site	Different estimates of annual runoff (m yr ⁻¹)	Annual TOC Flux g C m ⁻² yr ⁻¹		
		Flux	upper	lower
FA	1.9	98.2	111.3	85.1
FB		70.8	84.0	57.7
Mean		84.5	97.6	71.4
Difference between flux estimate and upper/lower bonds			13.1	13.1
FA	1.6	82.7	93.7	71.7
FB		59.7	70.7	48.6
Mean		71.2	82.2	60.1
Difference between flux estimate and upper/lower bonds			11.0	11.0

4.5 Discussion

4.5.1 TOC concentrations

TOC fluxes are comprised of two components i) fluvial organic carbon (DOC and POC) concentrations and ii) discharge. DOC formed the primary constituent of TOC (86-94%) across all landcover classes (Figure 4.17), with clear differences in TOC concentrations across the conversion gradient (Figure 4.15; Table 4.7). Significantly higher TOC concentrations were found in samples from FA than in all samples from plantations, across all drain types (Figure 4.15). This may reflect greater amounts of available organic matter in the forest, which has a dense canopy, continually supplying the forest floor with a diverse assortment of leaf litter and organic debris. In the oil palm monoculture, high quantities of labile carbon are lost early on in plantation development leaving a more limited amount of peat-carbon available to be incorporated into DOC (Freeman et al., 2001 b). TOC concentrations in FB were notably lower than in FA and were similar to those found in samples from the 6-year-old OPP stands (Figure 4.15). This is surprising because FB had a much lower (deeper) watertable (Figure 4.23), which should have resulted in higher decomposition rates. However, this could be a reflection of the more sparsely vegetated canopy at the FB site in comparison to the FA site, limiting organic matter input and thus, the DOC supply. Further work could attempt to evaluate total soil carbon stocks in these sites and the availability of mobile DOC.

The lower concentrations of TOC in samples collected from the P estates compared to those samples from the forest sites (Figure 4.15) could also reflect drainage-induced sulphate precipitation, in which peat soil aeration can promote the oxidation of sulphide into sulphate (Dowrick et al., 2015). The presence of sulphate increases soil acidity and ionic strength, altering the net charge of the DOC molecule and decreasing its solubility (Kalbitz et al., 2000; Clark et al., 2005; Monteith et al., 2007; Evans et al., 2012). However, this explanation was not supported by pH profile data, taken from Sabaju 4, which

showed relatively high pH values in the range of 3.5 – 4.5 at increasing core depth. This suggested the absence of potential acid sulphate soils which might be indicated by lower pH values (Appendix D).

TOC concentrations appeared to be higher within the 9-year-old P estates (Figure 4.15) compared to the 6-year-old estates. This may be due to a greater quantity and supply of carbon provided from the biomass of the more mature and developed oil palm stands. TOC concentrations in samples from the SE estate were significantly different ($p < 0.0001$) in comparison with those from the SA estates (Table 4.8; Figure 4.16). This could relate to the differing peat structure at the SE sites, with greater compaction of the peat surface carried out prior to plantation development (supported by higher BD measurements; 0.2 g cm^{-3} ; Appendix A). This suggests a greater density of carbon is above the watertable, at SE, leading to higher rates of organic matter decomposition and TOC production. Furthermore, compaction is likely to have caused large pores within the peat profile to collapse, reducing porosity (Whittington & Price, 2006), and decreasing hydraulic conductivity (K_{sat} ; slowing water movement through the peat). This could extend water residence times and allow more time for the mobilisation of DOC compounds. This is supported by Hribljan et al. (2014) who reported that hydraulically-altered fenlands in Michigan, with high BD and low K_{sat} values, had elevated DOC concentrations in comparison to intact sites.

TOC concentrations appeared to significantly increase during initial forest clearance and drainage (Figure 4.15). This is supported by the higher TOC concentrations exhibited by R-DF, suggesting a flushing out of fluvial carbon in direct response to conversion. This is supported by the observation of sudden pulses of high TOC concentration (e.g. June 2016 123 mg l^{-1}), shown in Figure 4.18, which are coincident with periods of land preparation activity (e.g. timber stacking and channel creation). Increases in DOC concentrations following disturbance have also been noted in temperate peat studies. For example, Glatzel et al. (2013) noted increases in DOC concentrations (from 110 mg l^{-1} to 188 mg l^{-1}) immediately following bog harvesting in eastern Québec.

The uncontrolled drainage experienced within R-DF, will alter peat hydrology (Qassim et al., 2014; Graham et al., 2016), potentially activating carbon pathways further down the peat profile with higher resultant DOC concentrations. Evidence for this mechanism is further provided by Baird et al. (2017) who modelled the differences in hydrological behaviour between natural and drained peat domes. Their model was designed to simulate OPP drainage systems revealing greater modelled losses of organic matter and lateral carbon export from these sites ($2.86 \text{ kg C m}^{-2}\text{yr}^{-1}$, OPP vs $0.09 \text{ kg C m}^{-2}\text{yr}^{-1}$, intact). In addition, the overlying vegetation biomass from recent deforestation (i.e. leaf litter), will supply R-DF with an assortment of organic matter, rich in fresh labile carbon which can be readily converted into DOC (Moore et al., 2013).

4.5.2 TOC concentration variability

The relatively stable TOC concentrations observed throughout the year within the plantation and, to a lesser degree, the forest sites (Figure 4.18) may reflect both natural (in the forest) and artificial (in the plantations) hydrological regulation. High TOC concentrations were noted during the first week of the investigation within the forests (Figures 4.18 and 4.19) but this may be a result of initial site set up, with dipwell insertion causing peat disturbance and thus, higher concentrations of POC/DOC to be released into the water. The otherwise stable TOC concentrations observed within the plantations (Figures 4.18 and 4.19), suggests that discharge must control the temporal pattern of TOC fluxes within this landcover class (Figure 4.30). Verification of this is provided by the strong relationship ($r^2 = 0.97$, $n = 132$; $r^2 = 0.96$, $n = 347$) observed between the weekly discharges and weekly TOC fluxes (Figure 4.31 c, d).

Overall there was no relationship observed between high discharge and corresponding increases in TOC concentrations (Figure 4.21). This relationship is reinforced by the low gradient solute rating curves (i.e. stable TOC concentrations even at high flows; Figure 4.22) which illustrate the

response of TOC concentrations to changes in channel discharge. As the watertable rises two things occur simultaneously i) discharge increases, causing saturated hydraulic conductivity (K_{sat}) to increase close to the peat surface and ii) the watertable comes into contact with more mobile TOC, increasing the TOC supply (Figure 4.33). As such, in order for these stable TOC concentrations to be observed at high flows (i.e. no dilution) the availability of TOC must be approximately proportional to the flow rate.

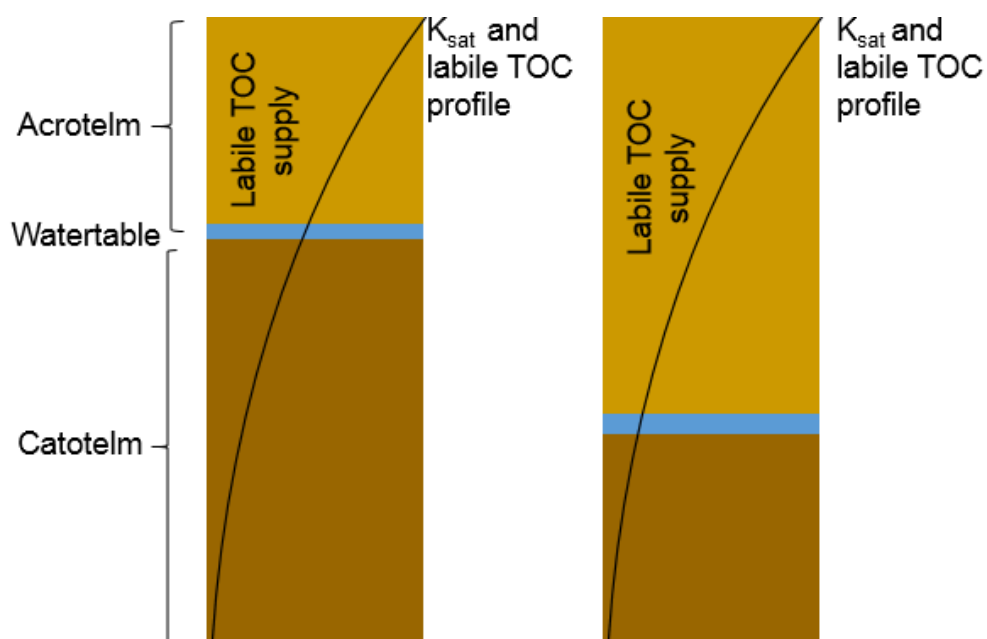


Figure 4.33 Diagram to illustrate the effect of high and low watertables on the hydraulic conductivity and TOC supply, within a peatland. The black line represents the K_{sat} and labile TOC profiles (i.e. decreasing values with increased peat column depth)

For the periods analysed, the majority of drains exhibited a counter clockwise hysteresis, with peak TOC concentrations occurring on the falling limb of the hydrograph (Figure 4.22). Previous research has attributed counter clockwise hysteresis to increases in catchment hydro-connectivity, increasing the number of transport pathways and thus, mobilization of DOC from previously disconnected sources (Strohmeier et al., 2013; Tunaley et al., 2016). Furthermore, low gradient solute rating curves observed during the wet season, particularly within the SA collection drains (Figure 4.22 a,b), reflect the

mechanisms outlined in Figure 4.33. Solute rating curves for the SE drains displayed clockwise hysteresis during the wet season (Figure 4.22 a, b). This could be due to the rapid flushing out of DOC accumulated in organic rich peat layers (McGlynn & McDonnell, 2003; Stutter et al., 2012) in response to high discharge on the rising limb of the hydrograph. Alternatively, the direction of the hysteresis could reflect the temporary depletion of the DOC supply during these high discharge periods, preventing concentrations from building up after peak discharge (Tunaley et al., 2016). Overall, the variability in hysteresis displayed (Figure 4.22) gives clues about the role of hydro-connectivity and DOC supply in the response of individual catchments to precipitation (Figure 4.30).

While mean TOC concentrations were relatively stable within both the forest and plantation landcover classes (Figure 4.18), at an individual estate scale there was some variability (Figure 4.20). Notable increases in TOC were observed just before peak monthly rainfall in November 2015 but also throughout periods of low monthly rainfall (Figure 4.20). The unpredictable response of TOC to rainfall is further highlighted within Figure 4.19, and is likely responsible for the lack of correlation between weekly TOC concentrations and weekly rainfall volume ($r^2 = 0.20$, $p > 0.05$, $n=220$). Increases in TOC production observed during months of low rainfall (Figures 4.18, 4.19 and 4.20) could reflect watertable drawdown, extending the depth of the aerobic peat column and thus, increasing organic matter decomposition and associated DOC production. In addition, sudden rainfall events during the dry season may result in a 'flushing out' of this DOC, built up during periods of low rainfall.

In contrast, samples from the R-DF and to a lesser extent DF sites, displayed higher variability in TOC concentrations (Figure 4.18). Concentrations were not always climatically related with low rainfall and consistently high TOC concentrations displayed within R-DF. This combined with the high SEMs and CVs for these sites (DF= 2.61 mg L⁻¹; CV = 34% and R-DF=8.27 mg L⁻¹; CV = 53%, respectively) imply a high degree of instability, indicative of anthropogenic disturbance. This finding is supported by Muller & Tankéré-Muller (2012) who found seasonal variations in DOC concentrations were

amplified in response to tree felling on Scottish bogs. Furthermore, the disturbance experienced may be exacerbated by natural forcing; large scale biomass loss coupled with intense drainage will lead to declines in interception loss and evapotranspiration plus increased run-off (throughflow and overland flow). The lack of canopy cover in these two landcover classes will expose the peat surface to a higher direct solar radiation flux density and higher daytime temperatures, potentially increasing microbial activity and enhancing organic matter decomposition (Jauhiainen et al., 2014). Thus, a combination of both anthropogenic and exacerbated natural forcing may account for the instability in TOC concentrations, particularly within R-DF, with small climatic perturbations impacting significantly on overall peatland functionality and fragility (Moore et al., 2013; Evans et al., 2014; Baird et al., 2017).

4.5.3 *Forest hydrology*

The watertables observed within the forest landcover class were much lower than expected (i.e. FB -75.7 cm). High watertables (> -40 cm) are typically characteristic of intact PSFs (Figure 4.23; Table 4.9). This is particularly evident within FB where watertables were consistently low (-52.0 cm to -109.3 cm) throughout the year (Figure 4.24). These low watertables may reflect interference from the plantation drainage system, with both sites in close proximity to plantation perimeter drains. In the case of the FB site, a 10-m deep perimeter drain ran adjacent to the site. This will tend to depress watertable depths for some distance away from it (Figure 4.34). It may, therefore, explain the dry conditions experienced in the adjacent forest. These data highlight the fact that forest fragments cannot be thought of as discrete hydrological units. Instead, they must be considered hydrologically connected to the wider plantation landscape (Dislich et al., 2016). This supports the notion that peatland OPPs can have negative impacts on surrounding peatland ecosystems; specifically forest fragments (Dislich et al., 2016). This has significant implications for forest conservation and throws into question the maintenance of buffer strips or riparian reserves as an effective conservation strategy in lieu of peatland OPP expansion (Marczak et al., 2010).

As such, the maintenance of forest reserves within a plantation landscape, does not necessarily dictate hydrological functionality, although other additional ecosystem services may be retained including: biodiversity (Brito et al., 2017), enhanced species richness (Lucey et al., 2014), reduced flood risk, reduced soil erosion (Gray & Lewis, 2014) and important wildlife corridors. Both the plantation and wider landscape need to be considered together and not in isolation. This supports criticism from Ewers et al. (2011) regarding the lack of guidance and ecological information concerning riparian zone management within tropical peatland landscapes

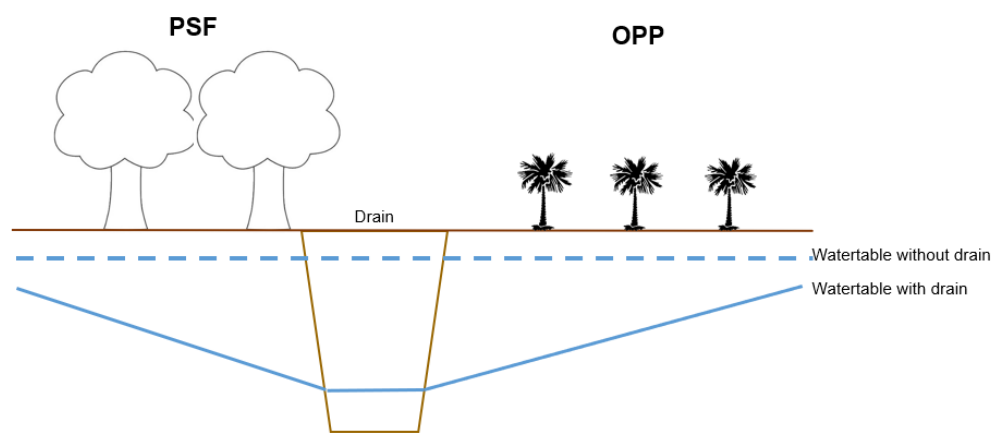


Figure 4.34. Diagram to illustrate the impact of plantation drainage channels on adjacent forest reserves

4.5.4 Interaction between watertable and TOC concentrations

The poor hydrological functioning of the forest buffer sites could help to explain the small differences in TOC concentrations observed between the forest, plantation and deforested sites (Figure 4.15). The mean TOC concentrations observed here for the forest sites (FA = 51 mg L⁻¹; FB=35 mg L⁻¹) were lower than those reported by Moore et al. (2013) for an intact PSF (68 mg L⁻¹) but similar to moderately and severely degraded PSFs (48.3 and 55 mg L⁻¹). In addition, mean TOC concentrations observed for the plantation landcover

class (29 - 39 mg L⁻¹) were lower than those reported by Moore et al. (2013) for a degraded PSF (48.3 and 55 mg L⁻¹). This could reflect the regulated watertable management within the OPP versus the uncontrolled drainage experienced within Moore et al.'s (2013) degraded PSF sites. The TOC concentrations measured in the degraded PSFs in this study (DF and R-DF; 46 and 63 mg L⁻¹) are comparable to those reported by Moore et al., (2013) for moderately and severely degraded PSFs.

Despite having lower watertables, FB displayed lower TOC concentrations than FA (Figures 4.15). However, a closer analysis of the watertable and TOC data (Figure 4.27) indicates that the watertables within FB were consistently low with limited variability. In contrast, watertables within FA were more variable from week to week (Figure 4.27). This is most noticeable at the start of January and in May 2016 in which changes of 52 cm and 16 cm were observed compared to the previous week (Figure 4.27). These alternating periods of low watertables followed by rapid rewetting may flush built up DOC out of the acrotelm contributing to higher TOC concentrations in the drainage water (Kalbitz et al., 2000; Strack et al., 2008). This mechanism could also account for the higher TOC fluxes within FA in comparison to FB (Table 4.13).

In general, watertables were high in the plantations, particularly in the dry season, with the watertable within the SA 1 and SA 3 estates shallower than 40 cm for 79% and 61% of the time, respectively (Figure 4.24). In SA 4 watertables were mostly in line with RSPO best management guidelines (i.e. -40 to -60 cm; Lim et al., 2012). The exception was SE which displayed the lowest but also the most variable watertable with depths of between +5 cm and -128 cm. These watertable extremes are similar to those observed for FA, and by the same logic could be used to explain the greater TOC concentrations and fluxes exhibited by SE (Figures 4.15; 4.16; 4.29); i.e. extreme watertable drawdown enhances organic matter decomposition. The low watertables within SE could also reflect the higher degree of peat surface compaction, which may limit water infiltration and hinder groundwater recharge (Tonk et al., 2017). Similar findings have also been reported from temperate peat studies (Schumman & Joosten, 2008) with compaction decreasing the storage

coefficient of peat leading to both larger watertable fluctuations and higher decomposition rates.

There was a weak, but significant, relationship between watertable and TOC concentrations (Figure 4.25) within two of the sample sites (FA and SA 3), with high TOC concentrations associated with high watertables. This is further reinforced by Figures 4.26 and 4.27. This trend is unexpected since previous research has reported increased DOC production under low watertables (Lou et al., 2014 and Laine et al., 2014). A possible explanation could be linked to the phenol oxidase enzyme. High watertables can create anoxic conditions throughout the peat profile, constraining the activity of phenol oxidase, which breaks down phenolic compounds (which inhibit microbial activity/ organic matter breakdown) (Freeman, 2001b). As a result, during anoxic periods, phenolic compounds are likely to build up, leading to enhanced TOC concentrations during high watertables (Figures 4.25, 4.26 and 4.27). However, research into the interaction between this enzyme and the release of labile DOC has produced tenuous links with contradictory findings (Peacock et al., 2014a; Kane et al., 2014). Freeman et al. (2001b) and Fenner et al. (2005) both report increases in phenol oxidase activity led to decreased phenolic concentrations but Peacock et al. (2014a) found no relationship between these two components.

4.5.6 Water sample properties (pH and EC)

Overall, water samples were acidic with pH averaging about 4 across all landcover classes (Table 4.10). This is typical of tropical peat black waters (Moore et al., 2011). The most acidic water samples were collected from DF (pH 3.8) and P (pH 3.9). The least acidic samples were from the forest sites (pH 4.8) and R-DF (pH 4.5). The EC averaged $148.4 \mu\text{S cm}^{-1}$, suggesting all samples contained freshwater with no evidence of saline intrusion (sea water influence is often defined as $\text{EC} > 200 \mu\text{S cm}^{-1}$; Moore et al., 2011). In general, TOC concentrations were not influenced by variability in either pH or EC (Figure 4.28), which was also observed by Yupi et al. (2016) for PSFs in

Sumatra, Indonesia. This contradicts research by Monteiro et al. (2013), within an Amazonian blackwater catchment, who found a strong relationship between EC and DOC concentrations ($r^2 = 0.98$) making it possible to predict DOC concentrations as a function of EC. Here, there was a statistically strong negative ($p < 0.0001$) correlation between TOC concentrations and pH, within the forest landcover class (Figure 4.28). This trend could reflect high humic acid concentrations within the forest sites, probably derived from lignin decomposition. This high humic acid concentration will work to both lower pH and contribute to the DOC/TOC pool, supporting the observed negative relationship between these two components (Pawson et al., 2008).

Recent research (Jones et al., 2016; Palmer et al., 2016; Pickard et al., 2017) has drawn attention to the occurrence of DOC processing 'hotspots' within peatland catchments, characterised by mixing zones of freshwater with differing water chemistries (i.e. different pH and EC). Large ranges in water chemistry were observed across the different landcover classes for the pH and EC data (i.e. pH ranged from 2.5 to 6.6). It is not unreasonable, therefore, to postulate that the mixing of these different drainage waters could create localised areas for rapid *in-situ* DOC turnover. However, further research would be needed to elucidate this.

4.5.7 Plantation and forest TOC fluxes

In terms of the plantation TOC fluxes, estimated annual fluxes ranged from 88.6 (SA 3.5) to 135.7 g C m⁻² yr⁻¹ (SE2) (Table 4.11). This translates into annual flux estimates of 104 ± 19.3 g C m⁻² yr⁻¹ and 109 ± 19.3 g C m⁻² yr⁻¹ for the main and collection drains, respectively. The higher flux estimates within the collection drains are suggestive of localised DOC processing (~ 5 g C m⁻² yr⁻¹) occurring before water reaches the main drains. This is further supported by Figure 4.17 which shows slightly lower TOC concentrations in the collection compared to the main drains, suggesting DOC degradation may have occurred whilst in transit to the main drains. While research into the degradation rates of tropical DOC is limited, studies have shown that DOC is susceptible to high

rates of instantaneous bacterial (Chen & Wangersky, 1996) and photo-degradation (Spencer et al., 2009), with DOC continuously metabolised throughout tropical aquatic systems (Richey et al., 2002),

In terms of the individual plantation estates, the highest fluxes were displayed in the SE plantation (Figure 4.29). In comparison, the lowest annual fluxes were displayed by SA 3, which also had a higher proportion of POC (mean ~11%; Figure 4.29) contributing to the overall TOC flux, in comparison to the other estates.

These trends mirror the variability in TOC concentrations observed between the plantation estates (Figure 4.16), with SE displaying the highest TOC concentrations and SA 3 the lowest. However, overall there was only a weak correlation observed between TOC concentrations and fluxes (Figure 4.31), due to the limited range of concentrations (< an order of magnitude) compared with discharge (two orders of magnitude; Figure 4.31). In addition, fluxes were observed across all drains throughout the year (Figure 4.30), with the exception of SA 4 C. This is probably due to the presence of deep artificial drainage channels, which allow for continuous peat drainage, despite dry periods with limited rainfall. Some daily discharge rates exceeded 34 mm day⁻¹ even during periods of low rainfall (Figure 4.14).

The fact that discharge exerted more control over the temporal variability in TOC fluxes (Figure 4.31 c, d and Figure 4.22) is supported by Li et al. (2017) who observed that global riverine DOC fluxes were highly correlated with discharge ($r^2 = 0.93$, $n = 109$). This was due to the contribution of i) the 'flushing effect' (Meybeck, 1982), where by increased discharge increases the dissolution and transportation of DOC and ii) peat erosion. Intense rainfall generates surface runoff, which will physically impact the peat surface, causing particles of peat to be dislodged and transferred into the drainage channels (Li et al., 2017). This will increase drainage channel POC/DOC concentrations adding to the TOC pool. The SE estate may experience higher rates of overland flow, as a result of compaction and a reduced infiltration capacity, increasing its susceptibility to peat erosion. This is supported by the

hydrographs (Figure 4.14) with the SE estate discharge exhibiting a quick and flashy response to precipitation. This could provide a further explanation for the significantly higher TOC concentrations and fluxes within this estate.

While the TOC concentrations for the degraded PSFs reported by Moore et al. (2013) are noticeably higher (48.3 and 55 mg L^{-1}) than those reported here for the plantation landcover class (33.5 mg L^{-1}) the overall annual TOC fluxes are comparable (i.e. degraded PSF = 97 $\text{g C m}^{-2} \text{ yr}^{-1}$ vs P = 104 $\text{g C m}^{-2} \text{ yr}^{-1}$). The lower TOC concentrations within the plantation were not counterbalanced by lower discharge rates. This is logical when considering the dense drainage network within the plantation, principally designed to efficiently and rapidly discharge water out of the system.

Mean forest fluxes ranged between 71.2 ± 11.0 $\text{g C m}^{-2} \text{ yr}^{-1}$ and 84.5 ± 13.1 $\text{g C m}^{-2} \text{ yr}^{-1}$, depending on runoff rates. The high fluxes reported for the FA site (82.7 ± 11.0 $\text{g C m}^{-2} \text{ yr}^{-1}$ to 98.2 ± 13.1 $\text{g C m}^{-2} \text{ yr}^{-1}$) are notably higher than fluxes reported elsewhere for intact PSFs within Sarawak (e.g. 63 and 64 $\text{g C m}^{-2} \text{ yr}^{-1}$; Moore et al., 2013; Muller et al., 2015). This could be due to the proximity of the OPPs to the F sites investigated here, and the associated effects on the watertable depth.

4.6 Conclusions

Overall, the findings from this Chapter suggest that the anthropogenic disturbance associated with the conversion of an intact PSF to OPP is responsible for increases in fluvial organic carbon fluxes. The fluxes from the 'minimally' disturbed forest sites estimated here were comparable with those from the OPPs. However, these forest fluxes were elevated compared to those reported elsewhere for intact PSFs (63 $\text{g C m}^{-2} \text{ yr}^{-1}$; Moore et al., 2013). Moreover, the TOC fluxes estimated for the plantation are approximately one third greater than those reported for an intact PSF. The low watertables observed in the forest sites may have been the result of groundwater drawdown by the drainage systems in the nearby OPPs (Figure 4.34). If this is

the case it suggests that OPPs can have an unseen and unintended impact on the water and carbon balances of adjacent forest fragments.

Fluvial organic carbon losses are an integral component of the tropical peatland carbon budget and represent a direct loss of carbon from the peat itself. Nevertheless, this aquatic component is often overlooked and is sometimes considered negligible in comparison to GPP and ecosystem respiration. According to the IPCC (2014) the mean NEE for an OPP on tropical peat is $+1,100 \text{ g C m}^{-2} \text{ yr}^{-1}$. Including an estimated fluvial carbon loss of $104 \text{ g C m}^{-2} \text{ yr}^{-1}$ (from this study), increases the carbon loss estimate to $+1,204 \text{ g C m}^{-2} \text{ yr}^{-1}$ (net carbon source; Figure 4.35). This approximates to a ~10% greater carbon loss than previously estimated using gaseous measurements alone (IPCC, 2014). I argue, therefore that including fluvial organic carbon fluxes in peatland carbon budgets is essential, particularly if the full impact of anthropogenic disturbance on these ecosystems is to be estimated. This supports the claim by Moore et al. (2013) that carbon from disturbed peatlands is underestimated by 22% if this aquatic carbon component is not included.

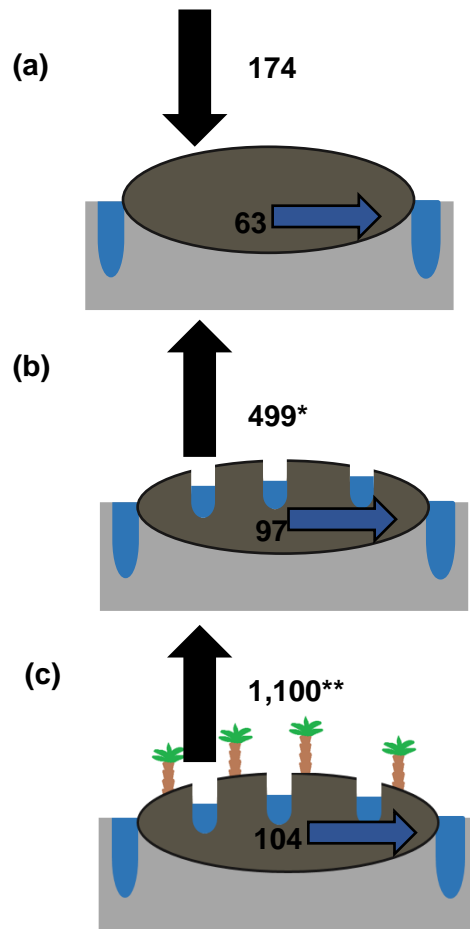


Figure 4.35 Schematic diagram to show NEE (black arrows; $\text{g C m}^{-2} \text{ yr}^{-1}$) and fluvial organic carbon loss estimates (dark blue arrow; $\text{g C m}^{-2} \text{ yr}^{-1}$) across the conversion gradient, including: (a) intact PSF, (b) degraded PSF, (c) OPP. *Net ecosystem exchange for the intact and degraded PSF are derived from Hirano et al., (2012) using tower based (eddy covariance) gas measurements, and the TOC fluxes obtained from Moore et al., (2013). **Net ecosystem exchange for the OPP obtained from IPCC (2014) and the TOC fluxes from this study. A net carbon gain is estimated from the intact PSF of $111 \text{ g C m}^{-2} \text{ yr}^{-1}$ ($-174 + 63 = -111$; net carbon sink) whereas there is a net carbon loss from the degraded and OPP of $596 \text{ g C m}^{-2} \text{ yr}^{-1}$ ($+499 + 97 = +596$) and $1,204 \text{ g C m}^{-2} \text{ yr}^{-1}$ ($+1,100 + 104 = +1,204$), respectively.

Chapter Five: Qualitative analysis of tropical dissolved organic carbon

5.1 Introduction

The role of fluvial organic carbon within the context of the global carbon cycle is becoming increasingly recognized (Evans et al., 2015), with the photolytic and biological breakdown of dissolved organic carbon (DOC) representing a significant carbon loss pathway to the atmosphere (Wit et al., 2015). The magnitude of carbon loss from tropical peatlands is strongly related to land management (i.e. deforestation and drainage) and the degree of peat degradation (Moore et al., 2013; Rixen et al., 2016). In Chapter Four I established that tropical peatland OPPs export large quantities of fluvial organic carbon, however, the importance of this exported carbon ultimately relies on its fate; whether it is stored or released into the atmosphere. This chapter considers this question through an analysis of the qualitative aspects of the DOC fraction, achieved through i) spectrophotometric techniques (SUVA₂₅₄ and E ratios) and ii) radiocarbon dating (¹⁴C), enabling the age, source and aromatic stability of the DOC compounds to be inferred.

5.1.1 Spectrophotometric techniques

The relative aromaticity of DOC determines how labile or recalcitrant it is and thus, how likely it is to be biodegraded and subsequently converted into gaseous carbon forms (Moore et al., 2013). Aromatic compounds are naturally very recalcitrant. They contain benzene rings, which are very stable because of their delocalized electrons, resulting in alternating single and double bonds within their structure (Clayden et al., 2001). SUVA₂₅₄ (Specific Ultra-Violet Absorption) is a useful tool for gaining an insight into the quality of DOC. It is the ultra-violet (UV) absorbance at 254 nm normalised to a water sample's DOC concentration (mg L⁻¹) and gives an 'average' absorptivity for all molecules comprising DOC (Weishaar et al., 2003). Absorbance at 254 nm is

commonly used as a surrogate for DOC aromaticity; DOC is largely comprised of aromatic humic substances, which absorb light in this particular part of the electromagnetic spectrum (Peacock et al., 2014b). High SUVA₂₅₄ correlates to high aromaticity and therefore indicates a high level of recalcitrance. If this is the case, it is likely that less carbon will be metabolized by in-stream fauna and will instead be buried in sediments, thus providing a long-term carbon store (Weishaar et al., 2003; Moore et al., 2013; Fellman et al., 2014).

The effectiveness of SUVA₂₅₄ as an indicator for DOC aromaticity was highlighted in a study by Weishaar et al. (2003) in which percentage (%) aromaticity of 13 organic matter isolates, from a range of aquatic environments (canal, creek, ocean, lake and river) were correlated with SUVA₂₅₄. The correlation between these two parameters was strong ($r^2= 0.97$, $n =13$; Weishaar et al., 2003) and subsequently, SUVA₂₅₄ has been used to determine the bioavailability of DOC in a number of investigations (Moore et al., 2013; Fellman et al., 2014; Whittinghill et al., 2014). In addition, absorbance values and ratios over a range of wavelengths can also be used to give an insight into the specific structural and compositional properties relating to DOC, as outlined in Table 5.1 (Thurman, 1985; Peacock et al., 2014b; Peacock et al., 2015).

Table 5.1 Various wavelengths and ratios used to determine specific properties relating to DOC, adapted from Peacock et al. (2014b).

Measure	Wavelengths (nm)	Property of DOC it determines	References
E2:E3 ratio	250:365	Molecular weight of humics/ aromaticity	Peuravuori & Pihlaja,, 1997
E2:E4 ratio	252:452	Coloured to uncoloured DOC	Graham et al., 2012
	254:436		Selberg et al., 2011
	254: 465		Park et al., 1999
E4:E6 ratio	400:600	Molecular weight and degree of humification	Moore., 1987
	450:650		Wilson et al., 2011
	460:660		Thurman, 1985
	465:665		Wallage et al., 2006

5.1.2 Radiocarbon dating

Radiocarbon dating (^{14}C) is an effective and widely employed method for quantifying the source age of DOC (Xu et al, 2004; Evans et al, 2007; Raymond et al, 2007; Moore et al, 2013; Evans et al, 2014; Campeau et al., 2017). The breakdown of DOC into CO_2 or CH_4 can be derived from either old peat material (^{14}C depleted), or recently (< 50 years) photosynthesised material (^{14}C enriched; Leach et al., 2016; Campeau et al., 2017). Quantifying the age of the carbon source is important for understanding the stability of the peatland carbon budget (Evans et al, 2012; Campeau et al, 2017) with the former indicating a loss in long-term carbon storage (Evans et al, 2007; Evans et al, 2012; 2014).

The ^{14}C content of organic matter reflects the isotopic signature of the atmosphere at the time of photosynthesis (Evans et al, 2007). During photosynthesis the plant assimilates CO_2 and the ^{14}C signature of the atmosphere is incorporated into plant biomass, where it remains even after

death (Evans, 2014). Overtime ^{14}C radioactively decays, causing ^{14}C to become depleted, providing an indication of the carbon age (Evans, 2014). Nuclear testing in the 1950s caused atmospheric ^{14}C enrichment (Figure 5.1; Levin & Kromer, 2004), which peaked in around 1960, leaving a ‘tracer pulse’ within the atmosphere (Evans et al, 2007). Carbon fixed prior to 1950 can be conventionally radiocarbon dated based on the radioactive decay of cosmogenic ^{14}C (Evans et al, 2007). However, post-1950 radiocarbon dating is complicated as the ^{14}C isotopic signature is likely to reflect a mixture of both old (pre-1950’s) and new (post bomb/ ^{14}C enriched) carbon, in varying amounts, thus, no single indicative ‘mean age’ can be ascribed to the sample (Evans et al, 2007; Moore et al, 2013). Nevertheless the following general assumptions can be made (Evans et al, 2007):

1. Samples with $^{14}\text{C} < 100\%$ modern (carbon capture pre 1955) must mainly contain pre-bomb carbon and a mean age can be assigned
2. Samples in the range of 100-106% modern will contain a large proportion of carbon fixed before 1957
3. $^{14}\text{C} > 106\%$ modern will contain a large proportion of carbon fixed since 1957

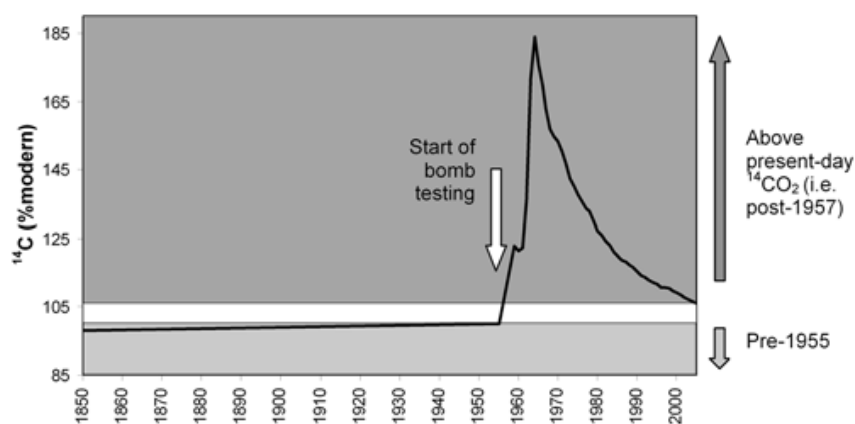


Figure 5.1 ^{14}C (%modern) levels of organic carbon photosynthesized from 1850-2000. Light shaded areas represent dateable carbon (pre-1955). Dark shaded areas represent bomb-enriched carbon, fixed between 1957 and 2000 (Evans et al, 2007)

The age of the sample can be expressed in conventional radiocarbon dating years relative to 1950 (before present, BP) or as %modern defined as,

$$\%modern = \left(\frac{A^{14C:13C}}{Ox^{14C:13C}} \right) \times 100 \quad (5.1)$$

Where, $^{14}C:^{13}C$ = the radioactivity, A = the sample under investigation, Ox = Oxalic Acid, with a radioactivity equivalent to the atmosphere in 1950 (i.e. 100 %modern = year 1950)

However, ascribing a mean age to ^{14}C values fails to capture the broad range of ages likely comprised by the DOC material. For example, conventional dating of a $DO^{14}C$ sample < 100% modern will assume that there is no bomb-enriched carbon. If any bomb carbon is present then the remaining carbon must be much older than the mean to compensate for this young carbon present (Evans et al., 2014). In order to overcome this problem Evans et al. (2014) developed an 'age attribution model' allowing an indicative age distribution for the organic carbon to be inferred. The model relates DOC production as a function of peat depth (Evans et al., 2014; equation 5.2), assuming that the greatest amount of DOC production occurs at the peat surface and is derived from photosynthetically fixed carbon in the same year of sampling (Moore et al., 2013; Evans et al., 2014). DOC production is then assumed to decline exponentially, with increasing peat depth, with each subsequent year (Moore et al., 2013).

$$DO^{14}C = \sum_{t=1}^{t=4,300} (^{14}CO_2t \times \exp(-kt)) \quad (5.2)$$

where, $DO^{14}C$ = the measured ^{14}C of the DOC sample, t = year prior to present day, $^{14}CO_2$ = the ^{14}C level of atmospheric CO_2 in year t , k = the exponential decay constant with a value between 0 and 1. k is solved for each sample by using excel 'goal seek' to fit the measured $DO^{14}C$ value (target value) to the

atmospheric sequence of $^{14}\text{CO}_2$, which becomes more depleted (lower values i.e. indicating older sources of carbon) with peat depth.

Existing data demonstrates that exported DO^{14}C is consistently modern from intact tropical peat swamp forests (PSFs; Moore et al., 2013; Evans et al., 2014; Gandios et al., 2014; Muller et al., 2015). However, there is limited DO^{14}C data in regards to degraded tropical peatlands and particularly from oil palm plantations (OPPs). Of the available data, DO^{14}C age signatures from waters draining disturbed PSFs correspond to ages of 92 to 2,260 BP (Moore et al., 2013), implying a loss of long-term stored carbon. Moore et al. (2013) present the first radiocarbon dates from two peatland OPPs with DO^{14}C levels corresponding to mean ages of around 4,000 years BP. While these are considered to be the oldest soil-derived natural surface-water DOC measurements to date (Moore et al., 2013), they are only based on two data points from Peninsular Malaysia, emphasizing the need to greatly increase the amount of radiocarbon data from this landcover type. Furthermore, it is likely that the DOC being lost will comprise of aged carbon from deep within the peat profile, indicative of older ^{14}C signatures (Moore et al., 2013; Evans et al., 2014; Evans, 2015). This is based on the rationale that:

- i) young carbon is progressively flushed from the system in the period following drainage
- ii) subsidence/oxidation means that it is necessary to progressively lower the water level to maintain the same depth of aerobic zone for the palm trees, thereby exposing older peat to oxidation.

Radiocarbon dating was used to help identify the most likely source of carbon being lost from the OPP sites and the relative contributions of recently photosynthesised carbon versus millennia-old carbon. This will be valuable in building a fuller picture of the temporal dynamics of DOC and potentially provide the basis for changes in plantation management in support of carbon conservation.

5.2 Methods

5.2.1 Sample collection

All samples collected for the determination of fluvial organic carbon (Chapter Four) were subject to spectrophotometric analysis. The samples were taken from the same locations as outlined in Chapter Two (section 2.2) resulting in four different landcover classes: Forest (F), Recently Deforested (R-DF), Deforested (D) and Plantation (P). The P landcover class was further subdivided into main (M) and collection (C) drains, and, for some analysis, grouped into respective plantation age categories (i.e. 6 years old, SA 3 + SA4, and 9 years old, SE + SA 1). Similarly, in some cases F was subdivided into FA and FB to ascertain differences between the two forest sample sites.

Samples were collected in 60 ml Nalgene® bottles and filtered through 0.45 µm cellulose nitrate membrane filters, using a hand-held vacuum pump within 24 hours of collection. Karanfil et al. (2003) cautions the use of some cellulose membrane filters for UV-vis analysis due to large amounts of leaching from the filter paper itself. Subsequently, to ensure their suitability a subset of filtered blanks were first analysed in the same manner as the water samples. Filters leached 0.008 absorbance at 254 nm and 0.4 mg L⁻¹ DOC; this was considered negligible in comparison to the relatively high DOC concentrations (> 20 mg L⁻¹) and absorbance values recorded for all samples (absorbance at 254 nm > 1.5).

UV-vis absorbance was measured using a Cole-Parmer UV/visible spectrophotometer (230 VAC, 50 Hz) at wavelengths of 254, 270, 350, 400, 600 and 700 nm. This allowed the quality of the DOC to be quantified by calculating the E2:E3 (254 nm: 350 nm), the E2:E4 (254 nm: 400 nm) and the E4:E6 ratios (400 nm: 600 nm, as outlined in Table 5.1), along with specific UV absorbance, at 254 nm. Samples were analysed immediately after filtration. SUVA₂₅₄ values were then calculated following equation 5.3 and percentage (%) of aromaticity using the equation outlined in Weishaar et al.

(2003), equation 5.4. Water samples with high levels of absorbance saturation (> 3.0) at 254nm were removed from the data set prior to analysis.

$$SUVA_{254} (l\ mg-C^{-1}\ m^{-1}) = (absorbance\ at\ 254 / DOC\ concentration) \times 100 \quad (5.3)$$

$$Aromaticity\ (\%) = (6.52 * SUVA_{254}) + 3.63 \quad (5.4)$$

An intense DOC collection experiment was carried out on the 29th and 30th August 2016, to provide a snapshot of DOC quality within the plantation estates. Water samples were collected from 17 collection and 3 main drains, within each of the 4 plantations, in 60 ml Nalgene® bottles (Figure 5.2). All samples were collected within 48 hours of each other, ensuring similar environmental and hydrological conditions. After collection, all samples were filtered and analysed, as described above, within 5 hours of initial collection ensuring minimal DOC degradation.

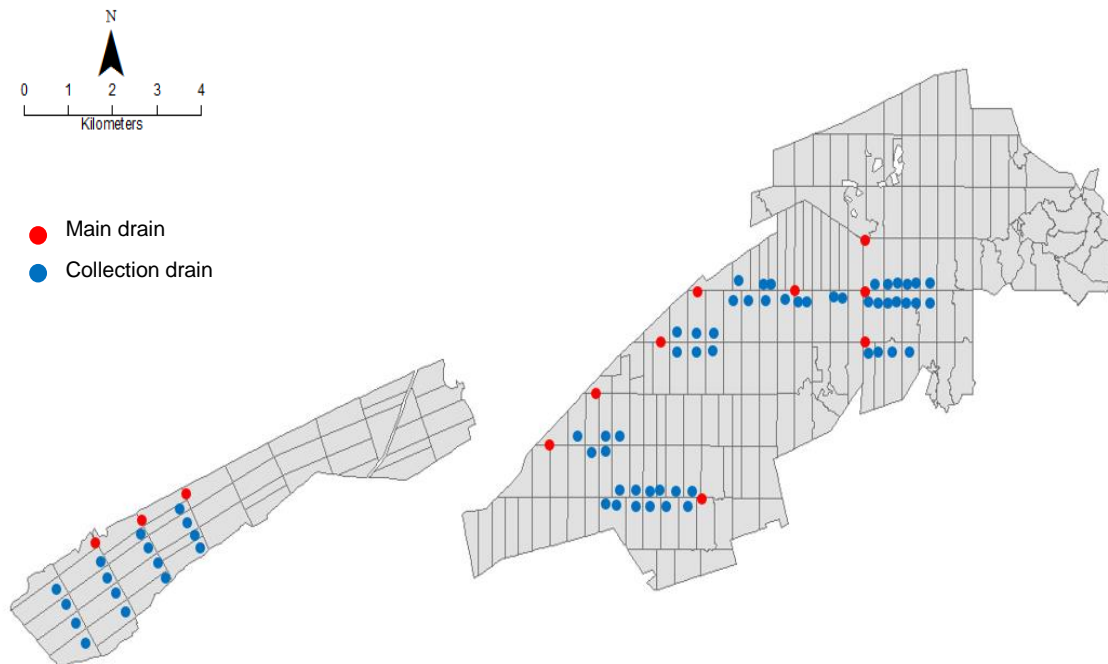


Figure 5.2 Approximate location of the main (red) and collection (blue) drains sampled for the intensive DOC collection experiment.

5.2.2 Radiocarbon dating

Samples for radiocarbon dating were acquired from three collection drains within both the SE and SA 3 plantation estates (6 samples total). Sample collection from main drains was avoided to prevent pseudo-replication. All samples were collected over the course of 24 hours in April 2016 in pre-rinsed (with sample) 500 ml polypropylene bottles and filtered using a 0.7- μm GF filter, as recommended by Evans et al. (2007). Water samples were collected from a central point immediately upstream from where the collection drain discharged into the main drain. All filters were pre-rinsed with deionised water and placed in a furnace for 3 hours at 550°C, before usage, to ensure the removal of any residual organic carbon pre-usage. After filtering, samples were kept in a darkened fridge at 4°C pending shipment back to the UK. Samples were shipped by international courier at the end of April 2016 and arrived early May 2016, where they were stored in a darkened fridge at 4°C, pending analysis. Samples were then transported to the NERC radiocarbon dating facility in Scotland, for analysis in early July 2017. While the samples were cold stored for approximately one year prior to analysis, research by Gulliver et al., (2010) has shown cold storage to be a viable method for the long-term preservation of carbon isotopic signatures ($^{14}\text{C}_{\text{DOC}}$).

An outline of the radiocarbon dating procedure method is illustrated in Figure 5.3. Upon arrival, at the radiocarbon dating facility, samples were prepared for analysis following the procedure outlined in Evans et al. (2007). Samples were first pre-treated by acidification (pH 4) with 2M hydrochloric acid (HCl) and then purged with helium and neutralised (pH 7) with 1M potassium hydroxide (KOH), rotary evaporated, frozen and freeze-dried. Weighted aliquots were then subsequently combusted with CO_2 at 900°C in vacuum sealed silica quartz tubes, containing copper oxide and silver foil. The gas was then converted to graphite by a Fe/Zn reduction (Evans et al., 2007). After this preparatory procedure the ^{14}C content was analysed by Accelerator Mass Spectrometry and normalized to $\delta^{13}\text{C}$ of - 25 ‰ and expressed as either

%modern or in conventional radiocarbon years (if carbon age < 1950) (Evans et al., 2007; Moore et al., 2013).

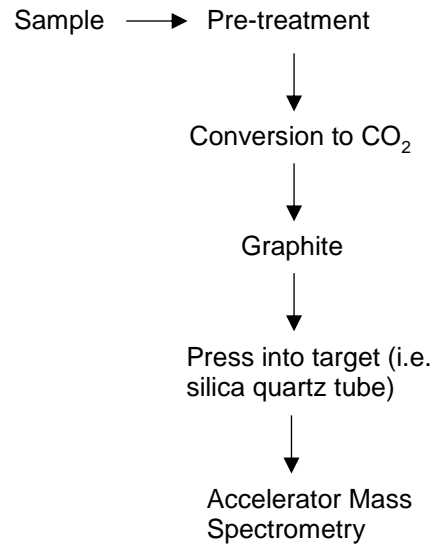


Figure 5.3 Outline of the radiocarbon dating method used on the DOC water samples

The age attribution model was then adapted to best represent the peat within the area sampled. Maximum peat ¹⁴C ages of 4,300 years BP have been recorded for this region (Dommain et al., 2011) thus, this was set as the model runtime limit. The model was applied to all samples and the DOC ages were separated into the following age categories 0-9, 10-49, 50-99, 100-299, 300-499, 500-699, 700-999, 1000-2999 and 3000+ years.

5.3 Results

5.3.1 DOC radiocarbon ages

All samples displayed %modern values indicative of DOC ages from a mixture of both pre-bomb and post-bomb carbon (Table 5.2). The greatest ^{14}C -enrichment was exhibited by SA 3.6 (102.6 %modern), with site SE 4 showing significant ^{14}C -depleted carbon (91.3 %modern, $p < 0.0001$; Table 5.2 and Figure 5.4). The values of $\Delta^{13}\text{C}_{\text{VPDB}}\text{‰}$ (Vienna Pee Dee Belemnite) were within the normal bounds for DOC (i.e. around -28; Gulliver et al., 2010) implying there had been no contamination with carbonate during analysis. The mean ^{14}C age appears to be positively related to depth of watertable and drainage severity (Figure 5.5). This is clearly demonstrated by site SE 4 which experienced the lowest average annual watertable (- 92 cm below peat surface) and greatest ^{14}C -depleted carbon, corresponding to a mean DO^{14}C age of 735 ± 37 years BP (Table 5.2). By contrast, sample sites with ^{14}C -enrichment clustered around higher mean watertables (i.e. -60 to -20 cm; Figure 5.5) and in some instances also experienced times of shallow flooding (i.e. SA 3.1, Table 5.2), i.e. standing water.

Table 5.2. Mean and standard errors for radiocarbon DO^{14}C expressed as %modern and in conventional radiocarbon years (years BP, relative to AD 1950), expressed at $\pm 1\sigma$ level, for individual samples sites across the Sebungan and Sabaju estates. Mean ^{14}C levels $>100\%$ modern cannot be assigned an age and are subsequently referred to as 'modern'. Mean annual watertable data for each site is also presented, alongside the maximum and minimum watertables recorded. Negative numbers indicate distance from the peat surface.

Plantation	Sample ID	Sample site	^{14}C (%modern)	DO^{14}C Age (years BP)	$\Delta^{13}\text{C}_{\text{VPDB}}\text{‰}$ (± 0.1)	Watertable (cm)		
						mean	maximum	minimum
Sebungan	SUERC-74555	SE 2	100.10 ± 0.46	modern	-29.2	-21	5	-58
	SUERC-74556	SE 3	99.57 ± 0.46	35 ± 37	-29.1	-52	-34	-89
	SUERC-74560	SE 4	91.26 ± 0.42	735 ± 37	-28.9	-92	-65	-128
Sabaju 3	SUERC-74561	SA 3.1	102.37 ± 0.47	modern	-29.1	-30	4	-56
	SUERC-74562	SA 3.3	99.63 ± 0.44	30 ± 35	-28.7	-39	4	-82
	SUERC-74563	SA 3.6	102.63 ± 0.47	modern	-29.1	-36	-14	-72

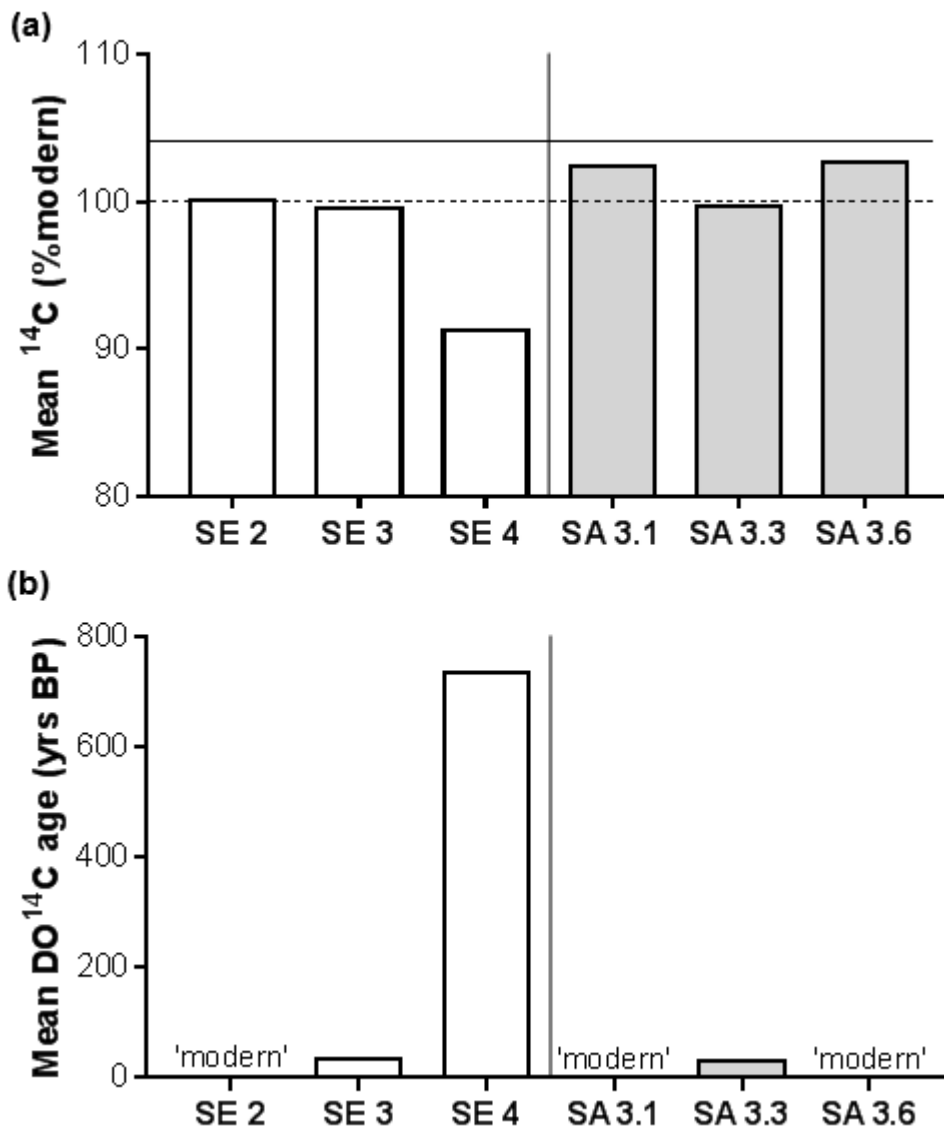


Figure 5.4 (a) Radiocarbon DO^{14}C levels (% modern) from the DOC samples analysed across the Sebungan (SE) and Sabaju 3 (SA 3) estates. Solid black line (104% modern) represents the current atmospheric $^{14}\text{CO}_2$ levels. Dashed line (100% modern) represents the atmospheric composition in 1950, prior to nuclear testing. **(b)** Radiocarbon DO^{14}C levels reported as conventional radiocarbon years (yrs BP, relative to 1950). Mean ^{14}C levels >100% modern cannot be assigned an age and are subsequently referred to as 'modern'.

Vertical grey line divides the Sebungan and Sabaju 3 sample sites.

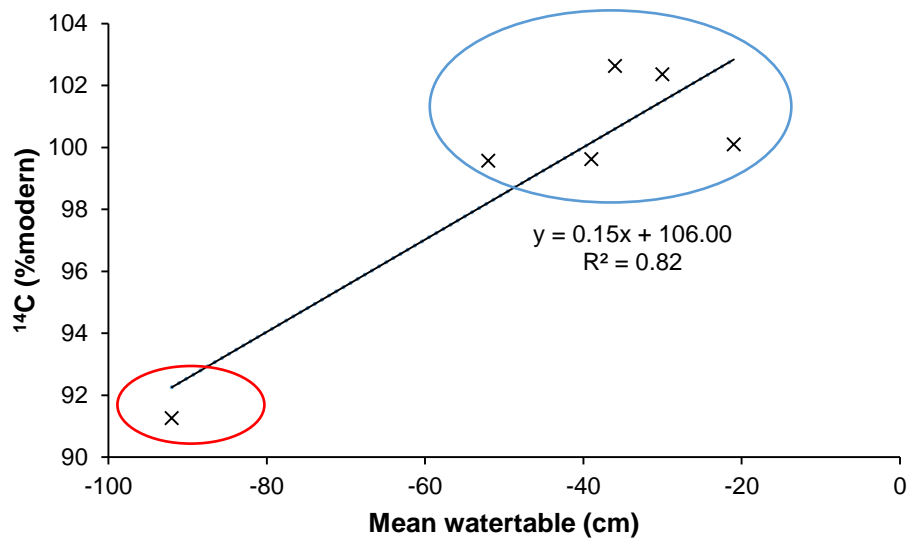


Figure 5.5. Mean watertable values plotted against ¹⁴C (%modern) for all six sites, alongside the line equation and regression metric (r^2). Minus numbers denote distance in relation to the peat surface. Coloured circles illustrate the clustering of sites with high (blue) and low (red) mean watertables.

The age attribution model provided a framework in which to greater interpret the data presented in Table 5.3, the results of which are presented in Table 5.3 and Figures 5.6 to 5.7. As expected samples contained a mixture of organic matter across a broad range of ages (Figures 5.6 and 5.7). The majority (> 30%) of carbon was derived from sources aged 100-299 years BP (Figure 5.6), with over 50% originating from carbon sources aged 100 – 499 years (Figure 5.7). Further to this, four out of the six sites displayed a small proportion of carbon fixed from sources exceeding ages of 3,000+ years BP (Figure 5.6). The SE estate contained a greater proportion of carbon from aged sources; on average 15% of peat carbon was derived from sources 1000-2999 years BP in comparison to only 3.5% in SA 3 (Figure 5.7). The data for SE 4 particularly stood out with over a third of the DOC derived from carbon exceeding 1000 years BP and only ~6% of peat carbon fixed from the atmosphere within the last 50 years (Figure 5.6 c).

Table 5.3. Sampling sites, together with conventional and modelled radiocarbon age estimates. As two solutions were possible for ‘modern’ samples (i.e. similar ¹⁴C values occur before and after the bomb peak) the decay constant (k) was modelled using a high (1.0) and low (0.0001) value. However, ¹⁴C values could only be reproduced using the ‘low k’ model suggestive of a predominately prebomb carbon content, as highlighted in bold.

Plantation	Sample ID	Sample site	DOC Age (years Before sampling Date)		
			Conventional	Modelled (High k)	Modelled (Low k)
Sebungan	SUERC-74555	SE 2	modern	No solution	351
	SUERC-74556	SE 3	35 ± 37	N/A	377
	SUERC-74560	SE 4	735 ± 37	N/A	904
Sabaju 3	SUERC-74561	SA 3.1	modern	No solution	255
	SUERC-74562	SA 3.3	30 ± 35	N/A	374
	SUERC-74563	SA 3.6	modern	No solution	246

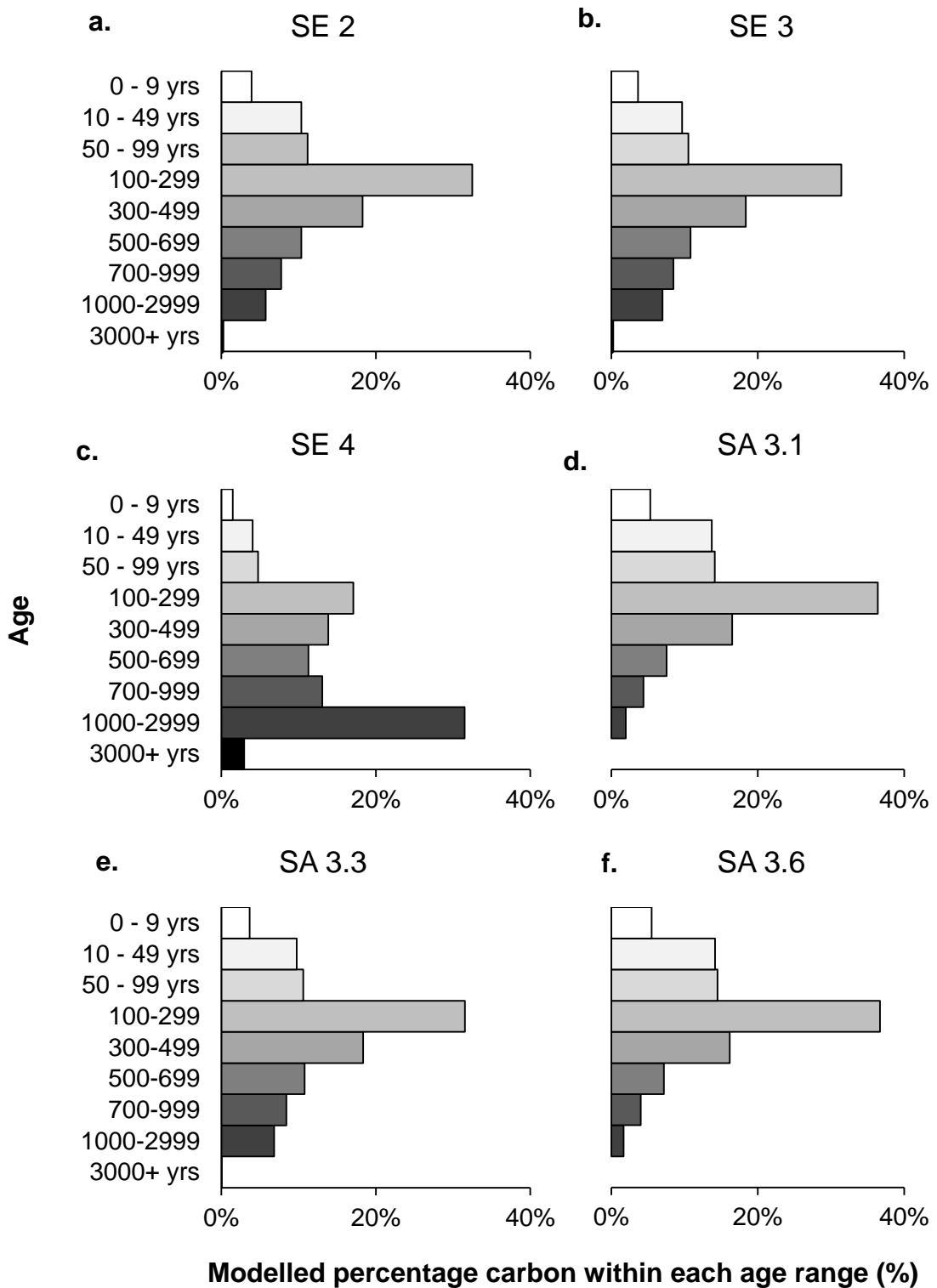


Figure 5.6. Modelled down-profile of DO^{14}C , as estimated from the age attribution model for all radiocarbon dated sites ($n=6$)

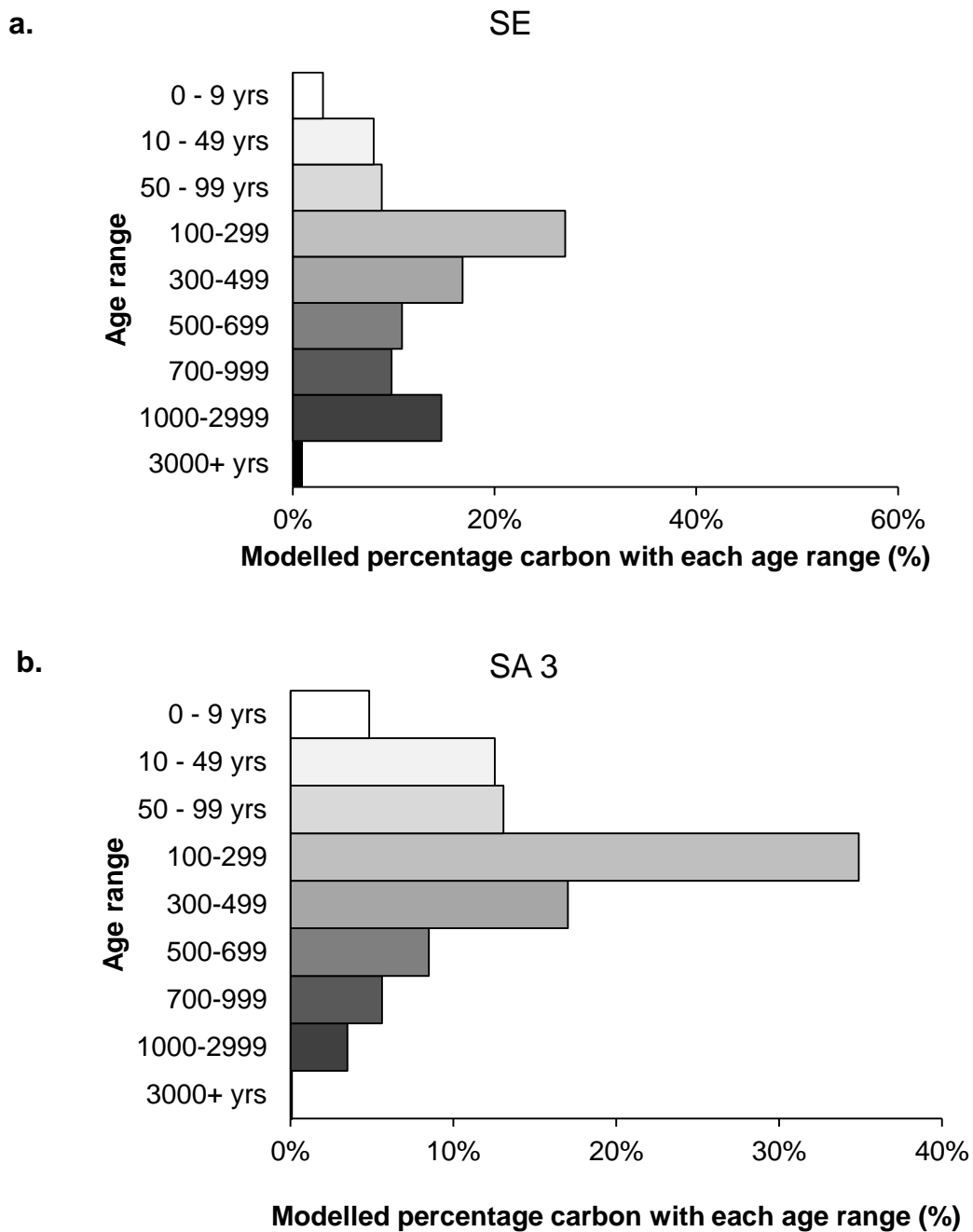


Figure 5.7. Modelled down-profile of DO^{14}C , as estimate from the age attribution model for all six radiocarbon dated sites grouped into their respective plantation estates **(a)** Sebungan and **(b)** Sabaju 3

5.3.2. Absorptivity and aromaticity

SUVA₂₅₄ data for the different landcover classes are displayed in Figure 5.8a and Table 5.4, and has also been converted to % aromaticity using the relationship described in Weishaar et al. (2003) (Figure 5.8b; Table 5.5). The overall trend shows differences in the spectrophotometric properties of DOC across the conversion gradient (Figure 5.8). Because the relationship between SUVA₂₅₄ and % aromaticity is based upon a straight line ($y = mx + c$), both data sets display the same trend. The highest SUVA₂₅₄ and % aromaticity was displayed by FB (6.3 l mg-C⁻¹ m⁻¹ and 44.5 %, respectively), which was significantly different to FA ($p < 0.01$; Table 5.5) and all plantation drain types (Table 5.5). In contrast the lowest values were displayed by the collection drain within the 6-year-old OPP with values for average SUVA₂₅₄ and % aromaticity of 5.2 l mg-C⁻¹ m⁻¹ and 37.0 %, respectively.

In terms of the plantations, the main drains displayed higher SUVA₂₅₄ values in comparison to the collection drains across all age categories (Figure 5.8; Table 5.4). When separated by age, the 9-year-old estates displayed slightly higher SUVA₂₅₄ values, across all drain types, in comparison to the 6-year-old plantations. This difference was significant between the collection drains (i.e. C6 vs C9, $p < 0.05$; Table 5.5) and between the collection and main drains (i.e. C6 vs M9, $p < 0.001$; Table 5.5).

Despite varying degrees of degradation there was very little difference in carbon quality between the forest sites (FA and FB) and the degraded landcover classes (R-DF and DF). Furthermore, carbon quality within DF was similar to that of the plantations, aside from the 6-year-old plantation collection drains (Table 5.5). Conversely, the carbon quality within R-DF was significantly different to the plantation collection drains, across all age categories (Table 5.5).

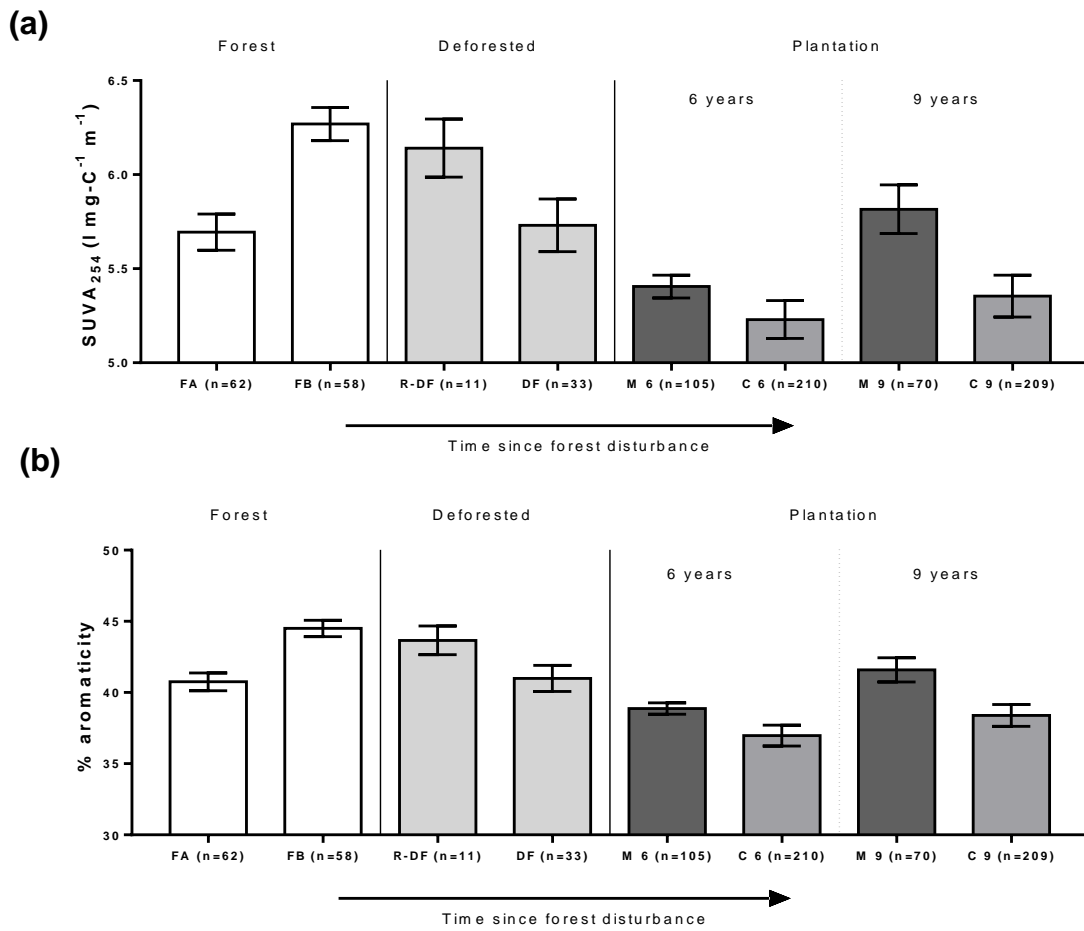


Figure 5.8. Mean (a) SUVA₂₅₄ data and (b) % aromaticity data during the study period for all landcover classes, along the conversion gradient. Error bars display the standard error of the mean.

Table 5.4. Summary of SUVA₂₅₄ and % aromaticity data for the landcover classes

Landcover class		Mean SUVA (l mg-C ⁻¹ m ⁻¹)	Mean % aromaticity
P	Main	5.6	40.0
	Collection	5.3	37.8
P 6	Main	5.4	38.9
	Collection	5.2	37.0
P 9	Main	5.8	41.6
	Collection	5.4	38.4
F	Overall	6.0	42.6
FA		5.7	40.8
FB		6.3	44.5
R-DF		6.1	43.7
DF		5.9	42.2

Table 5.5. Results of Kruskal-Wallis test (*post-hoc*) for SUVA₂₅₄ and % aromaticity applied to the different landcover classes. Where ns = no significant differences and * = the level of significance. Identical trends in significance were displayed between the two parameters

	FA	FB	R-DF	DF	M9	C9	M6	C6
FA		**	ns	ns	ns	ns	ns	***
FB			ns	ns	***	****	****	****
R-DF				ns	ns	*	ns	***
DF					ns	ns	ns	**
M9						ns	ns	***
C9							ns	*
M6								ns

The spectrophotometric differences in DOC across the four individual plantations are displayed in Figure 5.9. Only SUVA₂₅₄ data is displayed due to identical trends within the % aromaticity data set. Mean SUVA₂₅₄ values ranged from 5.1 – 6.5 l mg-C⁻¹ m⁻¹, irrespective of drain type. When analysed separately there are no consistent trends in relation to plantation age and DOC quality with significant differences observed between plantations of the same maturity (i.e. SE vs SA1; Figure 5.9). Significantly higher SUVA₂₅₄ values were displayed within the SE plantation, for both drain types, in comparison to all plantation estates. In contrast, the lowest values were observed within the collection drain within SA 4 (5.1 l mg-C⁻¹ m⁻¹) and the main drain within SA 3 (5.1 l mg-C⁻¹ m⁻¹). Slightly higher SUVA₂₅₄ values were found within the main drains of SA 4 and SE, in comparison to their collection drain counterparts, which was significant in the case of SA 4 (Figure 5.9).

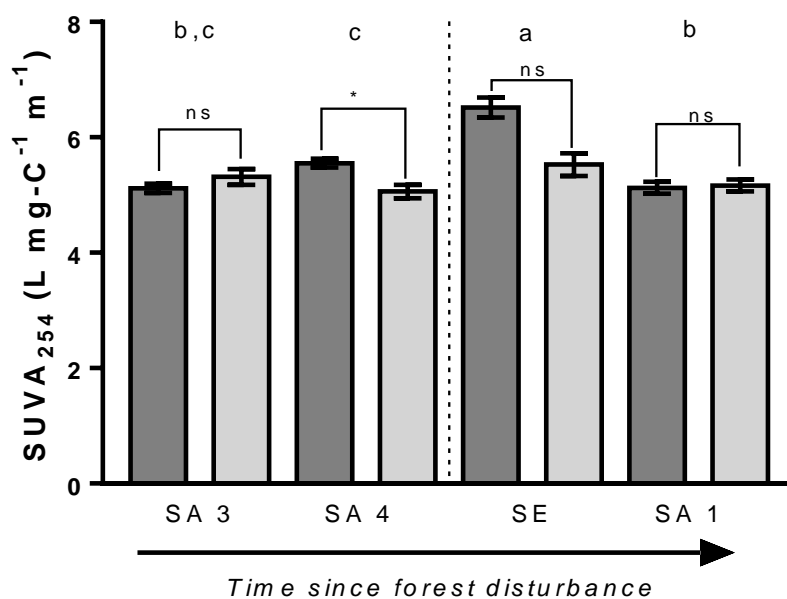


Figure 5.9. Mean SUVA₂₅₄ and % aromaticity data separated into the individual plantations, August 2015 – August 2016. Where: the dashed line represents the division between the young and old plantations and bars display the standard error of the mean. Main and collection drains are denoted by the dark grey and white bars, respectively. Letters a-c and (*) denote significant differences (Kruskal-Wallis test, *post-hoc*) between estates and drain types, respectively. Ns= no significant difference (P > 0.05).

5.3.4 Temporal dynamics of SUVA

Temporal variability in $SUVA_{254}$ values for each landcover class are displayed in Figure 5.10. The P landcover class displayed relatively stable $SUVA_{254}$ values throughout the year ranging from 4.3 to 6.7 $l\ mg-C^{-1}\ m^{-1}$, with no obvious seasonal trends (Figure 5.10). In contrast, both DF and to a lesser extent F, displayed greater seasonal variability, best illustrated by the sudden peak in $SUVA_{254}$ values in December 2015. Large increases in $SUVA_{254}$ are also apparent, within DF, in February 2016 and to a lesser extent in May 2016 (Figure 5.10). By contrast, both DF and F also show sudden episodic drops in $SUVA_{254}$ values, most noticeable in October 2015. In terms of R-DF, $SUVA_{254}$ values were relatively constant for the majority of the year, hovering between 5.8 $l\ mg-C^{-1}\ m^{-1}$ and 6.6 $l\ mg-C^{-1}\ m^{-1}$. The only noticeable trend is a sharp increase in February 2016, from 4.8 $l\ mg-C^{-1}\ m^{-1}$ to 6.4 $l\ mg-C^{-1}\ m^{-1}$, followed by a smaller increase in July 2016.

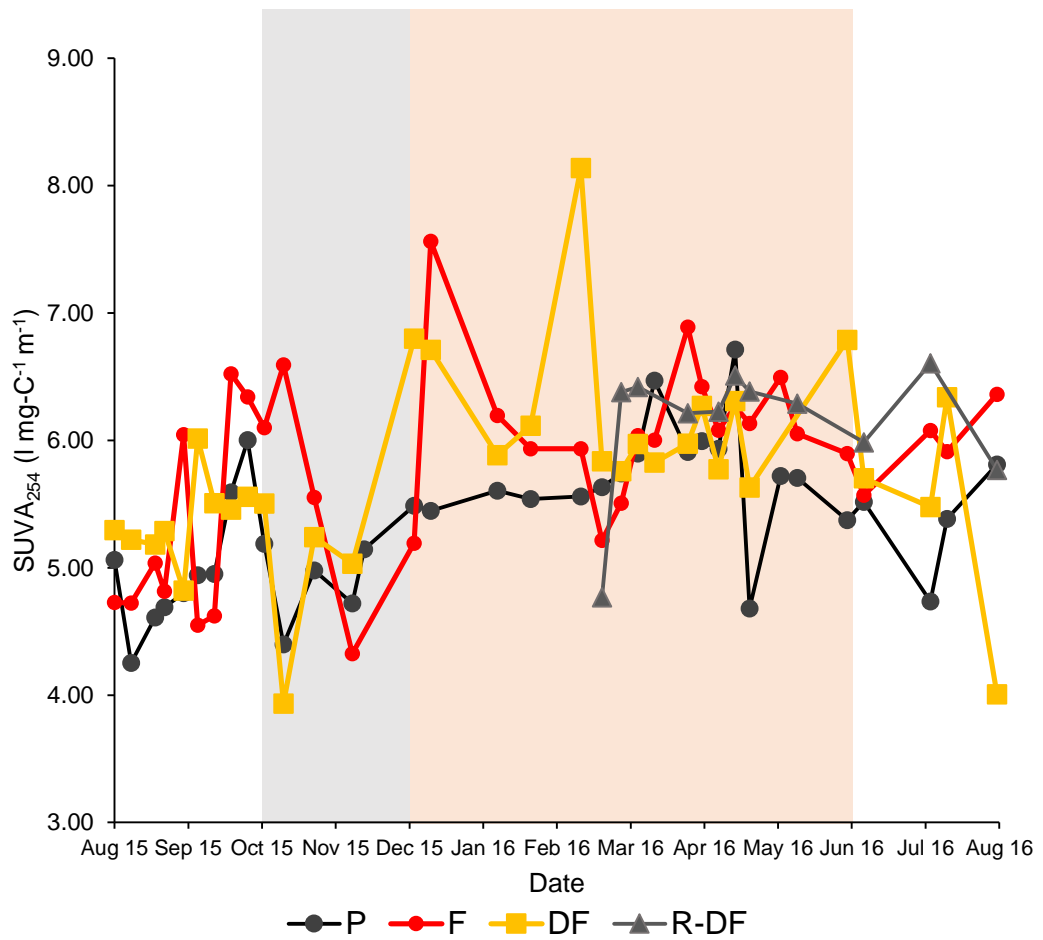


Figure 5.10 Weekly $SUVA_{254}$ data for the different landcover classes. Data presented is average weekly TOC concentrations from all drains within each landcover class. Weekly data for the P, F and DF landcover classes totals 54 weeks with the R-DF site totalling 25 weeks. The shaded areas indicate the timing of a distinct wet period (light grey; November to December, inclusively) and dry period (light orange; January to June, inclusively).

A closer analysis of the temporal dynamics of $SUVA_{254}$, alongside discharge and DOC concentrations are presented in Figures 5.11 to 5.12, for the SE and SA1 estates, respectively. These sites were selected based on their consistent annual discharges. DOC concentrations and $SUVA_{254}$ displayed a strong coupling with increased DOC associated with increases in the UV-range. There were some identifiable periods of increased discharge (red circles) which correlated to times of episodic increases in DOC and $SUVA_{254}$. This is particularly noticeable within Figure 5.11. In contrast, lower discharge months tended to be associated with lower $SUVA_{254}$ and DOC concentrations. Overall, the SA 1 plantation displayed a dampened response of the carbon metrics to discharge (Figure 5.12). This can be seen in direct contrast to SE which showed $SUVA_{254}$ and DOC readily responded to increases in discharge (Figure 5.11).

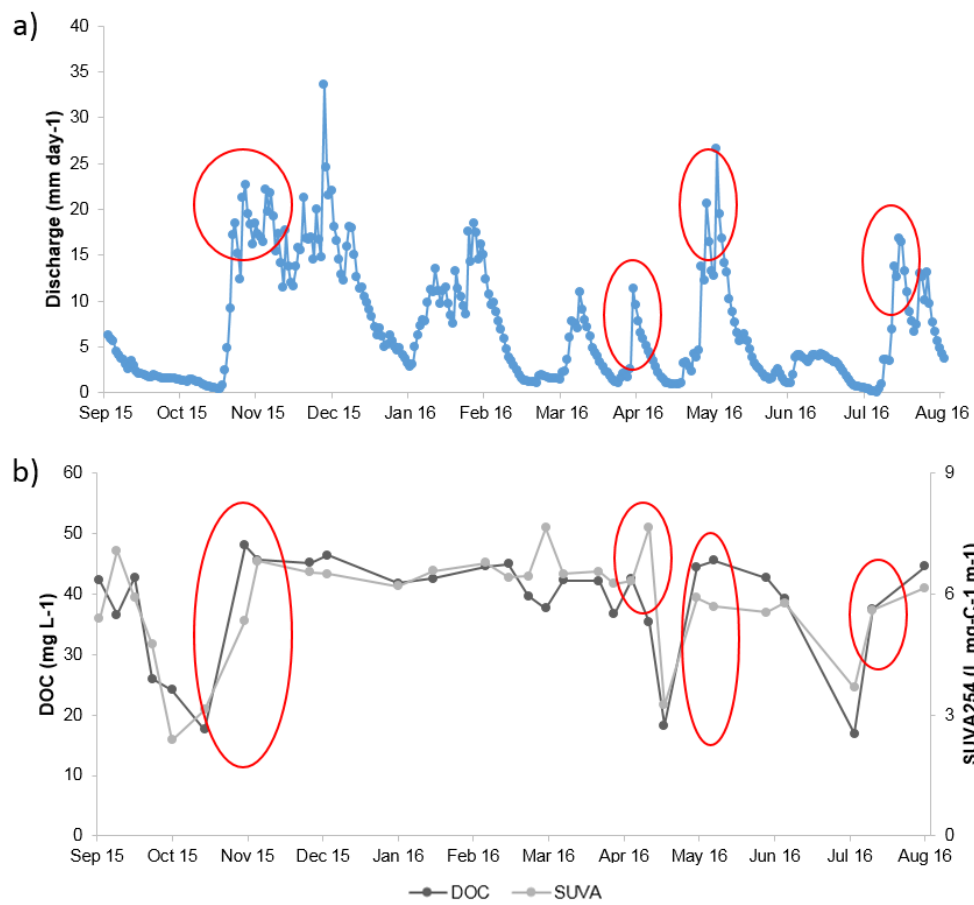


Figure 5.11. Temporal dynamics in mean (a) daily discharge and (b) DOC concentrations (blue line) and SUVA (orange line) for the Sebungan (SE) plantation. Red circles indicate periods of increased discharge and carbon quality metrics. Daily discharge readings are an average of the SE plantation sites installed within mini-divers.

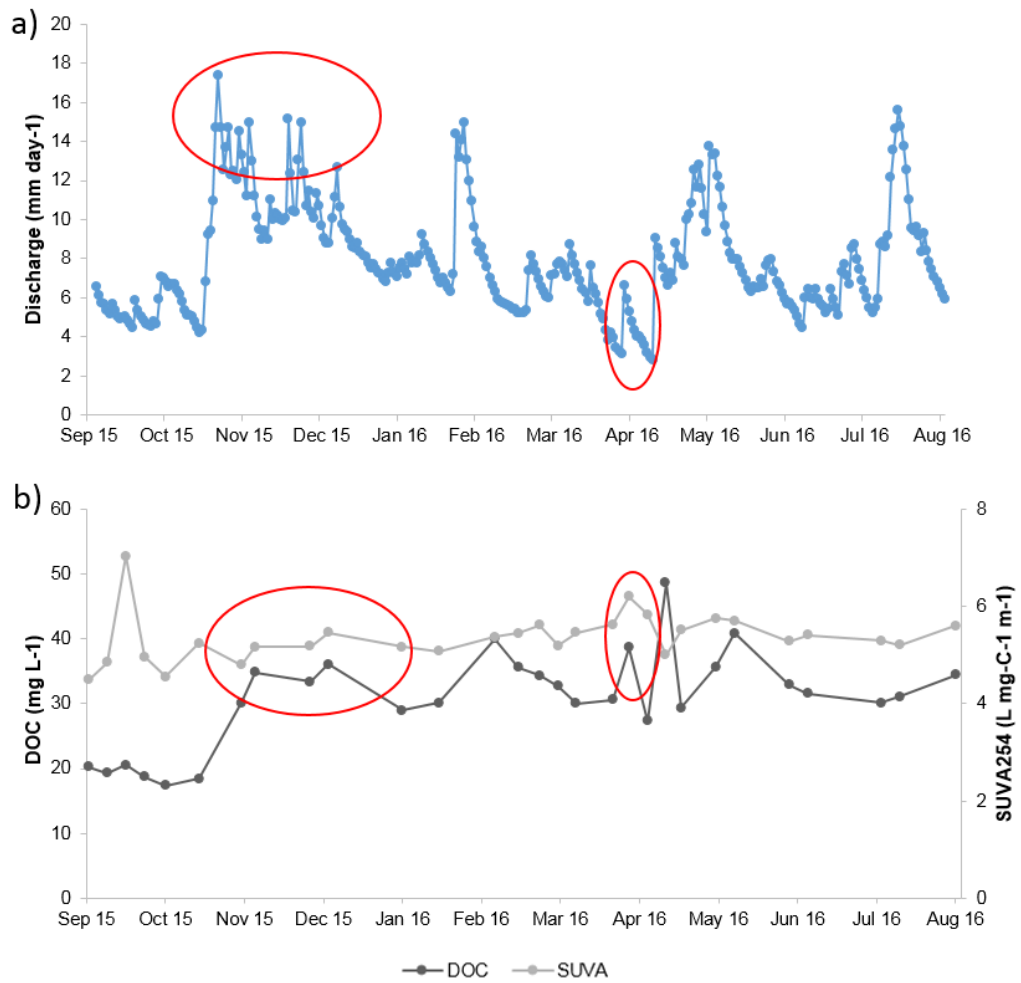


Figure 5.12. Temporal dynamics in mean (a) daily discharge and (b) DOC concentrations (blue line) and SUVA (orange line) for the Sabaju 1 (SA 1) plantation. Red circles indicate periods of increased discharge and carbon quality metrics. Daily discharge readings are an average of the SA 1 plantation sites installed within mini-divers.

5.3.5 E ratios

Overall, E ratios were largest within the P landcover class although differences between all sites were marginal (Table 5.6). All standard errors were small, particularly the E2:E3 ratio, which was an order of magnitude less than the other quotients. In general, the P landcover class tended to display the lowest standard error means, implying a greater degree of stability.

Table 5.6 Mean and standard errors for the three E ratios examined. n = the number of samples.

	P		F	DF	R-DF
	M	C			
n	175	419	120	33	11
E2:E3	3.4 ± 0.02	3.3 ± 0.03	3.1 ± 0.03	3.1 ± 0.06	3.0 ± 0.02
E2:E4	8.2 ± 0.10	8.2 ± 0.12	7.2 ± 0.13	7.1 ± 0.17	6.7 ± 0.11
E4:E6	8.6 ± 0.23	9.6 ± 0.32	9.2 ± 0.36	10.2 ± 0.85	6.7 ± 0.24

Weekly variation in all three E ratios, across the landcover classes, are displayed in Figure 5.13. The F and DF sites showed considerable weekly variation in all three E ratios, whilst P and R-DF were more stable by comparison. Regardless of landcover the E4:E6 quotient was the most erratic throughout the study period; there were sudden high increases within DF during September and November 2015 and gradual increases within F from November 2015 to January 2016. There was evidence of shared trends between the E2:E3 and E2:E4 ratios; for example, both displayed significant increases occurring in late November 2015, within F. In contrast, both P and R-DF displayed relatively stable annual E2:E3 and E2:E4 values, with equally stable E4:E6 ratios within R-DF.

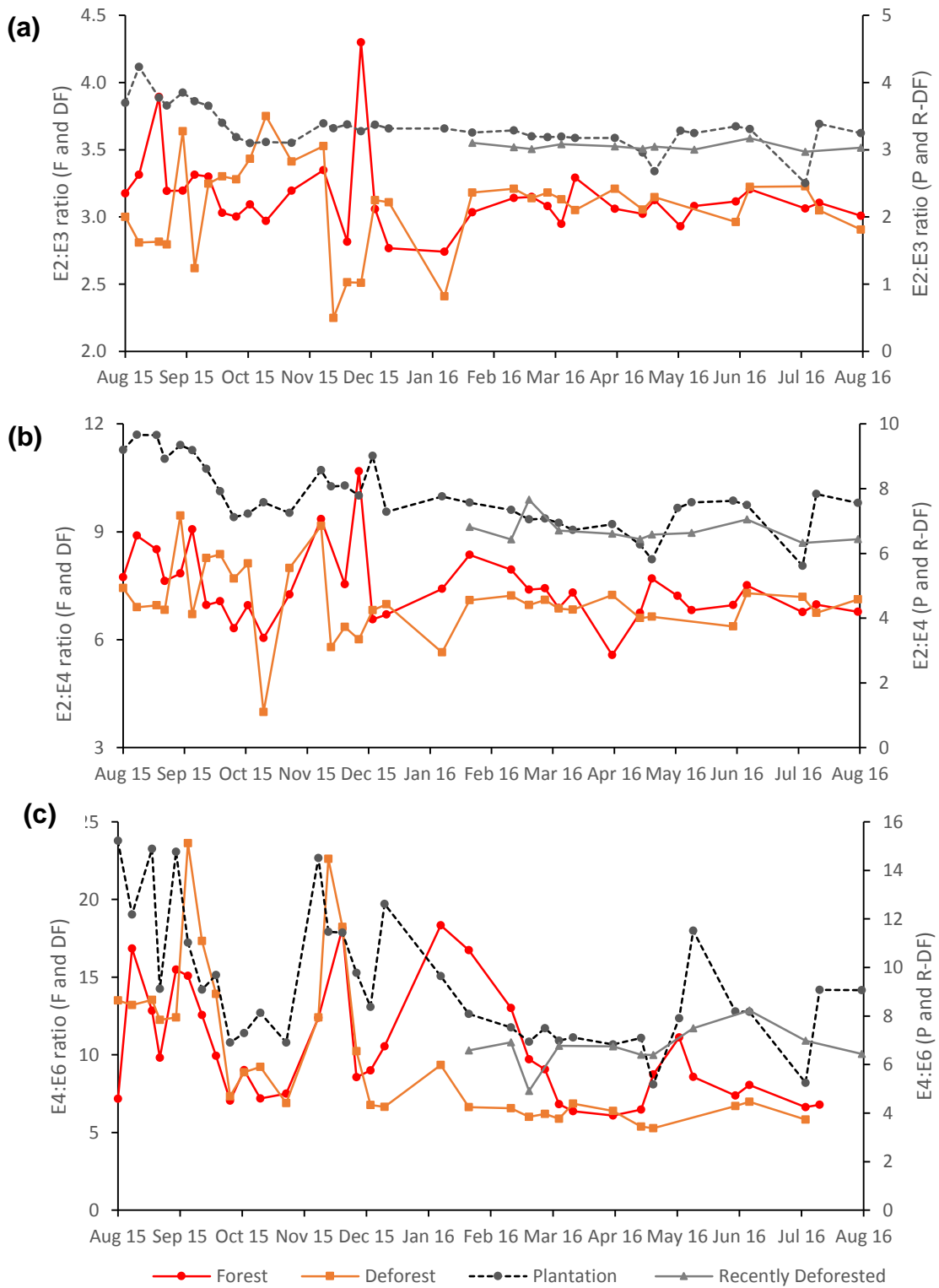


Figure 5.13 Weekly variability in mean values for all three E ratios (a) E2:E3, (b) E2:E4, (c) E4:E6, across the four landcover classes, during the study duration.

The relationship between % aromaticity and the quotients E4:E6 and E2:E3, indicators of aromaticity, are displayed in Figure 5.14. While there was no relationship observed between the E4:E6 quotient and % aromaticity data (Figure 5.14a), there was a weak yet statistically significant ($p < 0.0001$) negative relationship between the E2:E3 ratio and % aromaticity (Figure 5.14b).

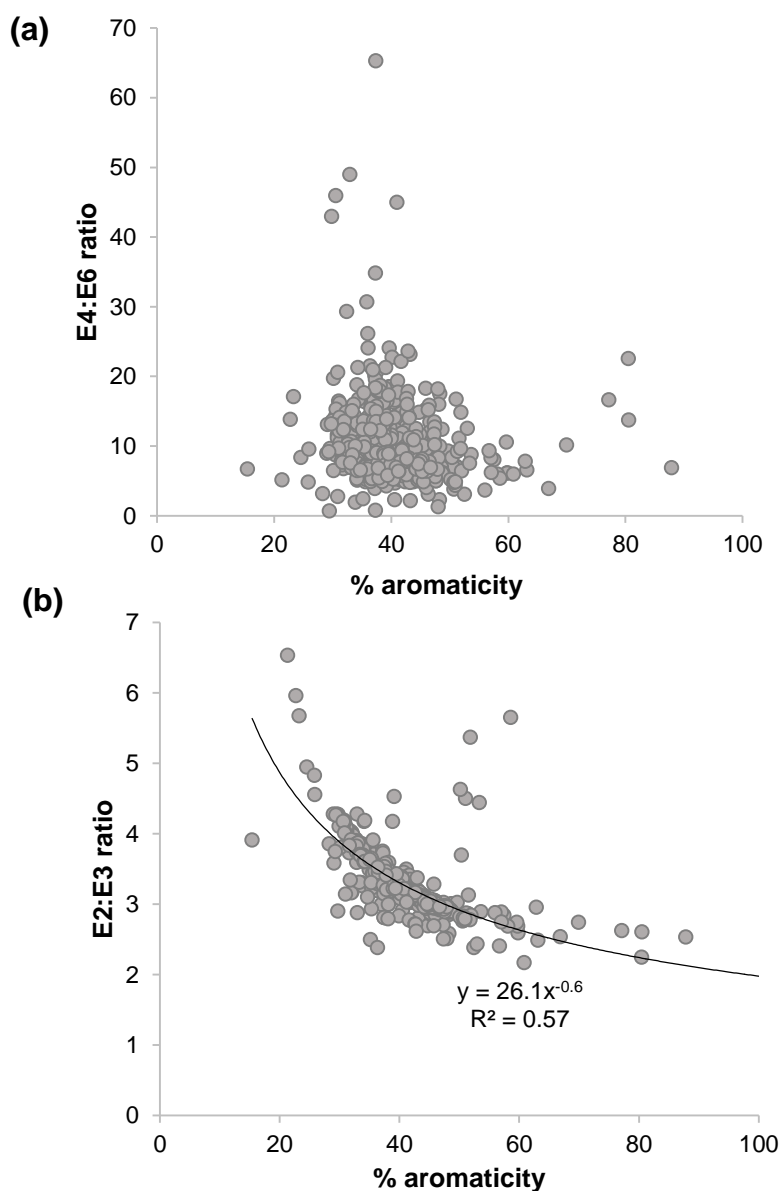


Figure 5.14 Correlation between % aromaticity and (a) E2:E3 ratio and (b) E4:E6 ratio. The correlation of fit (r^2) is displayed on (b) alongside the equation of the line.

5.3.6 Intense DOC collection experiment

The results from the intense DOC collection experiment are presented in Figure 5.15. The main drains showed consistently higher SUVA₂₅₄ and % aromaticity values throughout all the plantation study sites (Figure 5.15 b and c), by an average of 0.42 l mg-C⁻¹ m⁻¹ and 2.72 %, respectively. In contrast, DOC concentrations tended to be greater within the collection drains, by an average of 2.44 mg L⁻¹, with the exception of SA 3. However, it should be noted that there was no statistical significance between the main and collection drains for any of the three parameters.

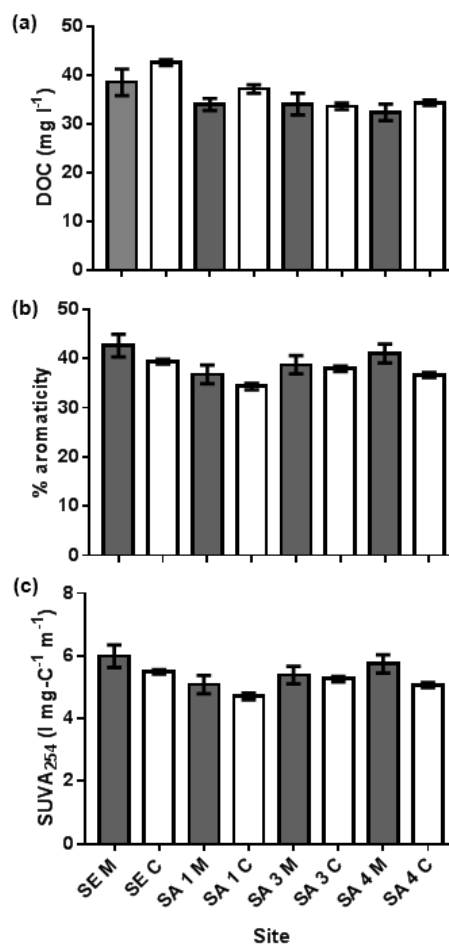


Figure 5.15 Mean (a) DOC concentrations, (b) % aromaticity and (c) SUVA₂₅₄ data from the intense DOC collection experiment. Bars displayed the standard error of the mean.

5.4 Discussion

5.4.1 DOC radiocarbon ages

Results from the radiocarbon dating suggested that the DOC contained a mixture of carbon from a range of ages (Table 5.2), which was more thoroughly examined with the age attribution model (Figures 5.6 and 5.7). The majority of all peat derived carbon was fixed from sources older than 100 years BP (Figure 5.6), with none of the modelled sites retaining their 'modern' conventional radiocarbon age (Table 5.3). On average only ~14% of the exported carbon was relatively young (< 49 years BP; Figure 5.7) and likely derived from the turnover of recently fixed carbon from the aboveground biomass. DOC from the channel draining site SE 4 displayed significant ^{14}C -depletion, equivalent to an age of 735 ± 37 years BP (Figure 5.4; Table 5.2), with a considerable fraction of peat carbon (> 33%) derived from aged sources (1000+ years BP). This implies that DOC export from these sites may represent a loss of long-term stored carbon derived from deep within the peat profile (Moore et al., 2013; Evans et al., 2014).

While attempts were made to minimize between-site variations in flow conditions (i.e. sampling sites on the same day) it is clear that there was watertable variability (Table 5.2). The watertable data coupled with the DO^{14}C values suggests watertable depth could determine the age of the exported carbon (Figure 5.5). Watertable drawdown is likely to expose deeper and older peat layers causing aged carbon to be leached out (Evans et al., 2014). This is in agreement with several studies (Moore et al., 2013; Evans et al., 2014; Butman et al., 2015) in which artificial drainage has been inputted causing instability deep within the peat column and resulting in the release of previously stable carbon stores. Alternatively, the older carbon may result from the mobilization of a finite and pre-existing ^{14}C -depleted DOC pool (Evans et al., 2014) that has no connection with drainage. However, this is unlikely considering these sites were drained 6 to 9 years prior to sampling, thus, this pool is likely exhausted. Taken together these findings help to reinforce the

RSPO watertable management guidelines, stipulating peatland OPP water levels should be maintained between -40 to -60 cm below the peat surface (Lim et al., 2012).

Overall, the radiocarbon data suggests DOC draining these tropical peatland OPPs is predominately sourced from carbon within the last three centuries (< 299 year BP). This conflicts with two previously collected samples corresponding to significantly older mean ages of 4,000 years BP (Moore et al., 2013). The presence of millennia year old carbon appears to be linked to drainage intensity (i.e. data from site SE 4) however, the lack of data from this landcover class, alongside differing watertable management regimes is necessary to gain a more complete understanding.

5.4.2 Bioavailability

There are clear differences in the bioavailability of carbon across the different landcover classes and subsequent conversion gradient (Figure 5.8). The main drains within the P landcover class displayed consistently higher $SUVA_{254}$ values (indicative of higher DOC aromaticity) in comparison to the collection drains (Figure 5.8; Table 5.4). This was significant in the case of SA 4 (Figure 5.9). This could indicate that localised DOC processing is occurring within the collection drains; labile aliphatic DOC compounds are already metabolised before reaching the main drains, leaving the more recalcitrant fraction behind. This is feasible with the processing of DOC reported to occur rapidly within peatland catchments (63% within 12 hours; Worrall and Moody, 2014). This concept is further supported by the results from the intense DOC collection experiment with consistently higher $SUVA_{254}$ and % aromaticity found within the main drains (Figure 5.15). In addition, slightly elevated DOC concentrations were exhibited by the collection drains in comparison to their main drain counterparts, further suggestive of differences in drainage channel DOC degradation rates (Figure 5.15). Conversely, both SA 1 and SA 3 exhibited greater $SUVA_{254}$ values within the collection drains (Figure 5.9). This inconsistency could reflect the fewer collection drains sampled in comparison

to the intensive DOC investigation, reducing spatial variability, and thus, precluding the identification of this trend within these individual plantation data sets.

Spectrophotometric differences in DOC were also observed between the plantation age categories (Figure 5.8). In general, the more mature plantations displayed greater $SUVA_{254}$ and % aromaticity values, suggestive of more recalcitrant DOC (Olefeldt et al., 2013). This is logical considering more time has passed since conversion and thus, the labile carbon pool has already been exhausted; an outcome of the longer exposure to both drainage and intensive soil management regimes (Kononen et al., 2016). Conversely, trends in age were not identified on an individual plantation basis (Figure 5.9). This is likely explained by the significantly higher ($p < 0.0001$) $SUVA_{254}$ values observed within the SE plantation, potentially skewing the data (Figure 5.8). As previously mentioned (Chapter Four), the SE estate has experienced greater compaction of the surface peat in comparison to the SA estate; this is reinforced by the bulk density data (Appendix A). This modification will restrict the movement of DOC through the peat profile by reducing pore volume and hydraulic conductivity (Whittington & Price, 2006). Subsequently, this impeded water movement could facilitate the build-up of DOC, rich in humic compounds, elevating $SUVA_{254}$ values (Clark et al., 2012). Alternatively, the lower watertables in SE (i.e. -1280 cm; Figure 4.11; Chapter Four) could also be contributing to the higher absorbance values. This is supported by several peatland studies (Lou et al., 2014; Hribljan et al., 2014) noting increases in coloured and phenolic DOC compounds at lower watertables, attributed to greater aerobic conditions and increased DOC mineralization.

Some of the highest $SUVA_{254}$ and % aromaticity values were displayed within the degraded sites (R-DF and DF), irrespective of statistical significance (Figure 5.8). This directly supports research by Kononen et al. (2016) suggesting a switch from more labile carbon, within a PSF, to more recalcitrant carbon in response to increased disturbance (i.e. active drainage). This will extend the aerobic zone within the peat column, exposing fresh layers of peat enriched in labile carbon substrates (Carlson et al., 2015). This creates

favourable DOC-decomposition environments quickly eliminating compounds such as labile hemicelluloses, uronic acids and cellulose (Kononen et al., 2016), leading to the build-up and enrichment of recalcitrant carbon units. This process will be further intensified by the presence of a more open canopy, enhancing photo and temperature induced degradation. The lack of a vegetation canopy will also limit the input and retention of fresh organic matter, reducing the presence of labile carbon, further enriching the peat in recalcitrant compounds. Furthermore, the peatland floor, within R-DF, was covered with woody debris which could be supplying the DOC pool with large quantities of recalcitrant lignin, further increasing SUVA₂₅₄.

As R-DF was more recently disturbed, in comparison to DF, labile carbon compounds are likely still present. However, this is not reflected in the carbon quality data with lower SUVA₂₅₄ values within DF (Figure 5.8). However, this could be a reflection of the priming effect of organic matter from recent deforestation (Fontaine et al., 2003). This will replenish the labile carbon pool which, in turn, will increase the amount of energy available for soil microorganisms accelerating carbon mineralization (Fontaine et al., 2003). Consequently, the higher SUVA₂₅₄ values within R-DF likely reflect a combination of more intensive and uncontrolled drainage, coupled with the priming effect of fresh organic matter input.

Following the same line of logic proposed by Kononen et al. (2016) it is expected that the forest sites would exhibit more labile carbon (i.e. lower SUVA₂₅₄). This is supported by the assumption that i) PSFs have a large input of fresh organic matter rich in young labile carbon (Kononen et al., 2016) and ii) the harsh acidic environments within PSFs inhibit microbial decomposition, thus, preserving these labile carbon compounds (Yule, 2010). While FA conforms to this assumption, FB displayed significantly higher values in comparison to FA and was more comparable to R-DF (Figure 5.8; Table 5.5). However, FB is likely to have a more favourable DOC-decomposition environment, substantiated by a more open canopy and thus, greater exposed peat surface. This is further reinforced by the watertable data presented in Chapter Four, showing significant drainage occurring within this site (i.e -75.7

cm; Figure 4.10). This, coupled with the priming effect described above could be causing the unexpectedly high SUVA₂₅₄ values within FB. Alternatively, Yule & Gomez (2009) have shown that in extreme environmental conditions (i.e. acidic PSF environments) microbial communities are able to adapt, allowing decomposition to take place. This makes the degree of leaf litter degradation more dependent upon the inherent physical and chemical properties of the leaves themselves, rather than microbial inhibition (Yule & Gomez, 2009). Consequently, labile DOC compounds can be utilized by PSF microbes (Yule & Gomez, 2009), despite these extreme environmental conditions, reinforcing the build-up of recalcitrant carbon compounds within the FB fluvial network.

The plantation sites exhibited the lowest SUVA₂₅₄ values, indicative of greater labile carbon enrichment. While this contradicts the findings by Kononen et al. (2016), it could suggest that PSF conversion to OPP is causing distinct changes to occur in the DOC compositional properties, unique to this form of conversion. It is not unreasonable to postulate this considering the differences in vegetation composition, canopy coverage and resultant temperature differences, with reported maximum soil temperatures in OPPs reaching ~8°C higher than intact PSFs (Comeau et al., 2013).

A closer analysis of the SUVA₂₅₄ data across the year revealed monthly variability (Figure 5.10), the greatest degree of which was displayed by both the F and DF study sites. This was most prominent during December 2015, corresponding to the region's wet season and is likely an outcome of increased DOC being flushed out of the system (Kalbitz et al., 2000; Strack et al., 2008). The variability in SUVA₂₅₄ within F could also reflect the lack of a stable and self-regulating watertable (Dommain et al., 2010); an outcome of the site's proximity to the plantation drainage ditches, compromising the resilience of these ecosystems to natural system perturbations. Considering this, it was somewhat surprising that the R-DF site exhibited more consistent SUVA₂₅₄ values (Figure 5.10). However, the sudden increase in values noted at the start of collection (February 2016), could reflect a lag-time in the system's response to ongoing disturbances, signifying a switch from more labile to more

recalcitrant carbon forms. This shift could be capturing the eventual depletion of the labile carbon pool (i.e. cellulose), following initial deforestation, leaving behind more refractory carbon compounds (i.e. lignin).

The consistent ranges in $SUVA_{254}$ observed within P, are likely an outcome of the regulated watertable management (Figure 5.10). However, a closer analysis of the dynamics between water quality, DOC concentrations and discharge reveal temporal changes (Figure 5.11 and 5.12). Several identifiable high discharge events are associated with episodic increases in both DOC and $SUVA_{254}$ values, more pronounced within Figure 5.11. As both DOC and $SUVA_{254}$ appear to increase together, then the increase in $SUVA_{254}$ must be proportionally larger than the increase in DOC (Weishaar et al., 2003). Subsequently, these high discharge events are leading to proportionally larger $SUVA_{254}$ increases.

The rewetting of peat, particularly following drought, has been linked to the flushing out of DOC rich in humic material, elevating $SUVA_{254}$ values (Clark et al., 2012). Conversely, lower rainfall periods are often associated with a decline in the humic acid fraction (Clark et al., 2012). This is seen within both Figures 5.11 and 5.12, with lower $SUVA_{254}$ values during lower discharge months (i.e. July 2016; Figure 5.11). This is caused by alterations in the ratio between hydrophilic and hydrophobic DOC components (Ritson et al., 2014), with drought associated with decreases in the hydrophobic humic component (Clark et al., 2012). Alternatively, changes in $SUVA_{254}$ values in response to hydrology can also indicate a change in the DOC source, with storm events often associated with more aromatic DOC (higher $SUVA_{254}$) in comparison to base flow (Hood et al., 2006). These $SUVA_{254}$ changes can also signify a switch in carbon sources with lower $SUVA_{254}$ values indicative of autochthonous sources (e.g. algae) and higher $SUVA_{254}$ suggestive of allochthonous derived carbon (i.e. terrestrial; Fasching et al., 2015). This is supported by visual field observations with the growth of algae on the surface waters during low flow/ stagnant periods. Furthermore, higher $SUVA_{254}$ values noted during high flow periods adds to the concept of increased hydro-

connectivity during storm events, increasing the number of terrestrially sourced carbon transportation pathways (Strohmeier et al., 2013; Tunaley et al., 2016).

It is important to recognise that while $SUVA_{254}$ and % aromaticity are useful for gaining an insight into the bioavailability of the DOC pool, they are proxy techniques. The 'fate' of the DOC pool is ultimately reliant upon the presence of particular microbial assemblages to metabolize this fraction (Jiao et al., 2010), without which even highly labile carbon will remain immobilized (i.e. net carbon sinks). Subsequently, an inventory of the microbial communities present would be necessary to ascertain the overall contribution of the DOC pool to net heterotrophy.

5.4.3 *E ratios*

The quotient E4:E6 has been used as an indicator of aromaticity, a larger ratio being indicative of more aromatic carbon (Worrall et al., 2002). A positive relationship would be expected between % aromaticity and respective E4:E6 ratios. However, no relationship was observed between these variables (Figure 5.14a), which agrees with previous research finding very little correlation between this ratio and DOC structural properties (Peuravuori & Pihlaja et al., 1997; O'Driscoll et al., 2006). An elevated E4:E6 ratio (8+) is indicative of DOC predominately derived from fulvic acids (Hriblijan et al., 2014), which accumulate from plant litter decomposition in aerobic environments (McKnight et al., 2001). Conversely, a quotient of 5+ is associated with the build-up of humic acids resulting from suppressed microbial decomposition during anaerobic conditions (Hriblijan et al., 2014). In general, all landcovers displayed mean E4:E6 values indicative of fulvic acids (Table 5.6), suggesting the prevalence of aerobic conditions, particularly at site DF. Surprisingly, site R-DF exhibited a lower E4:E6 ratio which was more suggestive of anaerobic conditions. However, this could reflect the uncontrolled drainage associated with recently cleared sites (Hooijer et al., 2011) causing the system to fluctuate between anaerobic and aerobic

conditions. This is further supported by Peacock et al. (2014b) noting a strong correlation between this quotient and temporal changes in DOC quality in response to environmental stimuli.

A negative relationship was observed between % aromaticity and the quotient E2:E3 (Figure 5.14a). This supports research by Peuravuori & Pihlaja (1997) who state that as the aromaticity and molecular size of an aquatic solute decreases (i.e. becomes more labile) the E2:E3 quotient increases. During the study year, both the E2:E3 and E2:E4 quotients were relatively stable, particularly within the P and R-DF landcover classes (Figure 5.13 a,b). However, all fluctuations in E ratio data will be, to some extent, driven by seasonal variability. This is supported by visual field observations finding clearer DOC water samples following some heavy precipitation events, a reflection of increased surface run-off and therefore increased channel water dilution.

The E2:E3 ratio, an indicator of molecular weight (MW), has also been linked to bioreactivity (Sinsabaugh and Forman., 2003), with higher MWs (lower E2:E3) associated with more stable, less-energetic, refractory carbon (Hribljan et al., 2014). However, the E2:E3 trends (Table 5.6) are in opposition to the SUVA₂₅₄ data (Figure 5.8 a). For example, the SUVA₂₅₄ results suggest that the P estates were dominated by labile carbon (low SUVA₂₅₄) yet, displayed the highest E2:E3 ratio indicative of aromatic carbon. Subsequently, despite the theoretical understanding, it is difficult to deduce from the E ratio data the overall fate of the DOC compounds (Amon & Benner, 1996).

5.5 Conclusions

The results presented within this chapter draw attention to the observed differences and behaviour of the carbon quality metrics (i.e. SUVA₂₅₄ and E ratios) across a peatland conversion gradient. These differences are suggestive of disturbances/ modifications in both the production and transportation of DOC (Wallage et al., 2006) within the peat profile. The R-DF

and DF sites represent the more heavily degraded areas with labile DOC already mineralised, leaving behind more stable recalcitrant carbon forms. In comparison, the OPPs exhibit the lowest SUVA₂₅₄ values, which can be interpreted as the DOC having a higher bioavailability, with this carbon more likely to be mineralised into CO₂. This implies more active microbial degradation is taking place within the peatland OPPs, primed by the input of fresh organic matter. This is, to some extent, supported by the 'modern' conventional radiocarbon ages reported for the samples. However, the age attribution model draws attention to the existence of older carbon sources (100 to 3,000+ years BP) present within the DOC, masked by the younger recently photosynthesised carbon. This, coupled with the SUVA₂₅₄ data suggest that not only are these areas losing historically aged carbon but that the fluvial carbon is more likely to be readily degraded and fed back into the carbon cycle as CO₂. The implications of this finding, in conjunction with the results of the quantitative study, are examined in Chapter Six. Here, the research outcomes are placed into both local and global contexts and the implications for the management of peatland plantations are discussed.

Chapter Six: General Discussion

The results from the Thermal Desorption-Proton Transfer Reaction – Mass Spectrometry experiment are published in Nature Scientific Reports: Materic, D., Peacock, M., Kent, M., **Cook, S.**, Gauci, V., Rockmann, T., Holzinger, R, 2017. Characterisation of the semi-volatile component of Dissolved Organic Matter by Thermal Desorption – Proton Transfer Reaction – Mass Spectrometry. Nature Scientific Reports 7: 15936

6.1 Introduction

The three primary investigations within this thesis have focused on: i) techniques to preserve and quantify tropical DOC (Chapter Three), ii) quantification of fluvial organic carbon export from peatland OPPs, at a sub-catchment level (Chapter Four) and iii) consideration of how land use change from PSF to OPP alters the qualitative aspects of the exported DOC, including bioavailability and age (Chapter Five). In this final chapter the results from the previous Chapters are synthesised and placed within a regional and global context. The implications for responsible peatland management are also discussed.

6.2 Fluvial organic carbon fluxes and carbon quality

The data presented in Chapter Four indicates that fluvial organic carbon concentrations and fluxes are high from peatland OPPs. Average DOC concentrations for the OPP landcover class ranged from 26.5 to 39.2 mg L⁻¹, an order of magnitude greater than those reported from studies of intact temperate peatlands (2.7 - 11.5 mg L⁻¹; Koehler et al., 2009). The annual TOC flux for the plantation land cover averaged 104 ± 19.3 g C m⁻² yr⁻¹, which is more than four times greater than TOC flux estimates for intact (15 to 25 g C m⁻² yr⁻¹; Koehler et al., 2009; Dinsmore et al., 2010) and disturbed (20 g C m⁻² yr⁻¹; Schwalm & Zeitz, 2014) temperate peatlands. The magnitude of the annual plantation flux is comparable to reported TOC values for degraded PSFs (94 to 108 g C m⁻² yr⁻¹; Moore et al., 2013; Muller et al., 2015) but is a third larger than TOC flux values reported for intact PSFs in Indonesia and

Sarawak, Malaysia ($63 - 64 \text{ g C m}^{-2} \text{ yr}^{-1}$; Moore et al., 2013; Muller et al., 2015). These differences are reinforced by Figure 6.1, which illustrates the plantation TOC fluxes in the context of other peatland studies across the world.

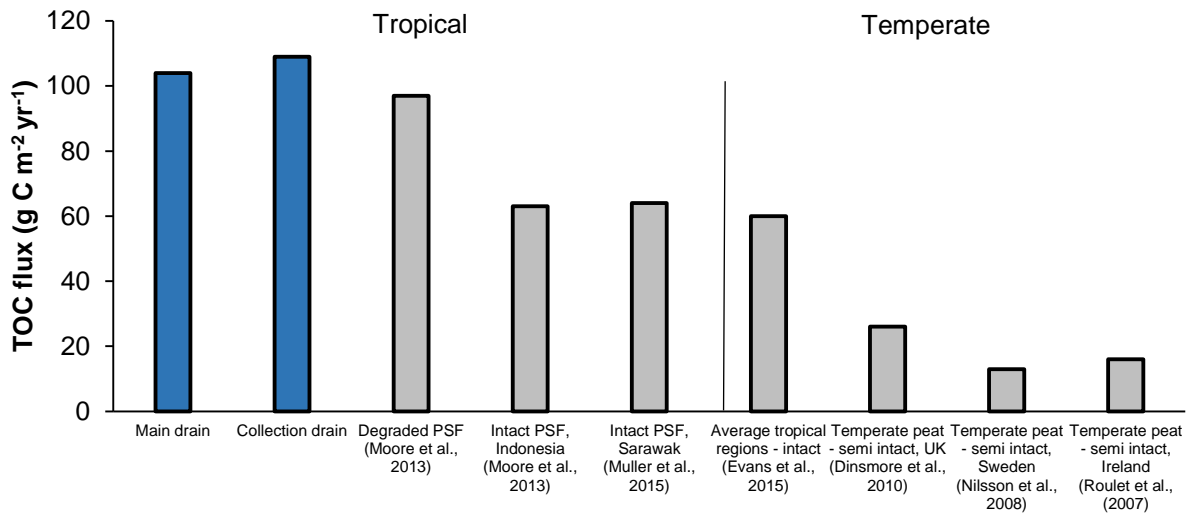


Figure 6.1 Comparison of TOC flux data from a range of peatland studies. Blue bars indicate the plantation fluxes from this study. Solid black line indicates the division between tropical and temperate peat fluxes.

To fully understand the significance of this land-use change on fluvial organic carbon losses, it is necessary to also consider the qualitative data, presented in Chapter Five. The spectrophotometric data revealed changes in the compositional properties of DOC across the land conversion gradient. Active disturbance (i.e. drainage) resulted in a switch from labile carbon, characteristic of DOC from PSFs (Kononen et al., 2016), to more recalcitrant carbon forms. Differences in DOC composition were also observed within the plantation drainage systems; the main drains were characterised by higher SUVA_{254} and higher TOC concentrations but lower overall TOC fluxes (Figure 6.2). The prevalence of more labile carbon compounds within the collection drains, coupled with their higher TOC flux, suggests the occurrence of

localised DOC processing within these drains of around $5 \text{ g C m}^{-2} \text{ yr}^{-1}$ or 5% of the total TOC (i.e. the difference between main and collection drain fluxes; $109 - 104 \text{ g C m}^{-2} \text{ yr}^{-1}$). Rixen et al. (2008) found that roughly 27% of DOC draining from a tropical blackwater, in Sumatra, was rapidly degradable (both biologically and photochemically), with a half-life of 43 hrs. As such, our processing loss rate (5%) is reasonable, and likely conservative (Kent, M, personal communication, 2017).

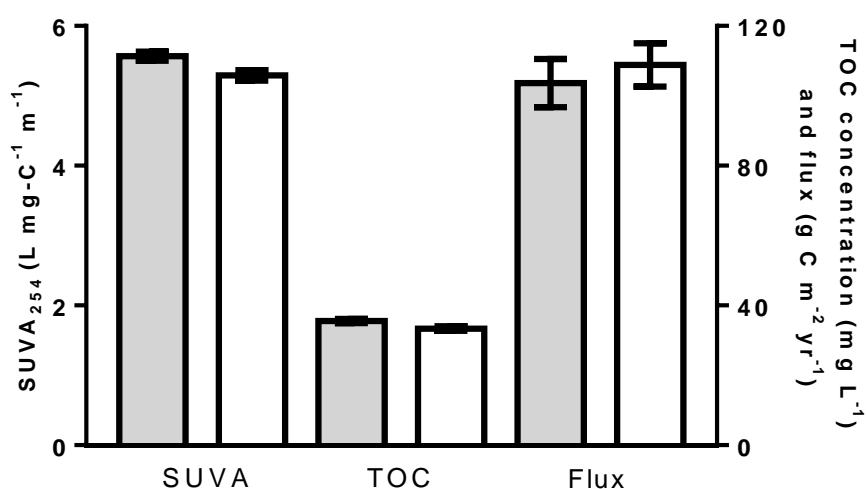


Figure 6.2 Summary graph comparing the SUVA, TOC concentration and TOC flux data for the main (grey) and collection (white) drains

The radiocarbon dating revealed that DO^{14}C ages could be linked to drainage severity. Site SE 4 displayed the lowest watertables (mean - 92 cm) with a comparable DO^{14}C age signature (91.3 % modern, equivalent to ~700 years BP) to that recorded for DOC in channels draining a moderately degraded PSF in Kalimantan, Southern Borneo (91.3 - 97.7 % modern; Moore et al., 2013). The application of the age attribution model revealed that the majority of the OPP peat carbon was derived from sources older than 100 years (BP), even for sites with 'modern' conventional radiocarbon ages. The proportion of aged carbon loss was greater under lower watertables (Figure 6.3), with higher drainage severity corresponding to increased losses of millennia old carbon. Sites with high watertables (between -20 cm to -60 cm) had DOC with <10%

carbon from sources older than 1000 year BP. This was in direct contrast to site SE 4 with a low mean watertable (-92 cm) and > 30% carbon from millennia old sources (Figure 6.3). There appears to be a ‘tipping-point’ with a disproportionately large increase in aged carbon released after watertables drop below – 60 cm (Figure 6.3). This also seems to directly relate to the proportion of time that the watertable remains below – 60 cm (Table 6.1); with the watertable for site SE 4 never recovering to levels above – 60 cm. Taken together, these observations strongly support the RSPO guidelines concerning the need for regulated stable watertables in OPPs (i.e. water tables should be in the range -40 to -60 cm below the peat surface throughout the year), which would ensure that less ancient carbon is released (Figure 6.3).

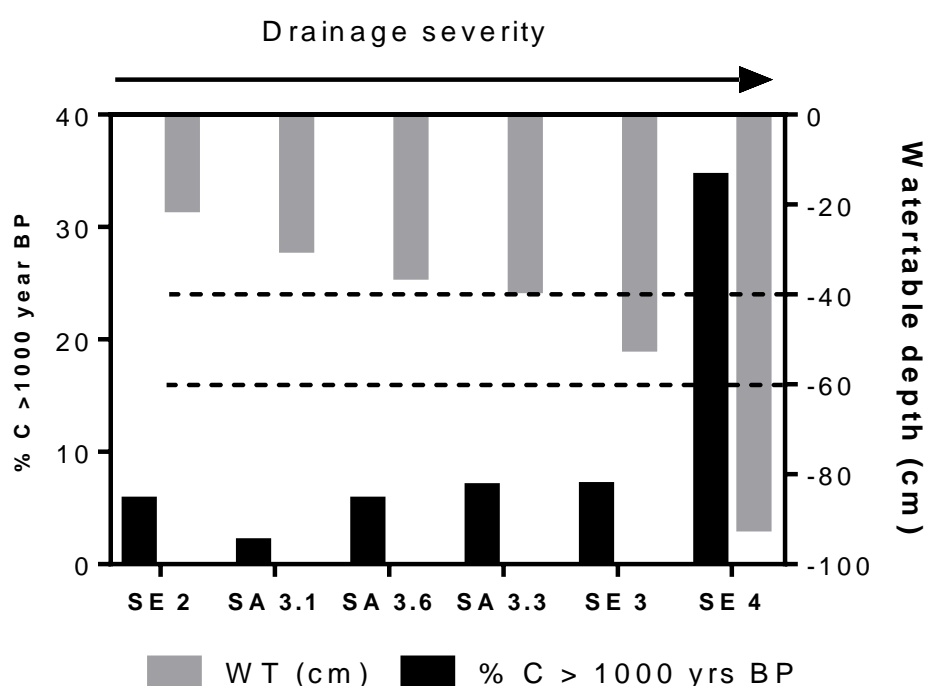


Figure 6.3 Comparison of mean watertable depth across the radiocarbon dated sites with the % of carbon greater than 1000 years (BP), as constructed from the age attribution model. Dashed lines indicate the RSPO watertable guidelines for OPP.

Dommain et al. (2011) report basal peat initiation dates and accumulation rates across Southeast Asia peatlands, with basal ages from the Baram river area,

Sarawak (~200 km from Bintulu), ranging from 3,864 to 4,819 years BP. This results in a mean basal peat age of ~4,300 years with an average peat accumulation rate of 1.77 mm yr⁻¹ (Dommain et al., 2011). Assuming a comparable rate of peat accumulation across the Sebungan and Sabaju study sites, an estimate of DOC source depth was calculated based on the DOC ages formulated from the age attribution model (Table 6.1). An assumption that recently fixed carbon occurred at the peat surface and that DOC age increased down the peat profile was also made. Some sites (i.e. SE 2) displayed similar DOC source depths in relation to maximum watertable drawdown, with the majority of sites (i.e. SA 3.1, 3.3, 3.6 etc.) showing estimated DOC sources above the maximum water level (Table 6.1). This is logical considering this is where the majority of aerobic decomposition will be taking place. By contrast, the estimated DOC source for site SE 4 is from much further down the peat column (i.e. 32 cm below the lowest watertable; Table 6.1). This is suggestive of deeper carbon instability within the peat profile and perhaps represents a legacy effect of previous, much deeper, watertables (Fenner & Freeman, 2011). This is reinforced by Bonnett et al. (2017) who report biochemical changes relating to the activity of phenol oxidase enzyme in a temperate peat site with a history of low watertables. The enzyme remained activated even under re-established anaerobic conditions (Fenner & Freeman, 2011). As such, more phenolic compounds (which inhibit microbial activity) were broken down, thereby increasing microbial growth, which led to increases in organic matter degradation and associated carbon release. As a result, accelerated carbon losses were reported in response to contemporary rewetting and higher watertables (Fenner & Freeman, 2011).

Table 6.1 Estimated depth of DOC source (cm), alongside maximum watertable drawdown, for the dated samples. Where +/- number represent a DOC source from higher/lower down the peat column, relative to the maximum watertable.

Site	Age estimated of DOC from Age Attribution model	Accumulation rate/year (cm)	Estimated depth of DOC source (below peat surface, cm)	Maximum watertable drawdown (below peat surface, cm)	Difference between estimated DOC source depth and maximum watertable depth (cm)	% of time the watertable was below – 60 cm
SE 2	351	0.177	62	58	-4	0 %
SE 3	377		67	89	+22	27 %
SE 4	904		160	128	-32	100 %
SA 3.1	255		45	56	+11	0 %
SA 3.3	274		66	82	+16	21 %
SA 3.6	246		44	72	+28	3 %

A new technique enabling water samples to be analysed using Thermal Desorption-Proton Transfer-Mass Spectrometry (TD-PTR-MS) was developed by Materic et al. (2017) and run on a small number of samples from the OPP sites (SE and SA 4) and forest (FA) sites. A copy of the resulting publication is provided in Appendix E. A principal component analysis (PCA) revealed that over 200 organic ions were present within the samples with a clear separation and clustering of samples from the OPP and PSF landcover classes (Figure 6.4). In general, the plantation samples displayed a higher contribution of semi-volatile DOC, relative to the total DOC concentration (Figure 6.5). In addition, a small number (n=2) of highly volatile compound signatures (i.e. m/z 63.024 and 81.036) were identified within the plantation data set, indicative of compounds from an anthropogenic origin and potentially connected with soil management alterations (Materic et al., 2017).

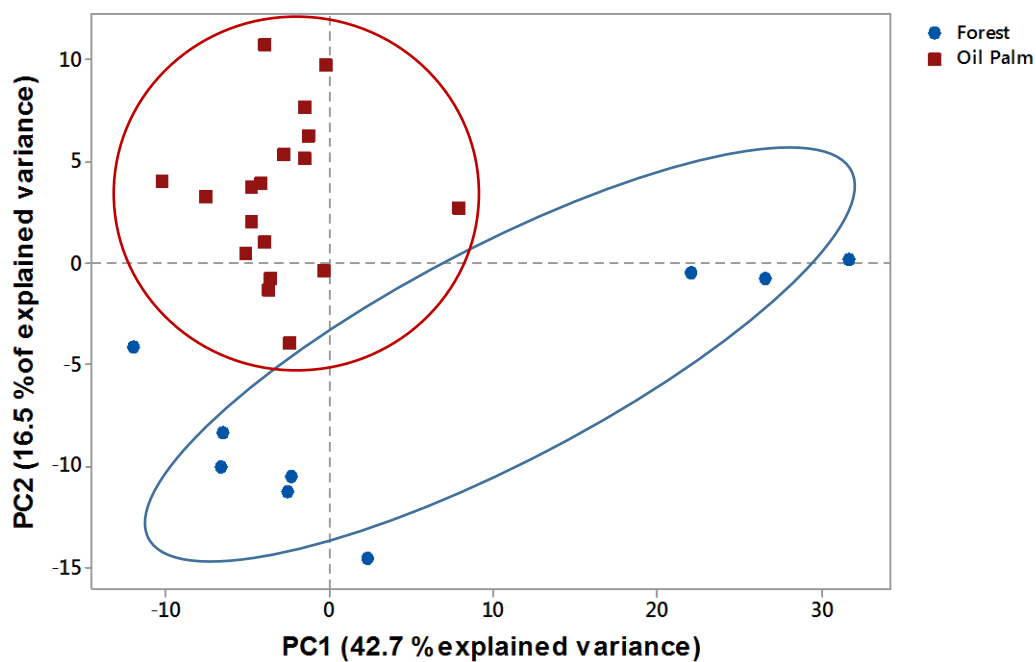


Figure 6.4 Principal component analysis from TD-PTR-MS for the forest and oil palm plantation samples.

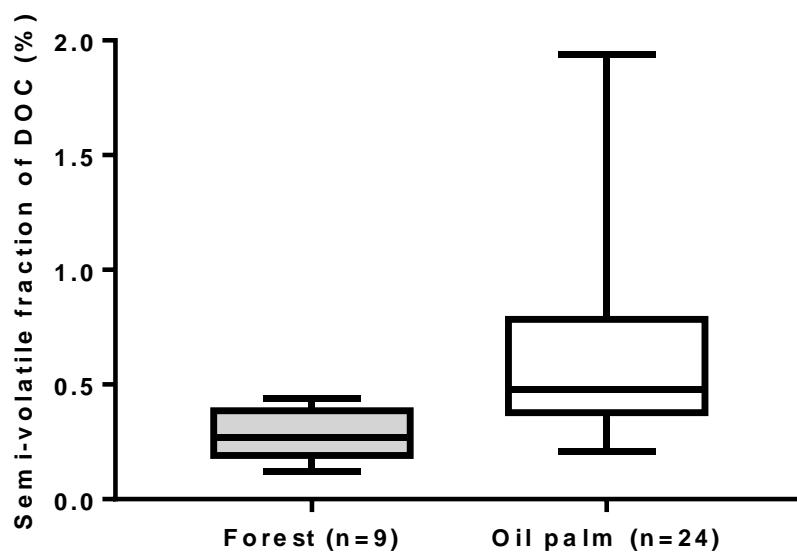


Figure 6.5 Boxplots of the fraction of semi-volatile (%) DOC normalised to the total DOC concentration. Horizontal lines; central = mean, upper = maximum and lower = minimum; Box = 75th and 25th percentiles.

Using the results of the TD-PTR-MS analysis the number of C, H, O and N atoms were analysed. From this, the mean oxidative state of the carbon (OS_C) and average number of carbon atoms per sample (n_C) were calculated, giving

a greater qualitative insight into the chemical processes driving the DOC composition (visualised in Figure 6.6). From these data it was apparent that the plantation samples were dominated by hydration/condensation reactions (i.e. gains and losses in water molecules affect both the O/C and H/C; Figure 6.6 a) whereas the forest samples were dominated by oxidation/reduction reactions (i.e. gains and losses in water only affected O/C). It is also worth drawing attention to the higher oxidative state of the plantation DOC samples (Figure 6.6 b) which suggests that the DOC is closer to being fully mineralised into CO₂. This reinforces the qualitative data presented in Chapter Five (Figure 5.8) showing that the plantation samples had a higher degree of carbon bioavailability. This, coupled with the radiocarbon data (Figure 6.3), suggests the potential mobilization of ancient carbon stores.

The effect of the depth of the watertable on DOC processes was also hypothesised by Materic et al. (2017). Three anomalous forest samples with high oxidative states were observed (Figure 6.6), corresponding to a sampling period following several months of drought (i.e. watertables below – 40 cm) and rapid rewetting (watertable – 13 cm). Materic et al. (2017) hypothesize that these anomalous data could reflect water stresses leading to changes in the oxidative state of the carbon. Overall, the conclusions drawn from this analysis suggest that the conversion of PSF to OPP could be causing distinct changes to occur in both the composition of the DOC and the underlying chemical processes governing its production. This directly supports the findings from Chapter Five which demonstrate differences in the carbon quality across the PSF conversion gradient. Overall, these results are suggestive of instability within the peat column, leading to the loss of long-term stable carbon stores in response to OPP conversion. The results also support the need for regulated watertable management in line with RSPO guidance.

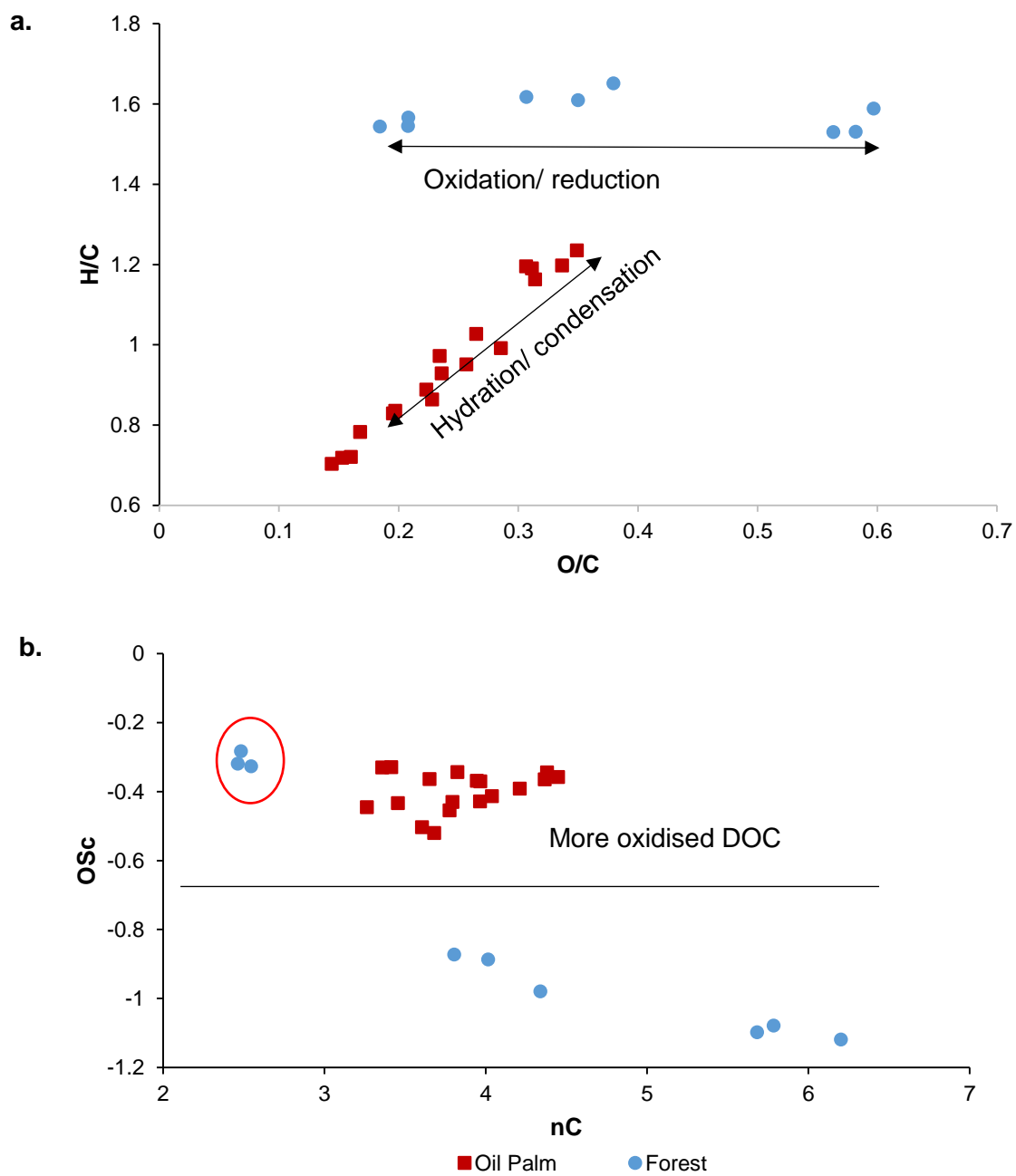


Figure 6.6 Van Krevelen plots displaying the **(a)** atomic ratio of O/C and H/C and **(b)** number of carbon atoms (nC) and oxidative carbon state (OSc) for the individual plantation and forest DOC samples. Red circle indicates three anomalous forest samples (see text above for further detail).

Materic et al. (2017) also include data from a selectively logged (KI) and extensively drained (KD) forest fragments in Kalimantan, Indonesia. While both the OPP and KD sites had been subjected to similar degradation regimes (e.g. both were extensively drained) they exhibit different biochemical characteristics. For example, the highly volatile compounds present within the oil palm sites were notably absent within the KD data set (Figure 6.7). While this could reflect the differences in geographical origin (i.e. North versus South Borneo) it could also be an outcome of differences in management (i.e. controlled drainage in the OPPs versus uncontrolled drainage in KD). Taken together, this conclusion further reinforces the concept that deforestation and drainage (i.e. PSF conversion to OPP) could bring about unique changes in the biochemical properties of DOC.

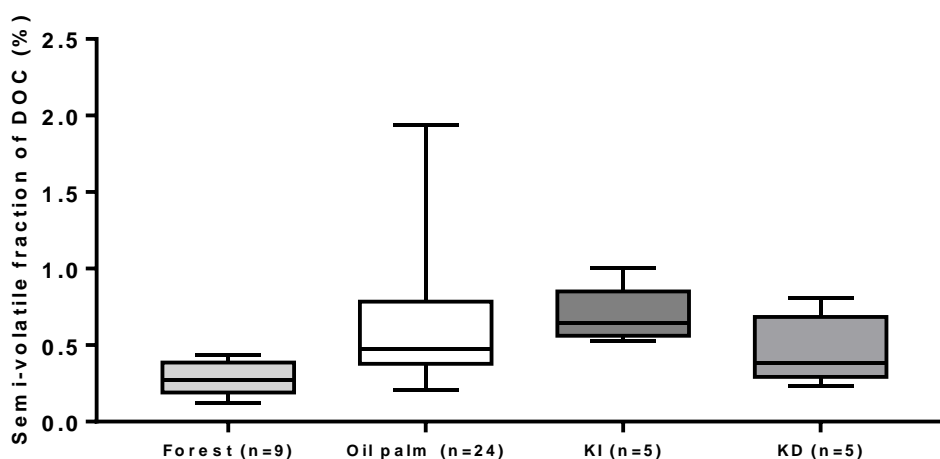


Figure 6.7 Boxplots of the fraction of semi-volatile (%) DOC normalised to the total DOC concentration for the Sarawak forest site and oil palm plantations, alongside the selectively logged (KI) and extensively drained (KD) Kalimantan sites. Horizontal lines; central = mean, upper = maximum and lower = minimum; Box = 75th and 25th percentiles.

The combination of the qualitative and quantitative data, alongside the watertable data, suggests that watertable plays a strong role in governing the fluvial organic carbon dynamics within the plantation landscape (Figure 6.8). Severe drought and sudden rewetting can destabilise carbon stocks. This is supported by the extreme watertable variability experienced within the SE estate (i.e. ranging between +5 to -128 cm over a period of 12 months) along with the higher overall TOC concentrations and fluxes reported from this site. Watertable variability may also influence carbon dynamics within the forest sites (FA and FB); while FA exhibited a higher overall watertable (mean -32.7 cm; range -66 cm to -5.3 cm), in comparison to FB (mean -75.7 cm; range -109.3 to -52 cm), it was more hydrologically dynamic which could have contributed to overall higher TOC concentrations and fluxes. The data also suggest that extreme watertable fluctuations can, in turn, lead to the release of aged carbon from deep down in the peat profile, which may be exacerbated in systems with a legacy of low watertables (i.e. SE 4). This can alter how microbial and enzymatic activity (i.e. phenol oxidase) responds to contemporary hydrological regimes (Bonnett et al., 2017). These alterations in DOC in response to watertables are also supported by the anomalous forest site data presented in Materic et al. (2017) with lower watertables leading to a higher oxidative state for DOC carbon. Taken together, these data suggest that regulation of high watertables within peatland OPPs should be paramount, with potential implications for carbon cycling and the loss of historically stored carbon – i.e. watertables should be kept as close to the peat surface as possible with minimal seasonal variation. This presents challenges for plantation management, since current oil palm cultivars grow best in a watertable range of 60 – 80 cm (Lim et al., 2012) and are less productive at higher watertables (Veloo et al., 2015). In addition, high watertables may limit on-site access, particularly during the wet season. Conversely maintaining high water tables during the dry season may be problematic since rainfall is the only source of water input to the peat surface on plantations where the entire peat dome has been converted.

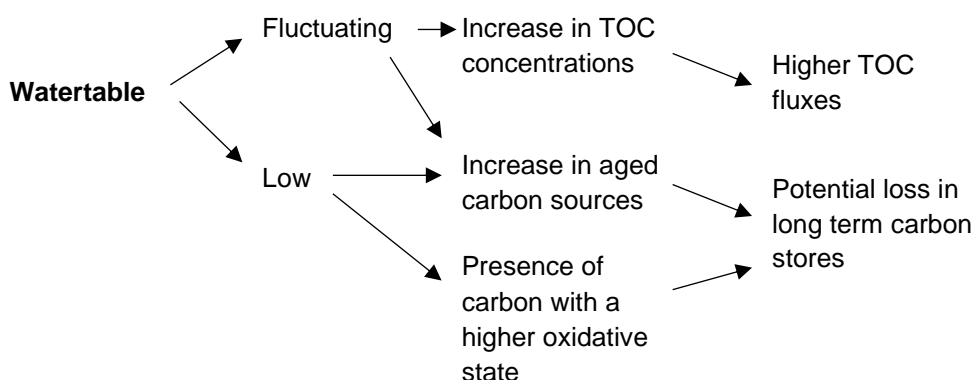


Figure 6.8 Schematic diagram to illustrate the role of the watertable in governing fluvial organic carbon dynamics within a peatland oil palm plantation

6.3 The Sebungan and Sabaju estates within a global context

Sampling campaigns across the plantation estates during the wet and dry seasons produced an estimated annual TOC export of $104 \text{ g C m}^{-2} \text{ yr}^{-1}$. The estates range in area from 1638 ha (SA 4) to 2526 ha (SA 1) covering a collective peatland area of 7526 ha. Taking the average annual TOC flux from the estate main drains and upscaling to represent the entire estates, results in annual TOC fluxes of 1.5×10^{-03} (SA 3) to 2.4×10^{-03} (SE) Tg C yr^{-1} (Table 6.2). This cumulatively results in an entire TOC flux for the sampled plantation area of $7.7 \times 10^{-03} \text{ Tg C yr}^{-1}$, with ~90% of this flux exclusively derived from DOC ($7.0 \times 10^{-03} \text{ Tg C yr}^{-1}$).

Table 6.2 Estimated fluvial organic carbon fluxes for the plantation estates based on the main drain TOC flux and total plantation area

Estate	Size (ha)	m^2	Main drain TOC flux ($\text{g C m}^{-2} \text{ yr}^{-1}$)	Plantation TOC flux (Tg C yr^{-1})	Plantation DOC flux (Tg C yr^{-1})
SE	1648	1.6×10^7	128.8	2.1×10^{-3}	2.0×10^{-3}
SA 1	2526	2.5×10^7	94.3	2.4×10^{-3}	2.1×10^{-3}
SA 3	1714	1.7×10^7	88.6	1.5×10^{-3}	1.3×10^{-3}
SA 4	1638	1.6×10^7	103.2	1.7×10^{-3}	1.6×10^{-3}
Totals	7526	7.5×10^7		7.7×10^{-3}	7.0×10^{-3}

Peatland coverage within Sarawak is estimated at 1,697,847 ha, with approximately 46% (as of 2016) of this peatland area dominated by OPP (~7810 km²; Wetlands International, 2016). Taking the average OPP TOC flux (104 g C m⁻² yr⁻¹) and extrapolating this to the total area of Sarawak peatland under OPP (7810 km²; Wetlands International, 2016), results in a yearly TOC flux of just under 1 Tg C yr⁻¹ (0.8 Tg C yr⁻¹) with a DOC flux of 0.7 Tg C yr⁻¹ (Table 6.3). These figures are comparable to the flux from a tropical blackwater river catchment (Sebangau, Indonesia) reported by Moore et al. (2011), with a TOC flux of 0.46 Tg C yr⁻¹ for a similar magnitude catchment size (5200 km²). Future projections suggest that by the year 2020, 84% (~14,262 km²) of Sarawak's peatland area will be under oil palm (Miettinen et al., 2012 b). This would result in a TOC flux of 1.5 Tg C yr⁻¹ (Table 6.3) with 1.4 Tg C yr⁻¹ derived exclusively from DOC. Placing this in a global context, Ludwig et al. (1996) estimate that 90.2 Tg C yr⁻¹ of DOC is derived from rivers within the tropical climate zone (TCZ; 23,633,00 km²). Based on the derived Sarawak OPP flux value above, this suggests that nearly 1% of the TCZ's total DOC flux is derived exclusively from the current peatland OPP area within Sarawak (7810 km²), increasing to a possible 1.6% contribution by the year 2020 (Table 6.3).

Table 6.3 Predicted future OPP expansion in Sarawak and associated TOC flux estimates

Sarawak total area under peat OPP	Size (ha)	Km²	Average main drain TOC flux (g C m⁻² yr⁻¹)	TOC flux (Tg C yr⁻¹)	DOC flux (Tg C yr⁻¹)
2016	781,009	7.8 x 10 ³	104	0.8	0.7
2020	1,426,191	14.3 x 10 ³		1.5	1.4

Wit et al. (2015) conservatively estimate that ~53% of leached organic carbon from tropical peat, is decomposed and emitted as atmospheric CO₂, as a result of photo and biological degradation. This is based on monthly measured CO₂ and DOC fluxes from six rivers across Malaysia and Indonesia, including two

catchments within Sarawak. Wit et al. (2015) estimate total riverine CO₂ fluxes from Malaysia and Southeast Asia at 6.2 Tg C yr⁻¹ and 66.9 Tg C yr⁻¹, respectively. Applying their outgassing estimate of 53% to the total OPP DOC flux (0.7 Tg C yr⁻¹) for Sarawak results in a DOC-CO₂ flux of 0.4 Tg C yr⁻¹ (Table 6.4). This represents 6% and 0.6% of the entire riverine CO₂ flux from Malaysia (6.2 Tg C yr⁻¹) and Southeast Asia (66.9 Tg C yr⁻¹), respectively (Table 6.4; Wit et al., 2015). However, considering predicted OPP expansion within Sarawak, by the year 2020 the future DOC-CO₂ flux could be contributing to 11% and 1% of this share, respectively (Table 6.4).

Table 6.4 Impact of Sarawak peatland OPPs on river outgassing, assuming 53% of DOC is decomposed and emitted as CO₂ into the atmosphere.

Location	Land-cover type	Area (Km ²)	DOC flux (Tg C yr ⁻¹)	DOC-CO ₂ flux (Tg C yr ⁻¹)	% contribution of Sarawak peatland OPPs to riverine CO ₂ flux in:	
					Malaysia	Southeast Asia
Sarawak						
2016	peatland OPP	7.8 x 10 ³	0.7	0.4	6.5	0.6
2020		14.3 x 10 ³	1.4	0.7	11.3	1.0

Moore et al. (2013) conservatively estimate total annual TOC fluxes from both remaining intact and degraded PSF areas in Peninsular Malaysia, Borneo and Sumatra, at 6.8 Tg C yr⁻¹, based on land cover area estimates from the year 2008. However, these estimates do not account for industrial peatland OPPs, which, in 2008, covered 2.3 Mha in this same geographical region (Miettinen et al., 2016). Combining this land cover area value with our mean OPP TOC flux (104 g C m⁻² yr⁻¹) results in a total TOC flux of 2.4 Tg C yr⁻¹ (Table 6.5). This, combined with the TOC flux for the remaining intact and degraded PSF areas estimated by Moore et al. (2013), elevates the annual TOC flux for this region by approximately one third to 9.2 Tg C yr⁻¹ (6.8 + 2.4 Tg C yr⁻¹). This

figure is more than twice the annual TOC flux for all peatland areas in Europe (4.3 Tg C yr⁻¹; Moore et al., 2013).

Table 6.5 Regional annual TOC fluxes for all peatland area covered by OPPs within Peninsular Malaysia, Borneo and Sumatra. Area estimates are taken from Miettinen et al., (2016) for the year 2008.

	Area (Mha)	Area (Km ²)	Mean TOC flux (g C m ⁻² yr ⁻¹)	Total TOC flux (Tg C yr ⁻¹)
Industrial OPP plantations on peat in 2008	2.3	23,000	104	2.4

However, land-use change within this region has progressed since the research by Moore et al. (2013) was conducted. This is supported by Miettinen et al. (2016) who provide updated land cover data for Peninsular Malaysia, Borneo and Sumatra, for the year 2015 (Table 6.6), with a 36% decrease in pristine PSF area occurring between the two studies (i.e. Moore et al. 2013; 15,600 km²; Miettinen et al. 2016; 9,960 km²; Table 6.6). Industrial peatland plantations have also increased in area and, in 2015, covered 4.3 Mha, with 73% of this under OPP (3.1 Mha; Miettinen et al., 2016). Taking these more recent land cover data into consideration and combining them with the TOC fluxes reported by Moore et al. (2013) for degraded and intact PSFs, along with the OPP values from this investigation, results in an overall TOC flux from this region of 10.4 Tg C yr⁻¹ (Table 6.7), with over a quarter of this (30%; 3.2 Tg C yr⁻¹) derived from industrial peatland OPPs.

Table 6.6. Peatland land cover estimates by Miettinen et al. (2016) and Moore et al. (2013), across Peninsular Malaysia, Borneo and Sumatra, for the years 2015 and 2008, respectively.

Land-cover	Peatland area in km ²	Peatland area in km ²
	(2015)	(2008)
Degraded PSF	68,423	60,205
Smallholder plantation	35,104	
Industrial plantation	42,861 (all)	
Oil palm	31,000	
Other (i.e. pulpwood)	11,861	
Intact PSF	9,960	15,600

Table 6.7 TOC flux estimates from PSF areas accounting for industrial oil palm plantations across Peninsular Malaysia, Borneo and Sumatra, for the year 2015. Area estimates are taken from Miettinen et al. (2016).

Landcover		TOC flux (g C m ⁻² yr ⁻¹)	Area (km ²)	Regional TOC flux Tg C yr ⁻¹
Plantation	Industrial oil palm plantations	104*	31,000	3.2
Forest	Degraded PSF	97**	68,423	6.6
	Pristine PSF	63**	9,960	0.6
				10.4

* TOC fluxes are taken from this investigation; average main drain OPP flux. **TOC fluxes are taken from Moore et al. (2013) for an intact (63 g C m⁻² yr⁻¹) and degraded PSF (97 g C m⁻² yr⁻¹)

The data sets presented so far do not account for TOC fluxes from smallholder (SMH) peatland OPPs. While TOC fluxes from SMH OPPs are yet to be quantified, the watertable levels are likely to be poorly controlled, given financial and labour constraints, and may therefore be similar to those found within the SE plantation. Consequently, the main drain TOC flux from SE (129 g C m⁻² yr⁻¹) may be considered to provide a good proxy for a SMH peatland OPP. Recent figures for peatland SMH land coverage are 3.5 Mha for Peninsular Malaysia, Borneo and Sumatra (Miettinen et al., 2016) with this area expected to continue to grow in coming years in both Malaysia and Indonesia (MPOB, 2012; Daemeter Consulting, 2015). Assuming, that 50% of this land is under oil palm gives a conservative TOC flux of 2.3 Tg C yr⁻¹ from SMH peatland OPPs (Table 6.8). This takes the regional TOC flux up to 12.7

Tg C yr⁻¹ which represents a potential threefold increase in fluvial TOC fluxes since 1990 (4.7 Tg C yr⁻¹; Moore et al., 2013) from this region.

Table 6.8 TOC flux estimates from all degraded PSF areas accounting for all industrial peatland plantations across Peninsular Malaysia, Borneo and Sumatra, for the year 2015.

Landcover		TOC flux	Area (km ²)	Tg C yr ⁻¹
Oil palm plantation	Industrial	104	31,000	3.2
	Smallholder	129	15,700	2.3
Forest	Degraded PSF	97	68,423	6.6
	Pristine PSF	63	9,960	0.6
				12.7

The total ‘best-estimate’ peat carbon emissions for this plantation study area and for Peninsular Malaysia, Borneo and Sumatra are presented in Tables 6.9 and Table 6.10, respectively. Fluvial carbon emissions make up approximately 16% of the total peat-carbon emission, from the Sabaju and Sebungan OPPs, with the largest emission (84%) derived from peat oxidation (Table 6.9; personal communication, Manning, F, 2017). From a regional perspective, peat oxidation makes up the greatest contribution to total peat-carbon emissions (51%; 146 Tg C yr⁻¹), followed by peat fires (43%; 122 Tg C yr⁻¹; Table 6.10) (Miettinen et al., 2017). The data from this study helps to complete Table 6.10, with fluvial carbon emissions making up approximately 4% of total peatland emissions and 6% of emissions from peat oxidation. It is, however, important to note that peat fires are not an annual occurrence and cause temporary emission peaks, whereas peat oxidation and TOC losses occur annually. Nevertheless, peat fires have attracted a high-degree of recent attention, particularly since the devastating impacts of the 2015 fire season (Konecny et al., 2015; Page and Hooijer, 2016; Huijknen et al., 2016; Miettinen et al., 2017), with the annual carbon emissions (fires + peat oxidation) from this year estimated at 289 Tg C yr⁻¹ (Huijknen et al., 2016) to 341 Tg C yr⁻¹ (Miettinen et al., 2017). In addition, burnt peatlands are an additional source of POC and DOC, particularly during the immediate post fire period (Moore et al., in prep.). Moore et al. (in prep) report a 32% increase in TOC fluxes from

deforested Indonesian peatlands, following the 2009 El Nino fires, over a 25 week period. This was attributable to changes in the hydrological regime leading to less evapotranspiration and increased DOC runoff. In comparison the intact forests remained resilient to the fires with no significant change in fluvial carbon export (0.8%) over the same period (Moore et al., in prep).

Table 6.9 Total carbon emissions for the Sebungan and Sabaju oil palm plantations

Carbon source	Emissions (Tg C yr ⁻¹)	% of total emissions
Peat oxidation*	4.0 x 10 ⁻²	84
Fluvial**	7.7 x 10 ⁻³	16
Total	4.8 x 10⁻²	

*peat oxidation rate of 5.32 Mg C yr⁻¹ was used (Manning, F, 2017, personal communication) for a total plantation size of 7526 ha. ** Fluvial carbon emissions are taken from Table 6.2

Table 6.10 Total carbon emissions from peatlands within Peninsular Malaysia, Borneo and Sumatra

Carbon source	Emissions (Tg C yr ⁻¹)	% of total emissions with/without fire
Peat oxidation	146.0*	51/90
Fires	122.0*	43
Fluvial	10.4	4/6
Total (with fire)	283.6	
Total (without fire)	161.6	

*Data taken from Miettinen et al., (2017)

6.4 Limitations and future research recommendations

6.4.1 TOC fluxes

This investigation has highlighted the challenges of conducting research within managed landscapes, specifically contending with the changing plantation hydrology in response to management efforts (i.e. channel blocking and rerouting). While this made determining area-specific TOC fluxes problematic, it created guidance for further plantation studies of this nature. However, the

resulting fluxes were subject to considerable uncertainties in (i) DOC concentration (C_i); (ii) the mean annual runoff (R_E) and (iii) channel discharge at the time of sampling (Q_i). To address this a sensitivity analysis could be undertaken using a Monte Carlo Simulation approach. Briefly, values for each variable could be selected randomly from probability density functions (pdf's) and run in a large number ($n= 5000$) of iterations. In all cases Gaussian pdf's would be used based on the assumption that the estimate of a statistic is normally distributed about the true value (central limit theorem) with the best-estimate value assumed for the mean and the standard error of the estimate (SEE) assumed for the standard deviation. The following variables could be sampled from their pdf's in calculating flux uncertainty for each plantation area: C_i , Q_i and R_E . The SEE for R_E could be derived by applying Equation (6.1) for site SE 1 in a Monte Carlo simulation in which SEE for A was assumed to be 10% of the best estimate and the SEE for each value of Q_h was derived from the SEE of Q in a linear regression fitted to the rating curve for this station.

$$R_E = \frac{Q_A}{A} = \frac{\sum_h^T Q_h}{A} \quad (6.1)$$

where Q_A is the measured mean annual discharge ($\text{m}^3 \text{yr}^{-1}$) estimated as the sum of hourly discharge h (Q_h ; $\text{m}^3 \text{h}^{-1}$) over T hours in a year and A is a known catchment area (m^2).

This would apply for estimates of Q_i in Equation (2.18, Chapter 2). For C_i , the SEE could be derived from the approach described by Waldron et al. (2014; Chapter 3B) for estimating uncertainties in DOC concentrations when using the approach adopted here (Cook et al., 2017). Furthermore, the relationship identified between the age of the exported DOC and watertable is also subject to uncertainty, given the reliance on effectively a single date for this interpretation. To address this more water samples would need to be dated across a broader range of watertable depths.

The forest TOC concentrations were derived from water samples extracted from dipwells, which acted as 'pseudo ditches' in the absence of clear discharge outlets. To test how representative the dipwell water replicated ditch water 22 water samples were extracted from the dipwells within the plantation and compared with the water from the plantation drains (Appendix G). All dipwell derived water exhibited a higher DOC concentration compared to their drainage water counterparts by an average of 5 mg L⁻¹. While this difference was not statistically significant (*t-test*, $p > 0.05$) it is likely that forest DOC concentrations, and therefore fluxes, are potentially greater than the values reported.

6.4.2 TOC upscaling

Up-scaling of the plantation TOC fluxes lends itself to a number of inherent limitations, this includes the assumption that the fluxes reported for this study are indicative of i) all OPPs across Southeast Asia and ii) all plantation sectors (smallholder vs large, industrial-scale). Firstly, the TOC data set for this study was obtained from four OPP estates in a small area of Sarawak Malaysia, and is thus unlikely to be representative of all peatland OPPs across Southeast Asia. In addition, while the management efforts within these four OPP estates were typical of those across Southeast Asia there will inevitably be variability across the board. For completeness of analysis, and to improve the reliability of up-scaling, continued collection of fluvial carbon data should be encouraged across different i) regions, ii) OPP ages, iii) plantation types and iv) plantation sectors.

6.4.3 Drivers of TOC variability

An extended temporal study (i.e. over at least a 3-year period) would help in building a fuller picture of the temporal dynamics of fluvial organic carbon within peatland OPPs. Longer timescales would permit the inclusion of stochastic climatic events, including the El Niño and La Niña. This, combined with the use of automatic water-samplers or deployment of *in-situ* UV

photometric sensors (Sandford et al. 2013), could help to generate high temporal resolution DOC data. This would enable pattern recognition and therefore the identification of potential drivers of DOC fluxes to be made, contributing to an improved understanding of peat carbon storage and export. Building on the concept of improved temporal data generation, absolute pressure water level loggers (i.e. Mini-Divers, Schlumberger, D1501), could be installed within the dipwells to continuously monitor fluctuations in watertable level. This, along with the use of automatic *in-situ* water samplers, could help in addressing the link between watertable depth and TOC export, which was not fully identified within this study.

The opportunity to sample from an area undergoing the initial stages of plantation development (R-DF) presented itself within this investigation. However, it would be of interest to continuously sample across the conversion gradient, capturing the initial stages of forest clearance (i.e. within the first few hours or days), through to plantation development and establishment. This would entail maintaining close communication with the plantation company to ensure sampling efforts captured specific conversion and development milestones i.e. undisturbed forest stand, initial forest clearance, stacking, initial drainage, and drain installation. In addition, continued data collection from peatland OPPs across different geographical locations and estates is paramount. This will help account for different climates and management regimes as well as adding to the limited amount of carbon data from this form of land-use change.

Significant differences in the quality and composition of TOC within the SE plantation compared with the other plantation blocks was observed during this study. One explanation for these differences could originate from the difference in land preparation prior to plantation development, with greater peat surface compaction taking place within SE. This has resulted in morphological differences, in the peat structure, between the two estates with a much higher bulk density (0.2 g cm^{-3}) within SE (Appendix A). These different land preparation methods could be responsible for the observed differences in TOC fluxes, (i.e. the TOC flux was greater from the more compacted peat site)

but more data would be necessary to confirm this observation. Peat compaction is undertaken in order to improve the rooting stability of palms and to help machinery move across the peat during harvesting (Melling & Henson, 2011). But the results presented here indicate that an unforeseen consequence may be a higher TOC flux.

Carbon losses from tropical peatlands are considered to be very high during the first five years following conversion (Hooijer et al. 2012; 2014). While this research did incorporate plantation estates of different age ranges, the two immature plantations sat outside this period of time (i.e. 6 years since development). Consequently, undertaking similar research on very young plantations (i.e. 1-3 years since conversion) in conjunction with studies of the scale of carbon loss occurring immediately following deforestation and drainage (as discussed above) could help to reveal differences in fluvial carbon fluxes at different stages of the plantation conversion cycle. Furthermore, all the estates investigated in this study were close in age (6 years versus 9 years) which may further explain why significant differences in plantation age were not uncovered within this study. In addition to very young plantations, it would also be of interest to extend the land conversion gradient to the other end of the plantation rotation and to collect data from much older OPPs which are coming to the end of their 25-year lifecycle. This would help to identify whether there are any differences in fluvial carbon dynamics across the full lifecycle of peatland OPPs.

6.4.4 The fate of DOC

Spectrophotometric techniques, including SUVA₂₅₄, were used to determine the potential fate of fluvial organic carbon within the context of a peatland OPP landscape. However, the ultimate fate of the DOC is reliant on the presence of particular microbial communities for the degradation of DOC into its metabolic components, without which even highly labile DOC will remain climatically neutral. Subsequently, an in-depth study of the microbial communities present

would be necessary to ascertain the true bioavailability of the DOC pool. This could be expanded to incorporate diurnal variations in both microbial assemblages and carbon concentrations, as well as the influence of photochemical oxidation.

The use of spectrophotometric data revealed that there were differences in the DOC composition between the plantation main and collection drains which suggested that *in-situ* DOC processing maybe occurring as the DOC moves from the collection drains to the main drains. However, an implication of significant processing of DOC across small spatial scales in the fluvial system is that comparisons of DOC status and fluxes between sites become more involved. For example, studies which collect water from further upstream may have higher resulting fluxes, as less DOC has had time to degrade, in comparison to samples collected further downstream. As such, it is essential that the uncertainty surrounding the fate of DOC is addressed and that is this acknowledged when interpreting data from different studies.

6.4.5 Forest buffer zones

More work is needed regarding the peatland edge/riparian zones within plantation landscapes. A key area to focus on is variability in watertable depth, as highlighted within this study, which is likely to influence both abiotic and biotic factors. Data presented in this study suggests that in some instances conserving larger areas of PSF, away from the OPP, would be more favourable than preserving small degraded forest patches. However, these areas may act as important biodiversity refuges and wildlife corridors, facilitating species movement across plantations. More data on the species diversity of these areas would contribute to a holistic assessment of the ecological value of these areas, enabling a more informed decision to be made concerning their maintenance.

6.4.6 Smallholder oil palm plantations

Over 50 % (7.8 million ha) of the remaining peatland areas within Peninsular Malaysia, Borneo and Sumatra are considered 'managed land'. Of this, 22.4 % is dominated by SMH plantations (Miettinen et al. 2016). Rapid expansion of SMH OPPs is imminent; between 2000 – 2009, SMH OPPs grew by approximately 11% within Indonesia alone, far exceeding growth rates of private companies (5.45 %) and government estates (0.37 %; Lee et al. 2014). Subsequently, while the exploitation and conversion of PSF to OPP has been largely dominated up until now by commercial sectors, this is changing, with the short-term economic needs of SMH communities playing an increasing role in this conversion. This was particularly evident during my time sampling within Sarawak, with many SMH plantations becoming established around the edges of the Sabaju and Sebungan estates. The dominance of peat within the coastal region of Sarawak, coupled with an otherwise hilly topography further inland which is less favourable for OPP, is forcing peat cultivation, which is seen as an 'easier' and more affordable alternative to terracing mineral soil. However, peat cultivation brings with it a unique set of challenges, a key issue being effective watertable management. Subsequently, SMHs cultivating peat represent a particularly vulnerable group, whose actions have both local consequences (i.e. increased local poverty, local deforestation) but also global ramifications (i.e. enhanced GHG emissions).

While the extent of SMH plantations across Southeast Asia is challenging to determine and, thus, remains largely unknown (Miettinen et al. 2017), the combined area of peat under SMH plantations will soon match that of industrial estates, making their presence significant. This is reinforced by Miettinen et al. (2017) who quantify the emissions arising from peat oxidation within Peninsular Malaysia, Borneo and Sumatra. They estimate that 44 % (64.3 Mt C yr⁻¹) of a total emission of 146 Mt C yr⁻¹ is derived from industrial plantations with a further 33 % (49.2 Mt C yr⁻¹) from SMH plantations. However, the estimate for SMH plantations could be as high as 52.7 Mt C yr⁻¹ if the IPCC

general emission factor for industrial plantations (non-crop specific) of 15 (t C ha⁻¹ yr⁻¹) is applied, making them comparable to large industrial estates.

At present, an accurate understanding of the peatland carbon budget within SMH plantations is lacking, with no available data on fluvial carbon emissions. While a single SMH (<10 ha) plantation is considerably smaller than that of an industrial estate (1,000+ ha), the management within SMH estates is likely poor, with many SMH farmers lacking agricultural knowledge relevant to peat. This, combined with their increasing numbers within Southeast Asia (Miettinen et al., 2016) could make the combined TOC flux from SMH areas just as significant as that from industrial estates.

6.5 Summary and overall conclusions

- Tropical DOC samples can be stored and analysed in remote field locations, with limited laboratory facilities, using inexpensive and robust methods.
- TOC concentrations varied across the PSF conversion gradient and responded positively to initial deforestation and drainage, with the DOC component accounting for >80% of the TOC concentration from all sites.
- The SE plantation exhibited significantly higher TOC concentrations and fluxes in comparison to the SA estates, irrespective of drain type (i.e. SE TOC fluxes range: 128.1 to 134.0 g C m⁻² yr⁻¹; SA flux range: 88.6 to 105.3 g C m⁻² yr⁻¹). This was attributed to greater peat compaction prior to development and more variable watertable levels.
- Forest reserves within peatland OPP landscapes are not hydrologically distinct which, without proper management, can lead to

lower watertables (i.e. FB = -75.7 cm) and higher TOC fluxes (71.2 to 84.5 g C m⁻² yr⁻¹) than expected, making them comparable to OPPs.

- The watertable strongly controls the fluvial carbon dynamics within a peatland OPP, with drought followed by sudden re-wetting increasing both the loss and age of DOC. This has important implications for peatland plantation management and emphasizes the need to follow RSPO watertable management standards.
- Qualitative analysis revealed differences in carbon bioavailability across the PSF conversion gradient. Consistently lower SUVA₂₅₄ and % aromaticity values were exhibited by the plantation collection drains, in comparison to the main drains, suggestive of the presence of more labile carbon compounds. This finding, coupled with the higher collection drain TOC fluxes (i.e. collection = 109 g C m⁻² yr⁻¹; main = 104 g C m⁻² yr⁻¹) suggests in-situ DOC processing is occurring within the collection drains, leading to the loss of ~ 5 g C m⁻² yr⁻¹ in the time taken for carbon to reach the main drain systems.
- The inclusion of the plantation TOC flux (104 g C m⁻² yr⁻¹) completes the carbon balance from peatland OPPs increasing NEE from 1,100 g C m⁻² yr⁻¹ to 1,204 g C m⁻² yr⁻¹ representing a 10% increase in carbon lost than previously estimated using gaseous carbon measurements.
- Extrapolation of the peatland OPP fluxes from this study to the total industrial OPP on peat, across Peninsular Malaysia, Borneo and Sumatra, suggests a total TOC flux of 3.2 Tg C yr⁻¹. This combined with estimates of TOC flux from the remaining intact and degraded PSF areas gives an updated TOC loss estimate, for the year 2015, of 10.4 Tg yr⁻¹ (intact + degraded + industrial OPPs). This represents 10% of the global fluvial organic carbon flux from the tropical climate zone (TCZ; 90.2 Tg C yr⁻¹; Ludwig et al., 1996), which is significant

considering this area only represents 0.5% (109,383 km²) of this TCZ by area (23,633,000 km²).

- From a more local perspective, the industrial peatland OPPs of Sarawak contribute nearly 1% (0.7 Tg C yr⁻¹) of the tropical climate zone total DOC flux, yet make up only 0.03% of this zone by area. Future OPP expansion projections will increase this contribution to 1.4 Tg C yr⁻¹ by 2020, making this area a hotspot for fluvial organic carbon losses.
- Fluvial carbon fluxes from Peninsular Malaysia, Borneo and Sumatra (10.4 Tg C yr⁻¹) represent 6% the total peat oxidation emissions (161.6 Tg C yr⁻¹; Miettinen et al., 2017).
- It is essential that SMH peatland OPPs are considered in future fluvial carbon loss estimates, with estimated fluxes (2.3 Tg C yr⁻¹) close to those of industrial estates (3.2 Tg C yr⁻¹).

7. References

- Abrams, J.F., Hohn, S., Rixen, T., Baum, A., Merico, A, 2015. The impact of Indonesian peatland degradation on downstream marine ecosystems and the global carbon cycle. *Global Change Biology* 22: 325-337
- Adon, R., Bakar, I., Wijeyesekera, D.C., Zainorabidin, A, 2012. Overview of the Sustainable Uses of Peat Soil in Malaysia with Some Relevant Geotechnical Assessments. *International Journal of Integrated Engineering Special Issue on ICONCEES* 4: 38-46
- Agus, F., Gunarso, P., Sahardjo, B.H., Harris, N., van Noordwijk, M., Killeen, T,J, 2013. Historical CO₂ emissions from land use and land use change from oil palm industry in Indonesia, Malaysia and Papua New Guinea. In: Killenn, T.J & Goon, J (eds.). 2013. *Reports from the Technical Panels of the 2nd Greenhouse Gas Working Group of the Roundtable on Sustainable Palm Oil (RSPO)*. RSPO, Kuala Lumpur, Malaysia
- Agus, F., Handayani, E., van Noordwijk, M., Idris, K., & Sabiham, S, 2010. Root respiration interferes with peat CO₂ emission measurement. In: 19th World Congress of Soil Science, Soil Solutions for a Changing World. Brisbane, Australia.
- Aitkenhead, J.A and McDowell, W.H, 2000. Soil C:N ratio as a predictor of annual riverine DOC flux at local and global scales. *Global Biogeochemical Cycles* 14:127-138
- Allen, R.G., Pereira, L.S., Raes, D., Smith, M, 1998. *FAO Irrigation and Drainage Paper No. 56 Crop Evapotranspiration*. Food and Agriculture Organization.
- Allen, R, 2003. Crop coefficients. *Encyclopedia of Water Science*. DOI: 10.1081/E-EWS 120010037

- Alongi, D.M., Sasekumar, A., Tirendi, F., Dixon, P, 1998. The influence of stand age on benthic decomposition and recycling of organic matter in managed mangrove forests of Malaysia. *Journal of Experimental Marine Biology and Ecology* 225: 197-218
- Anderson, J. A.R and Muller, J, 1975. Palynological Study of a Holocene Peat and a Miocene Coal Deposit from NW Borneo. *Review of Palaeobotany and Palynology* 19: 291-351
- Amon, R. M. W., and Benner, R, 1996. Bacterial utilization of different size classes of dissolved organic matter. *Limnology and Oceanography* 41: 41–51
- Arshad, A.M, 2014. Crop Evapotranspiration and Crop Water Requirement for Oil Palm in Peninsular Malaysia. *Journal of Biology, Agriculture and Healthcare* 4: 23-28
- Asmala, E., Stedmon, C.A., Thomas, D.N, 2012. Linking CDOM spectral absorption to dissolved organic carbon concentrations and loadings in boreal estuaries. *Estuarine, Coastal and Shelf Science* 111: 107-117
- Baird, A.J., Low, R., Young, D., Swindles. G.T., Lopez, O.R., Page, S, 2017. Higher permeability explains the vulnerability of the carbon store in drained tropical peatlands. *Geophysical Research Letters*, doi:10.1002/2016GL072245
- Bakoume, C., Shahbudin, N., Yacob, S., See Siang, C., Thambi, N.M.A, 2013. Improved Method for Estimating Soil Moisture Deficit in Oil Palm (*Elaeis guineensis* Jacq.) Areas with Limited Climatic Data. *Journal of Agricultural Science* 5: 57-65
- Bartlett, R.J and Ross, D.S, 1988. Colorimetric determination of oxidizable carbon in acid soil solutions. *Soil Science Society of America Journal* 52: 1191–1192

- Bastviken, D., Sundgren, I., Natchimuthu, S., Reyier, H., Galfalk, M, 2015. Technical note: cost-efficient approaches to measure carbon dioxide (CO₂) fluxes and concentrations in terrestrial and aquatic environments using mini loggers. *Biogeosciences Discussions* 12: 2357-2380
- Benner, R, 2004. What happens to terrestrial organic matter in the ocean? *Marine Chemistry* 92: 307–310
- Benner, R. and Kaiser, K, 2011. Biological and photochemical transformations of amino acids and lignin phenols in riverine dissolved organic matter. *Biogeochemistry* 102: 209–222
- Berglund, O and Berglund, K, 2011. Influence of water table level and soil properties on emissions of greenhouses gases from cultivated peat soil. *Soil Biology and Biochemistry* 43: 923-931
- Bernard, B.B., Bernarg, H., Brooks, J.M, 2004. Determination of Total Carbon, Total Organic Carbon and Inorganic Carbon in Sediments. Online: http://www.tdi-bi.com/analytical_services/environmental/noaa_methods/toc.pdf (Accessed 13/10/2014)
- Bianchi, T.S, 2007. *Biochemistry of estuaries*. Oxford: Oxford University Press
- Billett, M. F., Dinsmore, K.J., Smart, R. P., Garnett, M. H., Holden, J., Chapman, P., Baird A. J., Grayson, R., Stott, A.W., 2012. Variable source and age of different forms of carbon released from natural peatland pipes. *Journal of Geophysical Research*, 117, G02003, DOI: 10.1029/2011JG001807.
- Billett, M.F and Harvey, F.H, 2013. Measurements of CO₂ and CH₄ evasion from UK peatland headwater streams. *Biogeochemistry* 114:165–181

- Billett, M.F., Garnett, M.H., Hardie, S.M.L, 2006. A direct method to measure $^{14}\text{CO}_2$ lost by evasion from surface waters. *Radiocarbon* 48: 61-68
- Billett, M.F., Palmer, S.M., Hope, D., Deacon, C., Stroeton-West, R., Haregreaves, K.J., Flechard, C., Fowler, D, 2004. Linking land-atmosphere stream carbon fluxes in a lowland peatland system. *Global Biogeochemical Cycles*, 18, GB1024, DOI: 10.1029/2003GB002058
- Birgand, F., Appelboom, T.W., Checheir, G.M., Skaggs, R.W, 2011. Estimating Nitrogen, Phosphorus, and Carbon Fluxes in Forested and Mixed-Use Watersheds of the Lower Coastal Plain of North Carolina: Uncertainties Associated with Infrequent Sampling. *American Society of Agricultural and Biological Engineers* 54: 2099-2110
- Bjorkvald, L., Buffan, I., Laudon, H., Morth, C-M, 2008. *Geochimica et Cosmochimica Acta* 72: 2789 – 280
- Bonnett, S.A.F., Maltby, E., Freeman, C, 2017. Hydrological legacy determines the type of enzyme inhibition in a peatlands chronosequence. *Scientific Reports* 7: doi:10.1038/s41598-017-10430-x
- Brito, T.F., Phifer, C.C., Knowlton, J.L., Fiser, C.M., Becker, N.M., Barros, F.C., Contera, F.A.L., Maues, M.M., Juen, L., Montag, L.F.A., Wbster, C.R., Flaspohler, D.J., Santos, M.P.D., Silva, D.P, 2017. Forest reserves and riparian corridors help maintain orchid bee (Hymenoptera: Euglossini) communities in oil palm plantations in Brazil. *Apidologie*, DOI: 10.1007/s13592-017-0500-z

- Bruckner, M. Z, 2012. Measuring dissolved and particulate organic carbon (DOC and POC). Online:
http://serc.carleton.edu/microbelife/research_methods/biogeochemical/organic_carbon.html (Accessed 05/11/2014)
- Butman, D.E., Wilson, H.F., Barnes, R.T., Xenopoulos, M, A., Raymond, P.A, 2015. Increased mobilization of aged carbon to rivers by human disturbance. *Nature Geoscience Letters* 8: 112-116
- Campeau, A., Bishop, K., Billett, M. F., Garnett, M. H., Laudon, H., Leach, J. A., Nilsson, M. B., Öquist, M. G. and Wallin, M. B, 2017. Aquatic export of young dissolved and gaseous carbon from a pristine boreal fen: implications for peat carbon stock stability. *Global Change Biology*: doi:10.1111/gcb.13815
- Carlson, K.M., Curran, L.M., Asner, G.P., McDonald Pittman, A., Trigg, S.N., Adeney, J.M, 2012. Carbon emissions from forest conversion by Kalimantan oil palm plantations. *Nature Climate Change* 3: 283-287
- Carlson, K.M., Goodman, L.K., May-Tobin, C.C, 2015. Modeling relationships between water table depth and soil carbon loss in Southeast Asia plantations. *Environmental Research Letters* 10 074006
- Carpenter, P.D and Smith, J.D, 1984. Simultaneous spectrophotometric determination of humic acid and iron in water, *Analytica Chimica Acta* 159: 299–308.
- Carter, H.T., Tipping, E., Kopriyniak, J-F., Miller, M.P., Cookson, B., Hamilton-Taylor, J, 2012. Freshwater DOM quantity and quality from a two-component model of UV absorbance. *Water Research* 46: 4532–4542

- Causse, J., Thomas, O., Jung, A-V., Thomas, M-F. 2016. Direct DOC and nitrate determination in water using dual pathlength and second derivative UV spectrophotometry. *Water Research*, <http://dx.doi.org/10.1016/j.watres.2016.11.010>
- Cauwet, G, 2002. DOM in the coastal zone. In: Hansell, D.A and Carlson C.A.(eds.) *Biogeochemistry of Marine Dissolved Organic Matter*. San Diego: Academic Press, pp 579-609
- Chen, W and Wangersky, P.J, 1996. Rates of microbial degradation of dissolved organic carbon from phytoplankton cultures. *Journal of Plankton Research* 18: 1521-1533
- Chimner, R.A and Karberg, J.M, 2008. Long-term carbon accumulation in two tropical mountain peatlands, Andes Mountains, Ecuador. *Mires and Peat* 3: 1–10.
- Chow, A.T., Guo, F., Gao, S., Breuer, R., Dahlgren, R.A, 2005. Filter pore size selection for characterizing dissolved organic carbon and trihalomethane precursors from soils. *Water Research* 39: 1255–1264
- Clark, J.M., Chapman, P.J., Adamson, J.K., Lane, S.N, 2005. Influence of drought-induced acidification on the mobility of dissolved organic carbon in peat soils. *Global Change Biology* 11: 791- 809.
- Clark, J.M., Chapman, P.J., Heathwaite, A.L., Adamson, J.K, 2006. Suppression of dissolved organic carbon by sulfate induced acidification during simulated droughts. *Environmental Science Technology* 40: 1776-1783

- Clark, J.M., Bottrell, S.H., Evans, C. D., Monteith, D.T., Bartlett, R., Rose, R., Newton, J.R., Chapman, P.J, 2010. The importance of the relationship between scale and process in understanding long-term DOC dynamics. *Science of the Total Environment* 408: 2768-2775.
- Clark, J.M., Heinemeyer, A., Martin, P., Botrell, S.H, 2012. Processes controlling DOC in pore water during simulated drought cycles in six different UK peats. *Biogeochemistry*, 109: 253–270
- Clarke, D and Rieley, J, 2010. Strategy for responsible peatland management. International Peat Society (IPS): Finland
- Clayden, J., Greeves, N., Warren, S, 2011. *Organic Chemistry*. Oxford: Oxford University Press
- Clutterbuck, B and Yallop, 2010. Land management as a factor controlling dissolved organic carbon release from upland peat soils 2: changes in DOC productivity over four decades. *Science of the Total Environment* 408: 6179–6191
- Cole, J.J., Prairie, Y.T., Caraco, N.F., McDowell, W.H., Tranvik, L.J., Striegl, R.G., Duarte, C.M., Kortelainen, P., Downing, J.A., Middelbugh, J.J., Melack, J, 2007. Plumbing the global carbon cycle: integrating inland waters into the terrestrial carbon budget. *Ecosystems* 10:172–185
- Cole, J.J., Bade, D.L., Bastviken, D., Pace, M.L., Van de Bogert, M, 2010. Multiple approaches to estimating air-water gas exchange in small lakes. *Limnology and Oceanography: Methods* 8: 285-293
- Cole, L.E.S., Bhagwat, S.A., Willis, K.J, 2015. Long-term disturbance dynamics and resilience of tropical peat swamp forests. *Journal of Ecology* 103: 16-30

- Comeau, L-P., Hergoualc'h, K., Smith, J.U., Verchot, L, 2013. Conversion of intact peat swamp forest to oil palm plantation. Effects on soil CO₂ fluxes in Jambi, Sumatra. Working Paper 110. Indonesia: Centre for International Forestry Research
- Cook, S., Peacock, M., Evans, C.D., Page, S.E., Whelan, M., Gauci, V., Kho, L.K, 2016. Cold Storage as a method for the long-term preservation of tropical dissolved organic carbon (DOC). *Mires and Peat* 18: 1-8
- Cook, S., Peacock, M., Evans, C.D., Page, S.E., Whelan, M., Gauci, V., Kho, L.K, 2017. Quantifying tropical peatland dissolved organic carbon (DOC) using UV-visible spectroscopy. *Water Research* 115: 229-235
- Cory, R.M., Ward, C.P., Crump, B.C., Kling, G.W, 2014. Sunlight controls water column processing of carbon in arctic fresh waters. *Science* 345:925-928
- Couwenberg, J., Dommain. R., Joosten, H, 2010. Greenhouse gas fluxes from tropical peatlands in Southeast Asia. *Global Change Biology* 16: 1715-1732
- Couwenberg, J and Hooijer, A, 2013. Towards robust subsidence-based soil carbon emission factors for peat soils in south-east Asia, with special reference to oil palm plantations. *Mires and Peat* 12: 1-13
- Crump, J, 2017. Smoke on Water – Countering Global Threats From Peatland Loss and Degradation. A UNEP Rapid Response Assessment. United Nations Environment Programme and GRID-Arendal, Nairobi and Arendal. Online: https://gridarendal-website-live.s3.amazonaws.com/production/documents/s_document/372/original/RRapeatland_lores.pdf?1510738969 (Accessed 11/12/2017)

- Daemeter Consulting, 2015. Indonesian Oil Palm Smallholder Farmers: A Typology of Organizational Models, Needs, and Investment Opportunities. Daemeter Consulting, Bogor, Indonesia
- Dai, M., Yin, Z., Meng, F., Liu, Q., Cai, W-J, 2012. Spatial distribution of riverine DOC inputs to the ocean: an updated global synthesis. *Current Opinion in Environmental Sustainability* 4:170–178
- Dargie, G. C., Lewis, S.L., Lawson, I, T., Michard, E.T.A., Page, S.E., Bocko, Y.E., Ifo, S.A, 2017. Age, extent and carbon storage of the central Congo Basin peatland complex. *Nature DOI*: doi:10.1038/nature21048
- De Haan, H., De Boer, T., Kramer, H, A, Voerman, J, 1982. Applicability of light absorbance as a measure of organic carbon in humic lake water, *Water Resources* 16: 1047–1050
- Degens, E.T., Kempe, S. and Richey, J.E., 1991. Summary: Biogeochemistry of major world rivers. *SCOPE* 42: 323-347
- Del Grosso, S.F., Parton, W.J., Mosier, A.R., Holland, E.A., Pendall, E., Schimel, D.S., Ojima, D.S, 2005. Modelling soil CO₂ emissions from ecosystems. *Biogeochemistry* 73: 71–91
- Dinsmore, K. J., Billett, F. M., Skiba, U. M., Rees, R. M., Drewer, J., Helfter, C, 2010. Role of the aquatic pathway in the carbon and greenhouse gas budgets of a peatland catchment. *Global Change Biology* 16: 2750–2762
- Dislich, C., Keyel, A.C., Salecker, J., Kisel, Y., Meyer, K.M., Corre, M.D., Faust, H., Hess, B., Knohl, A., Kreft, H., Meijide, A., Nurdiansyah, F., Otten, F., Pe'er, G., Steinebach, S., Tarigan, S., Tschardtke, T., Tölle, M., Wiegand, K, 2015. Ecosystem functions of oil palm plantations -a review, *EFForTS Discussion Paper Series*, No. 16.

- Dislich, C., Keyel, A.C., Salecker, J., Kisel, Y., Meyer, K.M., Corre, M.D., Faust, H., Hess, B., Knohl, A., Kreft, H., Meijide, A., Nurdiansyah, F., Otten, F., Pe'er, G., Steinebach, S., Tarigan, S., Tschardtke, T., Tölle, M., Wiegand, K, 2016. A review of the ecosystem functions in oil palm plantations, using forests as a reference system. *Biological Reviews*: doi:10.1111/brv.12295
- Dommain, R., Couwenberg, J., Joosten, H, 2010. Hydrological self-regulation of domed peatlands in south-east Asia and consequences for conservation and restoration. *Mires and Peat* 6: 1-17
- Dommain, R., Couwenberg, J, Joosten, H, 2011. Development and carbon sequestration of tropical peat domes in south-east Asia: links to post-glacial sea-level changes and Holocene climate variability. *Quaternary Science Review* 30: 999-1010
- Dommain, R., Cobb, A.R., Joosten, H., Glaser, P.H., Chau, A.F.L., Gandois, L., Kai, F-M., Noren, A., Salim, K.A., Su'ut, N.S.H., Harvey, C.F, 2015. Forest dynamics and tip-up pools drive pulses of high carbon accumulation rates in tropical peat dome in Borneo (Southeast Asia). *Journal of Geophysical Research: Biogeosciences*, DOI: 10.1002/2014JG002796
- Dowrick, D.J., Freeman, C., Lock, M.A., Yusoff, F.M, 2015. Using Thermal Sensitivity Analysis to Determine the Impact of Drainage on the Hydrochemistry of a Tropical Peat Soil from Malaysia, *Communications in Soil Science and Plant Analysis*, DOI: 10.1080/00103624.2015.1069318
- EIA Report, 2006. Environmental impact assessment for the proposed Sarawak Oil Palm Berhad's Sebungan and Lavang Oil Palm Estates at Sebungan and Lavang area, Bintulu Division, Sarawak.

- Eisenlord, S, 2008. Does Atmospheric NO₃ Deposition Alter Actinobacterial Abundance and Community Composition in a Northern Hardwood Forest Ecosystem? MSc Thesis, Natural Resources and Environment at the University of Michigan
- Ekström, S.M., Kritzberg, E.S., Kleja, D.B., Larsson, N., Nilsson, P.A., Graneli, W., Bergkvist, B., 2011. Effect of acid deposition on quantity and quality of dissolved organic matter in soil-water. *Environmental Science and Technology*, 45: 4733-4739
- Evans, C.D., Monteith, D.T., Cooper, D.M, 2005 Long-term increases in surface water dissolved organic carbon: observations, possible causes and environmental impacts. *Environmental Pollution* 137: 55–71
- Evans, C. D., Chapman, P. J., Clark, J. M., Monteith, D. T., Cresser, M. S, 2006. Alternative explanations for rising dissolved organic carbon export from organic soils. *Global Change Biology* 12: 2044–2053
- Evans, C.D., Freeman, C., Cork, L.G., Thomas, D.N., Reynolds, B., Billett, M.F., Garnett, M.H., Norris, D, 2007. Evidence against recent climate-induced destabilisation of soil carbon from ¹⁴C analysis of riverine dissolved organic matter. *Geophysical Research Letters* 34, L07407, DOI:10.1029/2007GL029431
- Evans, C.D., Futter, M.N., Moldan, F., Valinia, S., Frogbrook, Z., Kothawala, D.N, 2017. Variability in organic carbon reactivity across lake residence time and trophic gradients. *Nature geoscience* 10: 832-835
- Evans, C.D., Jones, T.G., Burden, A., Ostle, N., Piotr, Z., Cooper, M.D.A., Peacock, M., Clark, J.M., Oulehle, F., Cooper, D., Freeman, C, 2012. Acidity controls on dissolved organic carbon mobility in organic soils. *Global Change Biology* 18: 3317–3331

Evans, C.D., Page, S.E., Jones, T., Moore, S., Gauci, V., Laiho, R., Hruška, J., Allott, T.E.H., Billett, M.F., Tipping, E., Freeman, C., Garnett, M.H., 2014. Contrasting vulnerability of drained tropical and high-latitude peatlands to fluvial loss of stored carbon. *Global Biogeochemical Cycles*, DOI: 10.1002/2013GB004782

Evans, C.D., Page, S., Morrison, R., Artz, R., Wijedasa, L., 2017. The potential of responsible peatland management to reduce global soil carbon loss and greenhouse gas emissions. *Global Symposium on soil organic carbon*. Online: <http://www.fao.org/3/a-bs027e.pdf> (Accessed 26/06/2017)

Evans, C.D., Renou-Wilson, F., Strack, M., 2015. The role of waterborne carbon in the greenhouse gas balance of drained and re-wetted peatlands. *Aquatic Sciences* 492:139-150

Evans, C, D, 2015. Biogeochemistry: old carbon mobilized. *Nature Geoscience* 8: 85-86

Ewers, R.M., Didham, R.K., Fahrig, L., Ferraz, G., Hector, A., Holt, R.D., Kapos, V., Reynolds, G., Sinun, W., Snaddon, J.L., Turner, E.C., 2011. A large-scale forest fragmentation experiment: the Stability of Altered Forest Ecosystems Project. *Philosophical Transactions of the Royal Society of London B-Biological Sciences* 366: 3292–3302

Fasching, C., Ulseth, A.J., Schelker, J., Steniczka, G., Battin, T.J., 2015. Hydrology controls dissolved organic matter export and composition in an Alpine stream and its hyporheic zone. *Limnology and Oceanography* 61: 558-571

Fellman, J.B., D'Amore, D.V., Hood, E., 2008. An evaluation of freezing as a preservation technique for analyzing dissolved organic C, N and P in surface water samples. *Science of The Total Environment* 392: 305-312

- Fellman, J.B., Fellman, D.V., D'Amore, E., Hood, R.D, 2008. Fluorescence characteristics and biodegradability of dissolved organic matter in forest and wetland soils from coastal temperate watersheds in southeast Alaska *Biogeochemistry*, 88: 169-184
- Fenner, N., and Freeman, C, 2011. Drought-induced carbon loss in peatlands, *Nature Geoscience* 4: 895–900
- Fenner, N., Freeman, C., Reynolds, B., 2005. Hydrological effects on the diversity of phenolic degrading bacteria in a peatland: implications for carbon cycling. *Soil Biology and Biochemistry*, 37: 1277-1287.
- Field, C.B and Raupach, M.R, 2004. *Global Carbon Cycle: Integrating Humans, Climate, and the Natural World*. Washington DC, USA: Island Press
- Fontaine, S., Mariotti, A., Abbadie, L, 2003. The priming effect of organic matter: a question of microbial competition. *Soil Biology and Biochemistry* 35: 837-843
- Freeman, C., Evans, C.D., Monteith, D.T., Reynolds, B., Fenner, N, 2001a. Export of organic carbon from peat soils. *Nature* 412: 785-785
- Freeman, C., Ostle, N., Kang, H, 2001b. An enzymatic 'latch' on a global carbon store. *Nature* 409: 149.
- Freeman, C., Fenner, N., Ostle, N.J., Kang, H., Dowrick-D.J., Reynolds-B., Lock, M.A., Sleep-D., Hughes, S., Hudson, J, 2004. Export of dissolved organic carbon from peatlands under elevated carbon dioxide levels. *Nature* 430: 195–198
- Furukawa, Y., Inubushi, K., Ali, M, 2005 Effect of changing groundwater levels caused by land-use changes on greenhouse gas fluxes from tropical peat lands. *Nutrient Cycling in Agroecosystems* 71: 81-91

- Gandaseca, S., Salimin, M.I., Ahmed, O.H, 2014. Effect of cultivation in different age's oil palm plantation on selected chemical properties of peat swamp soils. *Agriculture, Forestry and Fisheries* 3:6-9
- Gandois, L.M., Cobb, A.R., Chieng, Hei, I., Lim, L.B.L., Abu Salim, K., Harvey, C.F, 2013 . Impact of deforestation on solid and dissolved organic matter characteristics of tropical peat forests: implications for carbon release. *Biogeochemistry* 114: 183-199
- Gandois, L.M., Teisserenc, R., Cobb, A.R., Chieng, H.I., Lin, L.B.L., Kamariah, A.S., Hoy, A., Harvey, C.F, 2014. Origin, composition, and transformation of dissolved organic matter in tropical peatlands. *Geochimica et Cosmochimica Acta* 137: 35 - 47
- Garnett, M.H., Dinsmore, K.J., Billett, M.F, 2012. Annual variability in the radiocarbon age and source of dissolved CO₂ in a peatland stream. *Science of the Total Environment* 427-428: 277-285
- Germer, J and Sauerborn, J, 2008. Estimation of the impact of oil palm plantation establishment on greenhouse gas balance. *Environment, Development and Sustainability*, 10: 697-716
- Glatzel, S., Kalbitz, K., Dalva, M., Moore, T, 2003. Dissolved organic matter properties and their relationship to carbon dioxide efflux from restored peat bogs. *Geoderma* 113: 397-411
- Glendell, M and Brazier, R.E, 2014. Accelerated export of sediment and carbon from a landscape under intensive agriculture. *Science of the Total Environment* 476-477: 643-656
- Goldammer, J.G, 2007. History of equatorial vegetation fires and fire research in Southeast Asia before the 1997–1998 episode: A

reconstruction of creeping environmental changes. *Mitigation and Adaptation Strategies for Global Change* 12: 13–32

Gorham, E., 1991. Northern peatlands: Role in the carbon cycle and probable responses to climatic warming. *Ecological Applications* 1:182-195.

Goulsbra, C.S., Evans, M.G., Allott, T.E.H, 2016. Rates of CO₂ efflux and changes in DOC concentration resulting from the addition of POC to the fluvial system in peatlands. *Aquatic Sciences: DOI* 10.1007/s00027-016-0471-6

Graham, L.L.B., Giesen, W., Page, S.E, 2016. A common-sense approach to tropical peat swamp forest restoration in Southeast Asia. *The Society for Restoration Ecology* doi: 10.1111/rec.12465

Graham, M.C., Gavin, K.G., Kirika, A., Farmer, J.G, 2012. Processes controlling manganese distributions and associations in organic-rich freshwater aquatic systems: the example of Loch Bradan, Scotland. *Science of the Total Environment* 424: 239-250

Graneli, W., Lindell, M., Tranvik, L, 1996. Photo-oxidative production of dissolved inorganic carbon in lakes of different humic content. *Limnology and Oceanography* 41: 698 – 706

Gray, C.L and Lewis., O.T, 2014. Do riparian forest fragments provide ecosystem services or disservices in surrounding oil palm plantations. *Basic and Applied Ecology* 15: 693-700

Grayson, R.P and Holden, J, 2016. Improved automation of dissolved organic carbon sampling for organic-rich surface waters. *Science of the Total Environment* 543: 44-51

- Gulliver, P., Waldron, S., Scott, E.M. and Bryant, C.L., 2010. The effect of storage on the radiocarbon, stable carbon and nitrogen isotopic signatures and concentration of riverine DOM. *Radiocarbon* 52:1113-1122
- Hansen, M.C., Stehman, S.V., Potapov, P.V., Arunarwati, B., Stolle, F., Pittman, K, 2009. Quantifying changes in the rates of forest clearing in Indonesia from 1990 to 2005 using remotely sensed data sets. *Environmental Research Letters*, 4, 034001, doi:10.1088/1748-9326/4/3/034001
- Harris, N.L., Brown, K., Netzer, M., Gunarso, P., Killeen, T.J, 2013. Projections of oil palm expansion in Indonesia, Malaysia and Papua New Guinea from 2010 to 2050. In: Reports from the Technical Panels of the 2nd Greenhouse Gas Working Group of the Roundtable on Sustainable Palm Oil (RSPO) (eds Killeen, T.J; Goon, J), pp. 89–112. RSPO, Kuala Lumpur. Online: http://www.rspo.org/file/GHGWG2/6_emission_scenarios_from_land_use_change_Harris_et_al.pdf (16/10/2014)
- Harrison, J.A., Caraco, N., Seitzinger, S.P, 2005. Global patterns and sources of dissolved organic matter export to the coastal zone: results from a spatially explicit, global model. *Global Biogeochemical Cycles* 19: GB4S04, DOI: 10.1029/2005GB002480
- Hedges, J. I., Keil, R.G., Benner, R, 1997. What happens to terrestrial organic matter in the ocean? *Organic Geochemistry* 27: 195–212
- Helms, J.R., Stubbins, A., Ritchie, J.D., Minor, E.C, 2008. Absorption spectral slopes and slope ratios as indicators of molecular weight, source, and photobleaching of chromophoric dissolved organic matter. *Limnology and Oceanography* 53: 955 – 969

- Henriksen, H.J., Troldborg, L., Nyegaard, P., Sonnenborg, T.O., Refsgaard, J.C., Madsen, B, 2003. Methodology for construction, calibration, and validation of a national hydrological model for Denmark. *Journal of Hydrology* 280: 52–71
- Henson, I. E. and Harun, M. H, 2005. The influence of climatic conditions on gas and energy exchanges above a young oil palm stand in north Kedah. *Journal of Oil Palm Research* 17: 73–91
- Hergoualc'h, K. and Verchot, L. V, 2011. Stocks and fluxes of carbon associated with land use change in Southeast Asian tropical peatlands: a review. *Global Biogeochemical Cycles* 25: doi:10.1029/2009GB003718
- Hirano, T., Segah, H., Harada, T., Limin, S., June, T., Hirata, R., Osaki, M, 2007. Carbon dioxide balance of a tropical peat swamp forest in Kalimantan, Indonesia. *Global Change Biology*, 13: 412-425.
- Hirano, T., Jauhiainen, J., Inoue, T., Takahashi, H, 2009. Controls on the Carbon Balance of Tropical Peatlands. *Ecosystems* 12: 873-887
- Hirano, T., Segah, H., Kusin, K., Limin, S., Takahashi, H., Osaki, M, 2012. Effects of disturbances on the carbon balance of tropical peat swamp forests. *Global Change Biology* 18: 3410-3422
- Hirano, T., Kusin, K., Limin, S, Osaki, M, 2014. Evapotranspiration of tropical peat swamp forests. *Global Change Biology* 21: 1914-1927
- Holden, J., Chapman, P.J., Labadz, J.C, 2004. Artificial drainage of peatlands: Hydrological and hydrochemical process and wetland restoration, *Progress in Physical Geography* 28: 95–123.

- Holden, J., 2005. Controls of soil pipe frequency in upland blanket peat. *Journal of Geophysical Research* 110, F01002, DOI: 10.1029/2004JF000143.
- Holden, J., Green, S., Baird, A., Chapman, P., Evans, C., Grayson, R., 2016. Impacts of ditch blocking on peatland hydrology- the benefits of long-term monitoring. *Geophysical Research Abstracts* 18: EGU2016-3260
- Hood, E., Gooseff, M.N., Johnson, S.L., 2006. Changes in the character of stream water dissolved organic carbon during flushing in three small watersheds, Oregon. *Journal of Geophysical Research* 111: G01007, doi:10.1029/2005JG000082.
- Hooijer, A., Silvius, M., Wösten, H., Page, S., 2006. PEAT-CO2, Assessment of CO2 emissions from drained peatlands in SE Asia, Delft Hydraulics report Q3943.
- Hooijer, A., Page, S.E., Canadell, J.G., Silvius, M., Kwadijk, J., Wosten, H., Jauhiainen, J., 2010. Current and future CO2 emissions from drained peatlands in Southeast Asia. *Biogeosciences* 7:1505–1514
- Hooijer, A., Page, S. E., Jauhiainen, J., Lee, W. A., Idris, A., & Anshari, G, 2011. Land subsidence and carbon loss in plantations on tropical peatland: reducing uncertainty and implications for emission reduction options. *Biogeosciences Discussions* 8: 9311-9356
- Hooijer, A., Page, S. E., Jauhiainen, J., Lee, W. A., Idris, A., Anshari, G, 2012. Subsidence and carbon loss in drained tropical peatlands. *Biogeosciences* 9: 1053-1071

- Hooijer, A., Page, S., Navratil, P., Vernimmen, R., Van der Vat, M., Tansey, K., Konecny, K., Siegert, F., Ballhorn, U., Mawdsley, N, 2014. Carbon emissions from drained and degraded peatland in Indonesia and emission factors for measurement, reporting and verification (MRV) of peatland greenhouse gas emissions – a summary of KFCP research results for practitioners. IAFCP, Jakarta, Indonesia.
- Hooijer, A., Vernimmen, R., Visser, M., Mawdsley, N, 2015. Flooding projections from elevation and subsidence models for oil palm plantations in the Rajang Delta peatlands, Sarawak, Malaysia. Deltares report 1207384, 76 pp
- Hope, D., Billett, M.F., Cresser, M.S, 1994. A review of the export of carbon in river water: fluxes and processes. *Environmental Pollution* 84:301-324
- Horowitz, A. J., Lum, K. R., Garbarino, J. R., Hall, G. E. M., Lemieux, C., Demas, C. R, 1996. Problems Associated with Using Filtration to Define Dissolved Trace Element Concentrations in Natural Water Samples. *Environmental Science and Technology* 30: 954
- Houghton, R.A., House, J.I., Pongratz, J., van der Werf, G.R., DeFries, R.S., Hansen, M.C., Le Quere, C., Ramankutty, N, 2012. Carbon emissions from land use and land-cover change. *Biogeosciences* 9: 5125-5142
- Hribljan, J. A., Kane, E. S., Pypker, T. G., Chimner, R. A, 2014. The effect of long-term water table manipulations on dissolved organic carbon dynamics in a poor fen peatland. *Journal of Geophysical Research Biogeosciences* 119: 577–595,

- Hulatt, C.J., Kaartokallio, H., Asmala, E., Autio, R., Stedmon, C.A., Sonninen, E., Oinonen, M., Thomas, D.N, 2014a. Bioavailability and radiocarbon age of fluvial dissolved organic matter (DOM) from a northern peatland-dominated catchment: effect of land-use change. *Aquatic Science* 76: 393-404
- Hulatt, C.J., Kaartokallio, H., Oinonen, M., Sonninen, E., Stedmon, C.A., Thomas, D.N, 2014b. Radiocarbon Dating of Fluvial Organic Matter Reveals Land-Use Impacts in Boreal Peatlands. *Environmental Science and Technology* 48: 12543-12551
- Huijnen, V., Wooster, M. J., Kaiser, J. W., Gaveau, D.L. A., Flemming, J., Parrington, M., Inness, A., Murdiyoso, D., Main, B., van Weele, M, 2016. Fire carbon emissions over maritime Southeast Asia in 2015 largest since 1997. *Scientific Reports* 6: 26886
- Husnain, H., Wigena, P.I.G., Dariah, A., Marwanto, S., Setyanto, P., Agus, F, 2014. CO₂ emissions from tropical drained peat in Sumatra, Indonesia. *Mitigation and Adaption Strategies for Global Change* 19: 845-862
- Hwang, C. P., Lackie, T. H., Munch, R. R, 1979. Correction for Total Organic Carbon, Nitrate, and Chemical Oxygen Demand when Using the MF-Millipore Filter. *Environmental Science and Technology* 13: 871
- IPCC, 2014. 2013 Supplement to the 2006 IPCC Guidelines for National Greenhouse Gas Inventories: Wetlands (ed) Hiraishi, T., Krug, T., Tanabe, K., Srivastava, N., Baasansuren, J., Fukuda, M. and Troxler, T.G. International Panel on Climate Change (IPCC): Switzerland
- Jauhiainen, J., Takahashi, H., Juha, Heikkinen, E. P., Martikainen, P. J., Vasander, H, 2005. Carbon fluxes from a tropical peat swamp forest floor. *Global Change Biology* 11: 1788-1797

Jauhiainen, J., Hooijer, A., Page, S.E, 2012. Carbon dioxide emissions from an *Acacia* plantation on peatland in Sumatra, Indonesia. *Biogeosciences* 9: 617-630

Jauhiainen, J., Kerojoki, O., Silvennoinen, H., Limin, S., Vasander, H, 2014. Heterotrophic respiration in drained tropical peat is greatly affected by temperature—a passive ecosystem cooling experiment. *Environmental Research Letters* 9 105013: doi:10.1088/1748-9326/9/10/105013

Jauhiainen, J., Page, S.E., Vasander, H, 2016. Greenhouse gas dynamics in degraded and restored tropical peatlands. *Mires and Peat* 17: 1-12

Johnson, M.S., Lehmann, J., Couto, E.G., Filho, J.P.N., Riha, S.J, 2006. DOC and DIC in flowpaths of Amazonian headwater catchments with hydrologically contrasting soils. *Biogeochemistry* 81: 45-57

Jones, T.G., Evans, C.D., Jones, D.L., Hill, P.W., Freeman, C, 2016. Transformations in DOC along a source to sea continuum; impacts of photo-degradation, biological processes and mixing. *Aquatic Sciences* 78: 433-446

Jonsson, A., Algesten, G., Bergström, A.-K., Bishop, K., Sobek, S., Tranvik, L., Jansson, M. 2007. Integrating aquatic fluxes in a boreal catchment carbon budget. *Journal of Hydrology* 334: 141-150

Joosten, H, 2009. The Global Peatland CO₂ Picture Peatland status and drainage related emissions in all countries of the world. The Netherlands, Wetlands International

- Joosten, H. and Clarke, D. 2002. Wise Use of Mires and Peatlands .
Background and Principles Including a Framework for Decision-
Making. Devon: International Mire Conservation Group and
International Peat Society
- Kalbitz, K., Solinger, S., Park, J.H., Michalzik, B., Matzner, E, 2000. Controls
on the dynamics of dissolved organic matter in soils: A review. *Soil
Science* 165: 277–304
- Kalbitz, K and Kaiser, K, 2007. Contribution of dissolved organic matter to
carbon storage in forest mineral soils. *Journal of Plant Nutrition and
Soil Science* 170: 52-60
- Kallarackal, J., Jeyakumar, P., and George S. J, 2004. Water use of irrigated
oil palm at three different arid locations in Peninsular India. *Journal of
Oil Palm Research* 16: 45-53
- Kane, E.S., Mazzoleni, L.R., Kratz, C.J., Hribljan, J.A., Johnson,
C.P., Pypker, T.G., Chimner, R, 2014. Peat porewater dissolved
organic carbon concentration and lability increase with warming: a
field temperature manipulation experiment in a poor
fen. *Biogeochemistry* 119: 161–178
- Karanfil, T., Erdogan, I., Schlautman, M. A, 2003. Selecting Filter Membranes
for Measuring DOC and UV254. *Journal of American Water Works
Association* 95: 86
- Karanfil, T., Schlautman, M. A., Erdogan, I, 2002. Survey of DOC and UV
measurement practices with implications for SUVA determination.
Journal of American Water Works Association 94:68-80
- Kawahigashi, M and Sumida, H, 2006. Humus composition and physico-
chemical properties of humic acids in tropical peat soils under sago
palm plantation. *Soil Science & Plant Nutrition* 52: 153-161

- Kelly, T. J., Baird, A. J., Roucoux, K. H., Baker, T. R., Honorio Coronado, E. N., Ríos, M., Lawson, I. T, 2014. The high hydraulic conductivity of three wooded tropical peat swamps in northeast Peru: measurements and implications for hydrological function. *Hydrological Processes* 28: 3373–3387
- Khan, E and Subramania-Pillai, S, 2006. Effect of leaching from filters on laboratory analyses of collective organic constituents. *Proceedings of the Water Environment Federation*, 11-20: 901–918
- Khan, S., Yaoguo, W., Xiaoyan, Z., Youning, X., Jianghua, Z., Sihai, 2014. Estimation of concentration of dissolved organic matter from sediment by using UV-visible spectrophotometer. *International Journal of Environmental Pollution and Remediation* 2: 24-29
- Kho, LK and Jepsen, M.R, 2015. Carbon stocks of oil palm plantations and tropical forest ins Malaysia. *Singapore Journal of Tropical Geography*, DOI:10.1111/sjtg.12100
- Kling, G.W., Kipphut, G.W., Miller, 1991. Artic lakes and stream as gas conduits to the atmosphere: implications for tundra carbon budgets. *Science* 251: 298-301
- Kling, G.W., Miller, M.M., O'Brien, W.J, 2000. Integration of lakes and streams in a landscape perspective: the importance of material processing on spatial patterns and temporal coherence. *Freshwater Biology* 43: 477-497
- Koehler, A.-K., Murphy, K., Kieft, G., Sottocornola, M, 2009. Seasonal variation of DOC concentration and annual loss of DOC from an Atlantic blanket bog in South Western Ireland. *Biogeochemistry* 95: 231-242

- Koehler, A.-K., Sottocornola, M., Kiely, G, 2011. How strong is the current carbon sequestration of an Atlantic blanket bog? *Global Change Biology* 17: 309–319
- Koh, L.P., Miettinen, J., Liew, S.C., Ghazoul, J, 2011. Remotely sensed evidence of tropical peatland conversion to oil palm. *Proceedings of the National Academy of Sciences of the United States of America*, 108: 5127-5132. DOI: 10.1073/pnas.1018776108
- Kolka, R., Weishampel, P., Froberg, M, 2008. Measurement and Importance of Dissolved Organic Carbon. In: C.M. Hoover (ed.) *Field Measurements for Forest Carbon Monitoring*. New York: Springer + Business Media B.V, pp171-176
- Konecny, K., Ballhorn, U., Navratil, P., Jubanski, J, Page, S.E., Tansey, K, Hooijer, A., Vernimmen, R., Siegert, F, 2015. Variable carbon losses from recurrent fires in drained tropical peatlands. *Global Change Biology*, DOI: 10.1111/gcb.13186
- Kononen, M., Jauhiainen, J., Laiho, R., Spetz, P., Kusin, K., Limin, S., Vasander, H, 2016. Land-use increases the recalcitrance of tropical peat. *Wetlands Ecology and Management* 24: 717-731
- Kroon, P., Schrier-Uijl, A. P., Hensen, A., Veenendaal, E. M., Jonker, H. J. J, 2010. Annual balances of CH₄ and N₂O from a managed fen meadow using eddy covariance flux measurements. *European Journal of Soil Science* 61: 773-784
- Kumagai, T., Saitoh, T. M., Sato, Y., Takahashi, H., Manfroi, O. J., Morooka, T., Kuraji, K., Suzuki, M., Yasunari, T., and Komatsu, H, 2005 Annual water balance and seasonality of evapotranspiration in a Bornean tropical rainforest. *Agriculture and Forest Meteorology* 128: 81–92.

- Laine, M.P.P., Strommer, R., Arvola, L, 2014. DOC and CO₂-C Releases from Pristine and Drained Peat Soils in Response to Water Table Fluctuations: A Mesocosm Experiment. *Applied and Environmental Soil Science* 2014: 1-10
- Langner, A. and Siegert, F, 2009. Spatiotemporal fire occurrence in Borneo over a period of 10 years. *Global Change Biology* 15: 48–62
- Langner, A., Miettinen, J., Siegert, F, 2007. Land cover change 2002–2005 in Borneo and the role of fire derived from MODIS imagery. *Global Change Biology* 13: 2329–2340
- Larsen, S., Andersen, T., Hessen, D.O, 2011. Climate change predicted to cause severe increase of organic carbon in lakes. *Global Change Biology* 17: 1186-1192
- Leach, J.A., Larsson, A., Wallin, M.B., Nilsson, M.B., Laudon, H, 2016. Twelve year interannual and seasonal variability of stream carbon export from a boreal peatland catchment. *Journal of Geophysical Research: Biogeosciences* 121: 1851-1866
- Lee, J.S.H., Ghazoul, J., Obidzinski, K., Koh, L.P, 2014. Oil palm smallholder yields and incomes constrained by harvesting practices and types of smallholder management. *Agronomy for Sustainable Development* 34: 501-513
- Levin, I and Kromer, B, 2004. The tropospheric ¹⁴CO₂ level in midlatitudes of the Northern Hemisphere (1959 – 2003), *Radiocarbon* 46: 1261–1272
- Li, M., Peng, C., Wang, M., Xue, W., Zhang, K., Wang, K., Shi, Q., Zhu, Q, 2017. The carbon flux of global rivers: a re-evaluation of amount and spatial patterns. *Ecological Indicators* 80: 40-51

- Li, W., Pan, K.W., Wu, N., Wang, J.C., Wang, Y.J., Zhang, L, 2014. Effect of litter type on soil microbial parameters and dissolved organic carbon in a laboratory microcosm experiment. *Plant Soil Environmental* 60: 170-176
- Lim, K.H., Lim, S.S., Parish, F., Suharto, R, 2012. RSPO manual on best management practises (BMPs) for existing oil pal cultivation on peat. Kula Lumpur: RSPO
- Lindsay, J. B and Creed, I.F, 2006. Distinguishing actual and artifact depressions in digital elevation data, *Computers and Geosciences* 32: 1192–1204.
- Littlewood, I.G, 1992. Estimating contaminant loads in rivers: a review. Institute of Hydrology, Wallingford
- Littlewood, I. G., and Marsh, T.J, 2005. Annual freshwater river mass loads from Great Britain, 1975-1994: Estimation algorithm, database, and monitoring network issues. *Journal of hydrology* 304: 221-237
- Liu, C., Sun, G., McNulty, S.G., Noormets, A., Fang, Y, 2016. Environmental controls on seasonal ecosystem evapotranspiration/potential evapotranspiration ratio as determined by the global eddy flux measurements. *Hydrology and Earth System Science Discussions* , DOI: doi:10.5194/hess-2016-237
- López-Moreno, J.I., Hess, T.M., White, S.M, 2009. Estimation of reference evapotranspiration in a mountainous Mediterranean site using the Penman-Monteith equation with limited meteorological data. *Pirineos* 164: 7–31

- Lou, X-D, Zhai, S-Q., Kang, B., Hu, Y-L., Hu, L-L, 2014. Rapid response of hydrological loss of DOC to water table drawn down and warming in Zoige Peatlands: results from a mesocosm experiment. PlosOne, DOI: 10.1371/journal.pone.0109861
- Lucey, J.M., Tawatao, N., Senior, M.J.M., Khen, C.V., Benedick, S., Hamer, K.C., Woodcok, P., Newton, R.J., Bottrell, S.H., Hille, J.K, 2014. Tropical forest fragments contribute to species richness in adjacent oil palm plantations. *Biological Conservation* 169: 268-276
- Ludwig, W., Probst, J. L., Kempe, S, 1996. Predicting the oceanic input of organic carbon by continental erosion. *Global Biogeochemical Cycles* 10: 23–41
- Malcolm, R.L and McKinley, P.W, 1989. Methods and importance of suspended-organic-carbon determination in hydrologic studies. *Geological Survey Water-supply Paper 2326-A: 69-75*
- Marczak, L.B., Sakamaki, T., Turvey, S.L., Deguise, I., Wood, S.L., Richardson, J.S, 2010. Are forested buffers an effective conservation strategy for riparian fauna? An assessment using meta-analysis. *Ecological Applications*, 20: 126–134.
- Marthews TR., Metcalfe, D., Malhi, Y., Phillips, O., Huaraca Huasco, W., Riutta, T., Ruiz Jaén, M., Girardin, C., Urrutia, R., Butt, N., Cain, R., Oliveras Menor, I., and colleagues from the RAINFOR and GEM networks, 2012. Measuring Tropical Forest Carbon Allocation and Cycling: A RAINFOR-GEM Field Manual for Intensive Census Plots (v2.2). Manual, Global Ecosystems Monitoring network. Online: <http://gem.tropicalforests.ox.ac.uk/>. (Accessed 25.05.2015)

- Marvin-DiPasquale, M., Windham-Myers, L., Agee, J.L., Kakouros, E., Kieu, L.H., Fleck, J.A., Alpers, C.N., Stricker, C.A, 2014. Methylmercury production in sediment from agricultural and non-agricultural wetlands in the Yolo Bypass, California, USA. *Science of the Total Environment* 484: 288-299
- Marwick, T.R., Tamooh, F., Teodoru, C.R., Borge, A.V., Darchambeau, F., Bouillon S, 2015. The age of river-transported carbon: a global perspective. *Global Biogeochemical Cycles* 29: 122-137
- McDowell, W.H and Likens, G.E, 1988. Origin, composition and flux of dissolved organic carbon in the Hubbard Brook valley. *Ecological Monographs* 58: 177–195
- McGlynn, B. L and McDonnell, J.J, 2003. Role of discrete landscape units in controlling catchment dissolved organic carbon dynamics, *Water Resources Research* 39: 1090, doi:10.1029/2002WR001525.
- McKnight D.M., Boyer, E.W., Westerhof, P.K., Doran, P.T., Thomas, K., Andersen, D.T, 2001. Spectrofluorometric characterization of dissolved organic matter for indication of precursor organic material and aromaticity, *Limnology and Oceanography* 46: 38-48
- Medeiros, P. M., Seidel, M., Ward, N.D., Carpenter, E.J., Gomes, H.R., Niggemann, J., Krusche, A.V., Richey, J.E., Yager, P.L., Dittmar, T, 2015. Fate of the Amazon River dissolved organic matter in the tropical Atlantic Ocean. *Global Biogeochemical Cycles*, 29: 677–690
- Melling, L and Henson, I.E, 2011. Greenhouse gas exchange of tropical peatlands– a review. *Journal of Oil Palm Research* 23: 1087-1095
- Melling, L., Hatano, R., Goh, K.J, 2005. Soil CO₂ flux from three ecosystems in tropical peatland of Sarawak, Malaysia. *Tellus* 75:1–11

- Melling, L., Lau, J. U., Goh, K. J., Hartono, R., Osaki, M, 2006. Soils of Loagan Bunut National Park, Sarawak, Malaysia. Final Report, Peat Swamp Forests Project MAL/99/ G31, UNDP, GEF, Department of Agriculture, Sarawak, Malaysia.
- Melling, L., Goh, K.J., Beauvais, C., Hatano, R, 2007. Carbon flow and budget in a young mature oil palm agroecosystem on deep tropical peat. In: Rieley J.O., Banks C.J., & Radjagukguk B., (Ed.) Proceedings of the International Symposium and Workshop on Tropical Peatland, Yogyakarta, Indonesia
- Melling, L., Goh, K.J., Beauvais, C., Hatano, R, 2008. Carbon flow and budget in a young mature oil palm agroecosystem on deep tropical peat. *The Planter* 84: 21-25
- Melling, L., Goh, K.J, Chaddy, A., Hatano, R, 2014. Soil CO₂ flux from different ages of oil palm in tropical peatland of Sarawak, Malaysia. In: *Progress in Soil Science*. Switzerland: Springer International Publishing, pp 447-455
- Meybeck, M, 1982. Carbon, nitrogen and phosphorus transport by World Rivers. *American Journal of Science* 282: 401-450
- Meybeck, M, 1993. Riverine transport of atmospheric carbon: Sources, global typology and budget. *Water, Air and Soil Pollution* 70: 443-463
- Meyer, J.L., Wallace, J.B., Eggert, S.L, 1998. Leaf litter as a source of dissolved organic carbon in streams. *Ecosystems* 1: 240-249
- Miettinen, J and Liew, S.C, 2010a. Status of peatland degradation and development in Sumatra and Kalimantan, *AMBIO* 39: 394-401

- Miettinen, J. and Liew, S.C, 2010b. Degradation and development of peatlands in Peninsular Malaysia and in the islands of Sumatra and Borneo since 1990. *Land degradation and development* 21:285-296
- Miettinen, J., Hooijer, A., Shi, C., Tollenaar, D., Vernimmen, R., Liew, S.C., Malins, C., Page, S.E, 2012a. Extent of industrial plantations on Southeast Asian peatlands in 2010 with analysis of historical expansion and future projections. *Global Change Biology Bioenergy* 4: 908-918
- Miettinen, J., Hooijer, A., Tollenaar, D., Page, S., Malins, C., Vernimmen, R., Chi, C., Liew, S.C, 2012b. Historical Analysis and Projection of Oil Palm Plantation Expansion on Peatland in Southeast Asia. White Paper Number 17. Washington DC: International Council on Clean Transportation
- Miettinen, J., Shi, C., Liew, S.C, 2011. Deforestation rates in insular Southeast Asia between 2000 and 2010. *Global Change Biology* 17: 2261–2270
- Miettinen, J., Shi, C., Liew, S.C, 2016. Land cover distribution in the peatlands of Peninsular Malaysia, Sumatra and Borneo in 2015 with changes since 1990. *Global Ecology and Conservation* 6: 67-78
- Miettinen, J., Hooijer, A., Vernimmen, R., Liew, S.C., Page, S.E, 2017. From carbon sink to carbon source: extensive peat oxidation in insular Southeast Asia since 1990. *Environmental Research Letters* 12: 024014
- Mishra, S., Lee, W.A., Hooijer, A., Reuben, S., Sudiana, L.M., Idris, A., Swarup, S, 2014. Microbial and metabolic profiling reveal strong influence of water table and land-use patterns on classification of degraded tropical peatlands. *Biogeosciences* 11: 1727-1741

- Moatar, F and Meybeck, M, 2005. Compared performances of different algorithms for estimating annual nutrient loads discharged by the eutrophic River Loire. *Hydrological Processes* 19: 429-444
- Monteiro, M.T.F., Oliveira, S.M, Luizão, F.J., Cândido, L.A., Ishida, F.Y., Tomasella, J. 2013. Dissolved organic carbon concentration and its relationship to electrical conductivity in the waters of a stream in a forested Amazonian blackwater catchment. *Plant Ecology and Diversity*, 7, 205-213.
- Monteith, D.T., Stoddard, J.L., Evans, C.D., de Wit, H.A., Forsius, M., Høgasen, T., Wilander, A., Skjelkvale, B.L., Jeffries, D.S., Vuorenmaa, J., Keller, B., Kopacek, J., Vesely, J, 2007. Dissolved organic carbon trends resulting from changes in atmospheric deposition chemistry. *Nature* 450: 537–440
- Monteith, J.L, 1965. Evaporation and environment. *Symposia of the Society for Experimental Biology* 19: 205 - 234
- Monteith, J.L, 1995. A reinterpretation of stomatal responses to humidity. *Plant, Cell & Environment*, 18: 357–364
- Montgomery, D.R, 2007. Soil erosion and agricultural sustainability. *Proceedings of the National Academy of Sciences* 104: 13268-13272
- Moody, C.S., Worrall, F., Evans, C.D., Jones. T.G, 2013. The rate of dissolved organic carbon through a catchment. *Journal of Hydrology* 492: 139-150
- Moore, S., Gauci, V., Evans., C.D., Page, S.E, 2011. Fluvial organic carbon losses from a Bornean blackwater river. *Biogeosciences* 8: 901-909

- Moore, E., Evans, C.D., Page, S.E., Hoscito, A., Gauci, V, manuscript in preparation. A large fluvial carbon pulse from El Niño fire-affected tropical peatlands
- Moore, S., Evans, C.D., Page, S.E., Garnett, M.H., Jones, T.H., Freeman, C., Hooijer, A., Wiltshire, A., Limin, S., Gauci, V, 2013. Deep instability of deforested tropical peatlands revealed by fluvial organic carbon fluxes. *Nature* 493: 660-664
- Moore, T.R, 1987. A preliminary study of the effects of drainage and harvesting on water quality in ombrotrophic bogs near Sept-Iles, Quebec, 1987. *American Water Works Association* 23:785–791
- MPOB, 2008. Malaysian oil palm statistics 2007. 27th Edition. Kuala Lumpur: Malaysian Palm Oil Board, pp189
- MPOB, 2010. Best management practices for oil palm planting on peat: optimum groundwater table. MPOB Information Series, 472. Kuala Lumpur: Malaysian Palm Oil Board
- MPOB, 2011. Best management practices of oil palm cultivation on peatland. Online: [http://www.jkm.gov.my/file/3-%20MPOB%E2%80%99s%20Guidelines%20for%20Oil%20Palm%20on%20Peat%20\(Tarmizi\).pdf](http://www.jkm.gov.my/file/3-%20MPOB%E2%80%99s%20Guidelines%20for%20Oil%20Palm%20on%20Peat%20(Tarmizi).pdf) (Accessed 04/12/2014)
- MPOB, 2012. Malaysian Oil Palm Statistics 2012. Malaysian Oil Palm Board, Selangor
- Muller, D., Warneke, T., Rixen, T., Muler, M., Jamahari, S., Denis, S., Mujahid, A., Notholt, J, 2015. Later carbon fluxes and CO₂ outgassing from a tropical peat-draining river. *Biogeosciences* 12: 5967-5979

- Muller, D., Warneke, T., Rixen, T., Muler, M., Mujahids, A., Banges, H.W., Notholt, J, 2016. Fate of peat-derived carbon and associated CO₂ and CO emissions from two Southeast Asian estuaries. *Biogeosciences Discussion* 12: 8299-8340
- Muller, F.L.L and Tankéré-Muller, S.P.C, 2012. Seasonal variations in surface water chemistry at disturbed and pristine peatland sites in the Flow Country of northern Scotland. *Science of the Total Environment* 435-436: 351-362
- Murdiyarso, D., Hergoualc'h, K., Verchot, L. V, 2010. Opportunities for reducing greenhouse gas emissions in tropical peatlands. *Proceedings in National Academy of Science of the United States of America* 107: 19655-19660
- Murdiyarso, D and Kauffman, J.B, 2011. Addressing climate change adaptation and mitigation in tropical wetland ecosystems of Indonesia. Online:
http://www.cifor.org/publications/pdf_files/infobrief/3512-infobrief.pdf
(Accessed 14/10/2013)
- Mutabaruka, R., Hairiah, K., Cadisch, G, 2007. Microbial degradation of hydrolysable and condensed tannin polyphenol-protein complexes in soils from different land-use histories. *Soil Biology and Biochemistry* 39: 1479–1492
- Najmaddin. P.M., Whelan, M.J., Balzter, H, 2017. Application of Satellite-Based Precipitation Estimates to Rainfall-Runoff Modelling in a Data-Scarce Semi-Arid Catchment. *Climate*, DOI: 10.3390/cli5020032
- Nash, J.E and Sutcliffe, J.V, 1970. River flow forecasting through conceptual models part I—a discussion of principles. *Journal of Hydrology* 10: 282-290

- Nguyen, T., Roddick, F.A., Fan, L., 2012. Biofouling of Water Treatment Membranes: A Review of the Underlying Causes, Monitoring Techniques and Control Measures. *Membranes* 2: 804-840
- Norman, L and Thomas, D.N, 2014. Long-term storages of dissolved organic carbon. Technical note, Researchgate, DOI: 10.13140/2.1.3331.5200
- Norrman, B, 1993. Filtration of water samples for DOC studies. *Marine Chemistry* 41: 239-242
- O'Driscoll, N.J., Siciliano, S.D., Peak, D., Carignan, R., Lean, D.R.S, 2006. The influence of forestry activity on the structure of dissolved organic matter in lakes: implications for mercury photoreactions. *Science of the Total Environment* 366: 880–893.
- Olefeldt, D., Roulet, N. T., Bergeron, O., Crill, P., Backstrand, K., Christensen, T. R, 2012. Net carbon accumulation of a high-latitude permafrost palsamire similar to permafrost-free peatlands. *Geophysical Research Letters* 39: L03501, DOI:10.1029/2011GL050355
- Olefeldt, D., Roulet, N., Giesler, R., Persson, A, 2013. Total waterborne carbon export and DOC composition from ten nested subarctic peatland catchments- importance of peatland cover, groundwater influence, and inter-annual variability of precipitation patterns. *Hydrological processes* 27: 2280-2294
- Omar, W., Abd Aziz, N., Tarmizi, A., Harun, M.H., Kushairi, A, 2010. Mapping of oil palm cultivation on peatland in Malaysia (No. 529). Kuala Lumpur, Malaysia: MPOB
- Pacheco, F.S., Roland, F., Downing, J.A, 2013. Eutrophication reverses whole-lake carbon budgets. *Inland Waters* 4: 41-48

- Page, S.E., Rieley, J.O., Shoty, W. and Weiss, D. 1999. Interdependence of peat and vegetation in a tropical swamp forest. *Philosophical Transactions of the Royal Society, Series B* 354:1885–1897
- Page, S.E., Siegert, F., Rieley, J.O., Boehm, H-D.V., Jaya, A. and Limin, S.H. 2002. The amount of carbon released from peat and forest fires in Indonesia during 1997. *Nature* 420:61-65
- Page, S.E., Wust, R.A.J., Weiss, D., Rieley, J.O., Shoty, W. and Limin, S.H., 2004. A record of Late Pleistocene and Holocene carbon accumulation and climate change from an equatorial peat bog (Kalimantan, Indonesia): implications for past, present and future carbon dynamics. *Journal of Quaternary Science* 19:625-635
- Page, S.E., Hoscilo, A., Langner, A., Tansey, K., Siegert, F., Limin, S., Rieley, J.O. 2009. Tropical peatland fires in Southeast Asia. Pages 263–287 in Cochrane MA (eds.) *Tropical Fire Ecology: Climate Change, Land Use and Ecosystem Dynamics*. Springer, pp 263-287
- Page, S., Wust, R., Banks, C. 2010. Past and present carbon accumulation and loss in southeast Asian peatlands. *Scientific Highlights: Peatlands Pages News* 18: 25-26
- Page S. E., Morrison, R., Malins, C., Hooijer, A., Rieley, J. O., Jauhiainen, J, 2011a . Review of peat surface greenhouse gas emissions from oil palm plantations in Southeast Asia (ICCT white paper 15). Washington: International Council on Clean Transportation.
- Page, S.E., Rieley, J.O., Banks, C.J, 2011b. Global and regional importance of the tropical peatland carbon pool. *Global Change Biology* 17: 798-818

- Page, S.E and Baird, A.J, 2016. Peatlands and Global Change: Response and Resilience. *Annual Review of Environmental Resources* 41: 35-37
- Page, S.E and Hooijer, A, 2016. In the line of fire: the peatland of Southeast Asia. *Philosophical Transactions Royal Society B* 371: 20150176
- Palmer, S.M., Evans, E.D., Chapman, P.J., Burden, A., Jones, T.G., Allott, T.E.H., Evans, M.G., Moody, C.S., Worall, F., Holden, J, 2016. Sporadic hotspots for physio-chemical retention of aquatic organic carbon: from peatland headwater source to sea. *Aquatic Sciences* 78: 491-504
- Pan, F., Stieglitz, M., McKane, R.B, 2012. An algorithm for treating flat areas and depressions in digital elevation models using linear interpolation. *Water Resources Research* 48, doi:10.1029/2011WR010735
- Panetta, R.J., Ibrahim, M., Gelinas, Y, 2008. Coupling a High-Temperature Catalytic Oxidation Total Organic Carbon Analyzer to an Isotope Ratio Mass Spectrometer To Measure Natural-Abundance $\delta^{13}\text{C}$ -Dissolved Organic Carbon in Marine and Freshwater Samples. *Analytical Chemistry* 80: 5235-5339
- Pangala, S.R., Moore, S., Hornibrook, E.R.C., Gauci, V, 2013. Trees are major conduits for methane egress from tropical forested wetlands. *New Phytologist* 197: 524-531
- Pango, T., Bida, M., Kenny, J.E, 2014. Trends in Levels of Allochthonous Dissolved Organic Carbon in Natural Water: A Review of Potential Mechanisms under a Changing Climate. *Water* 6: 2862-2897
- Param Agricultural Soil Survey, 2013. Soils of Sebungun Estate, Bintulu Division, Sarawak, Malaysia

- Park, S., Joe, S, K.S., Han, H., Kim, H.S, 1999. Characteristics of dissolved organic carbon in the leachate from Moonam Sanitary Landfill. *Environmental Technology* 20: 419-424
- Pastor, J., Solin, J., Bridgham, S.D., Updegraff, K., Harth, C., Weishampel, P., Dewey, B, 2003. Global warming and the export of dissolved organic carbon from boreal peatlands. *Oikos* 100: 380–386
- Pawson, R.R., Lord, D.R., Evans, M.G., Allott, T.E.H, 2008. Fluvial organic carbon flux from an eroding peatland catchment, southern Pennines, UK. *Hydrology and Earth System Science* 12: 625 - 634
- Pawson, R.R., Evans, M.G., Allott, T.E.H, 2012. Fluvial carbon flux from headwater peatland streams: significance of particulate carbon flux. *Earth Surface Processes and Landforms* 37: 1203-1212
- Peacock, M., Burden, A., Cooper, M., Dunn, C., Evans, C.D., Fenner, N., Freeman, C., Gough, R., Hughes, D., Jones, T., Lebron, I., West, M., Zielinski, P, 2013. Quantifying dissolved organic carbon concentrations in upland catchments using phenolic proxy measurements. *Journal of hydrology* 477: 251-260
- Peacock, M., Jones, T.G., Airey, B., Johncock, A., Evans, C.D., Lebron, I., Fenner, N., Freeman, C, 2014a. The effect of peatland drainage and rewetting (ditch blocking) on extracellular enzyme activities and water chemistry. *Soil Use and Management*, DOI: 10.1111/sum.12138
- Peacock, M., Evans, C.D., Fenner, N., Freeman, C., Gough, R., Jones, T.G., Lebron, I, 2014b. UV-visible absorbance spectroscopy as a proxy for peatland dissolved organic carbon (DOC) quantity and quality: considerations on wavelength and absorbance degradation. *Environmental Science: Processes and Impacts* 16: 1445-1461

- Peacock, M., Freeman, C., Gauci, V., Lebron, I., Evans, C.D, 2015.
Investigations of freezing and cold storage for the analysis of peatland dissolved organic carbon (DOC) and absorbance properties. *Environmental Science: Processes and Impacts*, DOI: 10.1039/C5EM00126A
- Peh, K.S-H., Balmford, A., Field, R.H., Lamb, A., Birch, J.C., Bradbury, R.B., Brown, C., Butchart, S.H.M., Lester, M., Morrison, R., Sedgwick, I., Soans, C., Stattersfield, A.J., Stroh, P.A., Swetnam, R.D., Thomas, D.H.L., Walpole, M., Warrington, S., Hughes, F.M.R, 2014. Benefits and costs of ecological restoration: Rapid assessment of changing ecosystem service values at a U.K. wetland. *Ecology and Evolution*, DOI: 10.1002/ece3.1248
- Pereira, R., Bovolo, C.I., Spencer, R. G.M., Hernes, P.J., Tipping, E., Vieth-Hillebrand, A., Pedentchouk, N., Chappell, N.A., Parkin, G., Wagner, 2014. Mobilization of optically invisible dissolved organic matter in response to rainstorm events in a tropical forest headwater river. *Geophysical Research Letter* 41: 1202-1208
- Peuravuori, J and Pihlaja, K, 1997. Molecular size distribution and spectroscopic properties of aquatic humic substances. *Analytica Chimica Acta* 337:133-149
- Pickard, A.E., Heal, K.V., McLeod, A.R., Dinsmore, K.J, 2017.
Temporal changes in photoreactivity of dissolved organic carbon and implications for aquatic carbon fluxes from peatlands. *Biogeosciences* 14: 1793-1809
- Podgrajsek, E., Shalee, E., Bastviken, D., Holst, J., Lindroth, A., Tranvik, L., Rutgersson, A, 2014. Comparison of floating chamber and eddy covariance measurements of lake greenhouse gas fluxes. *Biogeosciences* 11: 4225-4233

- Posa, M.R.C., Wijedasa, L.S., Corlett, R.T, 2011. Biodiversity and conservation of tropical peat swamp forests. *Bioscience* 16: 49-57
- Pullan, S.P., Whelan, M.J., Rettino, J., Filby, K., Eyre, S., Holman, I.P, 2016. Development and application of a catchment scale pesticide fate and transport model for use in drinking water risk assessment. *Science of the Total Environment* 563-564: 434-447
- Qassim, S.M., Dixon, S.D., Rowson, J.G., Worrall, F., Evans, M.G., Bonn, A, 2014. A 5-year study of the impact of peatland revegetation upon DOC concentrations. *Journal of Hydrology* 517 part D: 3578-3590
- Quevauviller, P.P, 1995. *Quality Assurance in Environmental Monitoring: Sampling and Sample Pretreatment*. Germany: Wiley VCH Publishers
- Rais, D.S, 2011. Peatland hydrology and its role in tropical peatland sustainability. *Proceedings from National Symposium of Ecohydrology, Jakarta, March, 2011*
- Raymond, P.A and Bauer, J.E, 2001. Riverine export of aged terrestrial organic matter to the North Atlantic Ocean. *Nature* 497: 497-500
- Raymond, P.A., McClelland, J.W., Holmes, R.M., Zhulidov, A.V., Mull, K., Peterson, B.J., Striegl, R.G., Aiken, G.R., Gurtovaya, T.Y, 2007. Flux and age of dissolved organic carbon exported to the Arctic Ocean: A carbon isotopic study of the five largest arctic rivers. *Global Biogeochemical Cycles* 21, GB4011, DOI: 10.1029/2007GB002934

- Raymond, P.A., Hartmann, J., Lauerwald, R., Sobek, S., McDonald, C., Hoover, M., Butman, D., Striegl, R., Mayorga, E., Humborg, C., Kortelainen, P., Dürr, H., Meybeck, M., Ciais, P., Guth, P., 2013, Global Carbon dioxide emissions from inland waters. *Nature* 503: 355-359
- Reddy, K.R and DeLaune, R.D, 2008. *Biogeochemistry of wetlands: science and application*. Florida: Taylor & Francis Group
- Rehman, S.A,U., Ullah, W., Khurshid, M, 2014. Carbon Dioxide emissions from Tropical Peat swamp Forests: A review of Processes and Controls with special emphasis to Indonesia. *Science. Scientia Agriculturae* 2: 146-150
- Reijnders, L. and Huijbregts, M. A. J, 2008. Palm oil and the emission of carbon-based greenhouse gases. *Journal of Cleaner Production* 16: 477-482
- Reinhardt , G., Rettenmaier, N., Gaertner, S., Pastowski, A, 2007. Rain forest for biodiesel? Ecological effects of using palm oil as a source of energy. Frankfurt, Germany: WWF; 2007. Online: http://www.wwf.de/fileadmin/fm-wwf/pdf_neu/wwf_palmoil_study_english.pdf (Accessed 18/11/2014)
- Richey, J.E., Melack, J.M., Aufdenkampe, A.K., Ballester, V.M. and Hess, L.L, 2002. Outgassing from Amazonian rivers and wetlands as a large tropical source of atmospheric CO₂. *Nature* 416:617-620.
- Rieley, J., Siegert, F., Zhukov, B., Oeretel, D., Limin, S.H., Page S.E, 2004. Peat fires detected by the BIRD satellite. *Journal of Remote Sensing* 25: 3221-3230

- Rieley, J.O. and Page, S.E, 2005. Wise Use Guidelines for Tropical Peatlands. The Netherlands: Alterra, Wageningen
- Ritson, J.P., Graham, N.J.D., Templeton, W.R., Clar, J.M., Gough, R., Freeman, C, 2014. The impact of climate change on the treatability of dissolved organic matter (DOM) in upland water supplies: A UK perspective. *Science of the Total Environment* 473-474: 714-730
- Rixen, T., Baum, A., Pohlmann, T. Balzer, W., Samiaji J., Jose, C, 2008. The Siak, a tropical black water river in central Sumatra on the verge of anoxia. *Biogeochemistry* 90: 129-140
- Rixen, T., Baum, A., Wit, F., Samiaji, J, 2016. Carbon leaching from tropical peat soils and consequence for carbon balances. *Frontiers in Earth Science* 4, DOI: 10.3389/feart.2016.00074
- Roll, A., Meijide, A., Hardanto, A., Hendrayanto., Knohl, A., Holscher, D, 2015. Transpiration in an oil palm landscape: effects of palm age. *Biogeosciences* 12: 5619-5633
- Roulet, N. T., Lafleur, P. M., Richard, P. J. H., Moore, T. R., Humphreys, E. R., Bubier, J, 2007. Contemporary carbon balance and late Holocene carbon accumulation in a northern peatland. *Global Change Biology* 13: 397–411
- Sa'don, N.M., Abdul Karim, A.R., Jaol, W., Wan Lili, W.H, 2015. Sarawak Peat Characteristics and Heat Treatment. *UNIMAS e-Journal of Civil Engineering* 5: 6-12

- Sakata, R., Shimada, S., Arai, H, Yoshioka, N., Yoshioka, R., Aoki, H., Kimoto, N., Sakamoto, A., Melling, L., Inubushi, K, 2014. Effect of soil types and nitrogen fertilizer on nitrous oxide and carbon dioxide emissions in oil palm plantations. *Soil Science and Plant Nutrition*, DOI:10.1080/00380768.2014.960355
- Sandon, R.C., Hawkins, J.M.B., Bol, R., Worsfold, P.J, 2013. Export of dissolved organic carbon and nitrate from grassland in winter using high temporal resolution, in situ UV sensing. *Science of the Total Environment* 456-457: 384-391
- Sangkok, F.E., Maie, N., Melling, L., Watanabe, A, 2017. Evaluation on the decomposability of tropical forest peat soils after conversion to an oil palm plantation. *Science of the Total Environment* 587-588: 381-388
- SarVision, 2011. Impact of oil palm plantations on peatland conversion in Sarawak 2005-2010.
Online:<http://www.wetlands.org/Portals/0/publications/Report/Malaysia%20Sarvision.pdf> (Accessed 10/01/2015)
- Schlünz, B and Schneider R.R, 2000. Transport of terrestrial organic carbon to the oceans by rivers: re-estimating flux- and burial rates. *International Journal of Earth Sciences* 88: 599-606
- Schrier-Uijl, A. P., Veenendaal, E. M., Leffelaar, P. A., van Huissteden, J. C., Berendse, F 2010. Methane emissions in two drained peat agro-ecosystems with high and low agricultural intensity. *Plant Soil*, doi:10.1007/s11104-009-0180-1
- Schrier-Uijl, A.P., Silvius, M., Parish. F., Lim, K.H., Rosediana, S., Anshari, G, 2013. Environmental and social impacts of oil palm cultivation on tropical peat. A scientific review. Reports from the Technical Panels of the 2nd Greenhouse Gas Working Group of the Roundtable on Sustainable Palm Oil (RSPO).

- Schwalm, M and Zeitz, J, 2014. Dissolved organic carbon concentrations vary with season and land use – investigations from two fens in Northeastern Germany over two years. *Biogeosciences Discussions* 11: 7079-7111
- Schwalm, M and Zeitz, J, 2015. Concentrations of dissolved organic carbon in peat soils as influenced by land use and site characteristics — A lysimeter study. *CATENA* 127: 72-79
- Selberg, A., Viik, M., Ehapalu, K., Tenno, T, 2011. Content and composition of natural organic matter in water of Lake Pitkjarv and mire feeding Kuke River (Estonia). *Journal of Hydrology* 400: 274-280
- Shafer, M.M., Perkins, D.A., Antkiewicz, D.S., Stone, E.A., Qurasishi, T.A., Schauer, J.J, 2010. Reactive oxygen species activity and chemical speciation of size-fractionated atmospheric particulate matter from Lahore, Pakistan: an important role for transition metals. *Journal of Environmental Monitoring* 12: 704-715
- Sharp, J.H, 1993. The dissolved organic carbon controversy: an update. *Oceanography* 6: 45-50
- Sharp, J.H. Peltzer, E.T., Alperin., M.J., Cauwet, G., Farrington, J.W., Fry, B., Karl, D.M., Martin, J.H., Spitzzy,A., Tugrul, S., Carlson, C.A, 1993. Procedures subgroup report. *Marine chemistry* 41:37-49
- Sinsabaugh, S. E., and Forman, C.M, 2003. Integrating dissolved organic matter metabolism and microbial diversity: An overview of conceptual models, in *Aquatic Ecosystems: Interactivity of Dissolved Organic Matter* (eds) S. E. Findlay and Sinsabaugh, R.L. Academic Press, California, pp. 426–454

- Sivaprakasam, S., Murugappan, A., Mohan, S, 2011. Modified Hargreaves equation for estimation of ET_0 in hot and humid location in Tamilnadu State, India.
- Sjögersten, S., Black, C.R., Evers, S., Hoyos-Santillan, J., Wright, E.L., Turner, B.L, 2014. Tropical wetlands: a missing link in the global carbon cycle? *Global Biogeochemical cycles*. DOI: 10.1002/2014GB004844
- Smith, S. V., W. H. Renwick, R. W. Buddemeier, and C. J. Crossland. 2001. Budgets of soil erosion and deposition for sediments and sedimentary organic carbon across the conterminous United States. *Global Biogeochemical Cycles* 15 (3): 697– 707.
- Spencer, R. G. M., Butler, K.D., Aiken, G.R, 2012. Dissolved organic carbon and chromophoric dissolved organic matter properties of rivers in the USA, *Journal of Geophysical Research* 117: doi: 10.1029/2011JG001928.
- Spencer, R.G.M., Bolton, L., Baker, A, 2007. Freeze/thaw and pH effects on freshwater dissolved organic matter fluorescence and absorbance properties from a number of UK locations. *Water Research* 41: 2941-2950
- Spencer, R.G.M., Hernes, P.J., Ruf, R., Baker, A., Dyda, R.Y., Stubbins, A., Six, J, 2010. Temporal controls on dissolved organic matter and lignin biogeochemistry in a pristine tropical river, Democratic Republic of Congo. *Journal of Geophysical Research* 115, DOI: 10.1029/2009JG001180.
- Stallard, R. F. 1998. Terrestrial sedimentation and the carbon cycle: Coupling weathering and erosion to carbon burial. *Global Biogeochemical Cycles* 12:231– 257.

- Stets, E.G., Striegl, R.G., Aiken, G.R., Rosenberry, D.O., Winter, T.C., 2009. Hydrologic support of carbon dioxide flux revealed by whole-lake carbon budgets. *Journal of Biophysical Research: Biogeosciences*: DOI: 10.1029/2008JG000783
- Strack, M., Waddington, J.M., Bouronniere, R.A., Buckton, E.L., Shaw, K., 2008. Effect of water table drawdown on peatland dissolved organic carbon export and dynamics. *Hydrological Processes* 22: 3373-3385
- Strakova, P., Penttilä, T., Laine, J., Laiho, R., 2012. Disentangling direct and indirect effects of water table drawdown on above-and belowground plant litter decomposition: consequences for accumulation of organic matter in boreal peatlands. *Global Change Biology* 18: 322–335
- Strand, T.L., Abrahamsen, G., Stuanes, A.O., 2002. Leaching from organic matter-rich soils by rain of different qualities: I. Concentrations. *Journal of Environmental Quality* 31: 547-556
- Strohmeier, S., Knorr, K.H., Reichert, M., Frei, S., Fleckenstein, J.H., Peiffer, S., Matzner, E., 2013. Concentrations and fluxes of dissolved organic carbon in runoff from a forested catchment: insights from high frequency measurements. *Biogeosciences* 10: 905
- Stutter, M.I., Dunn, S.M., Lumsdon, D.G., 2012. Dissolved organic carbon dynamics in a UK podzolic moorland catchment: linking storm hydrochemistry, flow path analysis and sorption experiments. *Biogeosciences* 9: 2159-2175
- Suzuki, S., Nagano, T., Waijaroen, S., 1999. Influences of Deforestation on Carbon Balance in a Natural Tropical Peat Swamp Forest in Thailand. *Environmental Control in Biology* 37: 115-128

- Tamooh, K., Borges, A.V., Meysman, F.J.R., Van Den Meersche., Dehairs F., Merckx, R., Bouillon, S, 2013. Dynamics of dissolved inorganic carbon and aquatic metabolism in the Tana River, Kenya. *Biogeosciences* 10: 6911-6923
- Thurman, E.M, 1985. Developments in Biogeochemistry. In: Nijhoff, M (eds), *Organic Geochemistry of Natural Waters*
- Tipping, E., Corbishley, H.T., Koprivnjak, J-F., Lapworth, D.J., Miller, M.P., Vincent, C.D., Hamilton-Taylor, J, 2009. Quantification of natural DOM from UV absorption at two wavelengths. *Environmental Chemistry* 6: 472-476
- Tipping, E., Billett M.F., Bryant C.L., Buckingham S. and Thacker S.A, 2010. Sources and ages of dissolved organic matter in peatland streams: evidence from chemistry mixture modelling and radiocarbon data. *Biogeochemistry* 100: 121-137
- Tonks, A.J., Aplin, P., Beriro, D.J., Cooper, H., Evers, S., Vane, C.H., Sjögersten, S, 2017. Impacts of conversion of tropical peat swamp forest to oil palm plantation on peat organic chemistry, physical properties and carbon stocks *Geoderma* 289: 36-45
- Tranvik, L.J., Downing, J.A., Cotner, J.B., Loiselle, S.A., Striegl, R.G., Ballatore, T.J., Dillon, P., Finlay, K., Fortino, K., Knoll, L.B., Kortelainen, P.L., Kutser, T., Larsen, S., Laurion, I., Leech, D.M., McCalliser, S.L., McKnight, D.M., Melack, J.M., Overholt, E., Porter, J.A., Prairie, Y., Kenwick, W.H., Roland, F., Bradford, F., Sherman, B.S., Schindler, D.W., von Wachenfeldt, E., Wehenmeyer, G.A, 2009. Lakes and reservoirs as regulators of carbon cycling and climate. *Limnology and Oceanography* 54: 2298-2314

- Turetsky, M.R., Benscoter, B., Page, S., Rein, G., van der Werf, G. R., Watts, A, 2015. Global vulnerability of peatlands to fire and carbon loss. *Nature Geoscience* 8: 11-14
- Tunaley, C., Tetzlaff, D., Lessels, J., Souldby, C, 2016. Linking high frequency DOC dynamics to the age of connected water sources, *Water Resources Research* 52: 5232–5247
- Turunen, J., 2003. Past and present carbon accumulation in undisturbed boreal and subarctic mires: a review. *Suo* 54:15-28
- Valin, H., Frank, S., Pirker, J., Mosnier, A., Forsell, N., Havlik, P, 2014. Improvements to GLOBIOM for modelling of biofuels indirect land use change. Online : http://www.globiom-iluc.eu/wp-content/uploads/2014/09/GLOBIOM_All_improvements_Sept14.pdf (Accessed 24/11/2014)
- van Genuchten, M.Th., 1980. A closed-form equation for predicting the hydraulic conductivity of unsaturated soil. *Soil Science Society of America Journal* 44, 892–898
- Veloo, R., van Ranst, E., Selliah, P, 2015. Peat characteristics and its impact on oil palm yield. *NJAS, Wageningen Journal of Life Sciences* 72-73: 33-40
- Verwer, C., Meer, P.V.D., Nabuurs, G-J., 2008. Review of carbon flux estimates and other greenhouse gas emissions from oil palm cultivation on tropical peatlands - Identifying the gaps in knowledge. Wageningen, Alterra, Alterra-rapport 1731.
- Wagner, S., Jaffe, R., Cawley, K., Dittmar, T., Stubbins, A, 2015. Associations Between the Molecular and Optical Properties of Dissolved Organic Matter in the Florida Everglades, a Model Coastal Wetland System. *Frontiers in Chemistry* 3: 1-14

- Wallage, Z.E., Holden, J., McDonald, A.T, 2006. Drain blocking: an effective treatment for reducing dissolved organic carbon loss and water discolouration in a drained peatland. *Science of the Total Environment* 367:811–821
- Walling, D.E and Webb, B.W, 1985. Estimating the discharge of contaminants to coastal waters by rivers: Some cautionary comments. *Marine Pollution Bulletin* 16: 488-492
- Wang, G-S and Hsieh, S-T, 2001. Monitoring natural organic matter with scanning spectrophotometer. *Environmental International* 26: 205-212
- Wang, X., Liu, L., Piao, S., Janssens, I. A., Tang, J., Liu, W., Chi, Y., Wang, J., Xu, S, 2014. Soil respiration under climate warming: differential response of heterotrophic and autotrophic respiration. *Global Change Biology* 20: 3229–3237
- Ward, R.C and Robinson, M, 2000. *Principals of Hydrology*. McGraw Hill Publishing, London, pp 127- 130
- Weishaar, J.L., Aiken, G.R., Bergamaschi, B.A., Fram, M.S., Fujii, R. and Mopper, K., 2003. Evaluation of specific ultraviolet absorbance as an indicator of the chemical composition and reactivity of dissolved organic carbon. *Environmental Science and Technology* 37:4702-4708
- Wetlands International, 2010. A quick scan of peatlands in Malaysia. Wetlands International-Malaysia: Petaling Jaya, Malaysia. Online: http://www.wetlands.org/Portals/0/publications/Report/Quickscan%20of%20Peatlands%20in%20Malaysia_Feb3.pdf (Accessed 29.10.2014)

- Wetlands International, 2016. Towards Sustainable Palm Oil. Online:
<https://www.wetlands.org/casestudy/towards-sustainable-palm-oil/>
(Accessed 04.05.2017)
- Whalen, S.C and Cornwell, J. C, 1985. Nitrogen and phosphorus and organic-carbon cycling in an Arctic lake. *Canadian Journal of Fisheries and Aquatic Sciences* 42: 797-808
- Whelan, M.J and Gandolfi, C, 2002. Modelling of spatial controls on denitrification at the landscape scale. *Hydrological Processes* 16: 1437–1450.
- Whittington, P.N and Price, J.S, 2006. The effects of water table draw-down (as a surrogate for climate change) on the hydrology of a fen peatland, Canada. *Hydrological Processes* 20: 3589–3600
- Wicke, B., Dornburg, V., Junginger, J., Faaij, A 2008. Different palm oil production systems for energy purposes and their greenhouse gas implications. *Biomass and Bioenergy* 32: 1322-1337
- Wicke, B., Sikkema, R., Dornburg, V., Faaij, A, 2011. Exploring land use changes and the role of palm oil production in Indonesia and Malaysia. *Land Use Policy* 28: 193-206.
- Wickland, K.P., Neff, J.C., Aiken, G.R, 2007. Dissolved organic carbon in Alaskan boreal forest: sources, chemical characteristics, and biodegradability. *Ecosystems* 10: 1323-1340

Wijedasa, L. S., Jauhiainen, J., Könönen, M., Lampela, M., Vasander, H., Leblanc, M.-C., Evers, S., Smith, T. E. L., Yule, C. M., Varkkey, H., Lupascu, M., Parish, F., Singleton, I., Clements, G. R., Aziz, S. A., Harrison, M. E., Cheyne, S., Anshari, G. Z., Meijaard, E., Goldstein, J. E., Waldron, S., Hergoualc'h, K., Dommain, R., Frolking, S., Evans, C. D., Posa, M. R. C., Glaser, P. H., Suryadiputra, N., Lubis, R., Santika, T., Padfield, R., Kurnianto, S., Hadisiswoyo, P., Lim, T. W., Page, S. E., Gauci, V., Van Der Meer, P. J., Buckland, H., Garnier, F., Samuel, M. K., Choo, L. N. L. K., O'Reilly, P., Warren, M., Sukswan, S., Sumarga, E., Jain, A., Laurance, W. F., Couwenberg, J., Joosten, H., Vernimmen, R., Hooijer, A., Malins, C., Cochrane, M. A., Perumal, B., Siegert, F., Peh, K. S.-H., Comeau, L.-P., Verchot, L., Harvey, C. F., Cobb, A., Jaafar, Z., Wösten, H., Manuri, S., Müller, M., Giesen, W., Phelps, J., Yong, D. L., Silvius, M., Wedeux, B. M. M., Hoyt, A., Osaki, M., Hirano, T., Takahashi, H., Kohyama, T. S., Haraguchi, A., Nugroho, N. P., Coomes, D. A., Quoi, L. P., Dohong, A., Gunawan, H., Gaveau, D. L. A., Langner, A., Lim, F. K. S., Edwards, D. P., Giam, X., Van Der Werf, G., Carmenta, R., Verwer, C. C., Gibson, L., Gandois, L., Graham, L. L. B., Regalino, J., Wich, S. A., Rieley, J., Kettridge, N., Brown, C., Pirard, R., Moore, S., Capilla, B. R., Ballhorn, U., Ho, H. C., Hoscilo, A., Lohberger, S., Evans, T. A., Yulianti, N., Blackham, G., Onrizal, Husson, S., Murdiyarso, D., Pangala, S., Cole, L. E. S., Tacconi, L., Segah, H., Tonoto, P., Lee, J. S. H., Schmilewski, G., Wulffraat, S., Putra, E. I., Cattau, M. E., Clymo, R. S., Morrison, R., Mujahid, A., Miettinen, J., Liew, S. C., Valpola, S., Wilson, D., D'Arcy, L., Gerding, M., Sundari, S., Thornton, S. A., Kalisz, B., Chapman, S. J., Su, A. S. M., Basuki, I., Itoh, M., Traeholt, C., Sloan, S., Sayok, A. K., Andersen, R., 2017. Denial of long-term issues with agriculture on tropical peatlands will have devastating consequences. *Global Change Biology*, 23: 977–982.

- Wilson, L., Wilson, J., Holden, J., Johnstone, I., Armstrong, A., Morris, M, 2011. Ditch blocking, water chemistry and organic carbon flux: evidence that blanket bog restoration reduces erosion and fluvial carbon loss. *Science of the Total Environment* 409: 2010–2018
- Wit, F., Muller, D., Baum, A., Warneke, T., Pranowo, W.S., Muller, M., Rixen, T, 2015. The impact of disturbed peatlands on river outgassing in Southeast Asia. *Nature Communications* 6: 1-9
- Wittinghill, K.A., Finlay, J.C., Hobbie, S.E, 2014. Bioavailability of dissolved organic carbon across a hillslope chronosequence in the Kuparuk River region, Alaska. *Soil Biology and Biochemistry* 79: 25-33
- Waldron, S., Marian Scott, E., Vihermaa, L. E., Newton, J., 2014. Quantifying precision and accuracy of measurements of dissolved inorganic carbon stable isotopic composition using continuous-flow isotope-ratio mass spectrometry. *Rapid Communications in Mass Spectrometry*, 28: 1117–1126.
- Worrall, F., Burt, T., Jaeban, R., Warburton, J., Shedden, R, 2002. Release of dissolved organic carbon from upland peat, *Hydrological Processes*, 16: 3487–3504
- Worrall, F., Burt, T.P., Adamson, J.K, 2006. The rate of and controls upon DOC loss in a peat catchment. *Journal of Hydrology* 321: 311-325
- Worrall, F., Gibson, H.S., Burt, T.P, 2008. Production vs. Solubility in controlling runoff of DOC from peat soils—The use of an event analysis. *Journal of Hydrology* 358: 84–95
- Worrall, F., Burt, T.P., Rowson, J.G., Warburton, J., Adamson, J.K, 2009. The multi-annual carbon budget of a peat-covered catchment. *Science of the Total. Environment* 407: 4084-4094

- Worrall, F and Moody, C.S, 2014. Modeling the rate of turnover of DOC and particulate organic carbon in a UK, peat-hosted stream: Including diurnal cycling in short-residence time systems. *Journal of Geophysical Research: Biogeosciences* 119: 1934–1946
- Worrall, F., Chapman, P., Holden, J., Evans, X., Artz, R., Smith, P., Grayson, R, 2011. A review of current evidence on carbon fluxes and greenhouse gas emissions from UK peatlands. JNCC Report No.442. JNCC, Peterborough
- Wösten, J.H.M., Clymans, E., Page, S.E., Rieley, J.O., Limin, S.H, 2008. Peat–water interrelationships in a tropical peatland ecosystem in Southeast Asia. *Catena* 73: 212-224.
- Xu, S., Anderson, R., Bryant, C., Cook, G.T., Dougans, A., Freeman, S., Naysmith, P., Schnabel, C., Scott, E.M., 2004. Capabilities of the new SUERC 5MV AMS facility for C-14 dating. *Radiocarbon* 46:59-64
- Xu, X.K., Luo, X.B., Jiang, S.H., Xu, Z.J, 2012 Biodegradation of dissolved organic carbon in soil extracts and leachates from a temperate forest stand and its relationship to ultraviolet absorbance, *Chinese Science Bulletin* 57: 912-920
- Yamashita, Y., Maie, N., Briceño, H., Jaffé, R. 2010. Optical characterization of dissolved organic matter in tropical rivers of the Guayana Shield, Venezuela. *Journal of Geophysical Research*, 115, DOI: 10.1029/2009JG000987.
- Yew. F. K., Sundram, K., Basiron, Y, 2010. Estimation of GHG emissions from peat used for agriculture with special reference to oil palm. *Journal of Oil Palm and the Environment* 1: 17-25

- Yule, C.M, 2010. Loss of biodiversity and ecosystem functioning in Indo-Malayan peat swamp forests. *Biodiversity and Conservation* 19: 393–409
- Yule, C. M., and Gomez, L. N., 2009. Leaf litter decomposition in a tropical peat swamp forest in Peninsular Malaysia. *Wetlands Ecology and Management* 17: 231–241
- Yupi, H.M., Inoue, T., Bathgate, J., Putra, R, 2016. Concentrations, loads and yields of organic carbon from two tropical peat swamp forest streams in Riau Province, Sumatra, Indonesia. *Mires and Peat* 14: 1-15
- Yusop, Z., Chong, M. H., Garusu, G. J., and Ayob, K, 2008. Estimation of evapotranspiration in oil palm catchments by short-term period water-budget method. *Malaysian Journal of Civil Engineering* 20: 160–174
- Zhao, G-J., Gao, J-F., Tian, P., Tian, K, 2009. Comparison of two different methods for determining flow direction in catchment hydrological modelling. *Water Science and Engineering* 2:1-15
- Zhu, D., Chen, H., Zhu, Q., Wu, Y, Wu, N, 2011. High Carbon Dioxide Evasion from an Alpine Peatland Lake: The Central Role of Terrestrial Dissolved Organic Carbon Input. *Water, Air and Soil Pollution*, DOI: 10.1007/s11270-011-1048-6
- Zinck, J.A and O. Huber, 2011. Peatlands of the Western Guayana Highlands, Venezuela: Properties and Paleogeographic Significance of Peats. *Ecological studies* 217. Berlin, Heidelberg: Springer-Verlag

Appendix

Appendix A: Plantation bulk density estimates

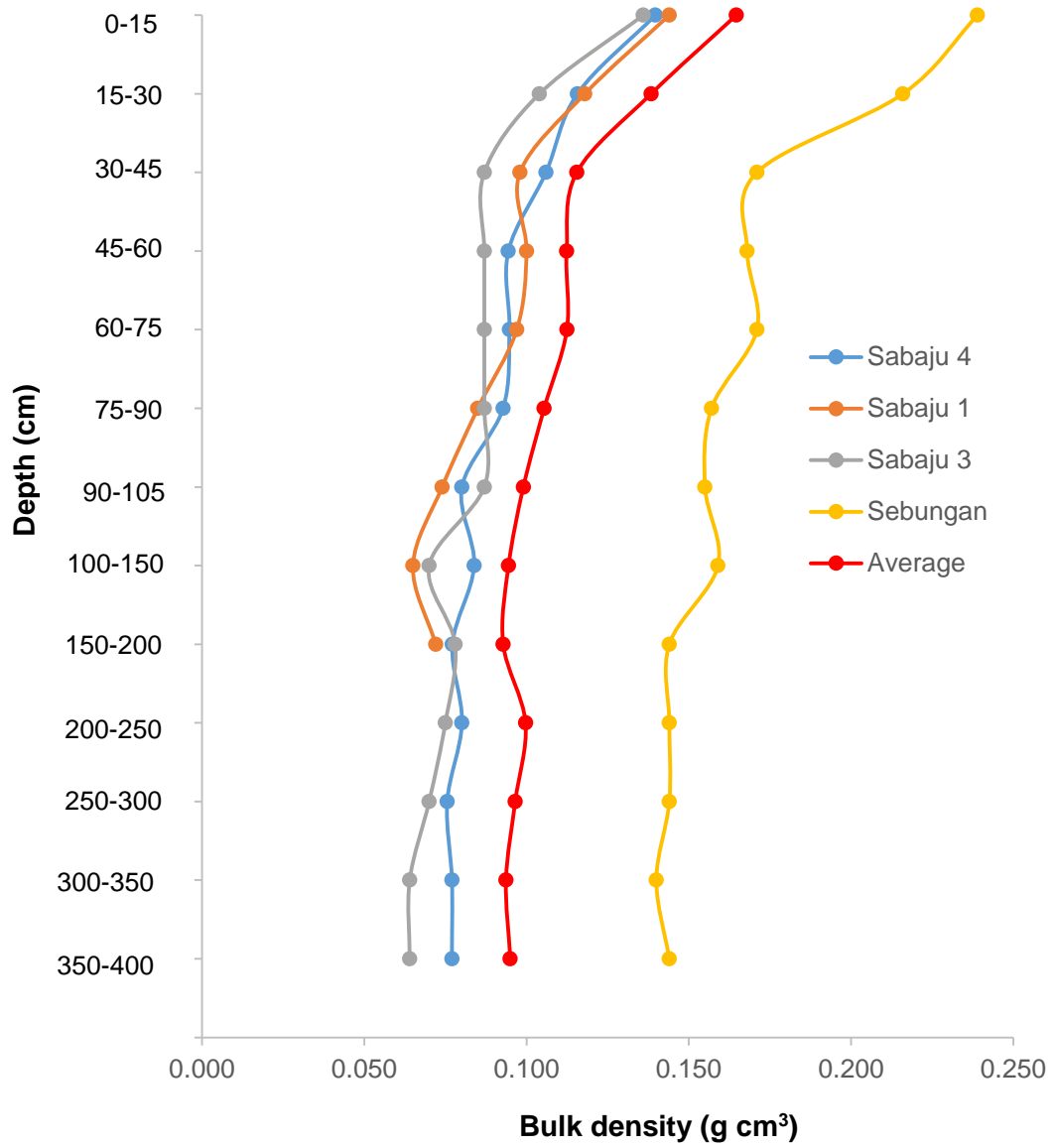


Figure A1. Peat profile bulked density estimates for the four plantation estates

Appendix B: Flow-weighted TOC concentration fluxes, a worked example

Date	Week	Site	DOC (mg/l)	POC (mg/l)	TOC (mg/l)	Stage height (m)	Q _i Corresponding discharge (m ³ s ⁻¹)	TOC _i x Q _i (g/m ³)
03.08.2015	1	SE 2	24.16	1.90	26.06	0.25	0.000	0.000
10.08.2015	2		44.49	1.50	45.99	0.40	0.018	0.821
20.08.2015	3		51.09	1.10	52.19	0.42	0.020	1.067
24.08.2015	4		45.31	1.90	47.21	0.24	0.000	0.000
01.09.2015	5		41.02	0.60	41.62	0.43	0.022	0.904
07.09.2015	6		55.63	1.50	57.13	0.42	0.020	1.168
14.09.2015	7		45.19	1.10	46.29	0.36	0.013	0.588
21.09.2015	8		44.67	3.20	47.87	0.21	0.000	0.000
28.09.2015	9		40.06	16.70	56.76	0.10	0.000	0.000
11.11.2015	15		46.31	4.00	50.31	0.37	0.014	0.704
16.11.2015	16		49.18	2.00	51.18	0.41	0.019	0.980
7.12.2015	19		47.34	1.80	49.14	0.37	0.014	0.688
14.12.2015	20		43.62	1.50	45.12	0.37	0.014	0.631
11.01.2016	24		43.89	2.60	46.49	0.23	0.000	0.000
25.01.2016	26		42.69	2.90	45.59	0.37	0.014	0.638
15.02.2016	29		41.45	0.30	41.75	0.32	0.008	0.315
24.02.2016	30		46.63	7.30	53.93	0.14	0.000	0.000
03.03.2016	31		40.19	2.90	43.09	0.00	0.000	0.000
10.03.2016	32		34.70	6.20	40.90	0.00	0.000	0.000
17.03.2016	33		42.50	4.10	46.60	0.30	0.005	0.232
31.03.2016	35		42.70	23.10	65.80	0.07	0.000	0.000
06.04.2016	36		35.61	4.70	40.31	0.28	0.002	0.096
13.04.2016	37		41.87	0.50	42.37	0.30	0.005	0.211
20.04.2016	38		31.54	2.20	33.74	0.12	0.000	0.000
09.05.2016	41		44.75	8.50	53.25	0.39	0.017	0.882
16.05.2016	42		45.33	2.90	48.23	0.35	0.01	0.551
06.06.2016	45		45.60	1.40	47.00	0.13	0.000	0.000
13.06.2016	46		40.16	1.60	41.76	0.26	0.000	0.000
18.07.2016	51		41.45	1.50	42.95	0.25	0.000	0.000
08.08.2016	54		43.16	2.00	45.16	0.27	0.001	0.050

<u>Carbon flux</u>		
$\sum Q_i$	0.22	
$\sum (TOC_i \cdot Q_i)$		10.53
$\frac{\sum (TOC_i \cdot Q_i)}{\sum Q_i}$	48.45	
R_E (m)	2.80	
$J_{a.s.y}$ (g C m ⁻² yr ⁻¹)	135.65	
<u>Catchment area</u>		
Q_A (m ³ s ⁻¹)	0.01	
Q_{av} (m ³ yr ⁻¹)	228380.56	
R_E (m)	2.80	
Area m ⁻²	81564.49	
Area ha	8.16	

Appendix C: Chloride mass balance

Example chloride mass balance for FA site. Data are questionable due to the effect of fertilizer.

Corresponding dates (to-from)	Week	Rain Sample Chloride (mg/L)	Forest A Chloride (mg/L)	Precipitation (mm) from MET station	ET _a (mm) calculated from Cl ⁻
03.08.2015-09.08.2015	W1	2	3.8	219.7	104.1
10.08.2015-16.08.2015	W2	2.9	8.4	85.8	56.2
17.08.2015-23.08.2015	W3	2.3	2.5	9.8	0.8
24.08.2015-30.08.2015	W4	1.2	2.5	110.8	57.6
31.08.2015-06.09.2015	W5	1	1.3	98.4	22.7
07.09.2015-13.09.2015	W6	1.2	1.3	100.1	7.7
14.09.2015-20.09.2015	W7	1.2	2.5	11.8	6.1
21.09.2015-27.09.2015	W8	2.9	3.8	26	6.2
28.09.2015-04.10.2015	W9	1.3	14.9	20.3	18.5
05.10.2015-11.10.2015	W10	1.2	3.0	35.8	21.5
12.10.2015-18.10.2015	W11	1.9	4.2	79.7	43.6
19.10.2015-25.10.2015	W12	0.9	4.2	27.6	21.7
26.10.2015-1.11.2015	W13	0.5	5.2	208.6	188.5
2.11.2015-8.11.2015	W14	0.1	5.2	224.9	220.6
9.11.2015-15.11.2015	W15	0.1	1.2	156	143.0
16.11.2015-22.11.2015	W16	0.2	2.0	163.8	147.4
23.11.2015-29.11.2015	W17	0.2	2.0	155.4	139.9
30.11.2015-06.12.2015	W18	0.2	2.0	218.1	196.3
07.12.2015-13.12.2015	W19	1	1.6	292.4	109.7
14.12.2015-20.12.2015	W20	0.2	3.3	166.8	156.7
21.12.2015-27.12.2015	W21	1	3.3	62.1	43.3
28.12.2015-03.01.2016	W22	0.1	3.3	46	44.6
TOTALS				2519.9	1756.6

Total rain = 2519.9

Daily ET_a = 11.41 mm day⁻¹

Total ET_a = 1756.6

Yearly rain = 5972 mm year⁻¹

Total Q = 763.3

Yearly ET_a = 4163 mm day⁻¹

Daily rain = 16.36 mm day⁻¹

Example chloride mass balance for SE plantation. Data are questionable due to the effect of fertilizer.

Corresponding dates (to-from)	Week	Rain Sample Chloride (mg/L)	Forest A Chloride (mg/L)	Precipitation (mm) from MET station	ET _a (mm) calculated from Cl ⁻
03.08.2015-09.08.2015	W1	2	7.5	219.7	161.0
10.08.2015-16.08.2015	W2	2.9	6.6	85.8	47.8
17.08.2015-23.08.2015	W3	2.3	7.8	9.8	6.9
24.08.2015-30.08.2015	W4	1.2	9.4	110.8	96.6
31.08.2015-06.09.2015	W5	1	10.8	98.4	89.2
07.09.2015-13.09.2015	W6	1.2	14.1	100.1	91.6
14.09.2015-20.09.2015	W7	1.2	9.1	11.8	10.2
21.09.2015-27.09.2015	W8	2.9	6.8	26	14.9
28.09.2015-04.10.2015	W9	1.3	12.1	20.3	18.1
05.10.2015-11.10.2015	W10	1.2	8.5	35.8	30.7
12.10.2015-18.10.2015	W11	1.9	15.7	79.7	70.0
19.10.2015-25.10.2015	W12	0.9	15.7	27.6	26.0
26.10.2015-1.11.2015	W13	0.5	17.2	208.6	202.5
2.11.2015-8.11.2015	W14	0.1	15.9	224.9	223.5
9.11.2015-15.11.2015	W15	0.1	19.9	156	155.2
16.11.2015-22.11.2015	W16	0.2	15.9	163.8	161.7
23.11.2015-29.11.2015	W17	0.2	15.9	155.4	153.5
30.11.2015-06.12.2015	W18	0.2	15.9	218.1	215.4
07.12.2015-13.12.2015	W19	1	13.4	292.4	270.5
14.12.2015-20.12.2015	W20	0.2	15.3	166.8	164.6
21.12.2015-27.12.2015	W21	1	15.3	62.1	58.0
28.12.2015-03.01.2016	W22	0.1	15.3	46	45.7
TOTALS				2519.9	2314

Total rain = 2519.9

Daily ET_a = 15.03 mm day⁻¹

Total ET_a = 2314

Yearly rain = 5972 mm year⁻¹

Total Q = 206

Yearly ET_a = 5486 mm year⁻¹

Daily rain = 16.36 mm day⁻¹

Appendix D: peat core pH profile

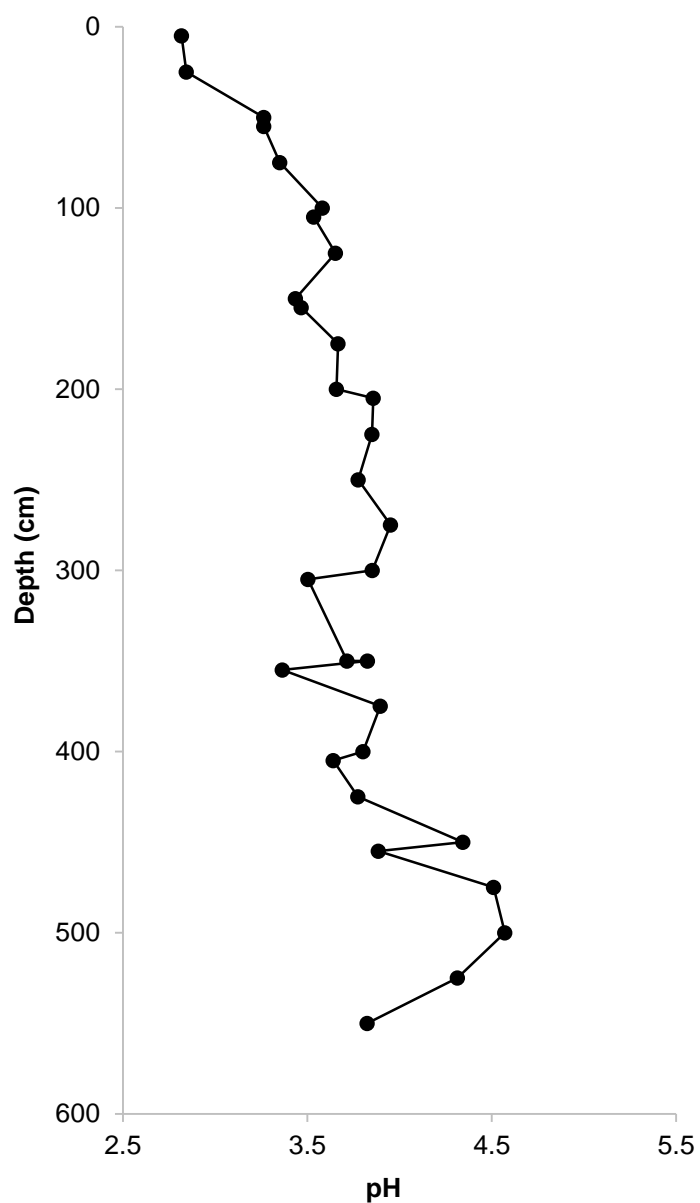


Figure D1. pH profile (5.5 m transect) of Sabaju 4 estate core. 20g of sample was taken at each interval and mixed with 20 ml of distilled water to form a slurry. No indication of potential acid sulphate soil present with high pH at greater depth.

Appendix E: Characterisation of the semi-volatile component of Dissolved Organic Matter by Thermal Desorption – Proton Transfer Reaction – Mass Spectrometry (Final submitted manuscript)

The following section is published in Nature Scientific Reports: Materic, D., Peacock, M., Kent, M., **Cook, S.**, Gauci, V., Rockmann, T., Holzinger, R., 2017. Characterisation of the semi-volatile component of Dissolved Organic Matter by Thermal Desorption – Proton Transfer Reaction – Mass Spectrometry. Nature Scientific Reports 7: 15936

Dušan Materić^{1*}, Mike Peacock^{2,4}, Matthew Kent², Sarah Cook³, Vincent Gauci², Thomas Röckmann¹ and Rupert Holzinger¹

¹Faculty of Science, Institute for Marine and Atmospheric Research, Utrecht University, Princetonplein 5, 3584 CC, Utrecht, Netherlands

²Faculty of STEM, School of Environment Earth and Ecosystems, The Open University, Milton Keynes, MK7 6AA, UK

³Centre for Landscape & Climate Research. University of Leicester, Geography, Leicester, LE1 7RH, UK

⁴Department of Aquatic Sciences and Assessment, Swedish University of Agricultural Sciences, 750 07 Uppsala, Sweden

*Corresponding author: dusan.materic@gmail.com

Abstract

Proton Transfer Reaction – Mass Spectrometry (PTR-MS) is a sensitive, soft ionisation method suitable for qualitative and quantitative analysis of volatile and semi-volatile organic vapours. PTR-MS is used for various environmental applications including monitoring of volatile organic compounds (VOCs) emitted from natural and anthropogenic sources, chemical composition measurements of aerosols, etc. Here we apply thermal desorption PTR-MS for the first time to characterise the chemical composition of dissolved organic matter (DOM). We developed a clean, low-pressure evaporation/sublimation system to remove water from samples and coupled it to a custom-made thermal desorption unit to introduce the samples to the PTR-MS. Using this system, we analysed waters from intact and degraded peat swamp forest of Kalimantan, Indonesian Borneo, and an oil palm plantation and natural forest in Sarawak, Malaysian Borneo. We detected more than 200 organic ions from these samples and principal component analysis allowed clear separation of the different sample origins based on the composition of organic compounds. The method is sensitive, reproducible,

and provides a new and comparatively cheap tool for a rapid characterisation of water and soil DOM.

Introduction

The fluvial export of dissolved organic matter (DOM) is a globally important process that represents a significant loss of terrestrial carbon. The biological and physico-chemical degradation of DOM in waters results in large emissions of carbon dioxide (CO₂) to the atmosphere^{1,2}. The magnitude of DOM losses can be influenced by anthropogenic disturbance acting on both large (i.e. continental) and small (i.e. catchment) scales. In addition to altering DOM quantity, both natural and anthropogenic processes can influence the composition and age of carbon exported as DOM³⁻⁶.

Due to the importance of DOM, numerous approaches have been used to study its composition. The simplest of these is UV-visible spectroscopy. Light absorbance at various wavelengths provides potentially useful compositional information, and 254 nm is perhaps the most popular measured wavelength. In addition to absorbance, fluorescence measurements are frequently used to study DOM, generally in conjunction with excitation-emission matrices (EEMs) and parallel factor analysis (PARAFAC)⁷. This approach reveals the presence of different fractions which may be, for example, protein-like (tryptophan) or due to the presence of soil fulvic acids. Complementing these simple optical measurements are simple chemical measurements. These can include measurements of hexose and pentose as indicators of whether DOM is predominantly derived from plants or microbes⁸, and a ratio of phenolic compounds to total DOM as a measure of aromaticity⁹.

Whilst the relatively simple methods above are widely used, there are also a range of analytical chemistry methods that provide information on DOM composition. For instance, high-performance size-exclusion chromatography with a UV detection wavelength of 254 nm can be used to determine DOM molecular weight¹⁰ (Zhou et al., 2000). Further basic information can be obtained using XAD fractionation which separates the hydrophobic and hydrophilic fractions of DOM¹¹. Also, pyrolysis and thermochemolysis gas chromatography – mass spectrometry (GC-MS) have been used to identify low molecular weight decomposition products, which belong to various categories (e.g. polysaccharides, proteins, aminosugars, etc.). The exact types and proportions of decomposition products can be used as a fingerprint for different organic materials^{12,13}. Ultimately, the development of high resolution mass spectrometry such as Orbitrap mass spectrometry¹⁴, Quadrupole time-of-flight mass spectrometry (QqTOF MS) and Fourier

transform ion cyclotron resonance mass spectrometry (FT-ICR MS) has opened new fields of DOM characterisation. FT-ICR MS has since been demonstrated to be a high resolution method for detecting individual compounds in carbon in natural waters, with one recent study identifying 4032 molecular formulae in 120 Swedish lakes ¹⁵. FT-IRC MS however, has numerous disadvantages including: low instrument availability, high cost, the requirement for a large sample size, low time resolution, and sample preparation that requires pre-concentration and non-established routine data analysis. Subsequently, this method is both time consuming and expensive, and leads to compromises in the experimental design such as running just one replica per sample. Thus, the method may not be suitable for wide usage.

Proton Transfer Reaction – Time of Flight – Mass Spectrometry (PTR-ToF-MS) is a real-time technique achieving time resolution <1s, has a mass resolving power of several thousands, and has sub-ppb sensitivity ¹⁶. The method utilises soft, chemical ionization by hydronium ions which results in low fragmentation of primary ions in gas stream compared to e.g. electrospray ionization. The technique allows manipulation of different energy conditions during ionization (E/N), it can use different ionization modes (H₃O⁺, NO⁺ and O₂⁺) and can be coupled with fastGC, which all increase analytical power at no or little time cost ^{17,18}.

PTR-ToF-MS has been used in many environmental studies that require high time and mass resolution such as: measurement of organic vapours concentrations/emissions in air, monitoring of oxidation processes of biogenic volatile organic compounds (BVOCs), measurement of chemical composition in organic aerosols etc. ^{19–22}. However, as the technique is developed for gaseous organic volatiles, analysis of water samples has been limited to the headspace analysis.

Here we present a rapid characterisation method of semi-volatile DOM based on PTR-ToF-MS and its first application to analyse water samples from tropical peatlands. We aimed to investigate the technique's potential to discover novel biomarkers linked to changes in land management.

Materials and Methods

Water samples were collected from different environments across a peat swamp forest oil palm plantation (SOP) and the surrounding natural forest buffer zone in Sarawak, Malaysian Borneo (SI); and intact, selectively logged forest (KI) and deforested, extensively drained land (KD) in Kalimantan, Indonesian Borneo. A complete list of all analysed samples is given in supplementary material (Table S1). All samples were filtered through 0.45

µm and stored at 4°C in the dark prior to analysis. This sampling and storage method has been shown to limit losses of total dissolved organic carbon (DOC) concentration and retain DOC composition, as measured using UV-visible spectroscopy, for periods of several months²³⁻²⁵. As the field location in Indonesian Borneo was remote and immediate refrigeration was not possible, samples were temporarily stored in the dark at ambient temperature in the coolest location at the field site (~20°C) for a month.

For analysis of DOC concentration, samples were first filtered through 0.2 µm cellulose nitrate membrane filters. Samples were then analysed as non-purgeable organic carbon (NPOC) using a Shimadzu TOC Analyzer and appropriate standards. All sample concentrations fell within the range of standards used (0 – 100 mg/L).

A clean, low-pressure evaporation/sublimation (LPE) system was adapted in order to achieve the following goals: (1) to remove water from the samples (2) limit the loss of the organic (semi-volatile) fraction of the sample and (3) limit the sample contamination from laboratory air. We used a rotary pump to achieve suitable vacuum followed by a liquid nitrogen cold trap (to trap water from the samples as well as oil vapours from backflow of the pump) (Figure 1a). The samples were placed in a desiccator and kept in 10 mL chromatography vials capped with Teflon caps which had two, 2 mm holes. Thus, all the internal parts of the system were glass, coated stainless steel (Restek Sulfinert) or Teflon.

The sample vials and caps were baked at 250°C overnight. 0.5 mL of the samples (and blanks) were loaded and the vials were placed in the desiccator followed by LPE, which was completed in 2 h. In order to reduce contamination between the samples and with laboratory air we re-pressurised the system by adding nitrogen slowly over 10 minutes. The vials containing the dehydrated samples were removed from the LPE system, capped with Teflon caps and analysed the next day.

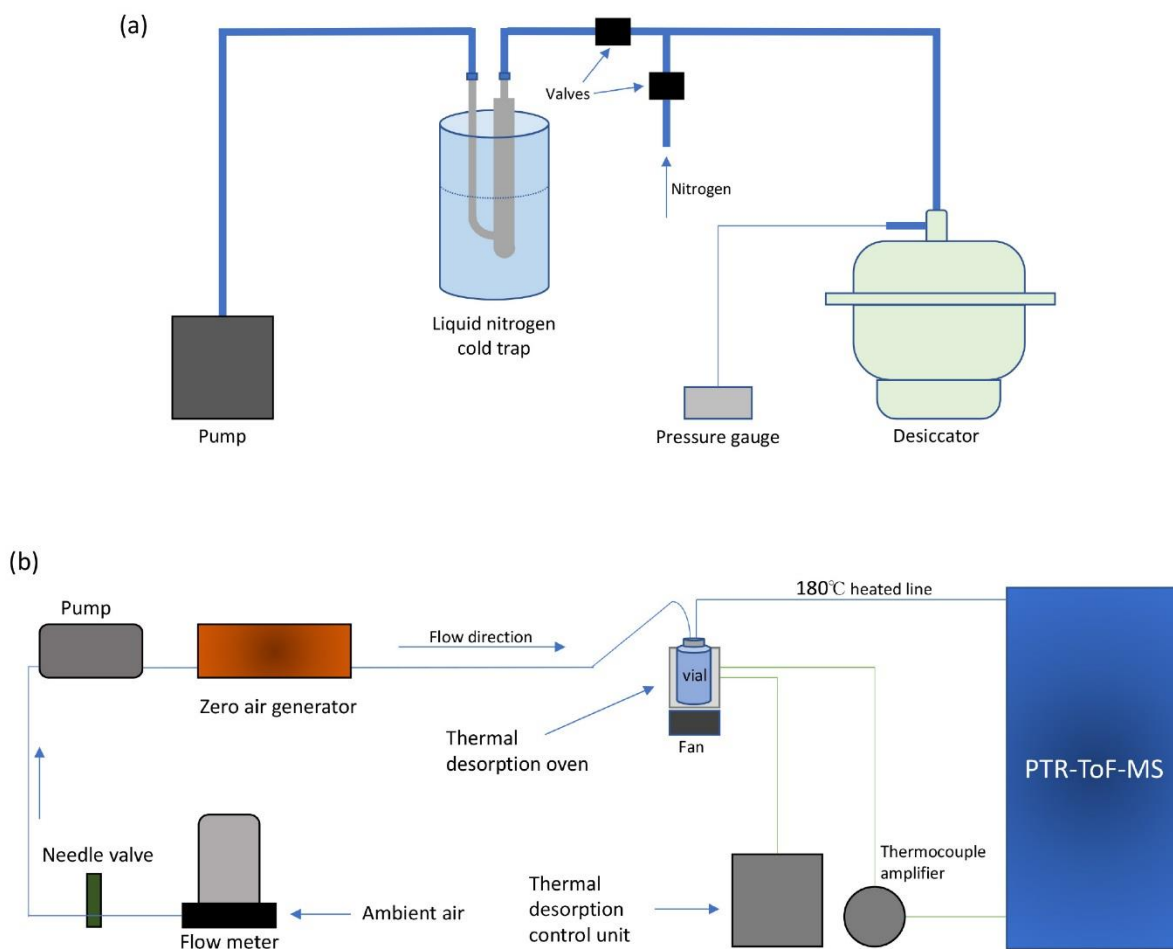


Figure 1. (a) Low pressure evaporation/sublimation system. (b) Thermal Desorption (TD) system coupled to PTR-ToF-MS.

The samples were loaded into a thermal desorption (TD) unit to enable transfer into the PTR-MS instrument in a clean carrier gas stream. The TD unit was designed to achieve the required temperature ramping conditions and accommodate the size of the vials (Figure 1b). The samples were loaded in the TD oven at a temperature $<35^{\circ}\text{C}$, after which the following TD sequence was started: (1) 1.5 min incubation at 45°C , (2) ramp to 220°C at a rate of $40^{\circ}\text{C}/\text{min}$, (3) 5 minutes at a constant 220°C , and (4) cooling down to $<35^{\circ}\text{C}$. Additional ramping to 250°C (after step 3) and 20 min at a constant 250°C was done for random long runs. During the TD, the samples were flushed with clean air at a flow rate of $50\text{ mL}/\text{min}$ as PTR-ToF-MS was sampling.

For the measurement of organic vapours, we used a PTR-TOF 8000 (IONICON Analytik, Austria), sampling up to m/z 1130, at a time resolution of

1 spectra per second and E/N (the ratio of the electric field strength E and the gas number density N) of 129 Td.

In order to assess the contamination from different sources, we analysed system blanks (clean vials), dry blanks (clean vials exposed to LPE system together with other samples), and ultrapure water blanks (vials loaded with 0.5 mL of HPLC water, VWR chemicals), which were evaporated together with other samples in the LPE system. We measured 3 replicates of each sample to assess the reproducibility of the method.

Raw PTR-ToF-MS data were analysed by PTRwid which performed peak identification and integration²⁶. Figure 2b shows a typical thermogram of a TD analysis. For each TD run, measured concentrations were integrated for 5 min starting from the point when the TD oven reached 50 °C (Figure 2a). The signal obtained from blanks measured during the same day was subtracted from each mass. The limit of detection (LoD) was established for each ion using the 3 σ method, so ions signals below the LoD threshold were excluded. We compared ion signals from different groups for statistical difference by t-test and performed principal component analysis.

The chemical formula for each peak was calculated and assigned using PTRwid and cross-compared using the open source mass spectrometry tool mMass.

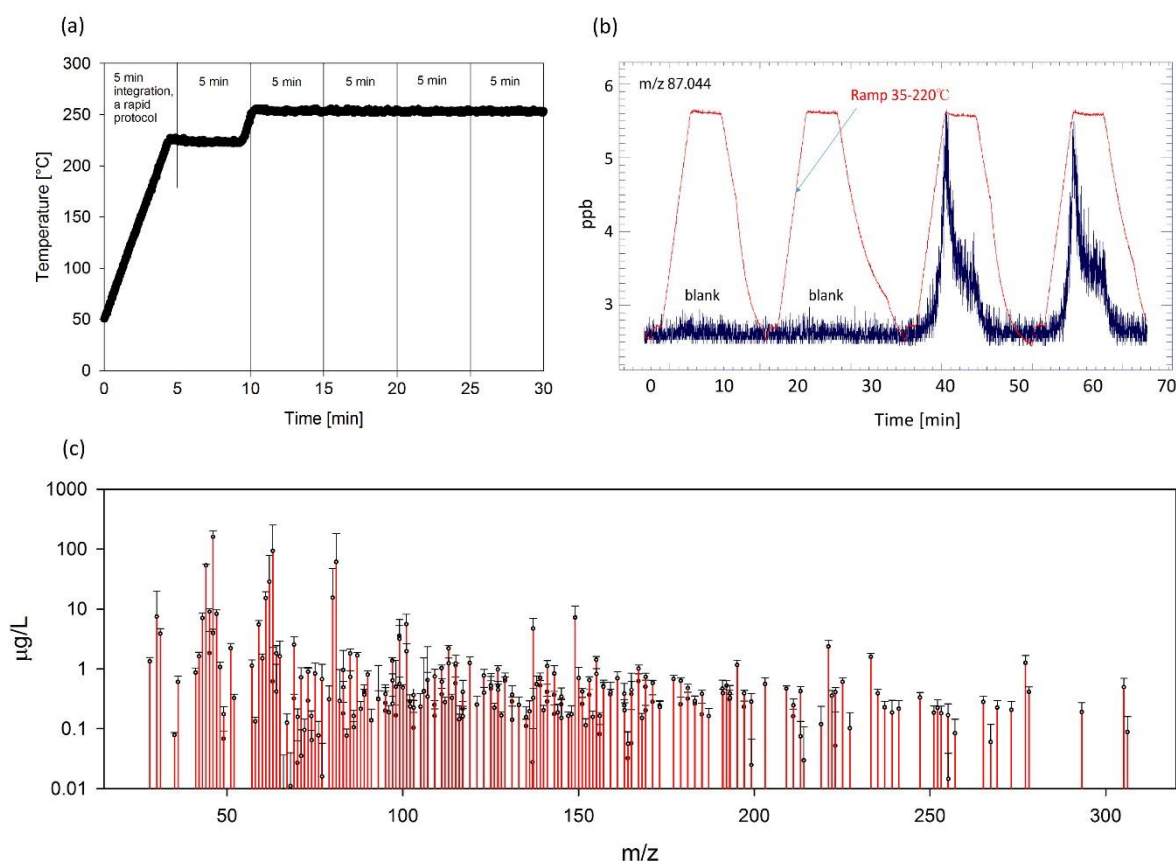


Figure 2. (a) Thermal desorption program and corresponding integration times. The rapid, 5 min heating program was used except in the long test runs. (b) Signal output of ion m/z 87.044 during 4 runs of thermal desorption (two blanks and two samples). (c) Typical mass spectrum gained after 5-minute integration (sample ID SE1W41). Note the log scale on the y-axis. Error bars present standard deviation over 7 replicas (error bars symmetrical, only top error bars plotted).

Method optimization

The PTR-ToF-MS analyser is so sensitive that it detects even small impurities that originate from different sources in the system. Exposure of vials to the laboratory air was minimized because longer exposure introduced clearly measurable impurities (e.g. m/z 63 and 41). These impurities were found to be higher in dry blanks than in blanks loaded with HPLC water. This could be due to the larger glass surface area in the dry blanks compared to blanks in which the bottom of the vials were covered with water. When comparing clean vials with vials exposed to the LPE system, several impurity masses were discovered, which all contained Si atoms. We attributed this

contamination to vapours originating from vacuum grease that was used to connect various parts of the system. However, these silica-based impurities are not an issue for data interpretation because they could easily be accurately identified and excluded. Nevertheless, this issue could be avoided in future by using a vacuum seal that does not use vacuum grease.

After optimization of the LPE and TD system we performed the measurements of samples together with blanks; dry blanks and HPLC water blanks were run at the beginning and at the end of measurements, at least 2 of each per day. Samples were randomly run in 3 replicates over the course of the experiment (3 weeks).

For data analysis, we found that averaging 3 replicas for each sample, subtracting the backgrounds measured on the same day, and then averaging them assures that masses close to the detection limit are retained.

Results and discussion

Utilising our method, we successfully separated more than 250 organic ions ranging from 28 to 305 m/z (Figure 2c). Ion concentrations were found to be reproducible over multiple replicates, which were run in a random order over the entire measurement. As PTR-ToF-MS is a soft ionization technique and we applied moderate temperatures during TD, we attribute most of these ions to be protonated molecular ions, rather than fragments of compounds of high molecular mass.

The semi-volatile fraction of DOM measured with our rapid qualitative TD-PTR-ToF-MS method is 0.6% on average of the total DOM present in samples. Higher 'recovery' values could be obtained with longer TD and using higher temperatures. However, high TD temperature and the increased exposure involve a risk of compound fragmentation and pyrolysis/thermolysis of high molecular masses. This would result in complex mass spectra ultimately not suitable for qualitative and quantitative analysis of the semi-volatile fraction of DOM, which is the main goal of this work.

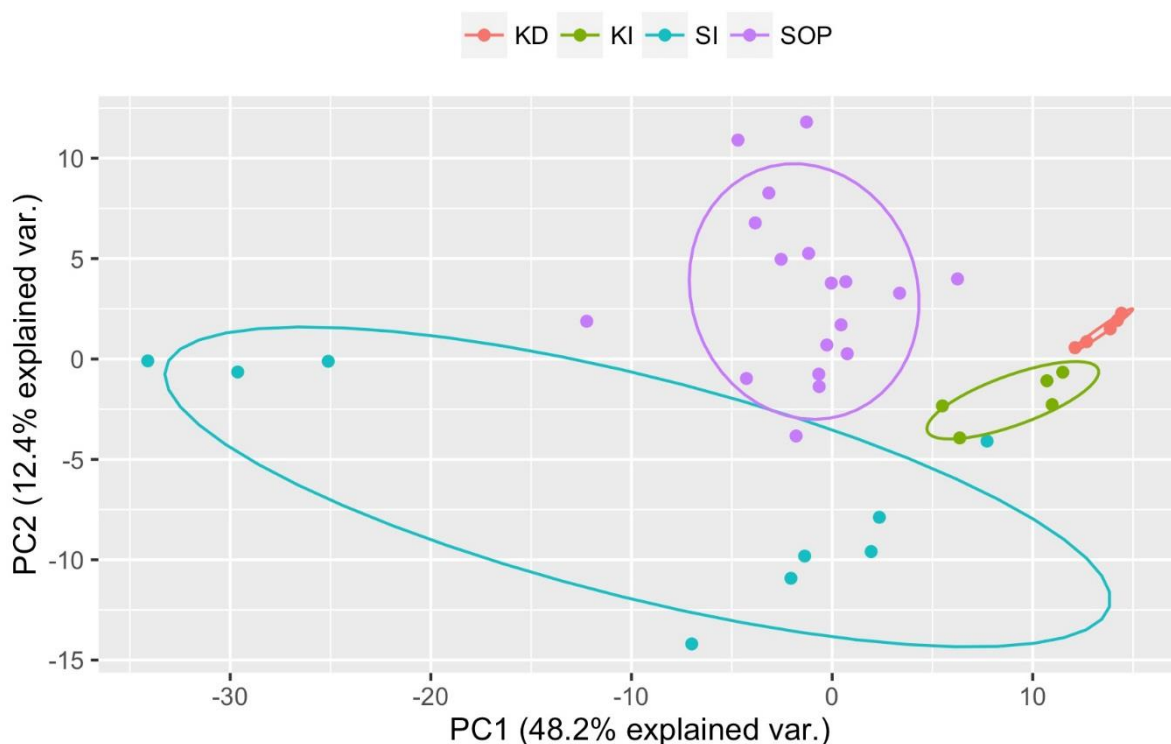


Figure 3. Principle component analysis of TD-PTR-ToF-MS. Samples from peat swamp forest oil palm plantation (SOP) and the surrounding natural forest buffer zones in Sarawak, Malaysian Borneo (SI); and intact, selectively logged forest (KI) and deforested, extensively drained land (KD) in Kalimantan, Indonesian Borneo.

Principal component analyses (PCA) is a useful tool for analysing and visualising complex PTR-MS data. As a first application and to demonstrate the power of this new technique, Fig. 3 shows the two first principle components resulting from a PCA of mass spectra obtained by TD-PTR-ToF-MS of water samples originating from tropical peatlands in Kalimantan and Sarawak. The data display a clear clustering related to sample origin. PC1 shows the highest values for Kalimantan samples with slightly higher values for the degraded site. Spread around zero are samples from both Sarawak groups with the exception of three samples that have extreme negative values. These samples might have undergone slightly different chemical processes than the rest of the group, which is discussed later (Figure 6c). PC2 shows a strong correlation with the level of the degradation/management compared to the intact state of the ecosystems,

with higher values seen in the samples coming from the degraded site of Kalimantan and the palm oil plantation of Sarawak.

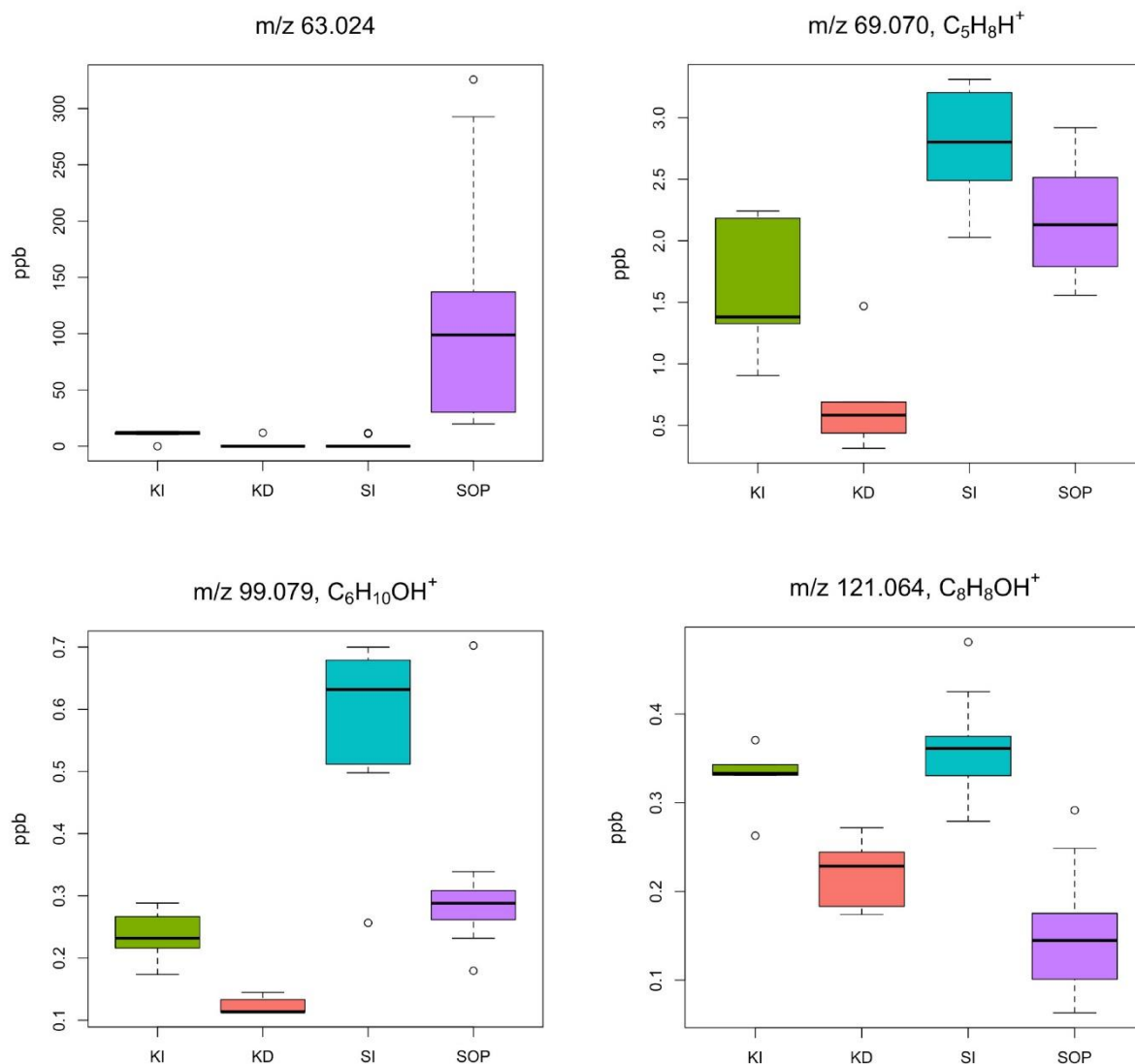


Figure 4. Boxplot of some significantly different organic ions ($p < 0.01$) with assigned chemical formula - potential biomarkers. Samples from peat swamp forest oil palm plantation (SOP) and the surrounding natural forest buffer zones in Sarawak, Malaysian Borneo (SI); and intact, selectively logged forest (KI) and deforested, extensively drained land (KD) in Kalimantan, Indonesian Borneo.

Analysis of the abundance of individual ions showed that many ions had strong significant differences ($p < 0.001$) between groups (supplementary Table S2 and S3). In most cases, the values are higher in the intact forest compared to degraded/oil palm ecosystems (e.g. ions m/z 69.070, 99.079, 121.064 in Figure 4). This could be related to higher mean values of total DOC measured within intact ecosystems. However, the relative contribution of semi-volatile DOM fraction to the total DOM also showed higher values only in the intact site in Kalimantan (Figure 5, supplementary Table S2). This suggests that the intact ecosystem in Kalimantan possesses a higher fraction of light DOM compounds, possibly due to the rich biodiversity and complex soil biogeochemical processes. On the other hand, the low fraction of semi-volatile DOM relative to the total, suggests that fluvial DOM in degraded ecosystems contains heavier, less semi-volatile compounds, which is in agreement with result showed in Figure 6b.

We also observed a small number of compounds which have higher values measured within the oil palm plantation (e.g. m/z 63.024, 81.036 etc.) compared to the intact site ecosystem of Sarawak (Figure 4, supplementary Table S3). Interestingly these compounds are highly volatile and have at least an order of magnitude higher levels, suggesting an anthropogenic origin possibly connected to agricultural processes or management-induced changes of the soil.

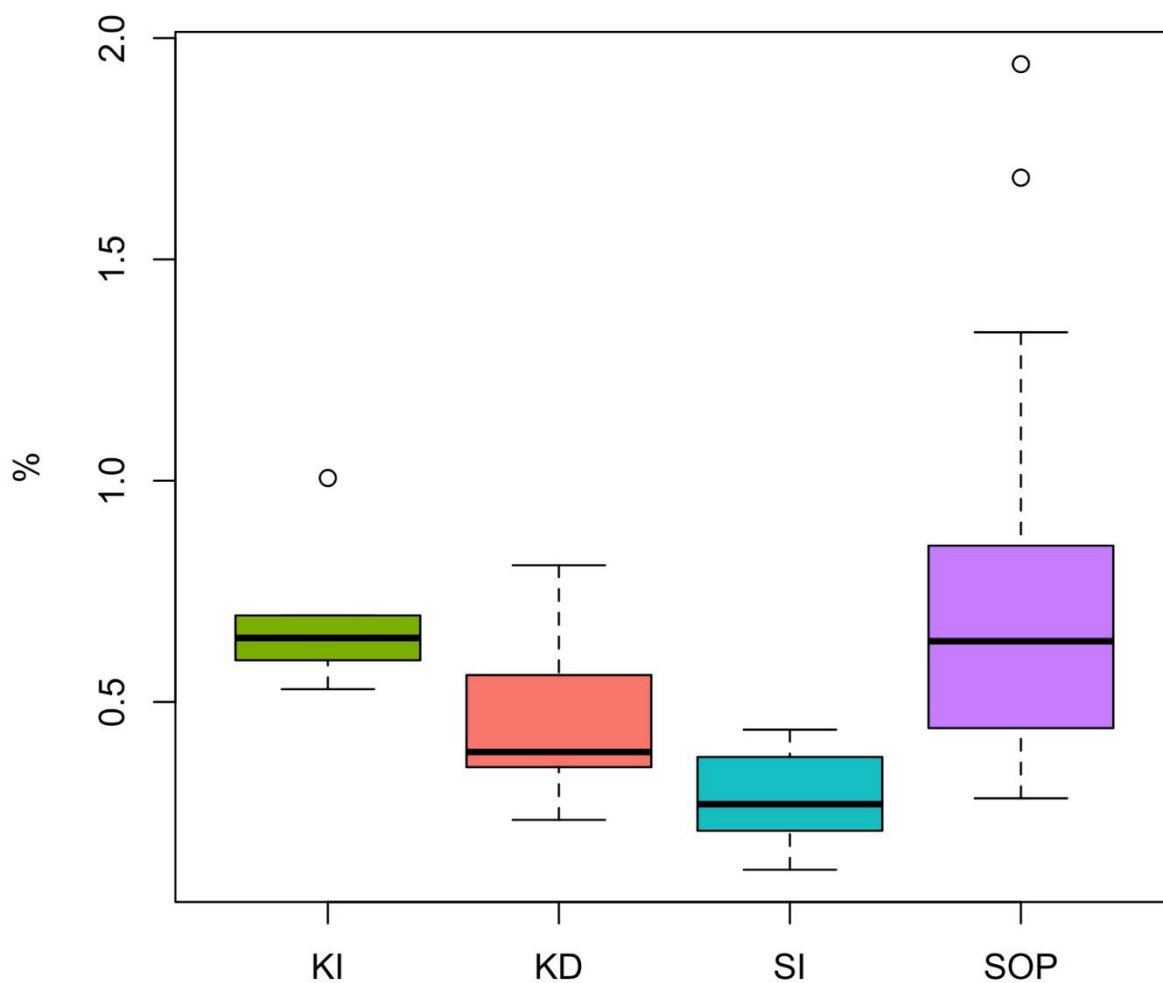


Figure 5. Semi-volatile fraction of DOM measured by TD-PTR-ToF-MS, normalised to the total DOM measured by TOC Analyzer.

Since the PTR-ToF-MS method is quantitative, the total number of C, H, O, N atoms can be calculated for each sample thus allowing the aromaticity index, mean oxidative state of carbon (OSc) and average number of carbon per sample molecule (nC) to be calculated. The data can then be visualised in a matrix e.g. similar to Van Krevelen plots (Figure 6a) ^{27,28}. These plots can reveal the major underlying chemical processes within the group (ecosystem). For example, Figure 6a shows that that major processes in Sarawak's intact forest are oxidation/reduction reactions (e.g. gaining/losing oxygen changes O/C and not H/C), whereas in the oil palm plantation the dominant processes are hydration/condensation (e.g. gaining/losing water molecule affects both O/C and H/C). This demonstrates that different biogeochemical processes are the dominant drivers of DOM composition for these two ecosystems. The mean oxidative state of carbon (OSc) in the Sarawak's oil palm plantation samples is indicating overall higher oxidation processes that might be affecting older, stored carbon (Figure 6c). This

might come as a result of low water table (drought stress) which is supported by the fact that three intact forest samples with OSC around -0.3 in Fig. 6c were sampled after low water tables were measured (drought-like conditions). Further analysis that involved placing the drought-stressed SI samples into a separate group improved PCA clustering and discovered ions associated with the stress condition (see supplementary Fig. S1). The mean numbers of carbon atoms of the organic compounds analysed with PTR-ToF-MS are higher in the samples coming from Kalimantan's degraded site compared to the intact site (Figure 6b), which suggests presence heavier semi-volatile DOM at this site possibly due to the mobilization of ancient carbon ²⁹.

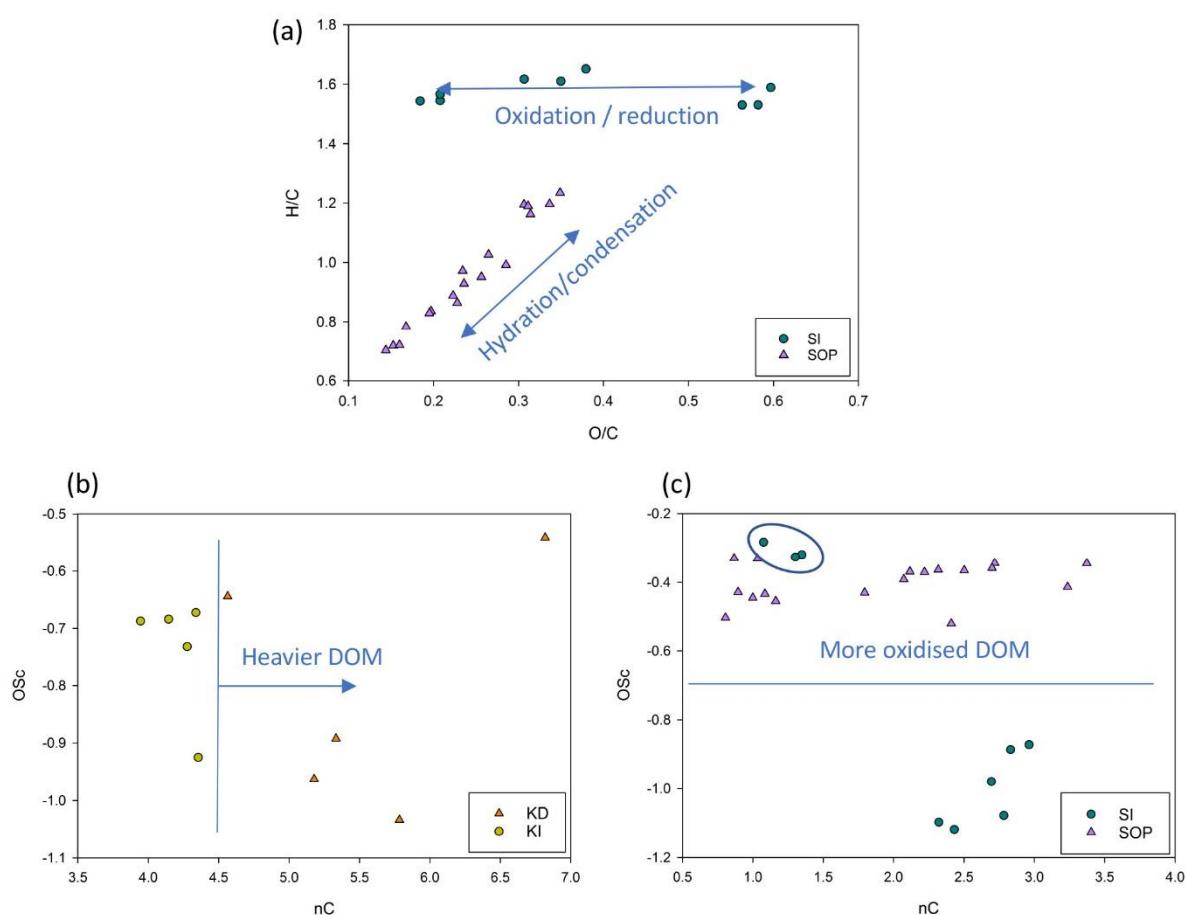


Figure 6. (a) Scatter plot of atomic ratio O/C vs H/C (Van Krevelen plot) in Sarawak samples - all ions summarised and presented as one point on the plot. (b) Scatter plot of chemical parameters nC and OSC for Kalimantan and (c) Sarawak samples.

Studying DOM has become an important method of assessing the stability of carbon-rich ecosystems such as peatlands⁶. Tropical peatlands, which are found in often rapidly developing equatorial nations, are undergoing large-scale disturbances as they are converted from natural swamp forest to large-scale agricultural use³⁰. For these plantations (often oil palm or paper pulp) the peatlands must be deforested and drained so that they are not waterlogged. Removing the near-constant waterlogged conditions means that the carbon-rich soils can be oxidised and leads to degradation and ecosystem instability, and studies have found that large quantities of historically stored carbon are being lost^{29,31,32}. The carbon lost from the ecosystems can be rapidly converted and emitted to the atmosphere as carbon dioxide³³. Understanding the altered carbon cycling and carbon-loss potential of degraded peatlands is therefore important to their restoration. TD-PTR-ToF-MS adds a fast and affordable technique to the biogeochemist's analytical toolkit and allows for further interpretation the fundamental changes the ecosystems are undergoing; specific compounds can be identified which could be used to elucidate process-level changes to biogeochemical interactions.

In conclusion, our rapid, high resolution TD-PTR-ToF-MS method for DOM characterisation could be potentially used both for fingerprinting approaches (untargeted) and biomarker discovery/monitoring (targeted). The advantages of our method are: (1) time resolution of a run < 10 minutes, (2) small sample size <1mL, (3) it does not require sample pre-concentration, (4) it is relatively inexpensive and (5) it is both qualitative and quantitative.-So far, the method is suitable for quantitative and qualitative analysis of lower molecular mass groups of compounds in DOM. However, the presented method can be modified to target molecules that have higher molecular masses. Strategies such as pre-treatment of the sample, sample degradation, running in a different ionization mode and coupling to a fastGC are some of the development options that can increase sensitivity and focus the technique on specific molecular targets in a complex chemical matrix of DOM.

References

1. Battin, T. J. *et al.* The boundless carbon cycle. *Nat. Geosci.* **2**, 598–600 (2009).
2. Cole, J. J. *et al.* Plumbing the Global Carbon Cycle: Integrating Inland Waters into the Terrestrial Carbon Budget. *Ecosystems* **10**, 172–185 (2007).
3. Butman, D. E., Wilson, H. F., Barnes, R. T., Xenopoulos, M. A. & Raymond, P. A. Increased mobilization of aged carbon to rivers by human disturbance. *Nat. Geosci.* **8**, 112–116 (2015).
4. Evans, C. D. *et al.* Contrasting vulnerability of drained tropical and high-latitude peatlands to fluvial loss of stored carbon. *Glob. Biogeochem. Cycles* **28**, 1215–1234 (2014).
5. Kothawala, D. N. *et al.* The relative influence of land cover, hydrology, and in-stream processing on the composition of dissolved organic matter in boreal streams. *J. Geophys. Res. Biogeosciences* **120**, 2015JG002946 (2015).
6. Moore, S. *et al.* Deep instability of deforested tropical peatlands revealed by fluvial organic carbon fluxes. *Nature* **493**, 660–663 (2013).
7. Stedmon, C. A. & Bro, R. Characterizing dissolved organic matter fluorescence with parallel factor analysis: a tutorial. *Limnol. Oceanogr. Methods* **6**, 572–579 (2008).
8. Strack, M., Zuback, Y., McCarter, C. & Price, J. Changes in dissolved organic carbon quality in soils and discharge 10 years after peatland restoration. *J. Hydrol.* **527**, 345–354 (2015).
9. Peacock, M. *et al.* Quantifying dissolved organic carbon concentrations in upland catchments using phenolic proxy measurements. *J. Hydrol.* **477**, 251–260 (2013).
10. Zhou, Q., Cabaniss, S. E. & Maurice, P. A. Considerations in the use of high-pressure size exclusion chromatography (HPSEC) for determining molecular weights of aquatic humic substances. *Water Res.* **34**, 3505–3514 (2000).
11. Leenheer, J. A. Comprehensive approach to preparative isolation and fractionation of dissolved organic carbon from natural waters and wastewaters. *Environ. Sci. Technol.* **15**, 578–587 (1981).

12. Frazier, S. W. *et al.* Characterization of organic matter from natural waters using tetramethylammonium hydroxide thermochemolysis GC-MS. *J. Anal. Appl. Pyrolysis* **70**, 99–128 (2003).
13. Leenheer, J. A. & Croué, J.-P. Characterizing aquatic dissolved organic matter. *Environ. Sci. Technol.* **37**, 18A–26A (2003).
14. Hawkes, J. A., Dittmar, T., Patriarca, C., Tranvik, L. & Bergquist, J. Evaluation of the Orbitrap Mass Spectrometer for the Molecular Fingerprinting Analysis of Natural Dissolved Organic Matter. *Anal. Chem.* **88**, 7698–7704 (2016).
15. Kellerman, A. M., Dittmar, T., Kothawala, D. N. & Tranvik, L. J. Chemodiversity of dissolved organic matter in lakes driven by climate and hydrology. *Nat. Commun.* **5**, 3804 (2014).
16. Ellis, A. M. & Mayhew, C. A. *Proton Transfer Reaction Mass Spectrometry: Principles and Applications*. (Wiley-Blackwell, 2014).
17. Jordan, A. *et al.* An online ultra-high sensitivity Proton-transfer-reaction mass-spectrometer combined with switchable reagent ion capability (PTR + SRI – MS). *Int. J. Mass Spectrom.* **286**, 32–38 (2009).
18. Materić, D. *et al.* Monoterpene separation by coupling proton transfer reaction time-of-flight mass spectrometry with fastGC. *Anal. Bioanal. Chem.* **407**, 7757–7763 (2015).
19. Holzinger, R. *et al.* Aerosol analysis using a Thermal-Desorption Proton-Transfer-Reaction Mass Spectrometer (TD-PTR-MS): a new approach to study processing of organic aerosols. *Atmos Chem Phys* **10**, 2257–2267 (2010).
20. Materić, D. *et al.* Methods in Plant Foliar Volatile Organic Compounds Research. *Appl. Plant Sci.* **3**, 1500044 (2015).
21. Park, J.-H. *et al.* Active atmosphere-ecosystem exchange of the vast majority of detected volatile organic compounds. *Science* **341**, 643–647 (2013).
22. Soukoulis, C. *et al.* PTR-ToF-MS, A Novel, Rapid, High Sensitivity and Non-Invasive Tool to Monitor Volatile Compound Release During Fruit Post-Harvest Storage: The Case Study of Apple Ripening. *Food Bioprocess Technol.* **6**, 2831–2843 (2013).
23. Carter, H. T. *et al.* Freshwater DOM quantity and quality from a two-component model of UV absorbance. *Water Res.* **46**, 4532–4542 (2012).

24. Cook, S. *et al.* Cold storage as a method for the long-term preservation of tropical dissolved organic carbon (DOC). *Mires Peat* **18**, 1–8 (2016).
25. Peacock, M. *et al.* UV-visible absorbance spectroscopy as a proxy for peatland dissolved organic carbon (DOC) quantity and quality: considerations on wavelength and absorbance degradation. *Environ. Sci. Process. Impacts* **16**, 1445–1461 (2014).
26. Holzinger, R. PTRwid: A new widget tool for processing PTR-TOF-MS data. *Atmos Meas Tech* **8**, 3903–3922 (2015).
27. Holzinger, R., Goldstein, A. H., Hayes, P. L., Jimenez, J. L. & Timkovsky, J. Chemical evolution of organic aerosol in Los Angeles during the CalNex 2010 study. *Atmos Chem Phys* **13**, 10125–10141 (2013).
28. Kroll, J. H. *et al.* Carbon oxidation state as a metric for describing the chemistry of atmospheric organic aerosol. *Nat. Chem.* **3**, 133–139 (2011).
29. Miettinen, J., Hooijer, A., Vernimmen, R., Liew, S. C. & Page, S. E. From carbon sink to carbon source: extensive peat oxidation in insular Southeast Asia since 1990. *Environ. Res. Lett.* **12**, 24014 (2017).
30. Miettinen, J. *et al.* Extent of industrial plantations on Southeast Asian peatlands in 2010 with analysis of historical expansion and future projections. *GCB Bioenergy* **4**, 908–918 (2012).
31. Evans, C. Biogeochemistry: Old carbon mobilized. *Nat. Geosci.* **8**, 85–86 (2015).
32. Hirano, T. *et al.* Effects of disturbances on the carbon balance of tropical peat swamp forests. *Glob. Change Biol.* **18**, 3410–3422 (2012).
33. Couwenberg, J., Dommain, R. & Joosten, H. Greenhouse gas fluxes from tropical peatlands in south-east Asia. *Glob. Change Biol.* **16**, 1715–1732 (2010).

Acknowledgements

This work is supported by Netherlands Earth System Science Centre (NESSC) research network. SC would like to thank the Malaysian Oil Palm Board (under MPOB grant: R010913000) in collaboration with University of Aberdeen, University of St. Andrews, and Sarawak Oil Palms Berhad, along with the Natural Environment Research Council (NERC) (grant number:

X402NE53). MK would like to thank the Center for International Cooperation in Sustainable Management of Tropical Peatland (CIMTROP) at the University of Palangkaraya, Indonesia, and the AXA Research Fund.

Author contributions

DM and RH designed the experiment and developed the system. DM performed PTR-MS and coordinate the project, MP performed DOC analysis, MK and SC collected the samples from Indonesian and Malaysian Borneo. All the authors contributed to constructing the manuscript.

Competing financial Interests

The authors declare that they have no competing interests.

Data availability

The datasets generated during and/or analysed during the current study are available from the corresponding author on reasonable request.

Supplementary material

Available online at:

https://static-content.springer.com/esm/art%3A10.1038%2Fs41598-017-16256-x/MediaObjects/41598_2017_16256_MOESM1_ESM.pdf

Appendix F: Annual TOC flux data calculations for all sites

Date	Week	Site	DOC (mg/l)	POC (mg/l)	TOC (mg/l)	Stage height (m)	Corresponding discharge (m ³ s ⁻¹)	TOC x Q (g/m ³)	TOC g C m-2 week-1
03.08.2015	1	SE 1	43.02	1.90	44.92	0.71	0.04	1.67	1.67
10.08.2015	2		47.54	3.00	50.54	1.01	0.12	6.10	6.11
20.08.2015	3		45.54	1.40	46.94	0.95	0.10	4.61	4.63
24.08.2015	4		43.39	2.20	45.59	0.80	0.06	2.52	2.53
01.09.2015	5		46.53	0.40	46.93	1.17	0.20	9.26	9.28
07.09.2015	6		40.99	2.80	43.79	1.03	0.13	5.64	5.66
14.09.2015	7		43.02	2.80	45.82	0.90	0.08	3.76	3.77
21.09.2015	8		38.98	3.20	42.18	0.80	0.06	2.33	2.34
28.09.2015	9		31.00	3.00	34.00	0.77	0.05	1.66	1.66
05.10.2015	10		35.19	3.40	38.59	0.73	0.04	1.57	1.58
13.10.2015	11		69.00	4.20	73.20	0.70	0.04	2.59	2.60
26.10.2015	13		40.66	3.60	44.26	0.60	0.02	0.94	0.94
11.11.2015	15		46.30	1.90	48.20	1.20	0.21	10.35	10.38
16.11.2015	16		48.64	2.60	51.24	1.38	0.34	17.56	17.61
7.12.2015	19		38.59	2.10	40.69	1.20	0.21	8.74	8.76
14.12.2015	20		45.44	1.20	46.64	1.30	0.28	13.09	13.12
11.01.2016	24		41.14	2.50	43.64	0.70	0.04	1.55	1.55
25.01.2016	26		40.11	3.20	43.31	1.01	0.12	5.23	5.24
15.02.2016	29		44.24	2.50	46.74	0.80	0.06	2.59	2.59
24.02.2016	30		45.35	1.30	46.65	0.58	0.02	0.88	0.88
03.03.2016	31		39.59	2.40	41.99	0.54	0.01	0.62	0.63
10.03.2016	32		34.29	2.70	36.99	0.54	0.01	0.55	0.55
17.03.2016	33		39.59	2.00	41.59	0.76	0.05	1.94	1.94
31.03.2016	35		38.66	4.10	42.76	0.55	0.02	0.68	0.68
06.04.2016	36		37.69	2.40	40.09	0.62	0.02	0.95	0.95
13.04.2016	37		40.43	2.00	42.43	0.72	0.04	1.65	1.66
20.04.2016	38		39.51	2.30	41.81	0.56	0.02	0.70	0.70
26.04.2016	39		38.64	2.60	41.24	0.52	0.01	0.54	0.54
09.05.2016	41		41.62	5.00	46.62	1.20	0.21	10.01	10.04
16.05.2016	42		41.82	1.60	43.42	1.00	0.12	5.07	5.08
06.06.2016	45		38.06	1.80	39.86	0.42	0.01	0.26	0.26
13.06.2016	46		37.39	2.60	39.99	0.51	0.01	0.49	0.49
11.07.2016	50		32.97	3.40	36.37	0.33	0.00	0.10	0.10
18.07.2016	51		36.04	2.20	38.24	0.48	0.01	0.38	0.38
08.08.2016	54		43.61	1.90	45.51	0.73	0.04	1.85	1.86
Carbon flux									
Q sum							2.79		
Sum of TOC x Q								128.41	
Vol. weighted mean TOC							45.99		
Runoff (m/yr)							2.80		
TOC flux (g C m⁻² yr⁻¹)							128.77		

Date	Week	Site	DOC (mg/l)	POC (mg/l)	TOC (mg/l)	Stage height (m)	Corresponding discharge (m ³ s ⁻¹)	TOC x Q (g/m ³)	TOC g C m-2 week-1
03.08.2015	1	SE 2	24.16	1.90	26.06	0.25	0.000	0.000	0.00
10.08.2015	2		44.49	1.50	45.99	0.40	0.018	0.821	10.59
20.08.2015	3		51.09	1.10	52.19	0.42	0.020	1.067	13.75
24.08.2015	4		45.31	1.90	47.21	0.24	0.000	0.000	0.00
01.09.2015	5		41.02	0.60	41.62	0.43	0.022	0.904	11.65
07.09.2015	6		55.63	1.50	57.13	0.42	0.020	1.168	15.05
14.09.2015	7		45.19	1.10	46.29	0.36	0.013	0.588	7.58
21.09.2015	8		44.67	3.20	47.87	0.21	0.000	0.000	0.00
28.09.2015	9		40.06	16.70	56.76	0.10	0.000	0.000	0.00
11.11.2015	15		46.31	4.00	50.31	0.37	0.014	0.704	9.07
16.11.2015	16		49.18	2.00	51.18	0.41	0.019	0.980	12.63
7.12.2015	19		47.34	1.80	49.14	0.37	0.014	0.688	8.86
14.12.2015	20		43.62	1.50	45.12	0.37	0.014	0.631	8.14
11.01.2016	24		43.89	2.60	46.49	0.23	0.000	0.000	0.00
25.01.2016	26		42.69	2.90	45.59	0.37	0.014	0.638	8.22
15.02.2016	29		41.45	0.30	41.75	0.32	0.008	0.315	4.06
24.02.2016	30		46.63	7.30	53.93	0.14	0.000	0.000	0.00
03.03.2016	31		40.19	2.90	43.09	0.00	0.000	0.000	0.00
10.03.2016	32		34.70	6.20	40.90	0.00	0.000	0.000	0.00
17.03.2016	33		42.50	4.10	46.60	0.30	0.005	0.232	2.98
31.03.2016	35		42.70	23.10	65.80	0.07	0.000	0.000	0.00
06.04.2016	36		35.61	4.70	40.31	0.28	0.002	0.096	1.24
13.04.2016	37		41.87	0.50	42.37	0.30	0.005	0.211	2.71
20.04.2016	38		31.54	2.20	33.74	0.12	0.000	0.000	0.00
09.05.2016	41		44.75	8.50	53.25	0.39	0.017	0.882	11.37
16.05.2016	42		45.33	2.90	48.23	0.35	0.01	0.551	7.10
06.06.2016	45		45.60	1.40	47.00	0.13	0.000	0.000	0.00
13.06.2016	46		40.16	1.60	41.76	0.26	0.000	0.000	0.00
18.07.2016	51		41.45	1.50	42.95	0.25	0.000	0.000	0.00
08.08.2016	54		43.16	2.00	45.16	0.27	0.001	0.050	0.64
Carbon flux									
Q sum							0.22		
Sum of TOC x Q								10.53	
Vol. weighted mean TOC							48.45		
Runoff (m/yr)							2.80		
TOC flux (g C m⁻² yr⁻¹)							135.65		

Date	Week	Site	DOC (mg/l)	POC (mg/l)	TOC (mg/l)	Stage height (m)	Corresponding discharge (m ³ s ⁻¹)	TOC x Q (g/m ³)	TOC g C m-2 week-1
03.08.2015	1	SE 3	49.22	2.50	51.72	0.23	0.017	0.897	6.10
10.08.2015	2		47.80	1.50	49.30	0.29	0.022	1.075	7.32
20.08.2015	3		47.53	1.70	49.23	0.29	0.022	1.074	7.31
24.08.2015	4		47.45	1.90	49.35	0.13	0.006	0.312	2.12
01.09.2015	5		43.16	1.40	44.56	0.23	0.017	0.772	5.26
07.09.2015	6		43.85	6.30	50.15	0.20	0.015	0.734	5.00
14.09.2015	7		44.07	2.10	46.17	0.17	0.012	0.531	3.62
21.09.2015	8		42.31	8.30	50.61	0.13	0.006	0.320	2.18
28.09.2015	9		67.04	19.80	86.84	0.05	0.000	0.000	0.00
05.10.2015	10		40.64	4.20	44.84	0.03	0.000	0.000	0.00
11.11.2015	15		46.03	5.10	51.13	0.23	0.017	0.886	6.03
16.11.2015	16		30.80	2.70	33.50	0.29	0.022	0.731	4.97
7.12.2015	19		45.66	1.40	47.06	0.25	0.019	0.892	6.07
14.12.2015	20		45.61	2.40	48.01	0.27	0.020	0.981	6.68
11.01.2016	24		45.00	2.00	47.00	0.1	0.001	0.059	0.40
25.01.2016	26		41.94	3.50	45.44	0.33	0.024	1.104	7.52
15.02.2016	29		44.49	2.00	46.49	0.29	0.022	1.014	6.90
24.02.2016	30		43.80	12.80	56.60	0.1	0.001	0.071	0.49
03.03.2016	31		45.65	4.40	50.05	0.03	0.000	0.000	0.00
10.03.2016	32		40.83	2.60	43.43	0	0.000	0.000	0.00
17.03.2016	33		41.64	1.80	43.44	0.25	0.019	0.823	5.60
31.03.2016	35		44.15	2.30	46.45	0.10	0.001	0.059	0.40
06.04.2016	36		36.30	4.20	40.50	0.17	0.012	0.466	3.17
13.04.2016	37		42.85	0.40	43.25	0.24	0.018	0.785	5.35
20.04.2016	38		42.21	2.60	44.81	0.13	0.006	0.283	1.93
09.05.2016	41		43.54	1.70	45.24	0.4	0.028	1.267	8.63
16.05.2016	42		44.15	1.30	45.45	0.31	0.023	1.050	7.15
06.06.2016	45		38.49	2.50	40.99	0.13	0.006	0.259	1.76
13.06.2016	46		40.60	1.90	42.50	0.26	0.020	0.837	5.70
18.07.2016	51		42.01	1.50	43.51	0.24	0.018	0.790	5.38
08.08.2016	54		45.09	2.40	47.49	0.21	0.016	0.740	5.04
Carbon flux									
Q sum							0.41		
Sum of TOC x Q								18.81	
Vol. weighted mean TOC							45.74		
Runoff (m/yr)							2.80		
TOC flux (g C m⁻² yr⁻¹)							128.08		

Date	Week	Site	DOC (mg/l)	POC (mg/l)	TOC (mg/l)	Stage height (m)	Corresponding discharge (m ³ s ⁻¹)	TOC x Q (g/m ³)	TOC g C m-2 week-1
03.08.2015	1	SE 4	35.06	3.30	38.36	0.50	0.024	0.92	5.69
10.08.2015	2		49.56	3.00	52.56	0.41	0.018	0.93	5.71
20.08.2015	3		51.62	1.90	53.52	0.44	0.020	1.05	6.49
24.08.2015	4		45.76	1.40	47.16	0.49	0.023	1.10	6.78
01.09.2015	5		49.44	1.90	51.34	0.42	0.018	0.94	5.79
07.09.2015	6		43.44	1.20	44.64	0.33	0.013	0.56	3.44
14.09.2015	7		36.50	1.50	38.00	0.30	0.011	0.41	2.52
21.09.2015	8		20.41	1.70	22.11	0.26	0.009	0.19	1.17
28.09.2015	9		32.88	5.40	38.28	0.22	0.007	0.25	1.56
05.10.2015	10		28.02	5.10	33.12	0.19	0.005	0.17	1.07
13.10.2015	11		27.59	2.70	30.29	0.17	0.004	0.13	0.82
26.10.2015	13		29.52	4.20	33.72	0.04	0.000	0.02	0.09
11.11.2015	15		53.26	8.20	61.46	0.55	0.028	1.72	10.60
16.11.2015	16		53.77	2.00	55.77	0.64	0.036	1.98	12.22
7.12.2015	19		49.08	2.30	51.38	0.57	0.030	1.52	9.38
14.12.2015	20		51.03	2.00	53.03	0.46	0.021	1.12	6.90
11.01.2016	24		37.14	2.50	39.64	0.20	0.006	0.23	1.39
25.01.2016	26		45.20	3.00	48.20	0.41	0.018	0.85	5.23
15.02.2016	29		47.93	4.20	52.13	0.40	0.017	0.88	5.44
24.02.2016	30		43.97	1.40	45.37	0.23	0.007	0.32	1.98
03.03.2016	31		33.27	1.70	34.97	0.29	0.010	0.36	2.20
10.03.2016	32		40.48	3.10	43.58	0.24	0.008	0.33	2.03
17.03.2016	33		45.22	3.30	48.52	0.37	0.015	0.73	4.48
31.03.2016	35		43.11	2.50	45.61	0.23	0.007	0.32	1.99
06.04.2016	36		36.92	1.20	38.12	0.25	0.008	0.31	1.90
13.04.2016	37		44.50	1.70	46.20	0.28	0.010	0.45	2.75
20.04.2016	38		27.90	2.30	30.20	0.20	0.006	0.17	1.06
26.04.2016	39		34.26	5.00	39.26	0.20	0.006	0.22	1.37
09.05.2016	41		47.99	4.40	52.39	0.45	0.020	1.07	6.59
16.05.2016	42		50.91	2.50	53.41	0.49	0.023	1.25	7.68
06.06.2016	45		48.25	1.40	49.65	0.23	0.007	0.35	2.17
13.06.2016	46		38.36	1.30	39.66	0.21	0.006	0.24	1.50
11.07.2016	50		34.51	5.40	39.91	0.10	0.002	0.08	0.47
18.07.2016	51		30.73	1.60	32.33	0.18	0.005	0.16	0.96
08.08.2016	54		46.30	2.30	48.60	0.26	0.009	0.42	2.57
Carbon flux									
Q sum							0.45		
Sum of TOC x Q								21.76	
Vol. weighted mean TOC							47.85		
Runoff (m/yr)							2.80		
TOC flux (g C m²yr⁻¹)							133.99		

Date	Week	Site	DOC (mg/l)	POC (mg/l)	TOC (mg/l)	Stage height (m)	Corresponding discharge (m ³ s ⁻¹)	TOC x Q (g/m ³)	TOC g C m-2 week-1
03.08.2015	1	SA 1.2	26.49	0.9	27.39	0.33	0.05	1.32	2.53
10.08.2015	2		37.88	0.6	38.48	0.5	0.08	2.94	5.62
20.08.2015	3		23.79	0.8	24.59	0.38	0.06	1.42	2.72
24.08.2015	4		21.93	1.3	23.23	0.31	0.04	1.02	1.96
01.09.2015	5		27.59	0.7	28.29	0.48	0.07	2.08	3.98
07.09.2015	6		24.88	1.7	26.58	0.4	0.06	1.63	3.11
14.09.2015	7		19.75	1.3	21.05	0.38	0.06	1.22	2.33
21.09.2015	8		18.38	2.1	20.48	0.24	0.03	0.55	1.05
28.09.2015	9		21.17	3.2	24.37	0.21	0.02	0.43	0.83
05.10.2015	10		18.06	1.8	19.86	0.22	0.02	0.42	0.79
13.10.2015	11		14.28	1.4	15.68	0.28	0.04	0.58	1.11
26.10.2015	13		16.17	6.4	22.57	0.23	0.02	0.54	1.03
11.11.2015	15		31.08	1.5	32.58	0.48	0.07	2.40	4.58
16.11.2015	16		37.28	4.2	41.48	0.38	0.06	2.40	4.58
7.12.2015	19		36.85	1.8	38.65	0.4	0.06	2.37	4.53
14.12.2015	20		39.67	2.1	41.77	0.34	0.05	2.10	4.02
11.01.2016	24		28.92	6.2	35.12	0.32	0.05	1.62	3.10
25.01.2016	26		32.17	2.9	35.07	0.27	0.03	1.22	2.33
15.02.2016	27		41.16	1.9	43.06	0.28	0.04	1.60	3.06
24.02.2016	29		36.43	1.5	37.93	0.25	0.03	1.12	2.14
03.03.2016	30		36.98	1.3	38.28	0.23	0.02	0.91	1.75
10.03.2016	31		33.83	1	34.83	0.27	0.03	1.21	2.31
17.03.2016	32		28.92	1.5	30.42	0.3	0.04	1.27	2.43
31.03.2016	33		30.75	4.8	35.55	0.27	0.03	1.23	2.36
06.04.2016	35		50.83	1.7	52.53	0.2	0.01	0.76	1.45
13.04.2016	36		30.12	2	32.12	0.22	0.02	0.67	1.28
20.04.2016	37		114.1	0.3	114.4	0.17	0.00	0.40	0.76
26.04.2016	38		31.53	1	32.53	0.3	0.04	1.36	2.60
09.05.2016	39		32.71	1.6	34.31	0.52	0.08	2.71	5.18
16.05.2016	41		42.86	3.2	46.06	0.36	0.05	2.49	4.77
06.06.2016	42		33.76	1.4	35.16	0.27	0.03	1.22	2.33
13.06.2016	45		32.56	1.5	34.06	0.22	0.02	0.71	1.36
11.07.2016	50		29.21	1.6	30.81	0.23	0.02	0.74	1.41
18.07.2016	51		30.97	0.8	31.77	0.44	0.07	2.15	4.11
08.08.2016	54		33.98	1.2	35.18	0.26	0.03	1.13	2.16
Carbon flux									
Q sum							1.46		
Sum of TOC x Q								47.94	
Vol. weighted mean TOC							32.74		
Runoff (m/yr)							2.80		
TOC flux (g C m²yr⁻¹)							91.68		

Date	Week	Site	DOC (mg/l)	POC (mg/l)	TOC (mg/l)	Stage height (m)	Corresponding discharge (m ³ s ⁻¹)	TOC x Q (g/m ³)	TOC g C m-2 week-1
03.08.2015	1	SA 1.3	27.95	1	28.95	0.36	0.02	0.54	1.28
10.08.2015	2		29.37	0.4	29.77	0.22	0.00	0.00	0.00
20.08.2015	3		28.14	2.6	30.74	0.22	0.00	0.00	0.00
24.08.2015	4		26.84	0.7	27.54	0.2	0.00	0.00	0.00
01.09.2015	5		30.47	0.8	31.27	0.47	0.05	1.57	3.73
07.09.2015	6		28.3	0.9	29.2	0.4	0.03	0.91	2.15
14.09.2015	7		23.17	1.6	24.77	0.3	0.00	0.00	0.00
21.09.2015	8		20.06	1.4	21.46	0.03	0.00	0.00	0.00
28.09.2015	9		18.58	3	21.58	0.02	0.00	0.00	0.00
05.10.2015	10		17.28	0.9	18.18	0.03	0.00	0.00	0.00
13.10.2015	11		20.98	2	22.98	0.35	0.02	0.35	0.83
26.10.2015	13		16.31	1.4	17.71	0.2	0.00	0.00	0.00
11.11.2015	15		33.81	0.5	34.31	0.7	0.10	3.35	7.93
16.11.2015	16		34.81	4	38.81	0.68	0.09	3.66	8.66
7.12.2015	19		35.63	0.9	36.53	0.67	0.09	3.38	8.00
14.12.2015	20		36.63	1.1	37.73	0.62	0.08	3.14	7.44
11.01.2016	24		32.01	3.3	35.31	0.6	0.08	2.80	6.63
25.01.2016	26		32.84	1.8	34.64	0.6	0.08	2.75	6.51
15.02.2016	27		39.42	13.9	53.32	0.56	0.07	3.79	8.98
24.02.2016	29		33.78	0.1	33.88	0.4	0.03	1.06	2.50
03.03.2016	30		31.7	14.6	46.3	0.33	0.01	0.38	0.91
10.03.2016	31		34.24	0.8	35.04	0.44	0.04	1.49	3.53
17.03.2016	32		32.3	0.7	33	0.4	0.03	1.03	2.43
31.03.2016	33		30.27	11.7	41.97	0.4	0.03	1.31	3.10
06.04.2016	35		32.01	1.2	33.21	0.2	0.00	0.00	0.00
13.04.2016	36		28.91	1.4	30.31	0.32	0.00	0.14	0.33
20.04.2016	37		26.69	0.3	26.99	0.1	0.00	0.00	0.00
26.04.2016	38		31.55	4.6	36.15	0.4	0.03	1.13	2.67
09.05.2016	39		39.14	1.3	40.44	0.6	0.08	3.21	7.60
16.05.2016	41		41.57	0.9	42.47	0.43	0.04	1.69	4.00
06.06.2016	42		33.15	3.2	36.35	0.4	0.03	1.13	2.68
13.06.2016	45		32	5	37	0.27	0.00	0.00	0.00
11.07.2016	50		31.44	5.4	36.84	0.37	0.02	0.81	1.91
18.07.2016	51		34.03	1	35.03	0.48	0.05	1.85	4.38
08.08.2016	54		33.87	6.5	40.37	0.53	0.06	2.61	6.18
Carbon flux									
Q sum							1.18		
Sum of TOC x Q								44.05	
Vol. weighted mean TOC							37.27		
Runoff (m/yr)							2.80		
TOC flux (g C m²yr⁻¹)							104.35		

Date	Week	Site	DOC (mg/l)	POC (mg/l)	TOC (mg/l)	Stage height (m)	Corresponding discharge (m ³ s ⁻¹)	TOC x Q (g/m ³)	TOC g C m-2 week-1
03.08.2015	1	SA 1.4	24.76	2.3	27.06	0.73	0.10	2.71	2.52
10.08.2015	2		27.09	1.7	28.79	0.72	0.10	2.84	2.64
20.08.2015	3		26.37	1.7	28.07	0.73	0.10	2.81	2.61
24.08.2015	4		27.46	1.8	29.26	0.57	0.08	2.31	2.15
01.09.2015	5		30.03	1.4	31.43	1	0.15	4.69	4.36
07.09.2015	6		26.59	3	29.59	0.7	0.10	2.84	2.63
14.09.2015	7		22.74	3.9	26.64	0.57	0.08	2.11	1.96
21.09.2015	8		23.52	4.7	28.22	0.5	0.07	2.01	1.87
28.09.2015	9		26.69	4.6	31.29	0.5	0.07	2.23	2.07
05.10.2015	10		20.28	3.4	23.68	0.49	0.07	1.66	1.55
13.10.2015	11		16.37	10.9	27.27	0.5	0.07	1.95	1.81
26.10.2015	13		23.48	5.7	29.18	0.43	0.06	1.88	1.74
11.11.2015	15		28.65	13.1	41.75	1.05	0.16	6.71	6.23
16.11.2015	16		33.87	6	39.87	0.75	0.10	4.11	3.82
7.12.2015	19		29.68	1.5	31.18	0.75	0.10	3.22	2.99
14.12.2015	20		32.22	1.6	33.82	0.7	0.10	3.24	3.01
11.01.2016	24		28.54	3.8	32.34	0.6	0.08	2.67	2.48
25.01.2016	26		27.45	4.4	31.85	0.54	0.08	2.41	2.24
15.02.2016	27		38.32	2.3	40.62	0.55	0.08	3.12	2.90
24.02.2016	29		34.54	2.7	37.24	0.46	0.07	2.50	2.33
03.03.2016	30		33.64	2.2	35.84	0.45	0.07	2.37	2.21
10.03.2016	31		31.09	1.7	32.79	0.52	0.07	2.41	2.24
17.03.2016	32		30.59	5.5	36.09	0.6	0.08	2.98	2.77
31.03.2016	33		31.04	0.6	31.64	0.5	0.07	2.26	2.10
06.04.2016	35		35.41	4.6	40.01	0.47	0.07	2.73	2.54
13.04.2016	36		24.31	7.1	31.41	0.42	0.06	1.99	1.85
20.04.2016	37		27.36	5	32.36	0.4	0.06	1.99	1.85
26.04.2016	38		27.74	3.7	31.44	0.51	0.07	2.28	2.11
09.05.2016	39		38.05	5.6	43.65	0.99	0.15	6.42	5.96
16.05.2016	41		41.02	1.7	42.72	0.63	0.09	3.69	3.43
06.06.2016	42		32.36	3.8	36.16	0.5	0.07	2.58	2.40
13.06.2016	45		31.8	6.5	38.3	0.44	0.07	2.50	2.32
11.07.2016	50		30.9	3.2	34.1	0.47	0.07	2.33	2.16
18.07.2016	51		31.62	1.1	32.72	0.92	0.13	4.34	4.03
08.08.2016	54		36.72	2	38.72	0.47	0.07	2.64	2.45
Carbon flux									
Q sum							3.01		
Sum of TOC x Q								101.53	
Vol. weighted mean TOC							33.68		
Runoff (m/yr)							2.80		
TOC flux (g C m²yr⁻¹)							94.31		

Date	Week	Site	DOC (mg/l)	POC (mg/l)	TOC (mg/l)	Stage height (m)	Corresponding discharge (m ³ s ⁻¹)	TOC x Q (g/m ³)	TOC g C m-2 week-1
06.08.2015	1	SA 3.1	24.38	8.2	32.58	0.57	0.11	3.69	3.41
13.08.2015	2		42.41	2.4	44.81	0.58	0.12	5.20	4.81
18.08.2015	3		26.39	2.7	29.09	0.56	0.11	3.22	2.97
27.08.2015	4		26.85	1.8	28.65	0.4	0.07	1.93	1.79
31.08.2015	5		29.83	1.2	31.03	1	0.23	7.12	6.58
09.09.2015	6		32.48	0.3	32.78	0.3	0.04	1.32	1.22
16.09.2015	7		27.72	1.4	29.12	0.39	0.06	1.88	1.74
23.09.2015	8		21.23	2.4	23.63	0.34	0.05	1.21	1.12
30.09.2015	9		21.55	3.7	25.25	0.36	0.06	1.43	1.32
06.10.2015	10		19.14	5.1	24.24	0.37	0.06	1.44	1.33
15.10.2015	11		21.27	2.3	23.57	0.3	0.04	0.95	0.88
28.10.2015	13		20.08	3	23.08	0.16	0.00	0.06	0.06
11.11.2015	15		20.08	3	23.08	1.1	0.26	5.92	5.47
16.12.2015	20		32.96	2.2	35.16	0.42	0.07	2.56	2.37
13.01.2016	24		27.74	2.3	30.04	0.3	0.04	1.21	1.12
27.01.2016	26		28.24	3.8	32.04	0.37	0.06	1.90	1.76
17.02.2016	29		33.78	1.6	35.38	0.37	0.06	2.10	1.94
22.02.2016	30		28.2	1.5	29.7	0.4	0.07	2.00	1.85
29.06.2016	31		28.97	1.3	30.27	0.26	0.03	0.90	0.83
07.03.2016	32		34.56	0.9	35.46	0.46	0.08	2.96	2.74
14.03.2016	33		29.12	4	33.12	0.9	0.20	6.70	6.20
28.03.2016	35		29.69	10.2	39.89	0.38	0.06	2.47	2.29
04.04.2016	36		27.11	1.6	28.71	0.43	0.08	2.17	2.00
11.04.2016	37		24.71	3	27.71	0.87	0.19	5.38	4.98
18.04.2016	38		25.95	0.5	26.45	0.4	0.07	1.78	1.65
25.04.2016	39		26.94	5.8	32.74	0.45	0.08	2.65	2.45
11.05.2016	41		41.91	1.7	43.61	0.55	0.11	4.70	4.35
18.05.2016	42		42.28	1.5	43.78	0.67	0.14	6.14	5.68
08.06.2016	45		30.99	2.7	33.69	0.62	0.13	4.27	3.95
15.06.2016	46		26.57	3	29.57	0.35	0.05	1.59	1.47
13.07.2016	50		25.62	3.7	29.32	0.3	0.04	1.18	1.09
20.07.2016	51		30.41	2.2	32.61	0.68	0.14	4.66	4.31
1.08.2016	53		30.41	2.2	32.61	0.47	0.09	2.81	2.60
10.08.2016	54		29.39	3.8	33.19	0.25	0.03	0.89	0.83
Carbon flux									
Q sum							3.03		
Sum of TOC x Q								96.38	
Vol. weighted mean TOC							31.84		
Runoff (m/yr)							2.80		
TOC flux (g C m⁻²yr⁻¹)							89.15		

Date	Week	Site	DOC (mg/l)	POC (mg/l)	TOC (mg/l)	Stage height (m)	Corresponding discharge (m ³ s ⁻¹)	TOC x Q (g/m ³)	TOC g C m-2 week-1
03.08.2015	1	SA 3.5	22.09	4.1	26.19	0.79	0.19	5.08	0.97
10.08.2015	2		24.35	4.1	28.45	1.3	0.40	11.33	2.16
20.08.2015	3		27.36	9.1	36.46	1.95	1.00	36.35	6.93
24.08.2015	4		20.74	6.9	27.64	1.3	0.40	11.01	2.10
01.09.2015	5		32.36	2.1	34.46	2	1.07	36.87	7.03
07.09.2015	6		27.93	3	30.93	1.45	0.49	15.23	2.90
14.09.2015	7		19.85	1.5	21.35	0.79	0.19	4.14	0.79
21.09.2015	8		16.02	6.1	22.12	0.7	0.17	3.78	0.72
28.09.2015	9		16.12	3.2	19.32	0.8	0.20	3.80	0.72
05.10.2015	10		15.72	5.5	21.22	0.75	0.18	3.89	0.74
13.10.2015	11		16.17	3.4	19.57	1.1	0.30	5.88	1.12
26.10.2015	13		14.68	6.7	21.38	1.13	0.31	6.70	1.28
11.11.2015	15		33.4	1.9	35.3	1.95	1.00	35.20	6.71
16.11.2015	16		37.35	1.3	38.65	2	1.07	41.36	7.88
7.12.2015	19		31.98	2.7	34.68	1.8	0.81	27.98	5.33
14.12.2015	20		26.01	1.6	27.61	1.2	0.35	9.55	1.82
11.01.2016	24		22.77	7	29.77	1.2	0.35	10.30	1.96
25.01.2016	26		27.08	5.5	32.58	0.79	0.19	6.32	1.20
15.02.2016	29		29	10	39	1.3	0.40	15.54	2.96
24.02.2016	30		21.35	5.3	26.65	1	0.26	6.95	1.33
03.03.2016	31		21.25	4.7	25.95	0.96	0.25	6.40	1.22
10.03.2016	32		29.67	0.6	30.27	0.85	0.21	6.39	1.22
17.03.2016	33		21.94	8.4	30.34	0.95	0.24	7.38	1.41
31.03.2016	35		24.17	8.6	32.77	1.1	0.30	9.84	1.88
06.04.2016	36		23.15	3.7	26.85	0.8	0.20	5.28	1.01
13.04.2016	37		19.41	3.3	22.71	1	0.26	5.92	1.13
20.04.2016	38		15.3	0.8	16.1	0.8	0.20	3.17	0.60
26.04.2016	39		23.22	2.5	25.72	1.1	0.30	7.73	1.47
09.05.2016	41		35.75	5	40.75	1.2	0.35	14.10	2.69
16.05.2016	42		38.34	1.5	39.84	1.5	0.53	21.05	4.01
06.06.2016	45		25.11	4.8	29.91	1.5	0.53	15.80	3.01
13.06.2016	46		17.78	4.1	21.88	1.38	0.45	9.76	1.86
11.07.2016	50		23.26	3.1	26.36	1.4	0.46	12.09	2.31
18.07.2016	51		28.83	13.8	42.63	1.7	0.70	29.87	5.69
08.08.2016	54		26.4	5.3	31.7	1.3	0.40	12.63	2.41
Carbon flux									
Q sum							14.69		
Sum of TOC x Q								464.67	
Vol. weighted mean TOC							31.63		
Runoff (m/yr)							2.80		
TOC flux (g C m⁻²yr⁻¹)							88.57		

Date	Week	Site	DOC (mg/l)	POC (mg/l)	TOC (mg/l)	Stage height (m)	Corresponding discharge (m ³ s ⁻¹)	TOC x Q (g/m ³)	TOC g C m-2 week-1
03.08.2015	1	SA 3.6	29.81	12.2	42.01	0.63	0.22	9.31	10.11
10.08.2015	2		28.17	1.5	29.67	0.62	0.21	6.32	6.86
20.08.2015	3		31.51	3	34.51	0.65	0.24	8.25	8.96
24.08.2015	4		27.41	1.4	28.81	0.47	0.11	3.11	3.38
01.09.2015	5		33.41	1.2	34.61	0.5	0.13	4.35	4.72
07.09.2015	6		29.02	2.3	31.32	0.4	0.07	2.28	2.47
14.09.2015	7		24.63	1.4	26.03	0.37	0.06	1.56	1.70
21.09.2015	8		21.74	3.3	25.04	0.32	0.04	1.05	1.14
28.09.2015	9		19.97	2.5	22.47	0.3	0.04	0.81	0.88
05.10.2015	10		21.26	9.3	30.56	0.35	0.05	1.60	1.74
13.10.2015	11		22.53	1.6	24.13	0.3	0.04	0.87	0.94
26.10.2015	13		22.84	1.7	24.54	0.23	0.02	0.46	0.50
11.11.2015	15		33.23	1.3	34.53	0.47	0.11	3.73	4.05
16.11.2015	16		35.66	0.6	36.26	0.42	0.08	2.97	3.23
7.12.2015	19		37.96	0.6	38.56	0.41	0.08	2.98	3.24
14.12.2015	20		32.36	0.2	32.56	0.41	0.08	2.52	2.73
11.01.2016	24		33.15	2.1	35.25	0.31	0.04	1.37	1.49
25.01.2016	26		30.14	3.4	33.54	0.4	0.07	2.44	2.65
15.02.2016	29		33.22	0.7	33.92	0.4	0.07	2.47	2.68
24.02.2016	30		27.92	0.8	28.72	0.44	0.09	2.64	2.87
03.03.2016	31		29.18	1.5	30.68	0.37	0.06	1.84	2.00
10.03.2016	32		33.26	3.5	36.76	0.23	0.02	0.69	0.75
17.03.2016	33		29.56	2.1	31.66	0.38	0.06	2.03	2.20
31.03.2016	35		33.08	1.6	34.68	0.4	0.07	2.52	2.74
06.04.2016	36		29.5	2.3	31.8	0.37	0.06	1.91	2.07
13.04.2016	37		29.68	1.3	30.98	0.4	0.07	2.25	2.45
20.04.2016	38		28.59	2.6	31.19	0.37	0.06	1.87	2.03
26.04.2016	39		28.94	6.2	35.14	0.42	0.08	2.88	3.13
09.05.2016	41		36.17	0.9	37.07	0.4	0.07	2.70	2.93
16.05.2016	42		41.15	3	44.15	0.37	0.06	2.65	2.88
06.06.2016	45		31.56	3.4	34.96	0.3	0.04	1.26	1.36
13.06.2016	46		26.84	3.2	30.04	0.21	0.01	0.45	0.49
11.07.2016	50		27.8	4.5	32.3	0.2	0.01	0.43	0.47
18.07.2016	51		31.38	7.2	38.58	0.3	0.04	1.39	1.51
08.08.2016	54		30.38	5.7	36.08	0.17	0.01	0.32	0.35
Carbon flux									
Q sum							2.58		
Sum of TOC x Q								86.29	
Vol. weighted mean TOC							33.46		
Runoff (m/yr)							2.80		
TOC flux (g C m²yr⁻¹)							93.70		

Date	Week	Site	DOC (mg/l)	POC (mg/l)	TOC (mg/l)	Stage height (m)	Corresponding discharge (m ³ s ⁻¹)	TOC x Q (g/m ³)	TOC g C m-2 week-1
03.08.2015	1	SA 4.1	28.65	1.1	29.75	0.83	0.09	2.79	0.95
10.08.2015	2		48.46	0.2	48.66	0.9	0.14	6.80	2.31
20.08.2015	3		34.65	1.7	36.35	0.88	0.13	4.60	1.56
24.08.2015	4		31.55	1	32.55	1.1	0.27	8.82	2.99
01.09.2015	5		37.5	1	38.5	1.3	0.40	15.47	5.25
07.09.2015	6		37.76	1.3	39.06	1.3	0.40	15.70	5.33
14.09.2015	7		53.06	1.4	54.46	1.14	0.30	16.18	5.49
21.09.2015	8		28.39	2.3	30.69	1.1	0.27	8.31	2.82
28.09.2015	9		26.62	12.9	39.52	1	0.21	8.11	2.75
05.10.2015	10		25.5	1.4	26.9	0.97	0.19	4.99	1.69
13.10.2015	11		24.44	1.9	26.34	1.04	0.23	6.10	2.07
26.10.2015	13		28.22	1.2	29.42	0.97	0.19	5.46	1.85
11.11.2015	15		34.02	1.5	35.52	1.2	0.34	11.95	4.05
16.11.2015	16		37.66	0.8	38.46	1.27	0.38	14.70	4.99
7.12.2015	19		36.57	1.1	37.67	1.15	0.30	11.44	3.88
14.12.2015	20		32.61	2.7	35.31	1.08	0.26	9.10	3.09
11.01.2016	24		29.29	2.2	31.49	1	0.21	6.46	2.19
25.01.2016	26		33.11	1.8	34.91	1	0.21	7.17	2.43
15.02.2016	29		35.84	1.1	36.94	1.1	0.27	10.00	3.39
24.02.2016	30		32.82	0	32.82	0.91	0.15	4.80	1.63
03.03.2016	31		26.44	5.5	31.94	1	0.21	6.56	2.22
10.03.2016	32		33.06	8.2	41.26	1.1	0.27	11.17	3.79
17.03.2016	33		30.35	2.2	32.55	1.1	0.27	8.82	2.99
31.03.2016	35		31.56	0.6	32.16	0.97	0.19	5.97	2.03
06.04.2016	36		31.81	1.4	33.21	1.05	0.24	7.91	2.68
13.04.2016	37		29.58	2.1	31.68	0.96	0.18	5.67	1.92
20.04.2016	38		28.26	3.5	31.76	0.94	0.17	5.27	1.79
26.04.2016	39		29.24	3.1	32.34	0.94	0.17	5.37	1.82
09.05.2016	41		36.41	1.1	37.51	1.09	0.26	9.91	3.36
16.05.2016	42		40.55	4.3	44.85	1.3	0.40	18.03	6.12
06.06.2016	45		32.37	1.8	34.17	1.03	0.22	7.69	2.61
13.06.2016	46		31.36	5.6	36.96	0.98	0.19	7.10	2.41
11.07.2016	50		30.56	1.9	32.46	0.96	0.18	5.81	1.97
18.07.2016	51		31.99	2.7	34.69	0.99	0.20	6.89	2.34
08.08.2016	54		34.66	2.50	37.16	0.98	0.19	7.14	2.42
Carbon flux									
Q sum							8.25		
Sum of TOC x Q								298.28	
Vol. weighted mean TOC							36.14		
Runoff (m/yr)							2.80		
TOC flux (g C m²yr⁻¹)							101.19		

Date	Week	Site	DOC (mg/l)	POC (mg/l)	TOC (mg/l)	Stage height (m)	Corresponding discharge (m ³ s ⁻¹)	TOC x Q (g/m ³)	TOC g C m-2 week-1
03.08.2015	1	SA 4.2	29.04	1.2	30.24	1.12	0.08	2.50	1.72
10.08.2015	2		32.7	9	41.7	1.2	0.11	4.53	3.12
20.08.2015	3		36.22	1.9	38.12	1.25	0.13	4.87	3.35
24.08.2015	4		31.89	1.9	33.79	1.07	0.07	2.33	1.61
01.09.2015	5		40.3	1.1	41.4	1.35	0.17	7.17	4.94
07.09.2015	6		37.2	6.3	43.5	1.36	0.18	7.76	5.34
14.09.2015	7		33.13	3.4	36.53	1.2	0.11	3.97	2.73
21.09.2015	8		29.27	2.6	31.87	1.16	0.10	3.03	2.09
28.09.2015	9		28.39	5.3	33.69	1.15	0.09	3.09	2.13
05.10.2015	10		25.81	1.9	27.71	1.14	0.09	2.46	1.69
13.10.2015	11		26.9	5.8	32.7	1.15	0.09	3.00	2.07
26.10.2015	13		27.37	1.2	28.57	1.1	0.08	2.20	1.51
11.11.2015	15		38.73	0.9	39.63	1.55	0.30	11.86	8.17
16.11.2015	16		55.01	0.7	55.71	1.4	0.20	11.15	7.67
7.12.2015	19		36.39	1.6	37.99	1.27	0.14	5.17	3.56
14.12.2015	20		32.68	1.6	34.28	1.2	0.11	3.73	2.57
11.01.2016	24		29.3	6.2	35.5	1.2	0.11	3.86	2.66
25.01.2016	26		32.21	3	35.21	1.2	0.11	3.83	2.63
15.02.2016	29		35.48	1.2	36.68	1.3	0.15	5.47	3.77
24.02.2016	30		29.89	1.1	30.99	1.14	0.09	2.75	1.89
03.03.2016	31		30.35	3.1	33.45	0.9	0.03	1.16	0.80
10.03.2016	32		32.57	5	37.57	1.15	0.09	3.45	2.38
17.03.2016	33		29.5	5.2	34.7	1.1	0.08	2.67	1.84
31.03.2016	35		31.92	0.7	32.62	1.2	0.11	3.54	2.44
06.04.2016	36		30.08	1.8	31.88	1.1	0.08	2.45	1.69
13.04.2016	37		29.93	2	31.93	1.1	0.08	2.46	1.69
20.04.2016	38		26.94	5.3	32.24	1	0.05	1.70	1.17
26.04.2016	39		32.79	1.2	33.99	1	0.05	1.79	1.24
09.05.2016	41		37.86	1.4	39.26	1.3	0.15	5.86	4.03
16.05.2016	42		39.11	6.6	45.71	1.6	0.34	15.52	10.68
06.06.2016	45		33.02	1.4	34.42	1.22	0.12	3.99	2.75
13.06.2016	46		31.17	1.7	32.87	1.28	0.14	4.61	3.18
11.07.2016	50		29.24	2.9	32.14	1.14	0.09	2.85	1.96
18.07.2016	51		31.36	3.7	35.06	1.15	0.09	3.22	2.22
08.08.2016	54		35.28	2	37.28	1.1	0.08	2.87	1.98
Carbon flux									
Q sum							4.07		
Sum of TOC x Q								152.88	
Vol. weighted mean TOC							37.60		
Runoff (m/yr)							2.80		
TOC flux (g C m²yr⁻¹)							105.27		

Date	Week	Site	DOC (mg/l)	POC (mg/l)	TOC (mg/l)	Stage height (m)	Corresponding discharge (m ³ s ⁻¹)	TOC x Q (g/m ³)	TOC g C m-2 week-1
04.08.2015	1	SA 4.3	30.36	1.3	31.66	0.56	0.00	0.00	0.00
13.08.2015	2		32.31	0.2	32.51	0.78	0.00	0.00	0.00
19.08.2015	3		32.8	0.5	33.3	0.78	0.00	0.00	0.00
25.08.2015	4		32.6	0.8	33.4	0.88	0.03	1.12	8.41
01.09.2015	5		34.34	0.4	34.74	0.87	0.03	1.03	7.73
08.09.2015	6		36.7	1.5	38.2	0.87	0.03	1.14	8.50
15.09.2015	7		31.23	0.8	32.03	0.83	0.01	0.45	3.37
22.09.2015	8		30.01	1.9	31.91	0.74	0.00	0.00	0.00
29.09.2015	9		29.25	5.1	34.35	0.4	0.00	0.00	0.00
05.10.2015	10		28.25	5.6	33.85	0.3	0.00	0.00	0.00
14.10.2015	11		29.61	2.7	32.31	0.7	0.00	0.00	0.00
27.10.2015	13		30.16	8.9	39.06	0.55	0.00	0.00	0.00
11.11.2015	15		31.47	1.3	32.77	0.87	0.03	0.98	7.29
19.11.2015	16		35.4	0.3	35.7	0.85	0.02	0.78	5.85
8.12.2015	19		34.86	0.4	35.26	0.85	0.02	0.77	5.78
15.12.2015	20		31.6	2.5	34.1	0.8	0.00	0.08	0.59
12.01.2016	24		29.52	2.7	32.22	0.67	0.00	0.00	0.00
26.01.2016	26		32.14	3.2	35.34	0.9	0.04	1.47	10.97
16.02.2016	29		36.61	1.1	37.71	0.98	0.07	2.75	20.55
23.02.2016	30		29.22	1.1	30.32	0.76	0.00	0.00	0.00
02.03.2016	31		28.56	8.3	36.86	0.42	0.00	0.00	0.00
09.03.2016	32		31.9	4.9	36.8	0.6	0.00	0.00	0.00
16.03.2016	33		31.1	3.3	34.4	0.79	0.00	0.00	0.00
29.03.2016	35		30.96	2	32.96	0.52	0.00	0.00	0.00
05.04.2016	36		28.02	6.9	34.92	0.2	0.00	0.00	0.00
12.04.2016	37		32.83	1.4	34.23	0.66	0.00	0.00	0.00
19.04.2016	38		27.83	1.4	29.23	0.26	0.00	0.00	0.00
11.05.2016	41		35.49	1.5	36.99	0.47	0.00	0.00	0.00
17.05.2016	42		37.97	1	38.97	0.99	0.08	2.99	22.38
06.06.2016	45		32.47	1.5	33.97	0.63	0.00	0.00	0.00
14.06.2016	46		29.11	2.2	31.31	0.39	0.00	0.00	0.00
19.07.2013	51		30.65	5.1	35.75	0.28	0.00	0.00	0.00
9.08.2016	54		34.1	2.4	36.5	0.59	0.00	0.00	0.00
Carbon flux									
Q sum							0.37		
Sum of TOC x Q								13.56	
Vol. weighted mean TOC							36.23		
Runoff (m/yr)							2.80		
TOC flux (g C m²yr⁻¹)							101.44		

Date	Week	Site	DOC (mg/l)	POC (mg/l)	TOC (mg/l)	Stage height (m)	Corresponding discharge (m ³ s ⁻¹)	TOC x Q (g/m ³)	TOC g C m-2 week-1
03.08.2015	1	SA 4.4	30.36	1.4	31.76	0.48	0.05	1.55	3.12
10.08.2015	2		32.31	0.8	33.11	0.42	0.03	0.93	1.88
20.08.2015	3		32.8	0.6	33.4	0.42	0.03	0.94	1.89
24.08.2015	4		32.6	0.6	33.2	0.58	0.08	2.77	5.56
01.09.2015	5		34.34	1.2	35.54	0.83	0.17	6.02	12.10
07.09.2015	6		36.7	1.9	38.6	0.78	0.15	5.88	11.81
14.09.2015	7		31.23	19.5	50.73	0.64	0.10	5.28	10.60
21.09.2015	8		30.01	2.6	32.61	0.55	0.07	2.38	4.78
28.09.2015	9		29.25	3.9	33.15	0.38	0.01	0.48	0.96
05.10.2015	10		28.25	4.4	32.65	0.28	0.00	0.00	0.00
13.10.2015	11		29.61	1.7	31.31	0.3	0.00	0.00	0.00
26.10.2015	13		30.16	1.4	31.56	0.33	0.00	0.00	0.00
11.11.2015	15		31.47	1.2	32.67	0.63	0.10	3.29	6.60
16.11.2015	16		35.4	1.6	37	0.67	0.11	4.23	8.50
7.12.2015	19		34.86	1.4	36.26	0.57	0.08	2.90	5.82
14.12.2015	20		31.6	1	32.6	0.55	0.07	2.38	4.78
11.01.2016	24		29.52	3.5	33.02	0.38	0.01	0.48	0.96
25.01.2016	26		32.14	2.3	34.44	0.64	0.10	3.58	7.20
15.02.2016	29		36.61	1.1	37.71	0.46	0.04	1.58	3.18
24.02.2016	30		29.22	5	34.22	0.34	0.00	0.02	0.05
03.03.2016	31		28.56	2.1	30.66	0.35	0.00	0.13	0.25
10.03.2016	32		31.9	1.8	33.7	0.45	0.04	1.30	2.61
17.03.2016	33		31.1	1.3	32.4	0.38	0.01	0.47	0.94
31.03.2016	35		30.96	1.4	32.36	0.5	0.06	1.81	3.63
06.04.2016	36		28.02	0.8	28.82	0.32	0.00	0.00	0.00
13.04.2016	37		32.83	1	33.83	0.31	0.00	0.00	0.00
20.04.2016	38		27.83	2	29.83	0.26	0.00	0.00	0.00
26.04.2016	39		29.04	2.1	2.1	0.28	0.00	0.00	0.00
09.05.2016	41		40.23	1	41.23	0.38	0.01	0.60	1.20
16.05.2016	42		43.07	1.2	44.27	0.44	0.04	1.55	3.12
06.06.2016	45		30.79	1.4	32.19	0.32	0.00	0.00	0.00
13.06.2016	46		30.1	0.8	30.9	0.29	0.00	0.00	0.00
11.07.2016	50		0	0	0	0	0.00	0.00	0.00
18.07.2016	51		29.12	6.4	35.52	0.29	0.00	0.00	0.00
08.08.2016	54		34.26	1.1	35.36	0.31	0.00	0.00	0.00
Carbon flux									
Q sum							1.39		
Sum of TOC x Q								50.56	
Vol. weighted mean TOC							36.28		
Runoff (m/yr)							2.80		
TOC flux (g C m²yr⁻¹)							101.57		

Appendix G: Comparison between dipwell and ditch water

Sample	DOC (mg/l) ditch	DOC (mg/l) dipwell	Difference (dipwell - ditch) (mg/l)
SE 2 W6	55.63	62.40	6.77
SE3 W6	43.85	47.34	3.49
SE4 W6	43.44	55.20	11.76
SA 1.1 W6	19.65	24.30	4.65
SA 1.2 W6	24.88	27.34	2.46
SA 1.3 W6	28.30	34.24	5.94
SA 3.1 W6	32.48	35.57	3.09
SA 3.3 W6	24.39	30.25	5.86
SA 3.6 W6	29.02	32.40	3.38
SA 4.3 W6	36.70	39.60	2.90
SA 4.4 W6	36.76	40.50	3.74
SE 2 W8	44.67	53.8	9.11
SE3 W8	42.31	46.2	3.92
SE4 W8	20.41	25.1	4.69
SA 1.1 W8	15.31	20.3	4.99
SA 1.2 W8	18.38	24.4	5.97
SA 1.3 W8	20.06	22.4	2.34
SA 3.1 W8	21.23	25.7	4.44
SA 3.3 W8	10.69	15.6	4.91
SA 3.6 W8	21.74	26.9	5.15
SA 4.3 W8	30.01	35.2	5.19
SA 4.4 W8	25.53	29.6	4.07
Average difference			4.95